Brain Imaging Exploration of the Representational Structures Supporting Observation of Abnormal Finger Postures.

Miguel Granja Espírito Santo

A thesis presented for the degree of

Doctor of Philosophy

School of Psychology, University of Nottingham

United Kingdom

Acknowledgements

I would like to thank Dr. Martin Schürmann, for all of these years of thoughtful, very considerate, and above all, patient supervision. Without his guidance many of the important milestones in my PhD, and life in general, would not have happened. I extend my gratitude to my second supervisor, Prof. Susan Francis. Her thoughtful consideration of my work, and the opportunities that she gave me was another reason why I was able to complete this crazy thing. I would also like to thank Dr. Rosa Sanchez-Panchuelo for all the quick replies to sometimes simple emails, and all the hours of help throughout these past four years with fMRI.

I would like to thank- Sally Eldeghaidy for her assistance and advice when conducting the very last few fMRI sessions; Octavian Maxim, for his assistance in acquiring EEG data, but more importantly his friendship; Joshua and Hsin-Yuang for their help with EEG experiments; Katherine Dyke, Christina Ralph-Nearman, Soyoung Kim, Sophia Pepes, Bev Brown, Hilmar Sigurdsson and Kanad Mandke for being my office mates and indulging me, maybe too often, in my procrastination sessions. Above all, thanks for their help with piloting, testing, and their understanding.

Entre família não se deve dizer obrigado, porque ninguem ajuda por obrigação, mas sim por amor. Mas depois deste tempo todo e distância, eu pelo menos preciso dizer que sem o meu pai, mãe, avó, avô, primos, tios e Marina nada disto seria possível. To Amma, Appa and Aashish, I am very happy that you have welcomed me into your family and treated me like your own. Without such kindness I would not be leading the life I am today. I could not have wished for better people to have become part of my life. Also, I am grateful to Asha, Colby, Lorna and Lottie for welcoming us into their family and being there for us during difficult times.

What to say to my wife, Smirithi? Our life was in hard mode for a long time, and it has been fun. Now the hard-mode is finished and we can start to look into the future with more crazy plans (like getting married in India while doing a PhD) because who wants to play life in boring-mode? I am lucky to always have you by my side. Without your love, support and above all patience, this would never have happened.

Abstract

Observing body related abnormalities such as broken limbs (like fingers) can lead to a vicarious somatosensory experience. Such responses depend on a complex interaction between different brain regions in order to give rise to a somatosensory experience based on visual stimulation alone. In this thesis, I use multiple imaging techniques to demonstrate this is an example of embodied simulation, an ingrained ability of the brain that allows an observer to simulate others' experiences based on somatosensory and lateral occipital involvement.

In the first stages of my PhD project I developed a novel procedure where realistic computer-generated 3D models of subjects' actual hands were created, and then tested their suitability for the neuroimaging experiments in this thesis. After finding the models suitable, I created images of salient hands with finger abnormalities, resembling broken fingers, in order to elicit a strong vicarious response. To investigate whether this response elicits somatosensory activity, I used 7T fMRI in combination with a highly specific tactile localiser to describe the involvement of different sub-regions of the S1 hand-area in the observation of distorted finger postures. Among the sub-regions distortion-related activation was the strongest in posterior regions of the S1 (BA 2). This was followed by two EEG experiments which investigated the involvement of the lateral occipital cortex in the processing of the observed finger abnormalities. This was assessed using the N1 ERP component, and larger amplitudes to the observation of distorted finger postures were found when compared to control conditions. Lastly, I used MEG to merge the findings made in the previous experiments. For the observation of distorted fingers compared to controls, the results of the MEG experiment revealed a complex temporal evolution: First, involving the visual areas; and then followed by sustained activity of ventral temporal areas in parity with involvement of somatosensory integration areas at later latencies.

This thesis describes with very good spatial and temporal resolution, the neural structures that support the observation of abnormal finger postures. It expands previous literature by showing primary somatosensory responses to body related visual stimuli

alone. It demonstrates that the visual body processing areas may initiate the mechanism for embodied simulation. And, it outlines the progression of activation from the visual areas to the somatosensory ones, creating the embodied simulation network.

Contents

Chapter 1

Introduction

A variety of anecdotal reports state that humans are able to create mental simulations of what others experience and create sensory experiences of their own. A famous case is that of somatosensory synesthetes. This very small group of individuals have a condition in which sensory stimulation in one modality is intrinsically linked with representations of another modality leading to an automatic experience of both. For 'mirror-touch' synesthetes (Banissy, Kadosh, Maus, Walsh & Ward, 2009), this is expressed as experiencing tactile sensations in a body part purely through observation of the same body part being touched in another person (Blakemore, Bristow, Bird, Frith & Ward, 2005). For example, in a brain imaging study, when a subject (named C) who experienced this condition, observed others being touched, significant brain activity in the primary and secondary (S1 and S2) cortices occurred (Blakemore et al., 2005). This activity was significantly higher compared to viewing objects being touched, but crucially, more activity was seen in S1 and S2 compared to control subjects. Blakemore et al. (2005) posited that everyone has some form vicarious representation of touch within the somatosensory cortices, since the controls also showed signific-

ant somatosensory activity, but with a variety of perceptual thresholds. Those that have lower thresholds, in which C is an extreme example, are likely to have localised representations and increased brain activity (Schaefer, Heinze & Rotte, 2012; Keysers & Gazzola, 2009), which in turn leads to more salient experiences. However, typical individuals do not report localised experiences as C does. Instead, they report some intransitive feeling that they cannot quantify, and qualify it as some form of wide-spread 'sensation'.

Everyone at some point, has experienced what other's experience. Observing a spider crawling over another person's hand, may elicit a shiver running down their spine. Observing people with an arm amputation may make one more aware of their own arm, in some cases, even create a weak tingling sensation in the same area. Watching broken limbs or even surgery on television, elicit a visceral, 'gut', reaction. These examples demonstrate that to some extent that typical individuals share some of the abilities that C has. Importantly, this highlights an embedded quality that humans have to model observed body related behaviour and experiences. The study of Blakemore et al. (2005) was one of the first to highlight that observation of others is not just simulated but also embodied.

The main focus of this thesis is to explore how this reaction arises and is represented within the human cortex, but with a particular focus on observing body abnormalities as may occur after an accident. These type of stimuli are of high importance to an observer, as they provides information not only about a potential inner state of a person, but also are an indicator of potential threats of the environment. Importantly, the thesis addresses questions about intrinsic aspects of the human brain: Are our brains modelling machines that allow the simulation of these events to elicit a sensory experience? Do these simulations

create specific representations in the brain? If so, where does it occur? What triggers a response such as this one?

By using highly realistic 3D models of real hands and distorting the appearance of the fingers to make them look they are broken (see Figure 1.1), I aim to induce a vicarious reaction in the observer and address the questions stated above. The reason for using hands as a tool to investigate embodied simulation stems from the simple reason of its somatosensory (Kaas, 1983; Baumgartner et al., 1991; Maldjian et al., 1999; Francis et al., 2000; Sanchez-Panchuelo, Francis, Bowtell & Schluppeck, 2010; Besle, Sánchez-Panchuelo, Bowtell, Francis & Schluppeck, 2013; Martuzzi, van der Zwaag, Farthouat, Gruetter & Blanke, 2014) and extrastriate cortex representations (Orlov, Makin & Zohary, 2010; Bracci, Ietswaart, Peelen & Cavina-Pratesi, 2010; Op de Beeck, Brants, Baeck & Wagemans, 2010). The borders of the somatosensory cortex and its sub-regions are well defined and explained in the literature allowing explicit hypotheses to be developed (Geyer, Schleicher & Zilles, 1999; Geyer, Schormann, Mohlberg & Zilles, 2000; Grefkes, Geyer, Schormann, Roland & Zilles, 2001). Similar arguments can be put forward for hand representation in the extrastriate cortex (Orlov et al., 2010; Bracci et al., 2010; Op de Beeck et al., 2010); and, due to the simple anatomical configuration of the hand, applying abnormalities in a controlled manner is considerably easy and effective.

In the current chapter, I will outline key concepts and literature which cover embodied simulation, the primary somatosensory cortex hierarchical structure and its vicarious activation, and the role of the extrastriate cortex in body detection and appraisal. Then, I will conclude with the framework of the thesis, which explores whether observation of abnormal hands leads to embodied simulation of

those abnormalities, and attempt to expand the current literature by investigating the interaction between extrastriate body area and primary somatosensory area.

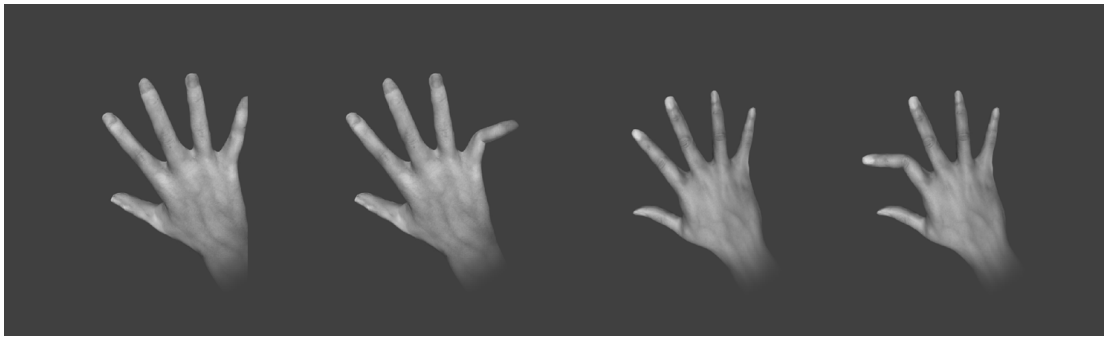

Figure 1.1: Example of realistic 3D models of actual human subjects, to which finger abnormalities were applied to mimic a joint dislocation. These stimuli are used in Chapters 5 and 7. For details on how they were constructed refer to Chapter 2.

1.1 Embodied Simulation

Exciting developments in neuroscience have demonstrated that the same neural structures involved in orienting and perceiving actions or sensations of our own body, are also involved in decoding others' body-related experiences and emotions. Crucially, this is an automatic, unconscious and reflexive simulation mechanism which allows functional representation in brain regions typically involved in own body experiences (Gallese, 2005). The term simulation is not necessarily reserved for body-related events but can also be applied to non-sensorial demands, such as being able to mentally simulate the rotation of shapes in one's head to achieve a desired angle. The key aspect is the term 'embodied' - in Gallese (2005, 2007) it is referred to as neural retrieval of a "pre-existing body model in the brain", which uses somato-motor regions as a scaffold for observed stimuli representation.

It must be highlighted that, whilst embodied simulation and mirror neuron system work for similar outcomes (understanding inner states) an important dif-

ference is made in the literature. The mirror neuron system, is a group of neurons which activates both when an action is conducted and observed (Rizzolatti, Fadiga, Gallese & Fogassi, 1996). In single-cell studies conducted in monkeys, the same group of neurons discharge when hand actions were executed to grasp an object, but also discharge when the monkey saw the experimenter executing the same action (Gallese, Fadiga, Fogassi & Rizzolatti, 2002). For an action to be embodied, the mirror neurons must be involved in the simulating outcomes of actions. In other words, embodied simulation is supported by the MNS, but is more than just mirroring. For example, Umilta et al. (2001) performed a study in which they showed monkeys two types of grasping actions: first, they showed an entire movement towards an object and measured neuronal discharge in parietal areas; second, they showed the exact same action, but just before the hand-object interaction, the movement was occluded. Neuronal measurements showed that more than half of the neurons active in response to the grasping action also fired during the hidden movement. This finding highlights that inferences of the goal of behaviours can be made without full information, the motor cortex simulates the rest of outcome, filling in the blank.

The previous example underlines the key ontological difference between mirror neuron system and embodied simulation. Whereas, the MNS is a group of neurons with a specific physiological characteristic related to action execution and observation (Buccino et al., 2004), the other is a higher level concept, which allows the simulation to occur based on previous body schematic information. A clear example for this explanation comes from an interesting study by Buccino et al. (2004). In this fMRI study, human subjects observed mouth actions performed by humans, monkeys and dogs, which could be object-oriented, like biting

on food, or indirect like mouthing words in case of humans, lip smacking for monkeys, and barking for dogs. The results showed that when viewing biting actions for all species, the mirror neuron network, encompassing the premotor cortex and posterior parietal areas, was active. When viewing silent communicative mouth actions, depending on the species, different patterns of activation were elicited. During the human silent mouthing condition, the left inferior frontal cortex and Broca's area- the speech production areas- were also active. When seeing lip-smacking in the monkey viewing condition, a similar but weaker bilateral pattern was observed. Finally, in the dog barking condition these areas were not active, and instead visual encoding areas in the fusiform and extrastriate cortices were involved in the neural representation of this stimulus. These differences demonstrate the distinction between mirroring and embodied simulation; those actions that are more related to the body-schema (i.e. the pre-existing body model) of the human subject, in this case observing a human or monkey, lead to recruitment of the areas involved in executing those actions. In the case of the dog barking, the propagation of visual information does not trigger a retrieval of body related information and instead is mapped based on visual properties.

In these examples, embodied simulation is using a combination of the motor repertoire and known physical properties of the bodies to develop an understanding of the consequences of an action. In this thesis, it is postulated that the observation of abnormal finger postures, is processed in a similar manner. The integration of highly salient visual information with stored body-schematic information may lead to the modulation of somatosensory areas in order to provide a somatic experience of the perceived abnormality.

1.2 Hierarchical Primary Somatosensory Cortex

As outlined above, embodied simulation allows inference about inner states and causality of a certain event via a visual integration mechanism, and therefore is likely involved in embodiment of distorted finger postures. Only recently, however, has the role of the somatosensory cortices been outlined within a model of simulation (see Keysers, Kaas & Gazzola, 2010), with particular focus on the primary somatosensory cortex (S1). Therefore, in this section I will focus on comparing the anatomy of different sub-regions of the S1, and how they lead to a hierarchical structure of somatosensory processing (Iwamura, 1998).

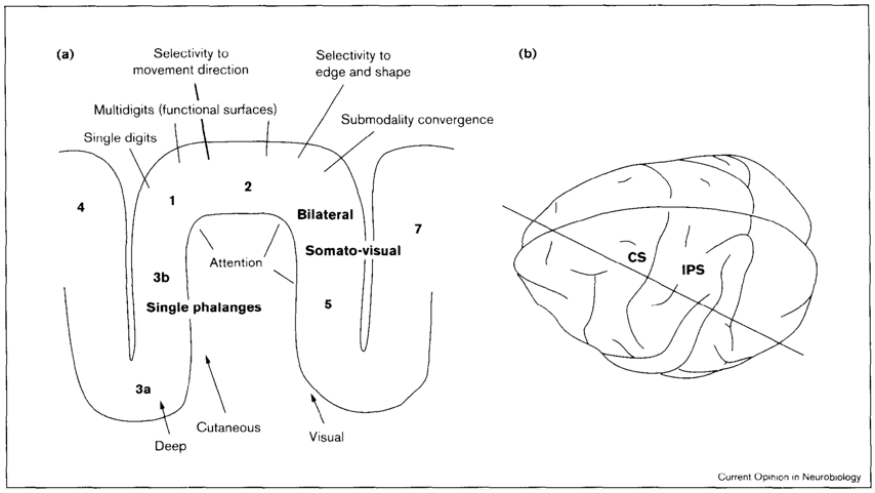

Figure 1.2: A. Schematic of a lateral of the postcentral gyrus corresponding receptive field functionality to different sub-regions of the S1 (Brodmann Areas). From anterior to posterior (i.e. 4 to 7) there is an increase in the complexity of the RF characteristic. B. Depiction of the Central Sulcus and Intra-parietal Sulcus of a monkey's brain. Diagonal line represents the section see in A. Figure extracted from Iwamura (1998).

Somatosensation arises in an orderly fashion, with post-central gyrus, comprising of the S1, showing a topographic arrangement of the contra-lateral body peripheral experience. This is referred to as the somatosensory 'homunculus', meaning that different regions of the body do not have a proportional region of cortex dedicated to their sensory processing. Instead, regions with higher numbers of receptors, such as the hand, lips, face and genitalia are over-represented

in comparison to other body parts (Penfield & Boldrey, 1937). Furthermore, these areas are sub-divided on the basis of their cytoarchitectonic structure and are identified as Brodmann Areas (BA) 3a, 3b, 1 and 2 (see Figure 1.2). These respectively correspond to the posterior bank of the central sulcus and anterior wall of the postcentral gyrus (PCG), the lip or crown of the PCG, and the posterior wall and bank of the post-central sulcus (PCS, Kaas, 2004; Geyer et al., 1999; Grefkes et al., 2001). It is important to note that all these regions have specificity of function derived from connections with the thalamus, pre-motor and motor regions, secondary somatosensory area (SII) and parietal input (Pons & Kaas, 1986; Kaas, 2004; see Keysers et al., 2010 for review). Depending on the type and number of connections between regions, a functional hierarchy is established. (Iwamura, 1998; Keysers et al., 2010). The BA 3a region receives direct input from ventral areas of the thalamus which carry signals from a wide range of muscle spindle receptors (Geyer, Schleicher & Zilles, 1997). Due to the proximity and parity in activity with area 4 (motor cortex), this region was thought to belong to the motor region. However, stark differences in muscarin and serotonin receptor concentrations, and similarity in density of ventrobasal thalamic connections with BA 3b, has conclusively defined this region as somatosensory (Geyer et al., 1997). Subregion 3b receives direct thalamic connections that can be traced directly to afferent cutaneous receptors on both glaborous and hairy skin (Craig, 2002b). Distinct functional representations of the skin are created, showing specific topographical representations for each body part (Eickhoff, Grefkes, Fink & Zilles, 2008). For example, studies using direct tactile stimulation of digits have shown clear definition of boundaries between digits' cortical representations, which (usually) have the same digit neighbours as the actual

hand (Sanchez-Panchuelo et al., 2010, 2012; Besle et al., 2013, 2014; Martuzzi et al., 2014, 2015). Other studies, investigating plasticity within the S1 have found that digit representation change mostly occurs in this area. For example, in owl monkeys trained in the use of three fingers together, receptive fields (RFs) changes were seen in BA 3b compared to untrained monkeys (Wang, Merzenich, Sameshima & Jenkins, 1995). In Besle et al. (2013), through the use of ultra-high field fMRI it was revealed that finger specificity was higher in anterior regions of the S1 (BA 3a, BA 3b), whereas finger specific ROIs overlapped considerably in posterior regions (BA1, BA2).

BA 1, is immediately posterior to BA 3b, has strong input from this region, and acts as a secondary processing unit of somatosensory input. Research shows that it has cutaneous RFs which are selective for perception of movement and direction selective (Hyvärinen & Poranen, 1978, Yau, Connor & Hsiao, 2013). Even though BA 1 has direct thalamic connections, ablation of BA 3b region leads to a profound impact on all somaesthic tasks (Randolph & Semmes, 1974). Inversely, ablation of BA 1 (and 2) does not affect BA 3a/b neuronal activity, suggesting a non-dependency on other regions, and processing at a lower level than BA 1 and 2 (Iwamura & Tanaka, 1991).

Lastly, BA 2 receives information and represents information about joint position (Kaas, 1993), and more complex cutaneous information such as roughness, pressure, orientation and direction of stimuli (Costanzo and Gardner (1980); but does not have as specific RFs as BA 1 [Iwamura (1998)]). Also, digit representations in this area overlap quite significantly (Besle et al., 2014; Martuzzi et al., 2014), indicating the presence of larger RFs in this region. Callosal connections from the contralateral S1 lead to bilateral representation of digits, although non-

specific, at BA 2 (Killackey, Gould, Cusick, Pons & Kaas, 1983; Iwamura, Iriki & Tanaka, 1994; Iwamura et al., 1994; Lederman & Klatzky, 2009). In a study conducted in awake monkeys, it was found that processing kinaesthetic and tactile information of body parts activated posterior regions of the S1. Stimulation of limb structures (arms, legs, shoulders, hands) more related to movement and actions, induced the largest neuronal, and bilateral activity compared with stimulation of body parts less involved in movement/action (such as trunk, abdmomen, oral cavity; Iwamura, Tanaka, Iriki, Taoka & Toda, 2002).

An important aspect of the posterior S1 is its relationship with the posterior parietal cortex (PPC). These two regions work in parity to integrate body-schematic information and somatosensory perception, making these very important areas of focus in the overall context of this thesis. For example, when observing goal-oriented actions and executing goal-oriented actions, or even when hearing action related noises (Keysers et al., 2004; Buccino et al., 2004; Keysers & Gazzola, 2009) BA 2, along with other areas of surrounding the posterior-central sulcus, show increased activity. Perhaps, the most important example is given by Iriki, Tanaka and Iwamura (1996). In this seminal study they were able to show the enlargement of RFs in posterior S1 as consequence of tool use. Experimenters placed food at different locations in front of the monkeys within or outside its reach. Using single recordings of the anterior bank and posterior lip, and fundus of the PCS, they were able to show that food within reaching distance lead to neuronal firing in the RFs of the monkey's shoulder. In another condition, the monkey was given a rake, when food was placed further away, outside of the reach with hand but still within the reach of the rake, the same neurons would fire. Another finding was that when food was placed within the monkeys'

reach (but before the monkey executed the task), a neuronal discharge also occurred, indicating a visual stimulation of somatosensory areas. These findings were the first to demonstrate a neurological basis of a body-schema and change in own body representation. Such a quick reflexive response reflects an aspect of motor imagery where the retrieval of body-schematic information generates an automatic reaction allowing one to predict and adjust behaviour (Hesslow, 2002). Therefore, an embodied simulation mechanism is supporting integration of visual information with the areas were involved in somatosensory behaviour.

This review of anatomical structure and function of the S1 generates a number of conclusions about the hierarchy of this region (see Figure 1.2). First, anterior regions have less complex RFs, and are tuned to particular characteristics of touch, therefore allowing low-level sensory perception of tactile and proprioceptive inputs. Complex information is transported further up the sulcus, allowing other posterior regions to infer on aspects of haptics. Second, BA 2 has a high degree of functional and structural connectivity with areas in the intra-parietal sulcus, thus, it is not surprising that this region is active during actions that require visual integration (Iriki et al., 1996; Grefkes et al., 2001). Third, clear hierarchical processing organisation is present within the PCG, making the BA2 and intra-parietal sulcus an area where body-schematic information is integrated with visual input. When considering that the focus of integration about body-schematic information changes with task demands (Iriki et al., 1996), it is proposed that if distorted fingers elicit embodied simulation, areas of BA2 and PCS should show increased activation as a consequence of the integration of visual body related information within somatosensory areas.

1.3 Vicarious Activation in SI

In the previous section it was demonstrated that within the S1 there are well defined borders not only for which body part is being stimulated but also for which type of stimulus is being delivered. It was highlighted that BA2 and the fundus of the PCS are areas of complexity, representing a wide range of body-related information, allowing integration of visual input with somatosensation (Keysers et al., 2010). Therefore, it is proposed that visual representation of bodies is to some extent linked to its somatosensory counterpart and that BA2/PCS are at the centre of embodied simulation. In this section, I will explain how events in observed bodies induce vicarious activation of S1, allowing inferences about body states and complex aspects of human social interaction to be made.

The findings of Iriki et al. (1996) outlined in the previous section tentatively demonstrate that by simply placing food visibly within the grasp of the monkey, somatosensory activity was elicited. This suggests body schematic information is automatically retrieved in order to simulate an outcome of body related events. Previous studies have suggested that this mechanism is the scaffold for being able to represent others' inner states (for review, Keysers et al., 2010, see Figure 1.3).

The reasoning behind this comes from studies which demonstrated the same areas of the body involved in representing one's own body are also involved in representing others' bodies. For example, observing facial expressions and imitation of those same expressions leads to overlapping brain activity (Carr et al., 2003). These data provide initial support that there is a tight link between understanding inner states of others and embodied simulation. However, a key weakness within this argument is the fact this could be simply categorized as a purely replicative mechanism, only involving the mirror-neuron system (MNS, Gallese,

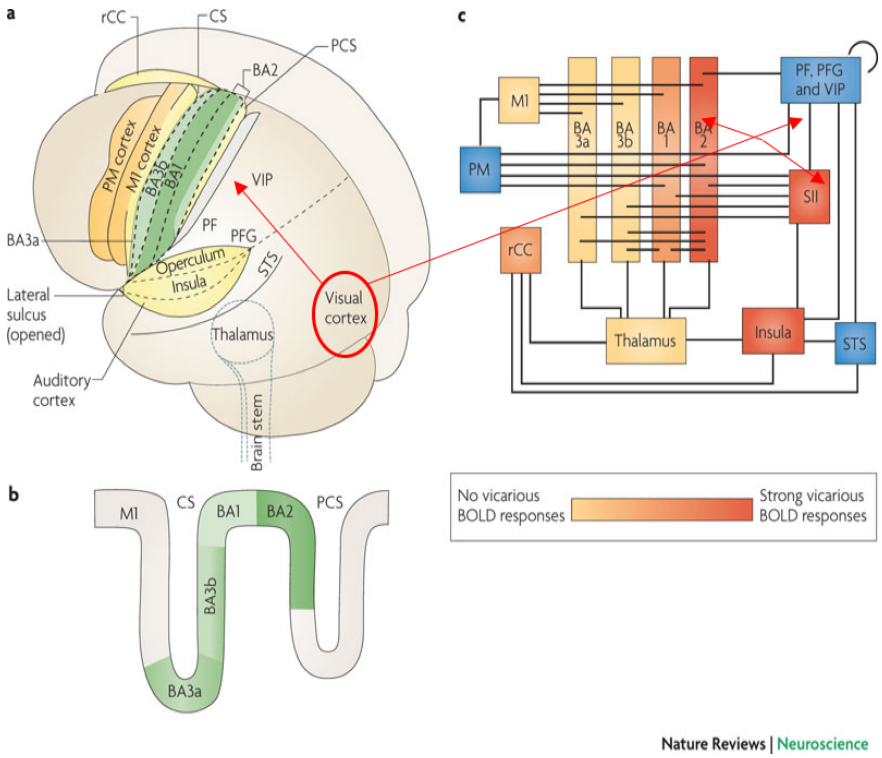

Figure 1.3: A) Areas involved in vicarious somatosensory representation. B) Diagram of pre- and post-central sulci showing the different Brodmann areas of S1 and other regions involving in vicarious touch processing. C) Diagram representing the somatosensory network colour coded to represent a function of strength of vicarious in areas of this network. Red arrows and oval, indicate the likely locations where EBA, as an area of higher-order visual processing, may influence this embodied simulation network (not in source image). Extracted from Keysers et al. (2010).

2005). In order to demonstrate otherwise, a causal link between brain representations and understanding inner states has to be established. This was provided by a study conducted by Oberman, Winkielman and Ramachandran (2007), where by placing objects in the mouth of the subject, experimenters were able to block specific muscles involved in smiling and frowning. As a consequence, recognition of others' happy facial expressions was significantly impaired during blocking when compared to no blocking. Their findings are consistent with the proposal that the human's ability to understand inner states of others derives from the simulation within the somatomotor network. Other emotions were not affected by the blocking the facial muscles, therefore suggesting those emotions do not rely on simulation via motor mimicry, but instead may rely on posture and body

schematic information (Reed, 2002). Considering that statement, Oberman et al. (2007) asked whether there is a somatosensory involvement in perceiving faces. A recent electrophysiological study that addresses this question was conducted by Sel, Forster and Calvo-Merino (2014). It combined tactile stimulation of the face and finger with visual presentation of facial expressions in order to address the involvement of S1, and consequently provided evidence of an embodied simulation mechanism. Sel et al. (2014) used source localisation of the ERP component of tactile stimulation to show stronger somatosensory activity when stimulation was combined with images of emotional faces compared to neutral faces. This study provides interesting evidence that the S1 is involved in emotional faces representation, however one concern with this research must be highlighted. Somatosensory activity increase during viewing of emotional faces occurred during both touch to the face (experimental condition) and touch to the finger (control condition). This peculiarity is explained by suggesting that embodied simulation elicits wide spread activation within the somatosensory cortices. However, based on anatomical connections within S1 this should not occur. From studies such as Iriki et al., (1996), the integration of visual and somatosensory information can extend towards the somatosensory areas, but is always within the boundaries of the somatosensory representation of that body part (Gallese, 2005; Chan & Baker, 2015). Furthermore, there was no actual comparison with somatosensory activation alone for either of the body parts. This is an important factor because it could be used as a localiser and improve the already limited spatial resolution. The source localisation of ERPs topography is widespread and includes parts of the anterior parietal lobe, and therefore the differences seen could be a consequence of serendipitous activity carried over from visual stimulation.

The studies described above provide a good case for embodied simulation, however the strongest evidence comes from touch and pain observation studies. One of the very first studies to show involvement of the S1 in touch observation was conducted by Blakemore et al. (2005). In this case study, C, a female synesthetic, experienced observed touch as if it was her own. Using fMRI, it was shown that S1 activity was larger when observing touch compared to controls subjects. This suggests that observing stimuli containing information related to a specific body triggers the embodiment of the observed stimulus, which is then reflected in the activation of the somatosensory areas (Pihko, Nangini, Jousmäki & Hari, 2010; Keysers et al., 2010). Further studies show that a similar process exists in the typical population, but without the sensory confusion of experiencing it as direct touch. Instead, it is likely that is an intrinsic sensation (Gallese, 2007) which does not trigger a specific mapping on areas such as BA 3a/b which represent cutaneous receptors (Iwamura, 1998). To demonstrate this, Bufalari, Aprile, Avenanti, Di Russo and Aglioti (2007) used EEG to take advantage of its high temporal resolution, and investigated how somatosensory-evoked potentials (SEP) created by median nerve stimulation, were modulated by the observation of touch or painful stimuli being applied to the same area. They found modulation of the P45 SEP in all observation conditions, with the pain condition (video clip of needle penetrating skin) eliciting the largest positive amplitude, followed by observing touch with a cotton bud. The latency of the component indicated a source arising from the posterior lip and wall of the PCG, as seen in Allison, McCarthy and Wood (1992)- where they used cortical and scalp electrodes, and found that early SEPs within 40ms reflect activity BA3 and subcortical activity, and later components, peaking between 45 to 60 ms, reflect activity in BA

1 and 2. Other neuroimaging studies using fMRI demonstrated that observation of painful stimuli pain (such as limbs being struck, or punctured) activates brain regions not involved with the somatosensory representation of those limbs (Singer et al., 2004; Jackson, Brunet, Meltzoff & Decety, 2006; Morrison, Peelen & Downing, 2006; Morrison & Downing, 2007; Lamm, Nusbaum, Meltzoff & Decety, 2007). Regions involved in cognitive processing such as the rostral cigulate cortex (rCC), dorsal anterior cingulate (aCC) and anterior insula were predominantly active when comparing noxious versus neutral conditions. In a few studies where subjects experienced the noxious event it self (e.g. needle prick) S1 and S2 activity was observed in conjunction with the other areas (Jackson et al., 2006; Morrison & Downing, 2007; Lamm et al., 2007; Costantini, Galati, Romani & Aglioti, 2008). These results point towards two components in vicarious experience: a somatic one (body related) and an affective one (emotion related). The former is of key importance for this thesis as it relates to the mechanism underlying embodied simulation.

More recently, two studies support the crucial role of the posterior regions of the S1 in embodied simulation. In Kuehn, Trampel, Mueller, Turner and Schütz-Bosbach (2013), subjects observed videos of their own hands touching sand paper, or others doing the same task in ego- or allocentric perspectives. Using 7T fMRI, they were able to demonstrate a main effect of touch observation located in the posterior S1 activity, only during the judgement of roughness sensation on another's hands. The results of the self-related touch condition showed no significant differences between observation and no touch. Furthermore, significant hand identity effects were found only during allocentric viewing, when subjects viewed another person's hand being touched. This finding fits with the results

from Bufalari et al. (2007), where touch observation led to lower increase of the P45 amplitude from baseline in comparison to pain observation, and also fits with other more recent studies combining own body presentation and SEPs. For example, in Cardini, Longo and Haggard (2011), congruent tactile stimulation and visual presentation of the subjects own hand or an object was done while measuring SEPs. They found that viewing their own hand suppressed the SEP response compared to viewing objects, likely due to shrinkage of somatosensory RFs. In light of these findings, Kuehn, Mueller, Turner and Schütz-Bosbach (2014), specifically tested RF shrinkage during touch observation for fingers. They found that a similar pattern of shrinking was seen with RFs in S1 tuned for tactile experience, and further found index and middle finger tactile representation overlapped in posterior areas of the S1 with those of observed touch to the same fingers.

1.4 Viewing Bodies

So far, it has been established that the sub-regions of the S1 have differential involvement in embodied simulation. A dichotomy is seen where anterior regions BA 3a/b are purely dedicated to direct tactile experiences, and anterior regions, particularly BA2, are the regions where own and other's experiences share a platform. Will the same occur for the observation of distorted fingers? That is, if perceived finger abnormalities are truly simulated (like touch), then a similar pattern of activation should be seen to those predicted and seen touch in observation research.

In the current literature only two studies (Avikainen, Liuhanen, Schürmann & Hari, 2003; Schürmann, Hlushchuk & Hari, 2011) have investigated how abnormal finger postures are processed in the brain. In order to study the embodiment of bodily abnormalities, which lead to reflexive and visceral responses, Schürmann

et al. (2011) conducted an fMRI study to investigate the differences between abnormal and natural finger postures. In addition, they investigated how social context influences somatosensory cortex activity; the stimuli were presented in the allocentric and egocentric perspectives. Significant activity of abnormal >natural postures was found in several regions of interest (ROI), but notably in S1 and MI, in which a (distorted 1^{st} - distorted 3^{rd} perspective) - (natural 1^{st} - natural 3^{rd} persepctive) contrast revealed significant activation. Furthermore, the authors noticed a cluster that overlapped with the typical location of the extrastriate body area (EBA) in the contrast distorted>natural postures. This area was also implicated in the cortical network of embodied simulation, which has not been detailed previously in Keysers et al. (2010) (see 1.3A).

Upon the first discovery of the EBA, Downing, Jiang, Shuman and Kanwisher (2001) proposed that this area is more sensitive to stimuli depicting bodies compared to faces and objects. Studies using electrophysiological measurements also have replicated a similar finding. Thierry et al. (2006), presented subjects with whole bodies (normal, silhouettes and scrambled), objects, scenes and faces. Using k-means clustering they were able to demonstrate different scalp topographies for each category, and in particular, the topography correlated with the occurrence of faces was maximal around 170ms (reflecting the N170, an ERP specific for faces (Bentin, Allison, Puce, Perez & McCarthy, 1996), whereas the correlation of the topography for bodies was maximal around 190 ms, henceforth known as the N190. Furthermore, the amplitude of the N190 decreased (i.e. became more positive) as stimuli looked less like bodies (pictures >silhouettes >scrambled). Once the topography was source localised, it revealed a source congruent with the location of the EBA.

It is also possible that the EBA encodes motion of specific body areas because of its proximity and overlap with the motion-sensitive middle temporal cortex (hMT; Downing et al., 2001, S. Ferri, Kolster, Jastorff & Orban, 2013), therefore allowing the reconstruction of the body in motion (Peelen, Wiggett & Downing, 2006). Orlov et al. (2010) conducted a study where they were able to show topographical organisation using different body parts using phase-encoding of voxel responses to viewing of specific body-parts. Importantly, they showed that body maps did not follow the 'nearest neighbour rule' like in the somatosensory cortex. Instead, those body parts that have wider range of movements largely overlapped with the hMT, and those that are restricted (e.g. trunk) had more ventral locations within the lateral occipital cortex. Other studies have demonstrated similar results (Bracci et al., 2010; Chan, Kravitz, Truong, Arizpe & Baker, 2010; Orlov, Porat, Makin & Zohary, 2014), and in particular, have shown that the EBA is involved in the identification and detection of bodies in the visual field. For example, when transcranial magnetic stimulation (TMS) is applied to the EBA, studies report weaker person detection in natural scenes and smaller BOLD responses to bodies and body parts (Downing et al., 2001; Downing & Peelen, 2016).

In Orlov et al. (2010) a positive linear correlation between body representations and motor representations (acquired during a motor mapping task) was seen. As a consequence they proposed that the lateral occipital cortex (which includes the EBA) receives motor, and perhaps, proprioceptive related input that may alter activity patterns of these regions. In line with the latter suggestion, results from Dinstein, Hasson, Rubin and Heeger (2007) showed lateral occipital cortex activity to both execution and observation of the same movement. More

recently, a study conducted on congenitally blind subjects found EBA activity using a visual-to-auditory sensory substituting device, which transforms visual images into auditory "soundscapes" by using a combination of rhythms and tones (Striem-Amit & Amedi, 2014). This demonstrated that the EBA is not only linked to visual information, but it also sends and receives inputs from other regions. As a consequence, the EBA may integrate information relevant for body perception from other areas of the brain by receiving efference copies or proprioceptive signals top-down to modulate its level of activation (Orlov et al., 2010). Therefore, relating this to the results in Schürmann et al. (2011) on viewing abnormal finger postures, it is likely that increased EBA activity seen here is an example of this mechanism.

Further evidence comes from an earlier magnetoencephalography (MEG) study (Avikainen et al., 2003). This study also showed abnormal finger postures to subjects during imitation and observation of the same postures. Mean amplitudes of right and left LOC ROIs showed significant differences (distorted>natural postures) between 250-600ms. This is in line with the findings stated above, where it was suggested that EBA activity occurs due to top-down modulation in order to provide extra attentional resources to process something unexpected. Like faces, hands benefit from extra processing resources (Orlov et al., 2010; Bracci et al., 2010, 2012; Orlov et al., 2014), but one question remains, is the processing of such a highly salient body posture really occurring so late? One criticism of this method was the use of data from large ROIs which lead to the loss of specific signals such as the MEG equivalent of the N170 or N190 (Bentin et al., 1996; Thierry et al., 2006), which typically occurs in EEG at very specific electrodes. Here, it is proposed that this difference can also oc-

cur during the earlier stage of a visual information processing stream. Such a difference in processing between distorted and natural postures would reflect a trigger mechanism for an embodied reaction. The findings seen in Avikainen et al. (2003) likely reflect sustained activity as a result of continuous re-appraisal of the distorted fingers. ERP studies report earlier difference in response to biologically salient stimuli. For example, Borhani, Làdavas, Maier, Avenanti and Bertini (2015) showed an increased N190 right hemispheric lateralisation of body postures depicting emotional content versus left lateralisation of body postures depicting motion. In a subsequent study by the same authors (Borhani, Borgomaneri, Làdavas & Bertini, 2016), alexithymia scores were taken into account. This is a trait which is expressed in the general population to different degrees, and one of its most relevant factors is the inability to describe and differentiating one's own feelings and sensations (Taylor & Parker, 1991; Herbert, Herbert & Pollatos, 2011). Another point of note, is that people with high trait alexithymia also experience difficulties in differentiating and describing what others are experiencing (Sifneos, 1971; Pouga, Berthoz, de Gelder & Grezes, 2010). This highlights the reliance on first-person sensorimotor and affective mechanisms to simulate what others are experiencing. The results of comparing N190 amplitude responses showed considerably larger emotional body posture modulation in low alexithymia group compared with no significant emotional body posture modulation in the high alexithymia group. This demonstrates the importance of understanding how the visual processing of the the body interacts with embodied simulation.

Other studies have taken the argument about latency even further, and propose that emotional modulations occur as early as 100 to 120 ms. For example,

in Meeren, Hadjikhani, Ahlfors, Hämäläinen and de Gelder (2008), faceless body postures of fearful or neutral valence were used as stimuli. They found significantly lower P1 amplitudes and earlier amplitudes over occipital electrodes for fearful body postures versus the same same condition scrambled by a spatial filter. Congruently, an MEG study (Meeren, Hadjikhani, Ahlfors, Hämäläinen & De Gelder, 2016) showed that fearful body postures are discernible from its scrambled control, as early as 80 ms. Using source analysis, this difference was localized to the right parietal cortex and included the IPS and PCS. This provides further evidence that emotional encoding of the body in the sense of translating a concrete visual stimulus to abstract code) occurs early in the processing stream, and crucially the locations align with other areas involved in embodied simulation as highlighted in the previous section.

The last four studies are at odds with each other suggesting the importance of different latencies. On one hand, Borhani et al. (2015) suggests that the P1 is not a good measurement of encoding because it is very sensitive to the physical qualities of stimuli (Halgren, Raij, Marinkovic, Jousmäki & Hari, 2000; Rossion & Jacques, 2008); whilst Meeren et al. (2008) suggests that the N170/N190 are still too late in light of how quick humans have to integrate information from their environment. Perhaps, a likely explanation is that there is some form of hierarchical processing of visual information, in which attention and coarse processing of bodies visual stimuli is processed earlier, and body part fine-grain information (i.e. shape and form) are processed at later stage as seen (Avikainen et al., 2003). Groves, Kennett and Gillmeister (2017) provides convincing evidence for this argument by studying the temporal dynamics of body viewing in female subjects with weight-restored eating disorders (ED). The ED group showed earlier

P1 latencies to viewing male and female bodies in comparison to controls. Conversely, the N190 ERP did not show latency differences, but instead viewing female bodies elicited significantly more negative amplitudes compared to male bodies. This dissociation merges the literature detailed above, by demonstrating that visual attention to bodies – and ED subjects are highly primed in this aspect – is encoded at the P1 latency, but body specific information, such as gender is encoded at the N1 latency.

In conclusion, viewing bodies operates through well defined regions in the extrastriate and fusiform cortex (Thierry et al., 2006; Orlov et al., 2010; Op de Beeck et al., 2010; Bracci et al., 2010, 2012; Downing & Peelen, 2011). Emotional content of a body leads to different outcomes in the processing stream, but recent evidence (Groves et al., 2017) suggests that the N1 ERP may be a good marker to test where and when the trigger for embodied simulation is likely to occur. That is, if observed distorted finger postures are truly simulated through this mechanism, then one should be able to trace the start of this process to the body areas in the extrastriate cortex, and be able to predict which stimuli will lead to larger somatosensory activity and which ones will not.

1.5 Thesis Statement and Structure

The thesis statement is that embodied simulation arises from a complex relationship between visual and somatosensory areas, leading to vicarious experience as a consequence of observing others' bodies.

In order to study this mechanism, I use hand images as they are salient social objects in human environment, are ideal as stimuli (Schürmann et al., 2011), and are well suited for neuroimaging. Stimuli of this type allow systematic and parametric control of their aspect to mimic abnormalities in the fingers. In the

development stage of this thesis I first studied the suitability of using realistic 3D computer-generated models of real hands for such explorations. Therefore, in Chapter 2, I describe the process by which subjects' real hands were modelled and validated through the use of psychological experiments.

The first experimental step in this thesis was the investigation of whether abnormal finger postures evoked a somatosensory response. For this purpose I use fMRI imaging at ultra-high field (7 Tesla) to achieve great spatial resolution which allows to explore the involvement of the S1 at sub-regions level. Therefore, in chapters 3, 4, and 5 respectively, I outline the theoretical background and the bio-physical aspects of fMRI, and discuss how they can be used to address the thesis statement. In chapter 4, I detail the results of a behavioural study, and a fMRI pilot experiments, in which I used repetition priming of finger abnormalities observation to explore how subjects engage with perceived finger abnormalities. The aim of this chapter was to investigate whether observing repeated finger abnormalities leads to fMRI suppression and consequently a more localised response (see 3.2.5 in Chapter 3). If this design approach was successful, then this would serve as the basis to compare overlapping responses between tactile and visually-induced S1 related activity. In Chapter 5, using ultra-high field fMRI, I perform a block experimental design to discern the involvement of different sub-regions of the hand area, acquired through tactile stimulation, in the representation of the perceived finger abnormalities. This chapter sets the foundation of the thesis by demonstrating that a similar embodied simulation mechanism is involved in the representation of abnormal body schema.

The second step of this thesis addresses one crucial element that is not well explored in the hierarchical processing of the S1, and embodied simulation mod-

els (Iwamura, 1998; Keysers et al., 2010) - the involvement of the extrastriate visual areas. As detailed in Section 1.4, the EBA plays a larger role in the embodied simulation cortical network (see Figure 1.3, red arrows). Hands have a large dedicated region of the lateral occipital cortex dedicated to their representation in comparison to other body parts (Orlov et al., 2010; Bracci et al., 2010; Op de Beeck et al., 2010). However, there are three factors that remain to be explored: First, the temporal dynamics of observing distorted finger postures have not been explored outside of Avikainen et al. (2003), as well as the categorical sensitivity of different ERPs to these stimuli; Secondly, even though Bracci et al. (2010) demonstrated that hand viewing is left-lateralised, this has not been directly tested using electrophysiology; lastly, according to M-EEG research (Meeren et al., 2008, 2016; Borhani et al., 2015, 2016), body postures containing affective information lead to right lateralisation and increase N1 ERP potentials, creating interesting hypothesises around observation of abnormal finger postures. Consequently, the second experimental step in this thesis was to investigate the responses of the N1 response to the observation of hands, and distorted fingers. Therefore, in chapter 6 I start by providing a M-EEG primer in order to familiarise the reader with the key biological concepts behind these techniques used in subsequent chapters to analyse and localise data. In chapter 7, I outline two experiments: the first experiment that attempts to demonstrate that hand viewing is left lateralised and that it is different from whole bodies; and in the second experiment I attempt to demonstrate modulation of the N1 component when observing finger distortions as a marker for the likelihood of embodiment simulation being performed.

In the last experimental step, reported in chapter 8, a similar experiment to

the second experiment in chapter 7 is described, but adapted for MEG analysis. This aimed to find if the activity (by means of the magnetic equivalent of the N1) in the lateral occipital cortex can be used to predict activity in the S1.

Lastly, Chapter 9 reviews the thesis statement made at the beginning of this section, reflects on the validity of the embodied simulation model, and attempts to develop a cortical network showing a flow of information from visual to somatosensory areas.

Summary

Embodied simulation on the involvement of different Subregions of the primary somatosensory cortex to represent finger abnormalities, and it modulates or is modulated by its representation in the extrastriate cortex.

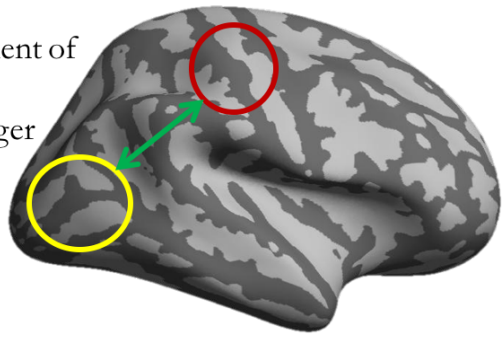

Step 1: **Find Somatosensory activity to finger abnormalities.**

Step 2: **Since the EBA is responsive to bodies/hands, it is also responsive to distorted fingers?**

Step 3: **How does EBA and S1 interact? Can EBA modulate S1 involvement?**

Key Points

- Embodied simulation is not the same as Mirror Neurons.
- Embodied simulation is well documented for observation of touch, the same cannot be said about observing abnormal body postures.
- SI shows Hierarchical Organisation.
- BA2 is probably an integrator of body information with known body schema.
- EBA is probably a modulator of how much recruitment there will be in somatosensory areas.
- Embodied Simulation depends on an interaction between visual and somatosensory areas, but there is a gap in literature with respect to this issue.

Chapter 2

Stimuli Development and Validation

2.1 Overview

To study the research questions outlined in the last section of Chapter 1, it was necessary to develop stimuli aimed at eliciting an embodied response. Development of stimuli was informed by the results conducted in my Masters' dissertation, which investigated the observation of abnormal finger postures using 7T fMRI. This study aimed to find S1 responses to the observation of images for distorted fingers postures in the vicinity of the somatosensory hand area (see Figure 2.1 A). Whilst a clear pattern of S1 activation was found in one subject, the results were inconsistent otherwise. Furthermore, comparisons between finger abnormalities in different perspectives also did not reveal any clear results.

Therefore the initial phase of this PhD project aimed to improve stimuli, replacing the low-feature 3D hand models with photo-realistic high-resolution 3D hand models (see Figure 2.1 B and C). In the first section of this chapter, I explain different procedures I used to improve the models by combining photo-

grammetry of the subject's real hand and 3D modelling techniques to generate high resolution 3D models. This aimed to increase vicarious S1 responses to the stimuli as previous studies have shown that seeing one's own body leads to increased involvement of S1 activity measurements during a variety of tasks (Urgesi, Calvo-Merino, Haggard & Aglioti, 2007; Cardini et al., 2011; Ferri, Frassinetti, Ardizzi, Costantini & Gallese, 2012).

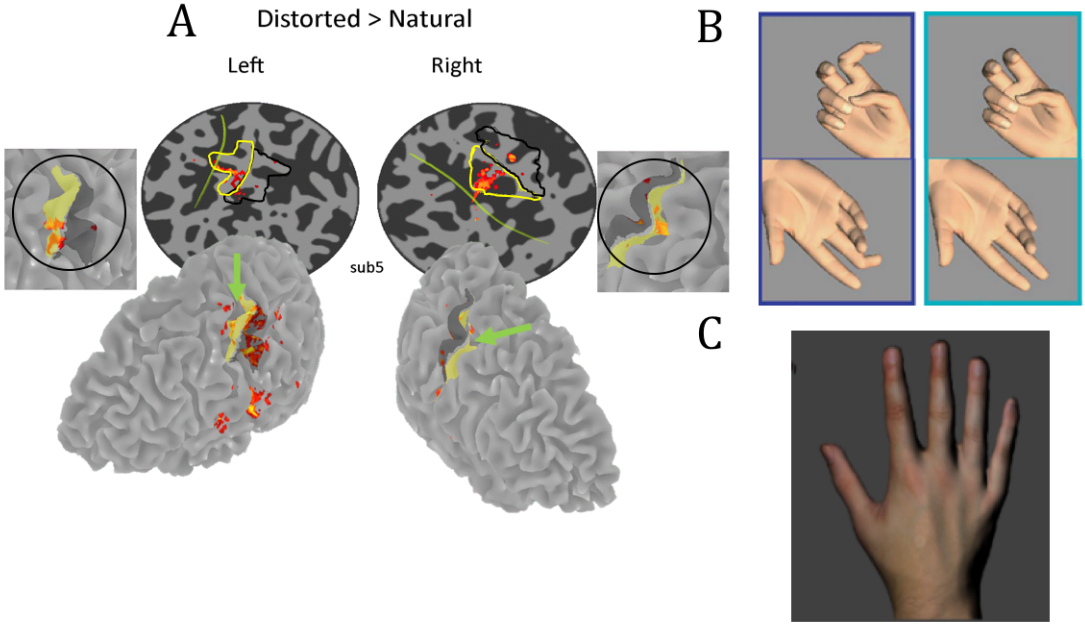

Figure 2.1: A. Extract from my MSc dissertation showing the results of a (Distorted<Natural) t-test in one subject that showed clear overlap with the S1 hand area. Within this panel the middle sections show flat maps of the area posterior central sulcus, with the yellow line indicating the location of the central sulcus, the black line of the flat maps indicating the region of interest. Bottom, and lateral panels Depictions of the left and right hemispheres with arrows pointing towards the vicinity of the somatosensory hand area.

The second section of this chapter investigates whether the developed 3D models are good visual representations of the subjects' actual hands. Two experiments are conducted that target the embodiment mechanism through the use of ownership illusions and mental rotation tasks. In addition, as the impact that viewing a hand in dorsal or palmar position was unaccounted for in the earlier

fMRI experiment, viewing different postures may have added unwanted variability as each aspect of the hand recruits the involvement of different strategies that rely on cognitive or proprioceptive mechanisms (see Brown, Morrissey & Goodale, 2009). Therefore, here I also explore how different hand viewing orientations (i.e. dorsal versus palmar) interact during the mentioned embodiment tasks (Ionta & Blanke, 2009, 2013) in order to decide which aspect to use in subsequent experiments.

2.2 Stimuli Creation

2.2.1 Computer Modelling of Real Hands

The generation of a 3D Model from images is a complex problem due to the relationship between the camera and the object. However, there are several freely available software packages that have dedicated algorithms to the creation of 3D meshes from photos. Here, I used Autodesk® 123D photogrammetry algorithms to create realistic stimuli. This software uses light intensity variation and image distortion (assuming that lighting is always constant) between photos to triangulate relative positioning between the cameras, creating a 3D Cartesian Coordinate system. Then, using a feature identification algorithm (similar to a k-means procedure) it assigns 3D coordinates for each pixel, in each image based on the triangulated distance calculated earlier (Luhmann, Robson, Kyle & Boehm, 2014). From there, a 3D matrix containing the common coordinates is put through a point cloud generation algorithm that uses a variation of Delaunay triangulation algorithms to generate a mesh of triangles with a coordinate system defined using the relative position of the cameras (see Figure 2.2). The procedure used here starts by acquiring between 30 to 50 photos around the hand from

different angles in the dorsal and palmar view. In order to aid with feature identification and coordinate assignment I also added a news paper as a background, which has very specific features regardless of camera position. Then, I run the reconstruction algorithms creating a mesh of each side of the hand.

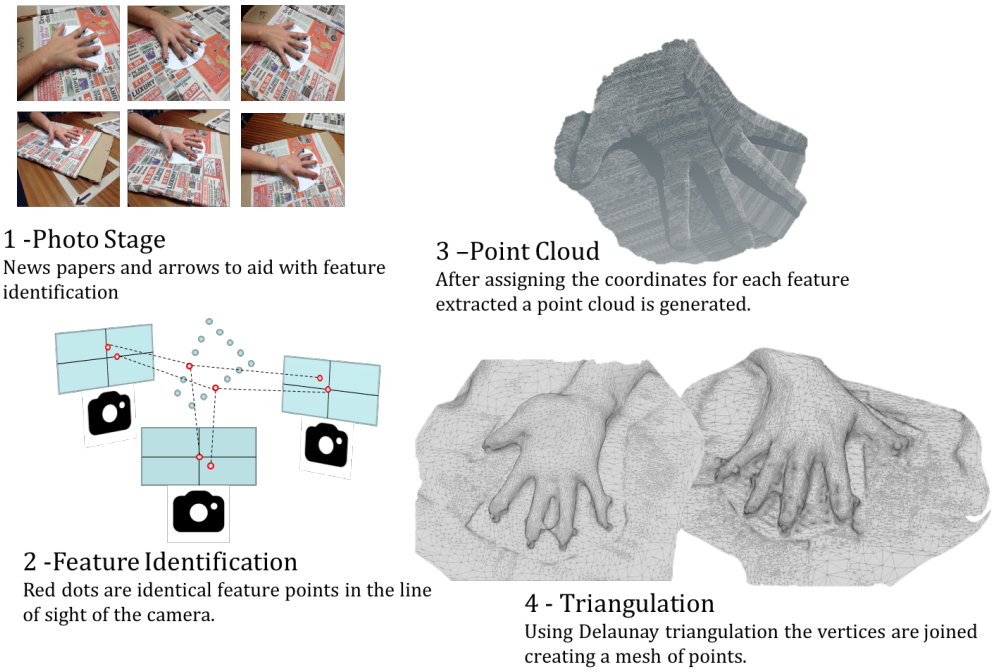

Figure 2.2: Visualisation of four crucial steps in the pipeline of the production of the 3D models from photos of the subject's real hand.

Once the meshes were acquired, they were imported into Blender 3D®, a free 3D modelling software https://www.blender.org, which contains an API that allows easy access to conduct any type of operations on interfaced data. These operations include alignment of each side of the hand, vertices stitching between meshes, decimation of the model in order to remove any outliers (such as floating vertices) and lowering the number of vertices, and a re-meshing algorithm that allows one to merge both models (palmar and dorsal) together whilst keeping the relative positioning of each vertices. Furthermore, as the remeshing algorithm also identifies common features between models, redundant vertices are removed resulting in a smoothing of the mesh, keeping large features that are hand shaped

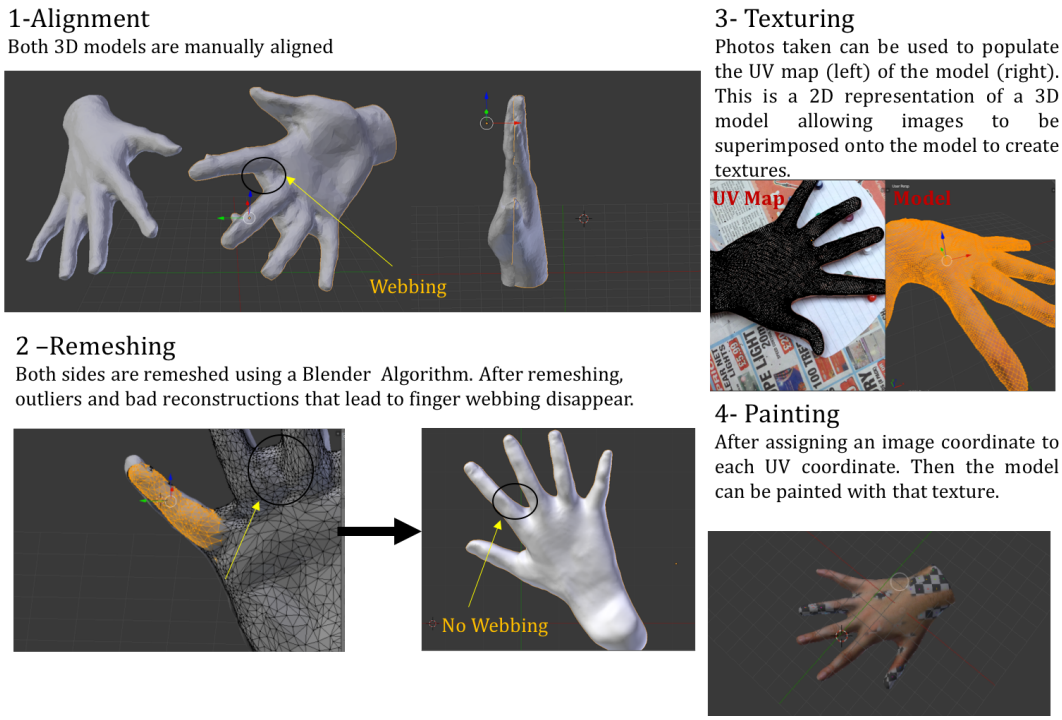

Figure 2.3: Visualisation of steps in creation of the 3D models acquired after putting the photos of the subjects real hand after the using the model reconstruction softwares and algorithms, all the way to applying skin textures to the models. Also of note, in steps points 1 and 2 arrows points towards the webbing problem I faced, and in step 2 the results of remeshing, now showing no webbing.

intact, but removing small features such as misaligned vertices or webbing (see Figure 2.3 steps 1 and 2). After these steps are conducted, the model is unwrapped using UV mapping, in which the 3D coordinates x,y,z of the models are converted into a 2D coordinates u,v (see Figure 2.3 step 3). Then, the UV map of the 3D hand model is imposed onto the image texture, allowing one to apply the texture to the face of the mesh and paint the model of the hand (see Figure 2.3 step 4), finalising the modelling process.

2.2.2 Distortion application

Another advantage of using the Blender is that the API allows the manipulation of the 'bone' structures that can be automatically matched to the surrounding vertices of a model. This provides perfect control over the degree to which

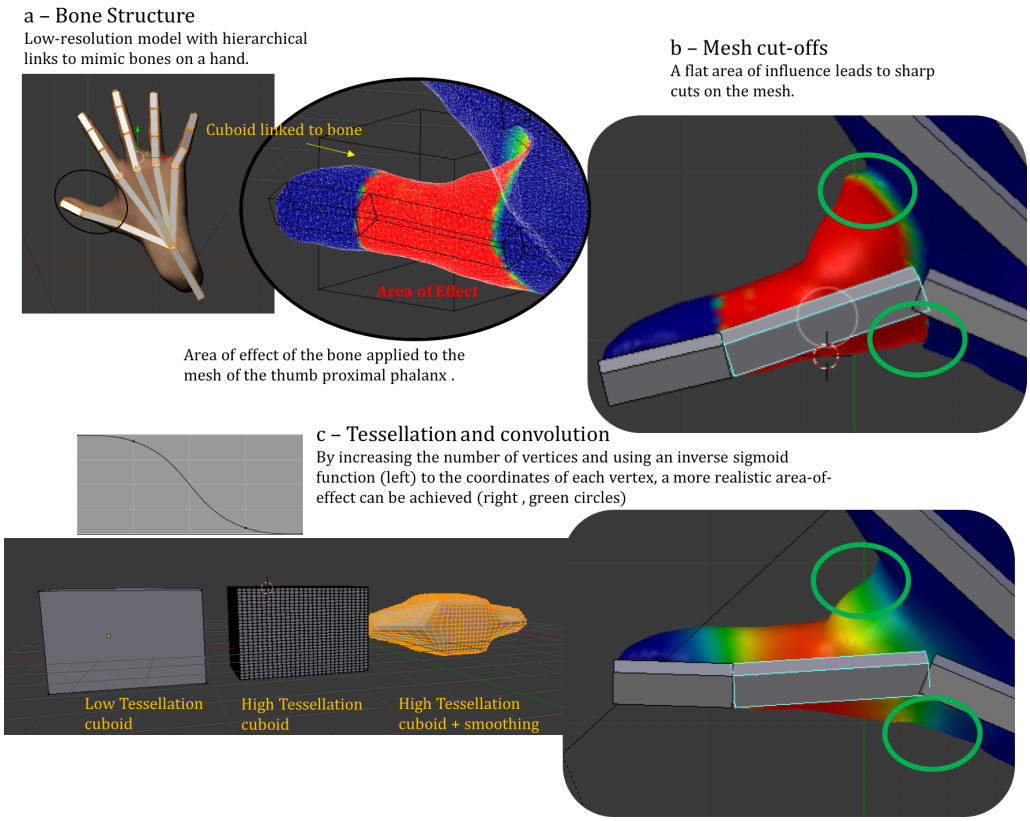

Figure 2.4: Description of the problem after linking a 'bone' structure as seen in a). The cuboid shape lead to a flat area (maximum in red) of influence that created sharp distortions in the mesh that lead to a non-biological appearance, as in b). To solve the problem the cuboid shape that exerted the area of influence of the mesh was modified in order to create a more realistic effect, see c)

finger distortions can be applied to the fingers by controlling the relative positions of the bones rather than the mesh itself. The bones are low-resolution models that I programmed to have an area of effect of a cuboid shape (see Figure 2.4 a) around the 3D hand mesh using Blender preset parameters. An issue was that the parameters created a flat area of influence with no fall-off (see Figure 2.4b). This meant that when controlling the bone to apply a distortion to the fingers, several parts of the mesh would overlap with each other creating a strange cut-off appearance of the hand (see Figure 2.4 b). This was solved by first increasing the tessellation of the cuboid by introducing 1000 randomly distributed vertices across the faces of the shape, then convolving that shape with a smoothing modifier, composed of an inverse sigmoid function (see Figure 2.4 c) with the highly

tessellated cuboid, resulting in a area of effect gradually falling off with distance. Once this new cuboid was applied to the mesh, smoother manipulations using the bone structure were achieved, with no cut-offs and mimicking the appearance of the skin stretching more realistically (Figure 2.4 c). Using this method, the smooth cuboid was linked to all the bones that control the mesh (see Figure 2.5 a and b).

Lastly, distortions were applied to the 3D models of the subjects as seen in several experimental sections of this thesis. The distortions are always applied at the joints of all digits, except thumb, between proximal and middle phalanges, in a combination of clockwise and anti-clockwise rotations. Then images were rendered with Blender camera presets (12:11 aspect ratio) with a focal length 35 mm, and 800 x 800 pixels resolution (see Figure 2.5 c and d).

2.3 Behavioural Testing

In this section, I proceed with the validation of the 3D models, and address how perception of the aspects (palmar and dorsal) of the 3D hand models interact with different viewing orientations in two experiments that typically use real hands (or rubber models), and images of real hands.

2.3.1 Laterality of Hands Task

2.3.1.1 Introduction

The laterality of hands task (Parsons, 1994) requires the subject to decide whether the viewed image is of a left or right hand. Parsons (1994) found that when the hand is presented at a medial angle (fingers point toward the mid-line of the body) reaction times (RTs) are shorter and accuracy is greater compared to lateral angles (fingers pointing away from the body, see Figure 2.7). This differ-

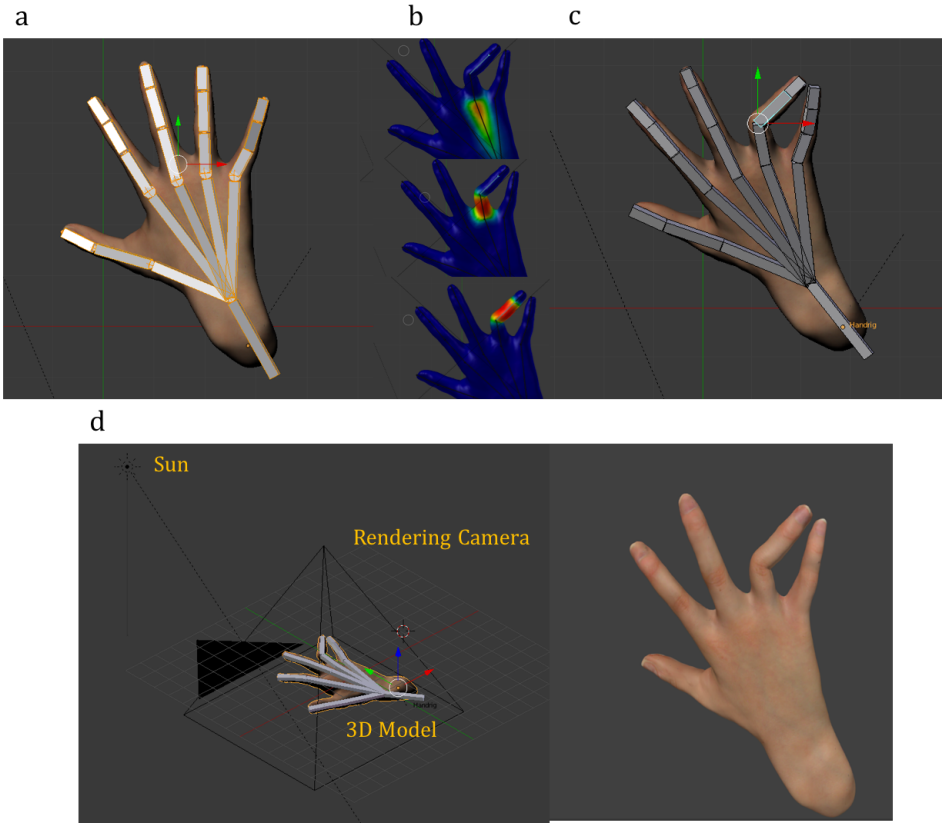

Figure 2.5: Description of the pipeline of distortion application and rendering set-up. a) bone structure applied to the mesh. b) result of applying the custom cuboid on the different bone structures and distortion of 40° along the y-axis of the ring finger. c) results aspect of the bone structure. d) Rendering set-up showing the relative positions of the rendering camera, sun (a Blender object that creates diffuse lighting in 3D space) to the 3D model. Also, the result of the rendering using this set-up.

ence suggests that subjects engage in mental rotation of their own hand to match the position of the viewed hand, and consequently the time taken to respond is proportional to the time taken to achieve that posture (Corradi-Dell'Acqua & Tessari, 2010). This finding indicates that a mental rotation process relies on proprioception, the feelings of one's body, to achieve success in this task. Therefore, it could be said that embodied simulation occurred (Brady, Maguinness & Choisdealbha, 2011). This finding has received more support recently; a similar laterality task to Parsons (1994), but showing images of the different aspects of the hand (Ionta et al., 2013) found that dorsal views of the hand induced significant differences between the egocentric and medial orientations (0°

and 90° respectively) when compared to more unfamiliar allocentric and lateral orientations (180° and 270°). However, this was not seen for the palmar viewing condition suggesting that multisensory integration of vison and proprioception tips in favour of the visual processing, and a object-oriented visual strategy is being used to make a decision when viewing this side of the hand (Wilson et al., 2004). These findings make this task particularly pertinent to determining the effect of palmar versus dorsal postures on mental rotation, and thus assess which side is likely to lead to more visual embodiment of the 3D model. Based on previous literature, it is predicted that: 1) Egocentric and medial (0° and 90°) perspectives will have shorter reaction times than allocentric and lateral (180° and 270°); and 2) perspective-related differences in reaction times will be stronger for images of hands in dorsal view (relative to palmar view).

2.3.1.2 Methods

Subjects. Eleven right handed students (male = 4, female =7) from the University of Nottingham took part in this experiment, with mean±SE = 25.71 ± 2.81 years.This experiment was approved by the ethics committee of the School of Psychology, University of Nottingham (Ref: 440).

Stimuli. Prior to conducting the experiment, subjects were required to come to the laboratory and have their right hand photographed. This would take approximately 10 to 15 minutes per subject. Right hand dorsal and palmar aspects were photographed (approximately 30-50 pictures each) from multiple angles, and then the pictures were uploaded separately onto Autodesk® 123D Catch. The models created through this software were then uploaded to Blender 3D® to create a fully malleable 3D mesh of the subjects hand (for more detail

on this procedure, see Section 2.2). Two grey scale images (one palmar and one dorsal posture) of the subjects' own hand were used. These were equally presented using Psychopy (Pierce, 2008), and rotated around the centre point of the monitor at 0°, 90°, 180°, 270°. Furthermore, the stimuli were horizontally flipped in order to mimic left hands (see Figure 2.6).

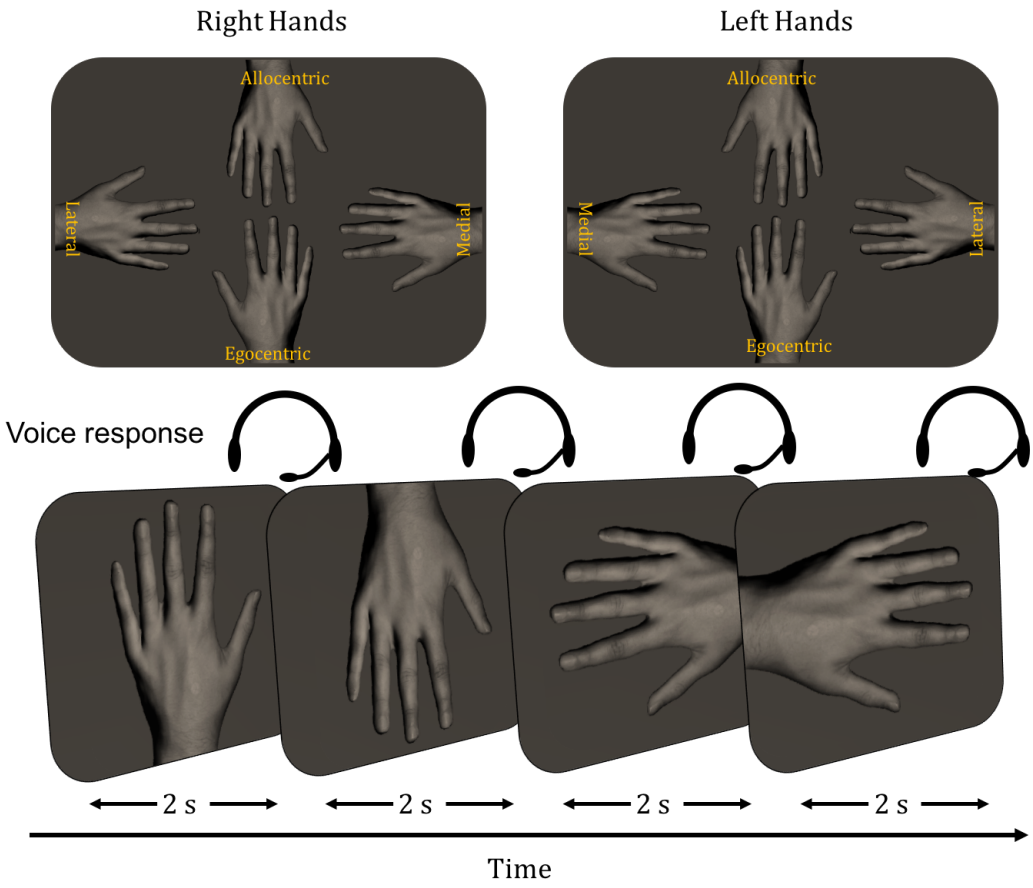

Figure 2.6: Top panel, example of Rotated hands. Each hand is presented individually with the following rotation angles, from bottom centre to middle left: 0°, 90°, 180°, 270°. Bottom panel, depiction of a typical experiment time line. Each hand was presented for 2 seconds, during which subjects had to make a voice response identifying the laterality of the hand observed. Images not to scale.

Procedure. Participants sat at approximately 60 cm from the screen, and were instructed verbally on how to complete the hand laterality judgement. This was followed by a practice session in which subjects had to complete 20 trials before the actual task. Subjects were required to make verbal responses (i.e. say left

or right), and were asked to place their hands underneath their legs in order to restrain any possible movements which may aid in laterality judgement (such as rotation of their own hands to fit with the observed stimulus). Sound was recorded using microphone connected to the stimulus computer, and sampled at 16 kHz. For each trial a .wav file was recorded with the duration of 2s. Stimuli were presented for two seconds, and responses recorded, for a total of 72 stimuli with 9 stimuli for each condition.

Preprocessing. Matlab (MATLAB 2012a, The MathWorks Inc., Natick, MA) was used to preprocess the sound files and extract voice onsets which were used as a measure of response time. A low-pass filter of 1 kHz was applied to each response to remove any random high frequencies, furthermore all sound files for each trial were normalised by dividing the sound file by its peak amplitude. This makes extracting approximate voice onsets easier for each subject as loudness of the voice, and speed of speech may vary. Only responses after 600ms were accepted as valid responses. This was done in order to avoid voice trail-offs from the previous trials. Voice onset response time (RT) was then extracted when the normalised amplitude was equal to or larger than 0.4.

Statistics. A 4x2, rotation angle (0°, 90°, 180°, 270°) x hand aspect (palmar, dorsal), ANOVA was conducted on accuracy measures and RT in order to test the effect of different hand postures and aspect in laterality judgements. Subsquent t-tests were corrected for multiple comparisons were corrected using a Bonferroni correction.

2.3.1.3 Results

A 4x2 ANOVA was conducted on angle and postures. A main effect on RT was found for angle, F(3,27) =7.395, p=.001, η^2 =.451, such that 180° hand viewing condition elicited significantly larger RT when compared to the 0° condition (mean difference = .204 ± .053 s , p = .024, 95 % CI[.025, .383]), and to 90° (mean difference = .172 ± .028 s, p <.001, 95% CI[.077, .267]), in addition no significant difference was found for 270° (mean difference =.143 ± .047, p= .089, 95% CI[-.017, .302]); A main effect of posture was found, F(1,9) = 9.540, p= .013, η^2 = .515, such that dorsal postures elicited significantly shorter RT compared to palmar (mean difference = −.148 ± .048). A significant angle*posture interaction was also found, F(3,27) = 11.637, p<.001, η^2= .564. To investigate the interaction, 4 t-tests for each angle between dorsal and palmar postures were conducted. This indicated that the mental rotation is driven by a significant difference between the dorsal postures at an angle of presentation of 0° (mean difference = −.347 ± 0.090, t(10)=-3.843, p = 0.012, 95% CI[-.549, -. 146]) and 90° (mean difference = −.197±0.06, t(9)=-3.209, p = 0.012, 95% CI[-.337,-.058]).

A 4x2 ANOVA was conducted on accuracy measures ($acc = \frac{TrueHits}{TrueHit+FalseHits} \times$ 100). There was no significant main effect of angle, F(3,27) =.639, p=.596, η^2 =.066, or posture, F(1,9) = 1.962, p=.195, η^2 = .179, and no significant angle*posture interaction, F(3,27) = 1.306, p=.293, η^2 = .127. In summary, the results indicate that the ability to mentally rotate hand postures is facilitated by dorsal postures at lower degrees of rotation (see Figure 2.7).

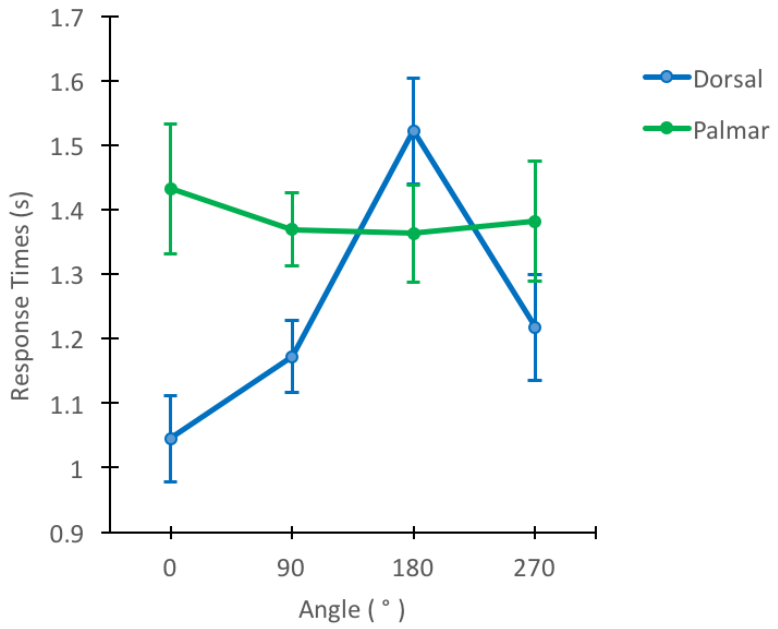

Figure 2.7: Line graph of response times for identification of laterality. 0° and 90° in dorsal position were significantly different from its palmar counterparts. Please refer to Results section for error values.

2.3.1.4 Discussion

It was predicted that dorsal postures would elicit better accuracy and faster responses. This was not found for accuracy measurements. However, evaluations of the RT data showed that egocentric (0°) and medial (90°) rotations of dorsal postures had faster responses. Palmar postures showed no interaction across rotation conditions.

According to Parsons (1994), the time taken for rotation is proportional to the actual physical time to achieve that posture, and dorsal postures are easier to simulate rotations of than palmar ones. This finding was replicated in this study. This difference arises from a dissociation of visual processing between the different aspects. Studies suggested that the space between and above the palms has increased perceptual salience and draw more attention than regions outside (Cosman & Vecera, 2010; Davoli & Brockmole, 2012; Qian, Al-Aidroos, West,

Abrams & Pratt, 2012). This supports the idea that observing the palms engages more visual mechanisms, rather than sensory-motor ones (Parsons, 1994; Ionta et al., 2013; Wilson et al., 2004). The 0° and 90° presentations of the dorsal side are more canonical postures, and elicit quick retrieval of body posture schemas. With 180° being an awkward position, which is less experienced, the slower RT seen is also congruent with the literature. The 270° viewing condition depicts the most awkward position of the hand, therefore should have comparable RTs to 180°. The comparison of RT between postures was not significant but below 0.1 chance level. This potential trend effect may have risen from the fact that the responses analysed here were for both left and right hands. Therefore, presentations of the left hand at 270° could have been seen as medial rotations rather than lateral ones, thus improving the measurements. This pattern of dorsal postures is very similar to the one obtained in Ionta et al. (2013) (see Figure 2.8).

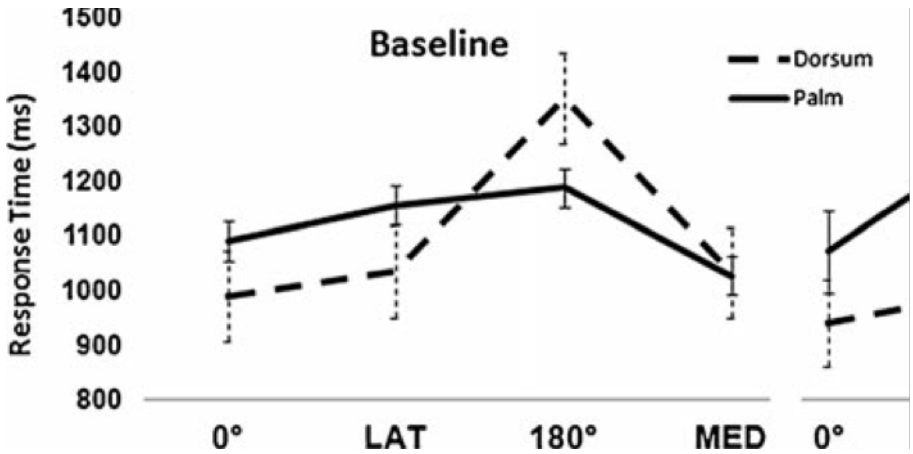

Figure 2.8: Extracted from Ionta et al. (2013) study, showing response times of a laterality task, after a baseline rubber hand illusion condition was conducted (only rubber hand stroking). LAT = 270° and MED = 90°.

Brain imaging studies offer a complementary explanation of this effect. Tactile fibres of the dorsal aspect of the hand have strong connections to areas involved in processing unfamiliar and affective sensory experience (such as the insula and secondary somatosensory cortex), and perspective processing (Chen et al., 2008;

Olausson et al., 2008; Keysers et al., 2010). This connection is likely responsible for increased visual salience, greater propensity of embodied simulation of the dorsal stimuli, and consequently greater facilitation effects in terms of mental rotation.

In conclusion, the results of this experiment support the assertion that the dorsal view seems to be more involved with sensory motor mechanisms than the palmar side. These findings point towards using images of hands in dorsal position in order to induce a more strongly embodied responses of finger abnormalities and that 3D models induced similar results to those in past literature.

2.3.2 Virtual Hand Illusion

2.3.2.1 Introduction

The purpose of this experiment is to compare hand postures in dorsal versus palmar views in a virtual variant of the rubber hand illusion paradigm. The rubber hand illusion is a common method to elicit body-ownership via manipulation of visual and somatosensory integration where one's own hand, typically unseen, is stroked synchronously with a fake rubber hand(Botvinick & Cohen, 1998; Tsakiris & Haggard, 2005). This may cause propriocetive confusion where subjects assign the feeling of the stroking to the rubber hand and report ownership of the hand. These reports make this task ideal to test the quality of the 3D models. One of the common measurements of the strength of the illusion is the proprioceptive drift. This measure outlines how much of a subjective bias there is towards the sensation of the 'fake' hand. When there is a strong illusion effect, subjects report the location of their real hand closer to the fake hand than its actual position. This sensation has been recently argued to represent the integ-

ration of visual and tactile percepts which leads to the mislocalisation of the real hand (Fuchs, Riemer, Diers, Flor & Trojan, 2016). Another way of measuring the effectiveness of the illusion is through a subjective questionnaire that assesses the strength of the illusion (Botvinick & Cohen, 1998).

In this experiment, the subject's 3D modelled hand ("the fake") was stroked by the experimenter's finger while their real hand was also being stroked synchronously. Commonly, in rubber (or virtual) hand illusion tasks the experimenter strokes the dorsal aspect of a real hand - which is abundant in C tactile-afferents (Olausson et al., 2002)- simultaneously with the fake hand. However, here the 3D model was stroked in both the dorsal and palmar views, alongside stroking of the real hand in the postures as the viewing position (dorsal or palmar). This aimed to address questions regarding the interaction between proprioception and vision of both hand aspects.

According to Ionta et al. (2013), who conducted a mental rotation task after inducing the rubber hand illusion effect, the effects of these tasks are supported by similar neural mechanisms involving premotor cortex and inferior parietal cortex. Taking into account the results of the previous behavioural experiment, in which dorsal postures rotated at egocentric and medial degrees (0° and 90° respectively) elicited faster RTs, it is predicted that dorsal postures will elicit strong embodiment reflected by larger values of drift and subjective measures on items related to illusion effects.

2.3.2.2 Methods

Subjects. Nine right handed students (male = 3 , female = 6) from the University of Nottingham took part in this experiment, with an mean±SE = 25.25±3.35 years. This experiment was approved by the ethics committee of the School of

Psychology, University of Nottingham (Ref: 440).

Stimuli. Some of the subjects that took part in the experint in Section 2.3.1, also took part in this task. The 3D hand models already existed, so please refer to Sections 2.3.1.2, and 2.2. The models were presented using online rendering options of Blender, and were seen from an orthographic perspective (see Figure 2.9a). The 3D models were rotated around the centre point of the screen (22 cm) and further rotated around the wrist to create dorsal and palmar postures (see Figure 2.9).

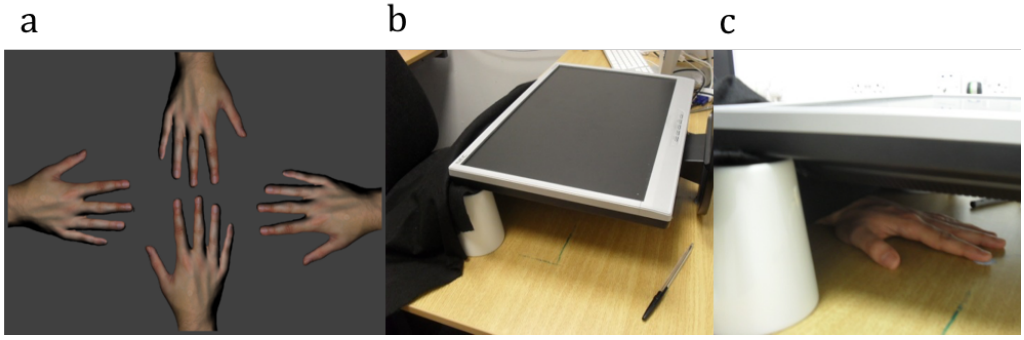

Figure 2.9: a) Depiction of the stimuli presented during virtual hand illusion. The virtual hands were seen at the centre of the screen, and the hands index fingers were stroked at the same time in order to elicit the illusion. b) Photo of experimental set-up for this task, subjects have their right arm under a blanket with their left arm visible next to the screen. Once underneath subjects placed the hand in the same posture as presented on the screen. c) the hand below the screen, matching the 0 posture on the screen.

Procedure. Subjects were asked to sit in front of a 19" LCD monitor positioned horizontally, lying approximately 14 cm above the table in a lowly lit room. A piece of Blu-tac was placed underneath the screen at 15 cm from the right bottom corner. The screen was turned on revealing the virtual hand, and subjects were asked to place their right hand on top of the screen in order to scale the model to approximately the same size as their real hand. Subjects' upper body was covered with a black blanket; then, they were asked to place their right hand underneath the screen, and their left hand on top of the table, next to the screen,

which was now visible. The index of the virtual hand was placed always at a centre point of the screen using the midpoint of the finger as a reference at 20 cm distance from the right bottom corner.

The subjects were informed that their right index finger would be stroked simultaneously with the index of the virtual hand for 2 minutes, and instructed to focus on the virtual hand being stroked. At end of each block, the screen was turned off and proprioceptive drift was measured. This was done by placing different sized rulers (custom made pieces of cardboard, selected at random) over the screen, on which the subject had to identify (by placing a piece of Blu-tac with their left hand) where they felt their real hand was, while keeping their right hand in place.

Table 2.1: Adapted questionnaire from Botvinick and Cohen (1998). The first three items measure the strength of the illusion, the last four are controls.

Type	Adapted Questions
Illusion 1	It seemed as if I felt the touch of the finger in the location where I saw the virtual hand being touched.
Illusion 2	It seemed as though the touch I felt was caused by the finger touching the virtual rubber hand.
Illusion 3	I felt as if the virtual hand was my hand.
Control 4	It felt as if my real (hand) was drifting towards the left.
Control 5	It seemed as if I might have more than one right hand or arm.
Control 6	It seemed as if the touch I was feeling came from somewhere between my own hand and the virtual hand
Control 7	It appeared (visually) as if the virtual hand was drifting towards the right (towards my hand).

The use of different sized rulers aimed at stopping the subject using the length and width of the cardboard as a potential landmark for where their hand was after continuous blocks of stimulation. Immediately after the drift measurement, subjects completed an adapted version of the rubber hand illusion questionnaire (Botvinick & Cohen, 1998) using a Likert scale from 1 (Strongly disagree) to 6 (Strongly agree). The order of the items was randomised for each viewing condition. For each block of this task, the virtual hand was placed at 0°, 90°, 180°, 270° in dorsal and palmar postures creating a total of eight postures.

Analysis. A 4x2 (rotation angle 0°, 90°, 180°, 270°) x hand postures (palmar, dorsal) ANOVA was conducted on drift measurements and subjective measures. Drift values were subtracted from 15 cm (distance from edge of screen to real hand), with larger values indicating a drift towards the 3D hand and smaller

values indicating less drift. The subjective measures were divided into illusion related questions, 1 to 3, see Table 2.1, and control questions, 4 to 7; then averaged creating an illusion and control score. Further post-hoc t-tests were conducted after on the illusion measures after the ANOVA. Multiple comparisons were corrected using Bonferroni correction.

2.3.2.3 Results

A two-tailed paired samples t-test between illusion questions and control questions showed a significant difference $t(8) = 7.13$, $p<.001$, such that illusion questions (mean±SE = $3.102 \pm .211$) scored higher than control questions (mean±SE = $2.467 \pm .211$), indicating that the models were successful in inducing the desired effect.

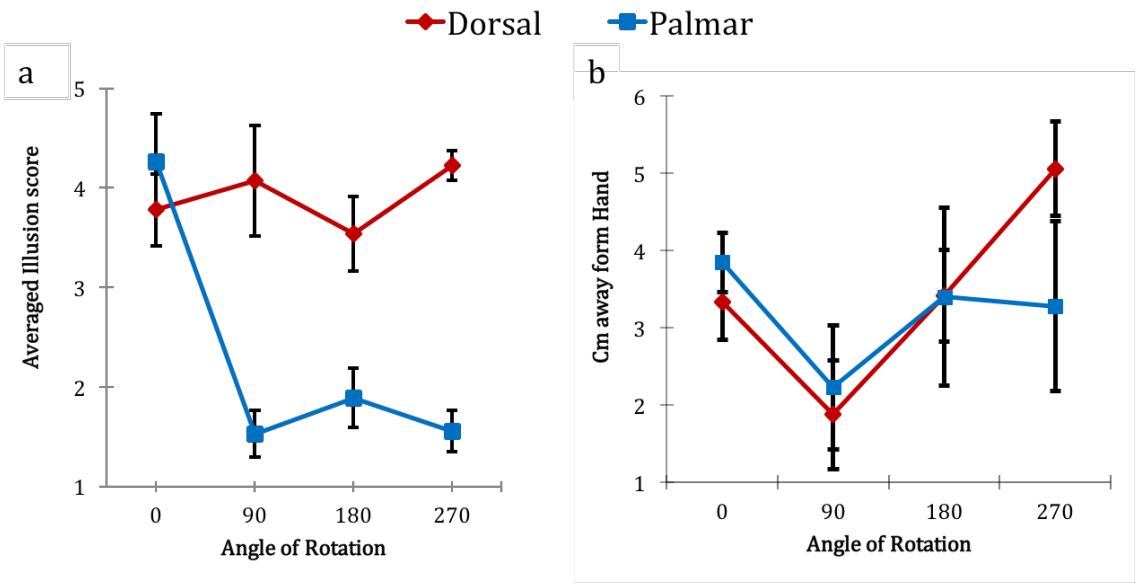

Figure 2.10: a) Average scores to the illusion related questions across 0° ,90°, 180°, 270° rotations of the 3D model. Significant dorsal vs palmar differences at all rotation angles except 0° and 270°. b) Average drift measure as cm away from the real hand 0° ,90°, 180°, 270° rotations of the 3D model. No significant differences found. Bars represent the standard error of the mean.

A more detailed analysis was conducted on just the effects of angle and postures on the scores of the illusion questions. A 4x2 ANOVA on subjective meas-

ures of illusion showed a significant main effect of angle on the illusion measures, F(1, 24) = 8.175, p = 0.001, η^2 = .505, in which the 0° condition was significantly different from the 180° condition (mean difference = 1.308±.278, p = .009, 95% CI[.337, 2.274]) and from the 270° condition (mean difference = 1.130±.306, p = .037, 95% CI [.065, 2.194]). A significant main effect of posture was also found F(1,8) = 38.374, p<.001, η^2 = .827, where dorsal postures elicited larger illusion scores compared to palmar (mean difference = 1.595/*pm*.257, 95% CI [1.001, 2.189]) with larger illusion scores. An interaction between angle*posture was found for illusion measures, F(3,24) = 12.561, p <.001, η^2 = .611. Further post-hoc t-tests were conducted on the illusion measures between dorsal versus palmar postures at 90°, 180° and 270°, but not for 0° as values were too close to be significantly different (see Figure 2.10a). Two-tailed paired samples t-tests showed a significant difference for 90° dorsal>90° palmar (mean difference= 2.546±.420], t(8) = 6.606, p <0.001), a trend difference 180° dorsal>180° palmar (mean difference = 1.648±.551, t(8) = 2.987, p = 0.051), and significant difference for 270° dorsal>palmar (mean difference = 2.666±.409, t(8) = 6.517, p<.001) see Figure 2.10). No significant main or interaction effects were found for drift measures. Multiple comparisons

In summary, the results showed dorsal postures elicit superior illusion experience compared to palmar even across awkward angles in which this effect should be smaller.

2.3.2.4 Discussion

It was predicted that as rotation of the hand moves away from the egocentric (0°) postures, the level of embodiment will decrease. This hypothesis was confirmed, but only partially. A significant interaction between posture and angle

of rotation was found, such that viewing the 3D model's palmar aspects at 90°, 180°, 270° elicited significantly lower levels of illusion compared to the dorsal aspects, except for 0°. The rubber hand illusion literature puts forward that when the 'fake' hand is placed in implausible locations, ownership of the hand decreases proportionally with the increasing degree of impossibility (see Tsakiris & Haggard, 2005 for a review). However, the results of the current experiments suggest that stimulating different aspects of the hand leads to intrinsically different ownership experience. A possible explanation for this result is linked to the anatomy and structural connections of the skin receptors, to the brain. The dorsal aspect of the hand is highly sensitive to affective stimulation (Morrison et al., 2011; van Stralen et al., 2014), it is rich in unmyelinated CT afferents which have strong connections to areas involved in affective experience, unfamiliar sensory experience, and perspective processing (Olausson et al., 2002; Chen et al., 2008; Morrison et al., 2011; Ionta et al., 2013). These connections may explain why dorsal postures did not show decreasing ownership with increasing angle (i.e. increasing degree of unfamiliarity). As hairy skin is mostly exposed to external stimuli (touch from others, heat, pain) it may have evolved the ability to be able to integrate proprioception regardless of any body related visual input. On the other hand, tactile experience of the glabourous skin (on the palm) likely leads to stronger somatosensory representation, which overrides any visual input that is not congruent with body related information being perceived.

2.3.3 Conclusion

The purpose of these experiments was to establish whether the 3D hand models are suitable for use in the subsequent experiments of this thesis. Based on these results, I ascertained that the results indeed are comparable to those

from previous literature, and provide new evidence towards a dissociation between processing styles of stimuli that are palm related or dorsum related.

Whereas processing of stimuli in dorsal view were more sensitive to angle manipulations in the experiment in Section 2.3.1, dorsal postures showed increased illusion scores regardless of viewing angle in the experiment in Section 2.3.2. Therefore, using the dorsal aspect of the hand is likely ideal for future use as it is more likely to elicit multisensory integration.

The finding that rotated 3D models in the palmar posture showed reduced illusion may be linked with the strength of tactile experience of the aspect of the hand. The glabourous skin of the palm has an estimated 70 units/cm^2 of tactile receptors, compared to the 5 units/cm^2 in hairy skin on the dorsal side (Brown et al., 2009). Therefore, this suggestion can explain the finding that when visual and tactile information are incongruent, the effect of the illusion is reduced.

This explanation can be extended to the laterality task results. In the absence of tactile input, observing the palm of the hand completely overrides the sensory integration mechanism that occurs for dorsal postures. Due to the increased focus of attention (Cosman & Vecera, 2010; Davoli & Brockmole, 2012), the observer is forced to rely on visual operations to complete the laterality task (see Figure 2.7), and therefore RTs show no differences between rotation angles of the model.

In conclusion, the 3D models are suitable stimuli for the neuroimaging investigations of this thesis. Furthermore, as the dorsal side of the human hand is exposed to more complex environmental stimuli, humans have likely developed the ability to integrate other senses better with those being received from the hairy skin. Therefore, for the purposes of neuroimaging experiments on embodied

simulation, results presented in this chapter point towards the use of dorsal-view hand images, as visual and somatosensory integration is more likely to occur. It is possible that presentation of a finger abnormality in a dorsal view will lead to stronger activity of the vicarious experience network activity (see Chapter 1, 1.2) and thus stronger activity of posterior regions of the S1.

Chapter 3

Functional Magnetic Resonance Overview and Methods

In this chapter, I outline a conceptual introduction to the bio-physical underpinnings of Magnetic Resonance Imaging (MRI). Then, I describe the key functional MRI methods used in Chapters 4 and 5 to measure brain activity.

3.1 Basic Principles of Functional Imaging using MRI

3.1.1 Nuclear Magnetic Resonance

Magnetic Resonance Imaging depends on the magnetic resonance property of atomic nuclei (Bloch, Hansen & Packard, 1946; Purcell, Torrey & Pound, 1946). The most commonly used nucleus in MRI is Hydrogen ^{1}H, as this is the most abundant nucleus in the human body, and this is used for the fMRI experiment in Chapters 4 and 5.

^{1}H is a protein and carries a positive charge and spins around its axis (see Figure 3.1).

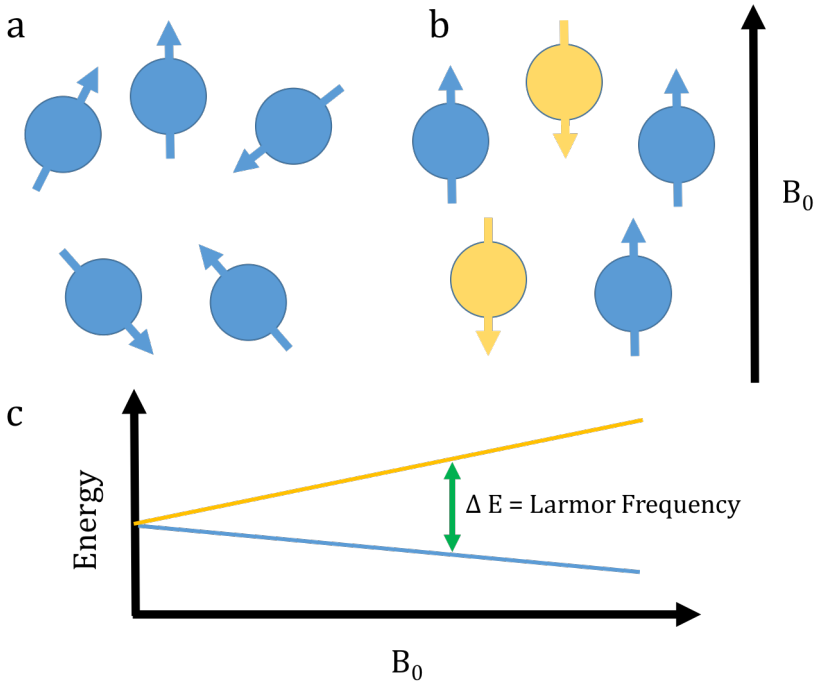

Figure 3.1: A) Spins in the absence of a magnetic field align randomly; B) In a magnetic field, B_0, spins arranged in either parallel (low energy state) in blue, or in anti-parallel (high energy state) in yellow; C) visual representation of the Zeeman effect, where the energy difference between the spin states linearly increases with B_0. This energy difference corresponds to the resonance frequency of spins, and it defines radio-frequency energy necessary to excite spins from the low energy to the high energy state.

This generates electrical current on the surface of the proton which, together with the spinning a magnetic field termed the magnetic momentum. Second, because the proton has odd-numbered positive charge, its moving mass generates angular momentum. Both of these properties are prerequisites for an atomic nucleus to be NMR sensitive, therefore each proton (now labelled as a spin) is a potential contributor to the MR signal.

Nuclei with spin can interact with a strong external magnetic field (B_0), and align themselves with it, resulting in a net magnetisation (M). This alignment can be parallel or anti-parallel to $_0$, and this means that there can be two energy levels in a spin system. Lower level spins are in the parallel state whereas higher

level are in the anti-parallel state (see Figure 3.1b). Since ^{1}H have the property of spin, they do not exactly align with B_0, but instead precess around its axis in a cone-shaped movement at the Larmor frequency (ω). The Larmor frequency is a special property of the spin, and the discrete difference in energy between the alignment states (see Figure 3.1c) of the spin system is equal to the photon energy according to the Planck relationship ($\hbar\omega$).

In equilibrium, there are slightly more spins (1 ppm) in the parallel state than in anti-parallel state, since it is at the minimum amount of energy required for stability. Applying a radio-frequency (RF) pulse at the Larmor frequency induces transitions between the parallel (low) and anti-parallel (high) energy states, driving the resonance of the system (see Figure 3.2a and 2b) and changing the overall net magnetisation. In addition, the RF pulse brings the spins in phase, and afterwards, the high-energy spins will return to the lower state and release the absorbed energy (see Figure 3.2c).

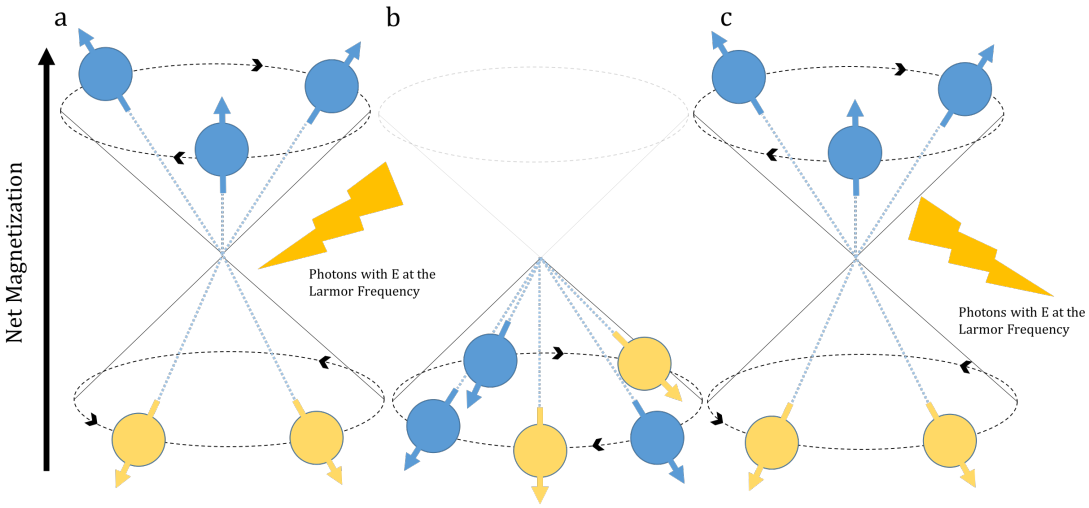

Figure 3.2: Visual representation of changes in the net magnetisation, after a pulse. A) photons at the Larmor frequency excite low energy spins in to the high energy state. B) now low energy become excited and are now precessing at high energy. C, once the excitation pulse ceases, some of the spins return to the low energy state and release the absorbed energy.

As alluded to in the previous paragraph, the MR signal detected after excita-

tion returns to a stable state after a set amount of time. This loss in magnetisation is referred to as relaxation, and explains how the spins return to the lower energy state. For example, T_1 refers to the time constant which describes the decay of the longitudinal magnetisation back to its equilibrium state, that is, the release of energy of spins from the higher energy state to the lower one (see Figure 3.3a), and the T_1 is in the order of seconds. Another relaxation constant is the T_2 decay. This constant describes the decay of the transverse magnetisation due to spin-spin interactions that cause the protons to go out of phase with each other over time (see Figure 3.3b), and reaches maximum decay in the order of milliseconds. Another consideration, for transverse decay is that of spatial inhomogeneity in the magnetic field, this causes additional dephasing.

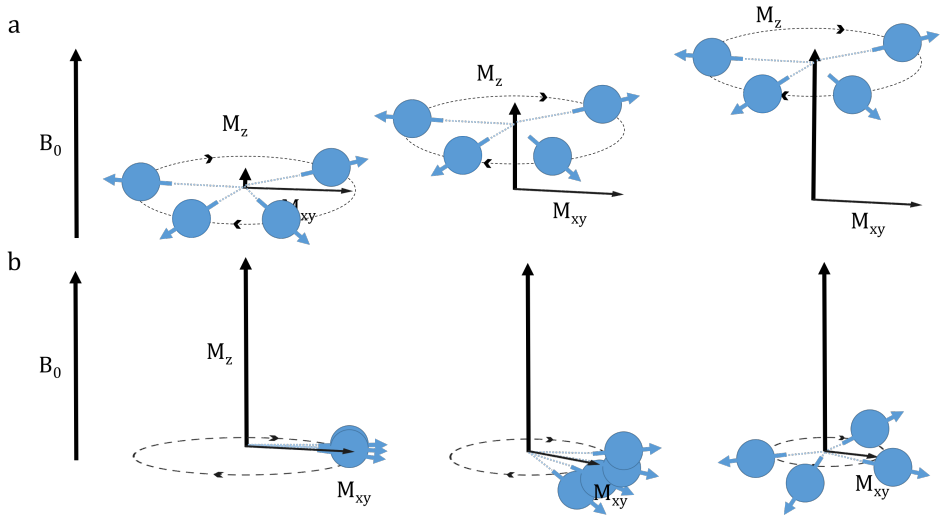

Figure 3.3: A) conceptual representation of the T_1 recovery along the longitudinal axis. After excitation, the longitudinal magnetisation, M_z tips into the transverse plane, then M_z slowly recovers and energy is released. B) representation of the T_2 decay after spins are tipped into the transverse plane. As time progresses the MR signal decays as the spins lose coherence with time and transverse magnetisation, M_{xy}, decreases.

This affects the decay of the transverse magnetisation because some spins will experience slightly stronger magnetic fields than others, causing them to have different dephasing effects, this cumulative dephasing has a time constant of T_2*. T_2* decay is of particular interest to this thesis as the fMRI relies on

the difference in the magnetisation of oxygenated and deoxygenated blood to derive a measurement of brain function.

3.1.2 Image Formation

The acquisition and formation of an MR signal into an image depends on a complex RF pulses, gradients and mathematical methods. Here, I give a short overview of these methods as further details are outside the scope of this thesis. In order to create a 3D image of the brain using the MR signal, a crucial aspect is to localise the signal. This is done by using superimposing gradient magnetic fields onto the main B_0 field in the x, y, and z-directions (see Figure 3.4).

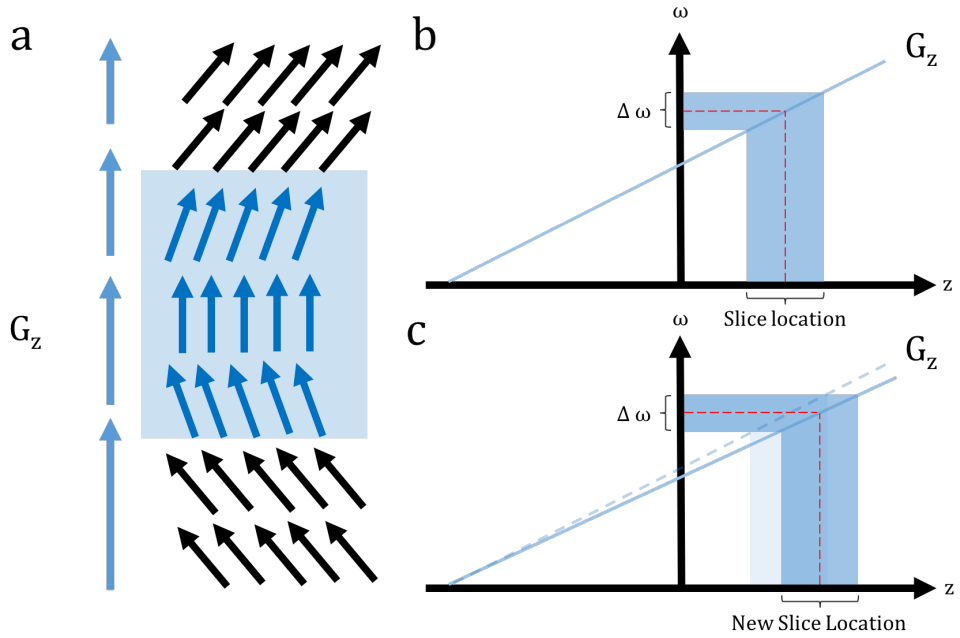

Figure 3.4: A) Slice selection diagram of the selection gradient at the Larmor frequency where the blue arrows represent the direction of the slice encoding gradient (G_z), the black arrows represent the spins in the magnetic field and in shaded blue the group of spins selected. B) a visual representation of the interaction between slice space, z, and frequency of excitation, ω. Where the bandwidth of the gradient, $\Delta\omega$, selects the slice thickness. C), by changing the slope of the gradient, whilst keeping the same bandwidth and new slice of the same thickness is selected (see slope change of the dashed line to solid line).

This makes small spatial variations in the precessing frequencies of the spins, making their specific resonant frequency depend on a function of their position, creating a linear variation along each axis. For the formation of the images,

usually three steps are involved. First, the slice selection: An initial RF excitation pulse is applied in the presence of a field gradient (G_z), only spins that have a corresponding Larmor frequency to the frequencies contained in the excitation pulse will tip into the transverse plane.

Depending on the desired slice thickness, and location it is possible to adjust the amplitude of the gradient and bandwidth of the RF pulse to acquire a 2D representation, or a single slice. Second, frequency encoding: once the slice is selected, a field gradient is now applied during image readout, instead of slice excitation, therefore affecting those spins already excited in that specific slice. By applying a linear gradient field in the x-axis (G_x), the resonant frequency of the spins in this slice will vary in the same way, and applying a Fourier transform to the signal will breakdown the intensity of those frequencies in the x-direction. Third, phase encoding: this step allows the localisation of the signal that is perpendicular to the frequency encoding direction, or the y-axis (G_y). In order to encode the spins in this direction, one gradient is applied before any MR signal is acquired, causing the spins along this axis to precess at different frequencies depending on their position – therefore, having different phases. By introducing different phase values under a specific frequency encoding pulse, a 2D image can be reconstructed using Fourier transform[1]. This will create a visual representation of a brain slice depending on the spatial configuration of each gradient and relaxation constants for each tissue (see Figure 3.5).

Any image can be represented as a combination of its underlying frequency features; samples from each coordinate can be extracted and the different trajectories of the spins can be plotted in k-space (Ljunggren, 1983). This concept can

[1]Mathematical method to convert a signal that changes of time into its underlying spectral composition. That is, any signal is a sum of any given number of cosine and sine waves which have a specific phase and amplitude.

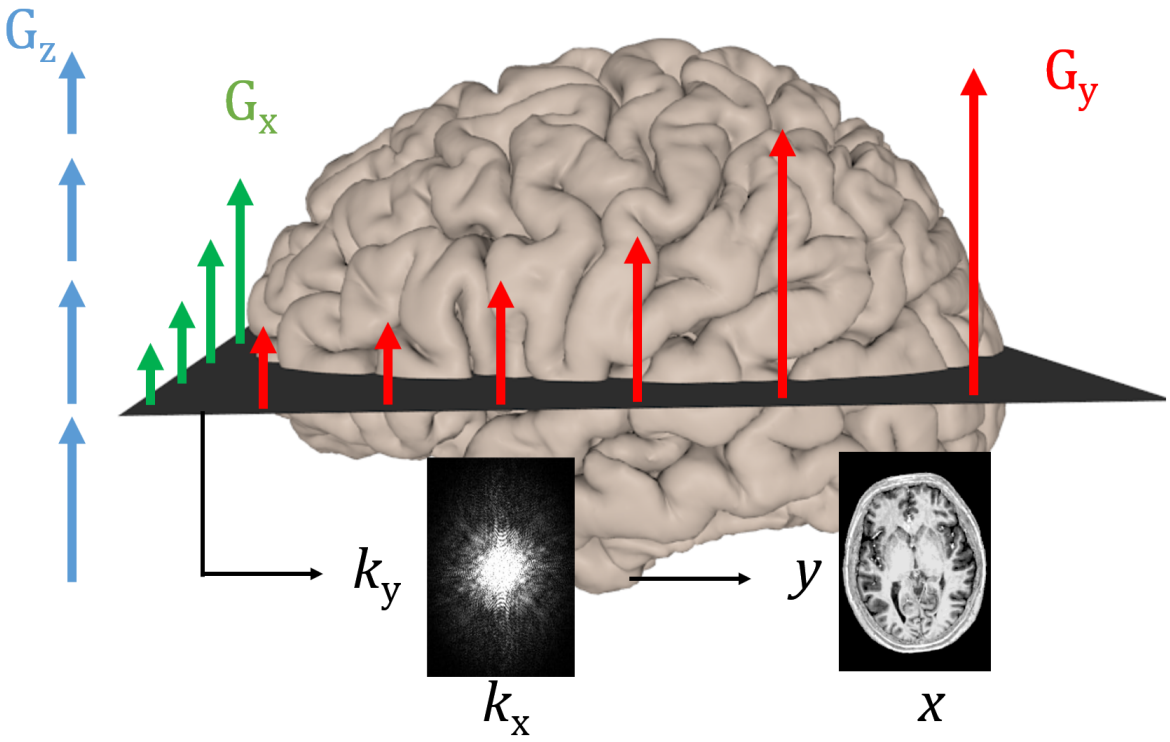

Figure 3.5: Summary of image formation, after applying the different gradients and acquiring a Raw signal for each coordinate . First, a gradient selects the slice, another two gradients that are frequency and phase encoded and tag different 2D areas. This is creates a 2D representation of the slice in the k-space, and then by means of inverse Fourier transforms the signal is converted to 2D space in Cartesian coordinates

be seen as an in-between stage of image formation, where the spatial frequency of the MR signal is represented in Fourier coordinates (k_x, k_y, k_z), before being converted to Cartesian coordinates (x, y, z). At the centre of the k-space projection, the image is brightest, and towards the edges it becomes darker. This illustrates that at the centre of the image, spins sampled have the same phase, and as the projection moves away from the centre spins are less and less in phase. During frequency encoding, the signal is recorded and projected along regular intervals in the k_x direction, while during phase encoding the location is changed without sampling the signal resulting in a change of of the sampled trajectory in the k_y

direction. As there is an inverse relationship between the spatial frequency and distance, the wider range of coverage, the higher spatial resolution will be, and therefore this measurement is a key factor in determining the Field-of-View of a scanning session. Other considerations such as pulse sequences, susceptibility effects, water and fat contents, and inhomogeneity mapping are also crucial for image formation. However, these concepts go beyond this purpose of this chapter. Although, some of these topics will be referred to in the following sections due to their relevance for T_2* contrast and the blood-oxygenation level dependent signal (BOLD).

3.1.3 MR Contrasts

The fact that different tissues have different relaxation times makes MRI a versatile tool for the generation of images. However, it is important to understand the intrinsic properties of different tissues and how to manipulate different instrumental variables to produce the desired image. There are two important factors that govern the type of MR image that is obtained. The first factor is the time interval between successive excitation pulses, and is known as the repetition time (TR). The second factor that governs the timing of MR image collection is the echo time (TE), the time between excitation and data collection (see Figure 3.6).

As different tissues have different T_1 and T_2/T_2* decays, through different combinations of TR and TE, it is possible to maximise the contrast between tissues. For example, T_1-weighted images are the most common structural contrast for anatomical images of the brain. At a very short TR, there is no time for the longitudinal magnetisation to recover, and thus no MR signal. Conversely, at very long TR values, the amount of signal produced by T_1-weighting from, say, tissue

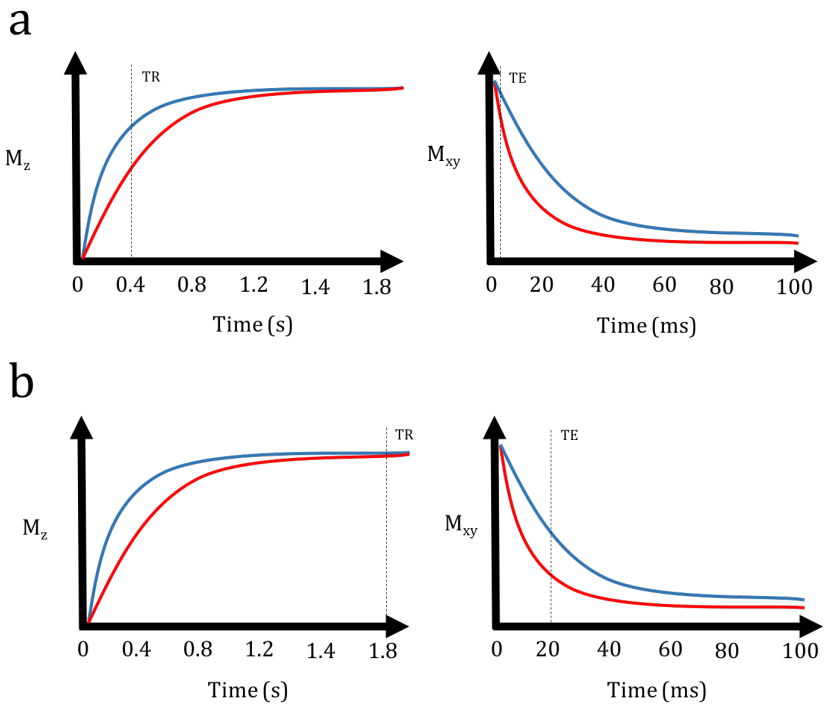

Figure 3.6: Representation of the T_1 recovery and T_2 decay across time and TR and TE combinations that select for optimum contrast (black dashed line) between tissue A (blue) and tissue B (red). A) medium TR and very short TE maximizes longitudinal magnetisation, M_z , and increases T_1-weight images contrasts in collected images. B) long TR and and medium TE maximizes transverse magnetisation, M_{xy}, differences between tissues and increasing T_2-weight contrast in collected images.

A and tissue B will be very similar. Therefore, in T_1-weighted images, TR take an intermediate value so as to maximise the differences between tissues which have different longitudinal relaxation times (see Figure 3.6 a). In order to have an exclusively T_1-weighted image, T_2/T_2* effects must be completely removed and thus the TE must be very short so that the transverse magnetisation is at its maximum (see Figure 3.6 b). In practice both gradient-echo pulse and spin-echo read-outs are used as the read-out schemes for T_1-weighed images. The hallmark of which is a spin-echo is the 180° refocusing pulse; this is applied shortely after the initial 90° excitation leading to a correction of the phase dispersion due to T_2 relaxation effects. A T_1 sequence elicits the most signal from white matter and bone marrow, due to their short T_1 values, and an intermediate amount of signal from grey matter. Since water has a very long T_1 value, very little signal

is recovered from cerebral spinal fluid. In order to increase the T_1 contrast, an inversion recovery technique can be used by adding a 180° inversion pulse before the standard read-out sequence. This has the effect of inverting the net magnetisation (i.e. more spins in higher energy state than in low energy state), and this doubles the dynamic range of the signal. By doing this, the range over which the signal recovers doubles, and in turn this increases the T_1 contrast between tissues (in Chapters 5, Methods section, an advanced version of this is used which allows better segmentation of grey- and white-matter). T_2-weighted images show the largest signal in regions containing fluids. For these images a spin-echo pulse sequence is used in combination with TR and TE times that remove the T_1 effect and at the same time maximise the difference between tissues (see Figure 3.6b). If the TE is too short, tissues have not had time to relax, and therefore no difference in tissue type is observed. the TE cannot be too long or all the transverse magnetisation would be lost and no signal would be collected.

Like T_2-weighted images, T_2* pulse sequences have a long TR and medium TE value but use a gradient-echo pulse sequence. However, when studying brain activation using BOLD, fast-imaging sequences must be used in order to capture the transient changes in signal. The first MR images were acquired by collecting one line of k-space per TR. This takes a long time to acqiuire the whole k-space, and for psychological experiments this method is not suitable. However, Mansfield (1977) proposed a new method where the entirity of k-space is filled using rapid gradient switching in a single TR. After the first excitation pulse, the phase and frequency encoding gradient are cycled very quickly removing the dephasing effects due to spin-spin interactions, but not re-phasing the susceptibility effects induced by, say, influx of oxygenated blood. A continuous gradient will trans-

verse the space chosen in a zig-zag, or rectilinear fashion with very quick data acquisition periods for each cycle, this acquisition was named single-shot echo planar imaging (EPI).

An EPI acquisition often results in large inhomogeneity of the B_0 field due to air-filled cavities and brain-tissue boundaries. In addition, due to longer TE, the system is more prone to distortions. Variations in magnetic field strength along the trajectory of the data acquisition results in pixel shifts of the image leading to the formation of geometric distortions. This can be corrected using image base shimming, which compensates for field inhomogeneity.

3.2 Methods for Functional Brain Imaging

This section outlines the different methods and statistical analysis used in Chapters 4 and 5 for the investigation of somatosensory responses to tactile stimulation and observed finger postures. First, I discuss theoretical aspects of BOLD imaging to measure brain activity, scanning at field strength, and multi-slice acquisition, and how it is used to measure brain activity. Then, I outline modelling and statistics applied to the BOLD response in fMRI experiments. Lastly, I briefly detail anatomical imaging and cortical reconstruction methods that are relevant for this thesis.

3.2.1 BOLD Imaging

Functional MRI is a technique that uses the intrinsic MR changes caused by neuronal activity during a certain task to create maps of brain activation. Perhaps the most common technique for fMRI is the blood-oxygenation level dependent (BOLD) contrast (Turner, Bihan, Moonen, Despres & Frank, 1991; Ogawa, Lee, Kay & Tank, 1990; Kwong et al., 1992; Bandettini, Wong, Hinks,

Tikofsky & Hyde, 1992). The following paragraphs give a pertinent overview of the theory and research of BOLD imaging that is used in fMRI experiments in Chapters 4 and 5.

In 1936, Pauling and Coryell, discovered that the haemoglobin molecule has different magnetic properties depending on whether or not it is bound with oxygen. In its bound state, (oxy)haemoglobin has no unpaired electrons and has weak magnetic susceptibility, or is diamagnetic. In its unbound state, (deoxy)haemoglobin has both unpaired electrons and significant magnetic moment. By separating venous from arterial blood, Pauling and Coryell showed 20% increase in magnetic susceptibility of deoxyhaemoglobin (see Figure 3.7).

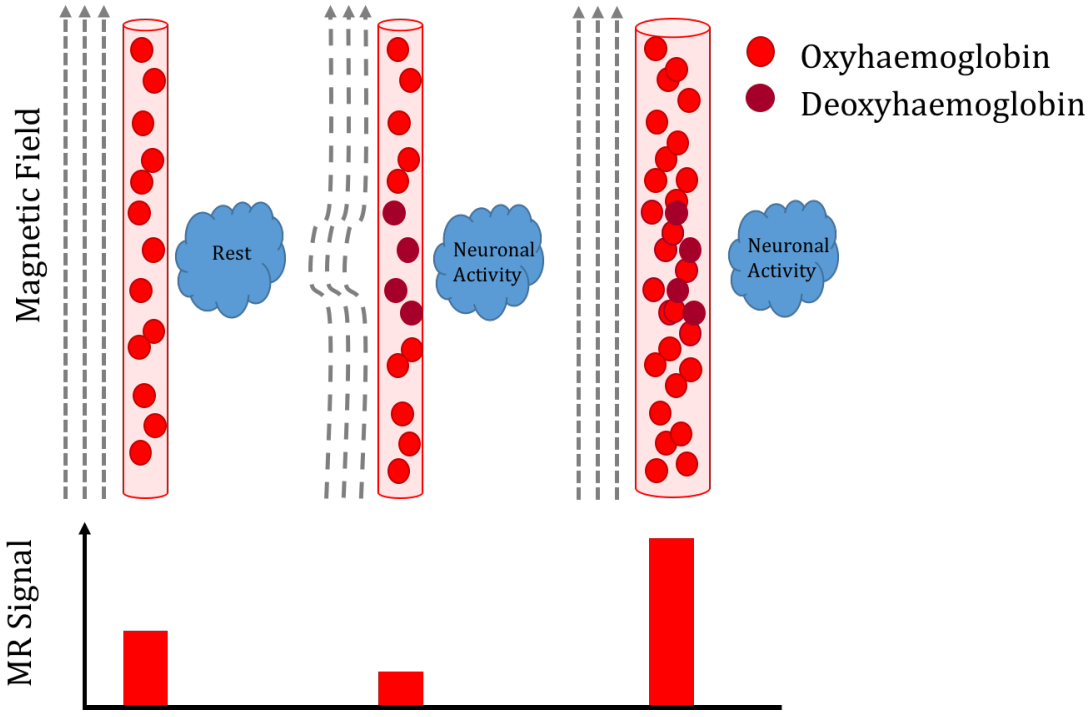

Figure 3.7: Visual depiction of the magnetic field interaction with oxygenated and deoxygenated blood during neuronal activity. First, as oxygenated blood is paramagnetic there is no disturbance of the magnetic field. Immediately after the onset of neuronal activity, there is a metabolic increase of deoxygenated blood which deforms the magnetic field and the MR signal decreases. After several second from the onset, the capillaries surrounding the active neurons dilate, leading to a influx of oxygenated blood which increases the MR signal arising from that region of the brain.

This discovery is crucial for BOLD imaging because paramagnetic substances influence the surrounding magnetic field, which in turn leads to nearby protons

to precess at different frequencies, resulting in a more rapid decay of T_2*. So, an MR pulse sequence targeting T_2* decay, should show MR signal contrast between deoxygenated and oxygenated blood. This prediction was verified by Thulborn, Waterton, Matthews and Radda (1982) who found that the decay of the transverse magnetisation is influenced by the volume of oxygenated blood in a solution. Furthermore, in order to acquire a significant contrast between blood oxygenation levels, B_0 magnetic field strength had to be 1.5T or greater. Later, Ogawa et al. (1990) expanded this finding and showed differences in brain oxygenation in anaesthetised rats undergoing MRI. Whilst inhaling pure oxygen, a noticeable increase in contrast was seen in the acquired images, therefore demonstrating the basis for BOLD contrast.

In this thesis, BOLD contrast is used to investigate brain function. Although not a direct measure of brain activity, BOLD assesses brain activity by measuring the change in blood supply after neuronal involvement. After, activation, an 'initial dip' has been suggested in the BOLD signal (explained to be due to local oxygenation consumption, see Yacoub et al., 2001a, also see 3.8), two seconds later, due to an influx of oxygenated blood, BOLD signal increases and peaks approximately 6 seconds after activity. Then in the next 20 seconds, it steadily decreases overshooting slightly from baseline, and is fully recovered after 60 seconds (see Figure 3.8). This response is well documented is referred as the 'Haemodynamic Response Function' (HRF, Yacoub et al., 2001b).

The BOLD signal is easily manipulated by different experimental designs, which can either be classified as blocked, event-related, or mixed. In a block design, a series of stimulations are presented in an ON/OFF fashion, in an event-related design, short trials (ranging from 100 ms to 3 s) of alternating conditions

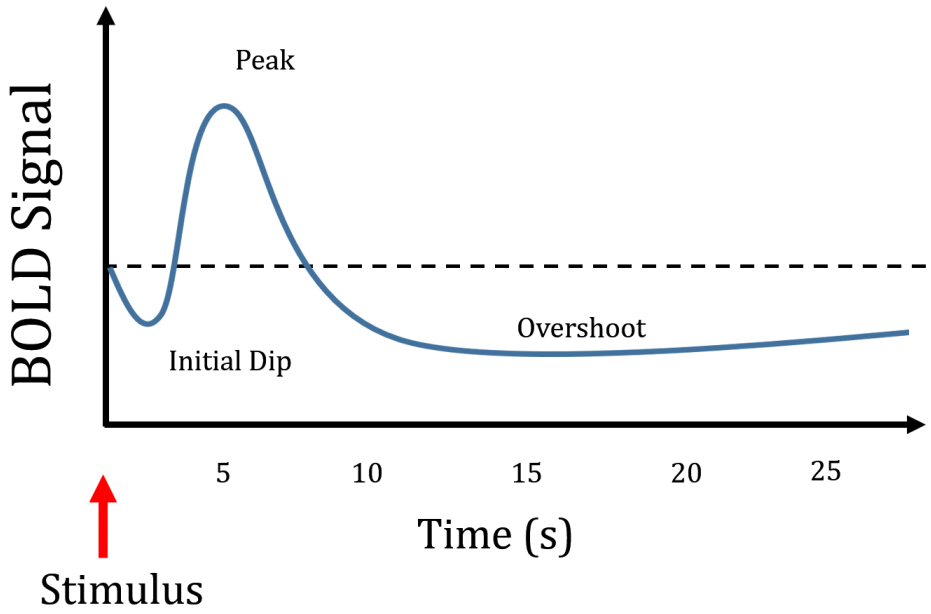

Figure 3.8: Schematic representation of the Hemodynamic Response Function (HRF) after a stimulus over time.

are presented with random inter-trial intervals. A mixed-design, combines the two methods and starts with an ON block, that has alternating trials, followed by an OFF period (see Figure 3.9).

In fMRI, the BOLD response occurs in an amount of time larger than time for the collection of slices for any given FOV. This means not enough samples are acquired to measure BOLD modulations. However, under the assumption that BOLD is a linear system, that does not vary with time, any stimuli sequence is equal to the summation of the BOLD responses to each stimulus (Boynton, Engel, Glover & Heeger, 1996). This assumption permits the convolution of the HRF with a stimulus input function, and allows modelling the events across a time-series, which can then be compared with the real data for statistical analysis (see Figure 3.10).

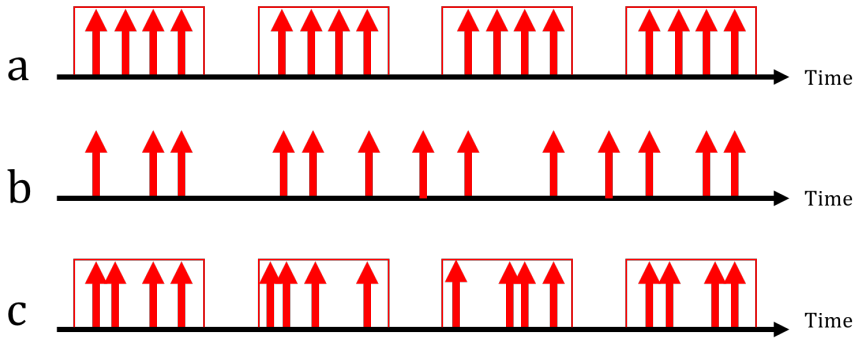

Figure 3.9: Schematic representation of the Haemodynamic Response Function (HRF) after a stimulus over time. Red arrows depicts the onset of the stimulus, and the box-car plot highlighting the blocked nature of the stimuli of the same category. A) a block design, where a series of stimuli are presented sequentially in for a specific amount of time. B) an event-related design, where stimulus onset and inter-stimuli interval is randomised. C) a mixed-design, with randomised trial onset within the same stimulus block.

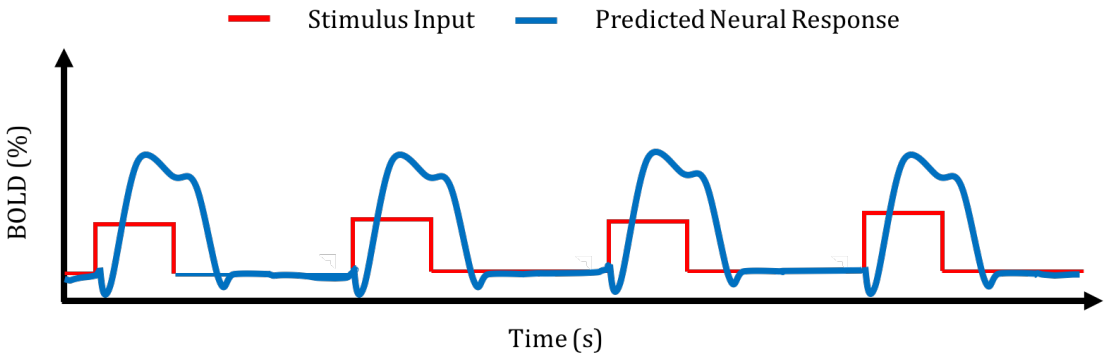

Figure 3.10: Stimulus input function (red) outlining the stimulation for the scanning duration. This is convolved with the HRF as in Figure 3.8, creating a predicted responses (blue) which will be tested to actual percentage change in the BOLD signal.

3.2.2 Imaging at Ultra-High Field Strength

To demonstrate that embodied simulation of observed finger abnormalities leads to overlap with regions dedicated to tactile experience, one crucial step is to obtain high spatial resolution measurements with fMRI. However, simply increasing spatial resolution is not enough as the signal-to-noise ratio (SNR) is reduced, and the BOLD SNR contrast is reduced. This can be particularly limiting for studies using tactile stimuli as the amplitude of the BOLD response is low (Stippich et al., 1999) and accurate representation of the finger tips is limited even at spatial resolution with high SNR (Triantafyllou et al., 2005).

Therefore, this calls for increasing the field strength to improve image SNR and intrinsic BOLD constrast. In Chapters 4 and 5, an ultra-high field scanner (7T) is used to acquire responses to tactile stimulation of the finger tips and observed distorted finger postures.

The impact of greater field strength on BOLD contrast is not trivial and depends on complex interactions of intra-[2] and extravascular[3] decay with the magnetic field. The intravascular contribution from large vessels drops out at high field strength because in larger vessels larger volume of spins will likely experience the same range of field gradients. However, in capillary vessels the spins will travel larger distances and as a consequence experience random dephasing, leading to an increase in T_2*-weighted contrast (Ogawa et al., 1993).

A significant challenge to fMRI experiments at 7T are the field-strength susceptibility-artefacts (Farahani, Sinha, Sinha, Chiu & Lufkin, 1990). Regions close to air-filled sinuses and other air-filled cavities will interact with the surrounding magnetic fields and change the magnetic gradients locally. Any tissue close to air will experience the same change leading to a drop in SNR, and potentially become distorted. However, because smaller vessels are located near the site of neural activity of interest, increasing the field strength will result in an increase in the specificity of the signal. For example, Krüger, Kastrup and Glover (2001) investigated the effect of field strength (1.5 vs 3T) using a task-based fMRI. In addition to an overall increase in functional SNR, they found that functional SNR increased by a factor of 1.8 in areas that correspond to large blood vessels, and by factor 2.2 in areas of active grey matter. In a comparison between 4T and 7T field strengths, the microvascular contribution to the BOLD

[2] T_2 and T_2* relaxation rate depending on the amount of water inside blood vessels.
[3] T_2 and T_2* relaxation depending on the water outside the vessels.

signal was significantly improved because the TE is at 25 ms (Yacoub et al., 2001, see Figure 3.11). This means that only quick dephasing effects related the small vessels neighbouring areas of activity are contributing to the BOLD signal.

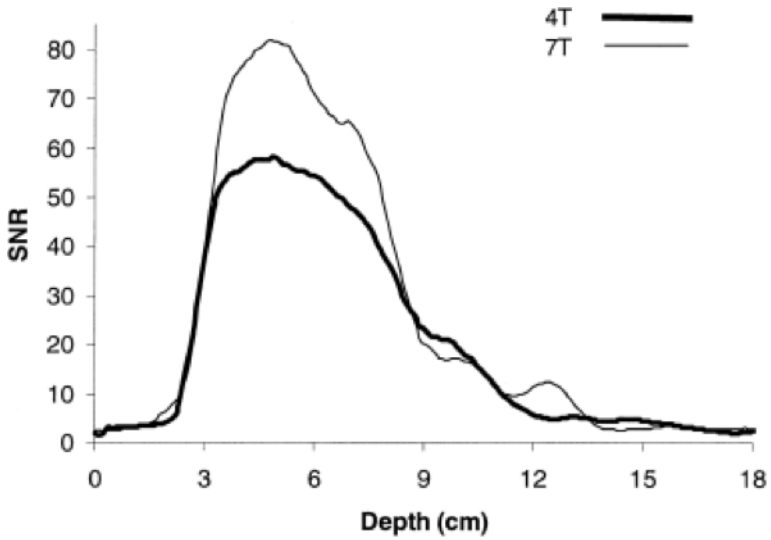

Figure 3.11: Imaging brain function in humans, a comparison between 4T and 7T fMRI response. At 7T SNR is larger at the same cortical depth as differences in TE lead to 7T being more tuned to measuring T2* decay from the rapidly dephasing effects from blood in small vessels. Extracted from Yacoub et al., (2001).

Another consequence of increasing field strength is the increase of spatial extent of activation, with results showing increases as high as 70% to 100% of the number of active voxels during active tasks for a given threshold (Yang et al., 1999). However, this is somewhat contradictory with the increase in special specificity. This is because the gain in extent comes from increased SNR, and voxels were more likely to be labelled as significant.

Given the increase of functional SNR, the detection of highly spatially localised and/or weak signal functional changes is hypothesised to be improved at 7T. Using 7T to study somatosensory responses to both tactile and observed stimuli is particularly pertinent to this thesis because somatosensory responses are small and sensitive to partial volume effects (Scouten, Papademetris & Constable, 2006). Furthermore, most functional studies apply smoothing depending on the

voxel size (Weibull, Gustavsson, Mattsson & Svensson, 2008), causing blurring of the spatial response, then register their fMRI data to standard Talairach space or MNI template space. More recently, a series of somatosensory studies (Sanchez-Panchuelo et al., 2010, 2012; Besle et al., 2013, 2014) showed that accurate mapping can be acquired at 7T with no smoothing required, on an individual subject basis, as the BOLD contribution is well modulated by stimulus input and highly spatially specific with well delineated borders between fingers.

3.2.3 Multiband fMRI Acquisition

Multiband scanning (MB; Nunes, Hajnal, Golay & Larkman, 2006) refers to slice acquisition sequences where the excitation of different slices occurs simultaneously - this is also known as simultaneous multislice (SMS). This allows for an improvement in coverage in a given TR period or a dramatic reduction in TR to produce more samples of the same time-series. For example, with an MB factor of 2, two slices are acquired allowing the number of slices to be doubled, or the TR to be halved. This allows for the acquisition of whole brain images with high temporal resolution (J. Cheng et al., 2015). In short, MB sequences rely on the varying sensitivities of receiver coils and the application of slice selection pulses that are phase encoded along the z-axis of B_0. Then reconstruction can be achieved using the sensitive encoding (SENSE) algorithms for parallel imaging (Blaimer et al., 2004).

While the increase in temporal resolution may not offer immediate benefits to the BOLD signal, as the HRF is particularly slow, the higher sampling rate provides more independent data for statistical analysis methods. Furthermore, the noise influence on the statistical measures is further reduced as with more data points the averaging of repeated measurements leads to noise cancelling, and

better estimates of activity (Miller, Bartsch & Smith, 2015). With this sequence increased coverage can be achieved while maintaining the same TR (Moeller et al., 2010), and gain further sensitivity to BOLD response.

In addition to using a 7T scanner, in Chapters 4 and 5, a MB sequence with factor 2 is used in the event-related fMRI session to increase the BOLD contrast-to-noise ratio.

3.2.4 General Linear Model for fMRI

In fMRI experiments, the process of inferring statistical significance depends on the ability of rejecting the null hypothesis, which is the probability that the experimental manipulation had no effect on the data. The most common way of achieving this is to use a General Linear Model (GLM) where a linear combination of different explanatory variables (EV), $X(t)$, and uncorrelated noise, $\epsilon(t)$, are considered to derive a value of how well the model predicts (β_{1-n}) the real BOLD signal, $Y(t)$. This method uses a multiple regression analysis as follows:

$$Y(t) = X_1(t) \times \beta_1 + ... + x_n(t) \times \beta_n + \epsilon(t) \tag{3.1}$$

This allows the creation of a line of best fit, where the slope parameters or beta values that best explains the fMRI time-series whilst minimising the noise contribution. The β value can be used to make an inference about whether there is a meaningful relationship between Y and X. To do this, first we assume that noise has no temporal structure, and that the EVs are temporally independent from each other. These requirements are important because if there is similar temporal structure, i.e. temporal correlation, to a set of EVs it would be impossible to decide which of the combinations of β values would best explain the data. For

example, this would happen if two stimuli are always presented together. Under this assumption then there is an unique set of β values that can explain the noise contribution:

$$\beta = (X^T - X)^{-1} \times X^T \times Y \tag{3.2}$$

The signal variation after sensory stimulation follows a HRF and as such the BOLD time-series can be predicted by convolving this function with the design matrix, i.e. the EVs, of the model. If, when solving the GLM based on a specific EV, it reaches a significant level ($p<.05$), this means that the null hypothesis is not responsible for the changes in the data observed taking into account the contribution of the other parameters combined. In order to understand whether one EV is eliciting more BOLD signal than another, their contribution to the signal must be compared. This can be done using t-tests and attributing contrast weight to each β value. For example, if:

$$Contrast = C \times \beta^T \tag{3.3}$$

where C is a vector containing $\beta_1 = 1$, and β_2 =-1, and β^T is a transposed matrix with β values derived from the GLM, then, the t-statistic T for a certain voxel is derived as follows:

$$T = \frac{C^T}{\sqrt{\frac{C^T \times (X^T X)^{-1} \times C \times \sigma^2}{n-p-1}}} \tag{3.4}$$

where X is the predicted time-series, n is the number of samples, p the number of predictors, and σ^2 is the variance calculated from the residual sum of squares (RSS). The residuals for any combination of parameters, are derived from the

difference between the actual time-series Y and the model $X\beta$.

$$\epsilon = Y - X \times \beta \tag{3.5}$$

This means that the RSS can be found the by sum of the squared residual values, $\sum \epsilon^2$, and the variance for any combination of EVs is simply:

$$\sigma^2 = \frac{RSS}{n - p - 1} \tag{3.6}$$

This statistical methodology is used in Chapters 4 and 5 to investigate the brain responses to the observation of distorted finger (and natural) postures. The T-value obtained can then be normalised and transformed to a Z-value, that represents the standard normal distribution value of that probability.

As this is a mass-univariate approach, where every voxel of interest is being tested for significance, this creates a multiple comparison problem. By repeatedly conducting the same type of statistical test, the family-wise error rate increases. In order to control for this, a Bonferroni correction is used where the probability of significance decreases proportionally with number of tests (or voxels) conducted.

This is a conservative correction method as it applies a stringent threshold without any consideration of the analysed data (Benjamini & Hochberg, 1995; Genovese, Lazar & Nichols, 2002). In the fMRI experiments reported here, an alternative method is used. The False Discovery Rate (FDR), describes the probability of having at least one false positive within a number of significant results (Benjamini & Hochberg, 1995; Benjamini, Krieger & Yekutieli, 2006). This becomes less strict than Bonferroni correction, as the value depends on the distribution of the p-value, and assumes that only within that set of significant tests, you

will see false-positives. In this research, activity is focal and specific to certain areas of the brain (i.e. grey matter), therefore this method increases statistical inference power.

3.2.5 Repetition Suppression

Repetition suppression is used as an experimental tool to explore the selectivity of neuronal populations to any given repeated stimulus. For example, single-cell recording studies in macaques show that neuronal spiking rates exponential decrease with repetition number in the visual cortex (Xiang & Brown, 1998). In BOLD imaging, this relationship is more complex and demands certain assumptions. Broadly speaking, it is assumed that increasing the signal recorded from single cells positively correlates with local field potential (LFP) signal, which in turn correlates with BOLD activity (Logothetis, Pauls, Augath, Trinath & Oeltermann, 2001). Current theories that explain this reduction in BOLD response and spiking rates, suggest a complex interaction between stimulus input and neuronal biophysiology.

The *Fatigue Model* explains that the repeated presentation of the same stimulus leads to an equivalent reduction in neuron firing rate with no temporal difference nor pattern difference across a different group of neurons (see Figure 3.12). One mechanism for this model potentially occurs via firing-rate adaptation, in increasing potassium ion currents due to increased firing rate, decreasing membrane potential and its conductance, and consequently leading to a lower probability for spiking (Carandini & Ferster, 1997). Another mechanism which can also explain a fatigue model is synaptic depression, in which continuous firing leads to a reduction in neurotransmitter release, reducing spiking and consequently the BOLD signal (see Gordon, Choi, Ellis-Davies & MacVicar, 2008 and Lauritzen,

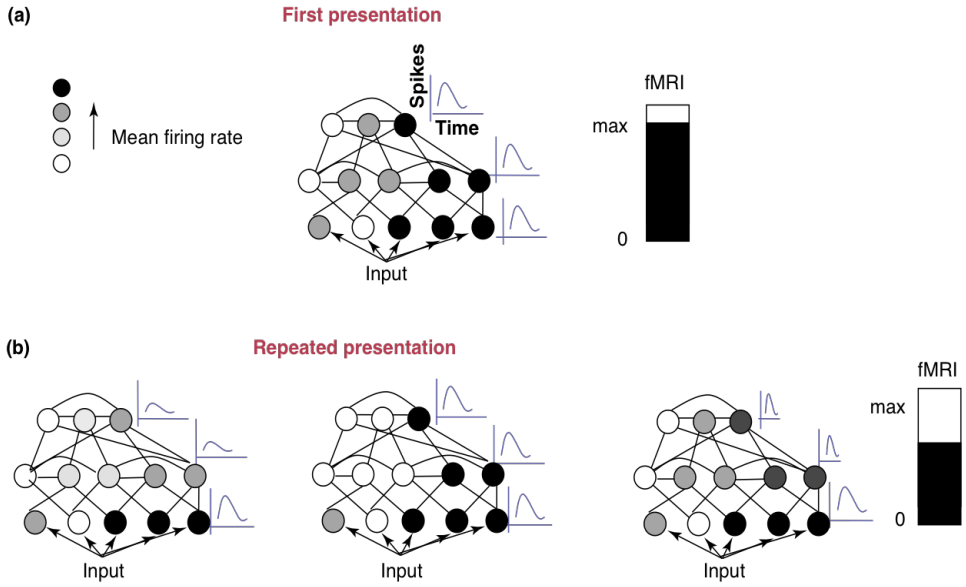

Figure 3.12: a) Schematic representation of repetition suppression theoretical Models, to a hypothetical stimulus. The blue graphs show spiking rates with highest response at each stage (indicated by black circles). b) The three models predict reduced BOLD for repeated stimuli, but for different reasons: Fatigue model (left, lower firing rates); Sharpening model (centre, fewer neurons responding); Facilitation model (right, shorter duration of neural processing). Extracted from (Grill-Spector, Henson & Martin, 2006).

2005).

The *Sharpening Model* suggests that repetition results in a more specific neuronal representation of the stimuli. Hence, it is assumed that certain groups of neurons are specifically tuned to certain stimuli, and the responses of other neurons are 'trimmed off'. The response curve of these stimuli becomes narrower, and more specific to certain neuronal populations, as sparser representations may allow for more efficient and faster processing (Henson & Rugg, 2003).

The *Facilitation Model* explains that repetition causes faster processing, shorter latency, and shorter spike trains. These facts combined, explain how a haemodynamic signal will become smaller with repetition; with integration of neural activity occurring over large periods of time (in comparison to electrophysiology), this shorter duration will lead to significantly smaller BOLD signal in repeated conditions as a consequence of facilitation.

In summary, through the use of repetition suppression, CNR, and voxel specificity to different conditions is increased. This approach is suitable for exploration of the research aims established in the first step of the thesis. Visually induced S1 activity maybe be low and non-specific and this type of design aims to possibly counteract these effects.

3.2.6 Travelling wave fMRI protocols

A travelling wave refers to the property of a wave, or in this case a signal, where its maximum and minimum amplitude change with time and space (see Figure 3.13). This concept was first applied in visual neuroscience to study mapping of different visual areas and demonstrate a topographical organization of the visual field in the occipital cortex (Sereno et al., 1995, Engel, Glover & Wandell, 1997). As neighbouring areas of the visual field are represented in neighbouring areas of the primary visual cortex, presenting periodical stimuli that change in eccentricity or polar angle will lead to periodical fluctuations of the BOLD signal in voxels in the corresponding brain areas to the stimulated visual field (see Figure 3.13). This concept has been also successfully applied to somatosensory representations of different locations in a single finger (Overduin & Servos, 2004, 2008) and to representations of different fingers (Sanchez-Panchuelo et al., 2010, Besle et al., 2013) and therefore is of importance to this thesis.

As the response elicited by a travelling wave method of stimulation is cyclical, disentangling the contribution of the different areas of the brain (such as those that represent different fingers) becomes a Fourier problem. As explained in section 3.1.2 *Image Formation*, any temporal signal can be represented as a sum of any sine and cosine waves of different frequencies, where in this case the amplitude corresponds to the intensity of BOLD signal. As different SI areas also have

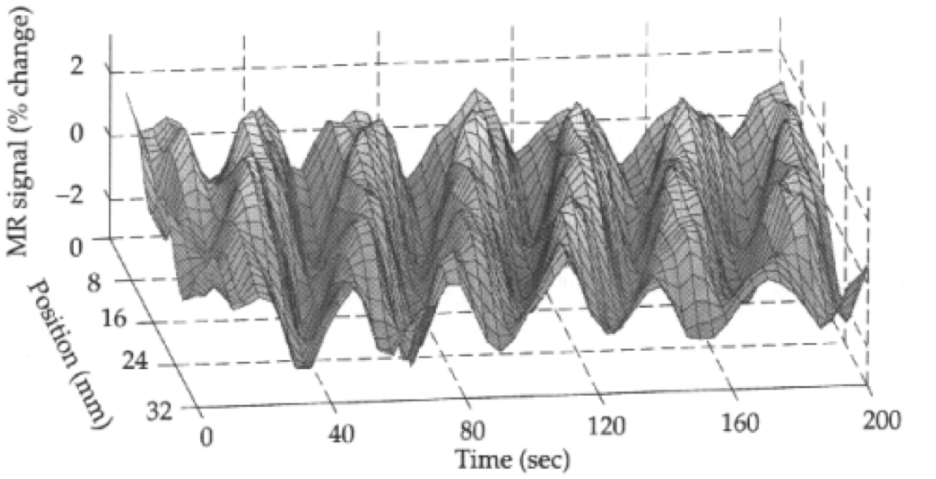

Figure 3.13: Depiction of a patch of the visual cortex undergoing cyclical stimulation using a travelling wave method. As time progresses the MR signal for different position changes leading to a wave-like appearance of the MR signal which can be easily modelled with a sinusoidal function. Extracted from (Engel et al., 1997).

limited receptive fields corresponding to different body parts (see Figure 3.14a), applying a Fourier transform to BOLD responses elicited by cyclical stimulation of different body parts will allow one to the delineate the borders of those body parts. This is possible because at a given stimulation frequency, each body part will correspond to a specific phase angle expressed in radians. Therefore, as phase progresses brain regions representing different fingers will show significant coherence creating a topographical map of the stimulation (see Figure 3.14).

The advantage of using this method to measure responses to stimulation is it creates well delineated topographical representations, with non-overlapping responses as the phase of stimulation corresponds to a specific moment in time in a specific location. Whereas in the GLM analysis, the specificity of a certain voxel depends on the statistical contrasts introducing more potential for multiple comparisons errors, and leading to wide-spread, non-specific activation (Sanchez-Panchuelo et al., 2010,Besle et al., 2014, Martuzzi et al., 2014), which can be an issue with respect to specificity of location of the SI.

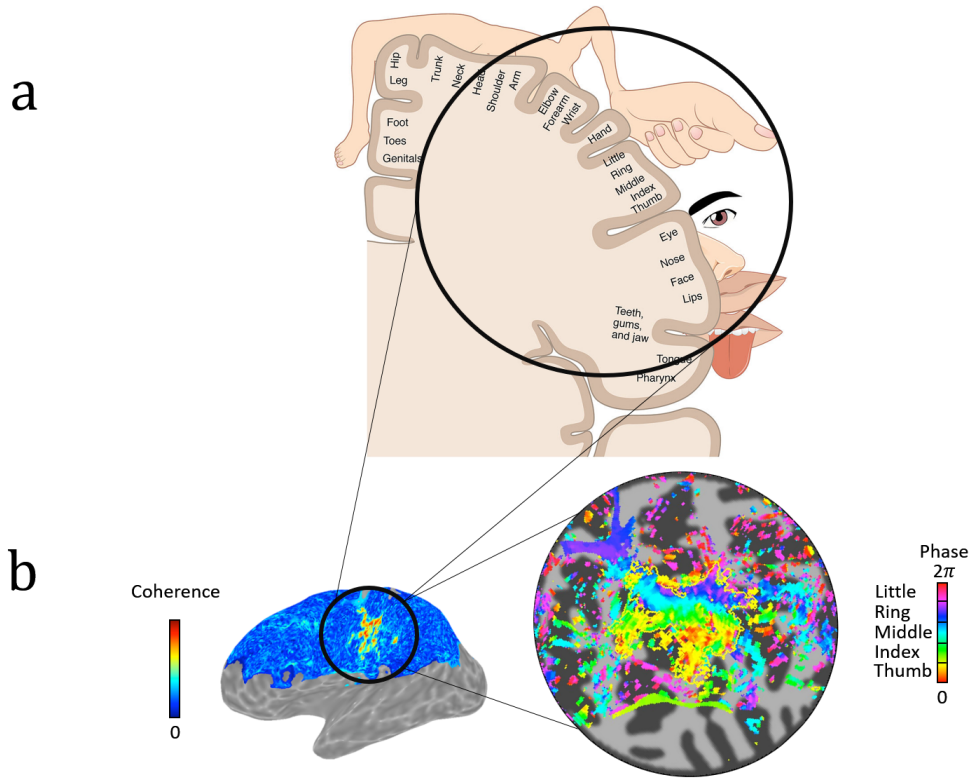

Figure 3.14: A) Schematic representation of the somatotopic representation of different body parts in the primary somatosensory cortex showing that there is well defined borders between them. Illustration from Anatomy & Physiology, Connexions Web site. http://cnx.org/content/col11496/1.6/. B) Inflated surface showing the overlay of the coherence with the frequency of stimulation of different digits. Largest coherence is seen over the SI (circled) and once this transformed into the corresponding phase values, as seen in the flat map, different fractions of 2 correspond to the stimulation of different fingers.

3.2.7 3D Cortical Flattening and Surface Based Atlas

In order to visualise and interpret the spatial locations of the SI regions underlying representation of different digits, cortical reconstruction and flattening was used. This is crucial for the fMRI experiments as finger areas in the brain can be located at the bottom of the sulci of the grey matter and due to the highly folded nature of the human brain visualisation can be difficult. In this thesis, Freesurfer (http://surfer.nmr.mgh.harvard.edu/, Fischl, 2012) was used to to achieve surface reconstructions of grey matter as this brain tissue is responsible

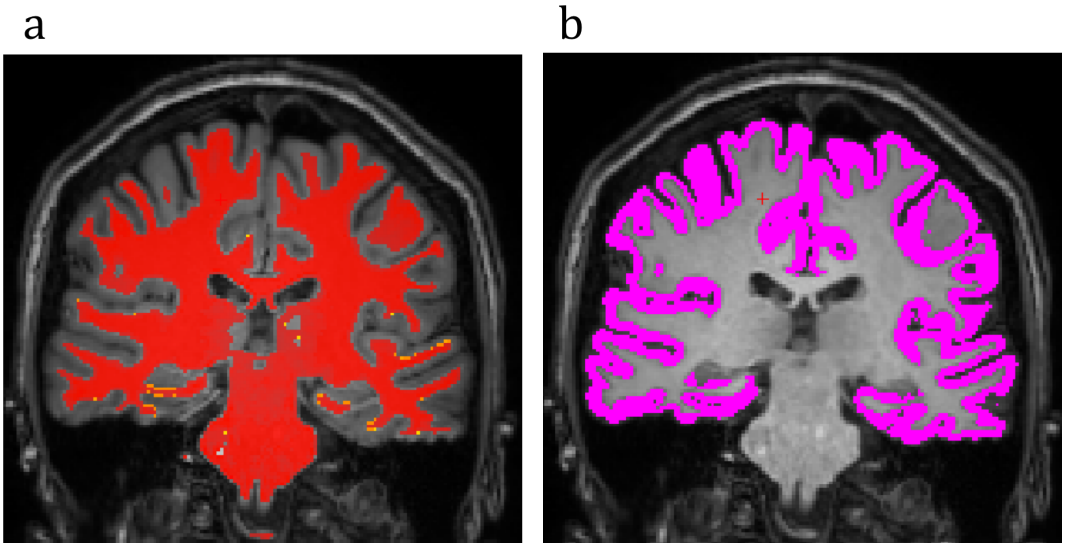

Figure 3.15: A), Freesurfer results of white matter segmentation in red, overlaid on a anatomical brain image. B) results of extending the boundaries of the white matter until there is an intensity drop in the MR signal, and therefore finding the limits of the grey matter, in pink.

for the generation of the signals of interest.

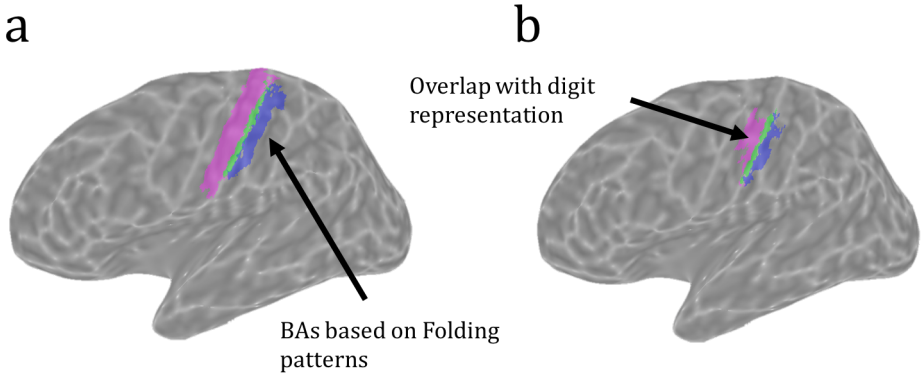

Figure 3.16: A), Freesurfer results of white matter segmentation in red, overlaid on a Anatomical brain image. B) results of extending the boundaries of the white matter until there is an intensity drop in the MR signal, and therefore finding the limits of the grey matter, in pink.

The pipeline starts by using a T_1-weighted image and registering it to an MNI template (Collins, Neelin, Peters & Evans, 1994), assuring that all dimensions and orientations are properly arranged, as different unfolding/reconstruction templates will be used in the later stages. Then, image intensity is corrected and normalised by using different points of the white-matter estimated from the template locations and divided by the estimated variation across voxels to remove

potential intensity bias caused by the receiver coils. This allows for the next step, skull-stripping, to occur with as much accuracy as possible as different tissues will have specific intensity ranges that do not overlap. Using machine-learning algorithms, the boundaries of the white matter are classified, and then right and left hemisphere are separated based on the location of the corpus callosum and pons, which are heavily dense white matter structures. An initial white matter segmentation is generated by filling the space outside this boundary using the intensity ranges that do not correspond to white matter (see Figure 3.15). Then, grey matter segmentation is generated by expanding the outer boundaries of the white-matter until there is significant drop in the intensity, which suggests that there is no more relevant brain tissue. This process is highly dependent on the quality of the skull-stripping procedure, as dura matter can remain and that can have similar intensities to the grey matter, therefore manual corrections were used to complement this step. The distance between grey and white matter boundaries give the cortical thickness at each location in the cortex; this an important measurement, as it allows one to compute the curvature and surface area of the brain, which then allows the surface to be tessellated and reconstructed to create a 3D visualisation.

Another important step is the inflation and specification of the surface as it allows registration to an anatomical atlas based on the folding patterns of the brain (see Figure 3.16) but also allows the flattening of the sections of the cortex (see Figure 3.16). Fischl et al., 2007 showed that folding patterns can be used to predict the underlying cytoarchitecture of different Brodmann areas (BA).

In this, they used their Freesurfer algorithm to reconstruct the 3D surfaces of 10 post-mortem brains. They conducted a histological study and mapped 8 BAs

of 10 different brains. Then, they found the probability distribution of different subjects' curvature parameters falling within the BA labels that were histologically defined. This resulted in showing that folding patterns can accurately predict boundaries of BAs with good spatial overlap between subjects. As explained in Chapter 1, I have developed hypotheses with explicitly reference to BAs 1, 2 and 3, and therefore this method was used to separate them based on subject specific folding patterns.

Chapter 4

Repetition priming of Abnormal Finger Postures: Behavioural study and fMRI piloting

4.1 Overview

In this chapter I address the first hypothesis of this thesis that the primary somatosensory cortex (S1) of humans has simulative qualities through which humans are able to develop an understanding of others' feelings. This hypothesis relies on the hierarchical processing structure of the S1 (Iwamura, 1998) and the vicarious network model proposed by Keysers et al. (2010), see Chapter 1 section 1.2: *Hierarchical Primary Somatosensory Cortex*; and section 1.3: *Vicarious Activation in SI*. This chapter is divided into two sections; in the first, I report the results of a behavioural experiment in which I first test a finger abnormal-

ity priming paradigm and in the second I report fMRI results using the same paradigm in two pilot subjects.

4.2 Repetition Suppression of Finger Postures

4.2.1 Behavioural Priming

4.2.1.1 Introduction

Repetition suppression (RS) is said to occur when the fMRI BOLD response reduces after repetition of the same stimuli (Grill-Spector et al., 1999; Grill-Spector, Sayres & Ress, 2006; Cross, Mackie, Wolford & Hamilton, 2010), this also is known as fMRI adaptation. For example, in Cross et al. (2010) BOLD activity differences related to the observation of bodies in contorted or normal postures was found after repeated observation of the same posture. In their paradigm they used the repetition of contorted bodies to sharpen the location of the hemodynamic response, and compare it to the activation of repeated body postures in normal postures. They found activity differences in both the extrastriate body area (EBA) and fusiform body area (FBA). The usefulness of RS for the purpose of the behavioural research conducted in this section, is promoted by the idea that lowering of the BOLD responses suggests priming, i.e. a facilitation process, which is linked with performance improvement both in reaction times and accuracy, and may underline the adaptation findings from earlier studies on the early visual areas (Henson & Rugg, 2003; Wig, Grafton, Demos & Kelley, 2005).

The link between priming and suppression is overwhelmingly seen across the literature (see Vuilleumier, Henson, Driver & Dolan, 2002; Wig et al., 2005; Grill-Spector, Sayres & Ress, 2006). Therefore, in preparation for the fMRI study of

repetition suppression, I investigated whether the underlying neural processes of embodied simulation would manifest in a behavioural measure. As such, the aim of this behavioural study was to demonstrate that it is possible to facilitate finger abnormality detection using a repetition suppression paradigm. To explore the effect of different viewing perspectives, as done in the experiments in Chapter 2 the hand (right) will be shown in egocentric and allocentric perspectives. Similarly to what was shown in Section 2.3.1, viewing hands in dorsal postures induces a proprioceptive reliant processing style. Consequently, in order to investigate the processing of the viewed abnormality, priming will occur either in congruent or incongruent perspectives with respect to the target stimulus. It was hypothesised that: 1) primed stimuli elicit faster RT and better accuracy than unprimed; 2) primed stimuli in first person perspectives have faster response times and accuracy, as no mental rotation of the stimulus will be necessary (and possible interaction with no. 1); and 3) primed stimuli have slower RT and accuracy when the prime is presented in incongruent perspectives (and possible interaction with no. 1).

4.2.1.2 Methods

Subjects. A total of 24 subjects (male = 4, female = 20) participated in this experiment (mean±SD = 19.72 ± 2.03 years). This experiment was approved by the ethics committee of the School of Psychology (Ref: 440).

Stimuli. Subjects that took part in this experiment had their hand modelled as explained in sections 2.3.1 and 2.3.2. In preparation for the experiments, scripts were developed to create a large number of stimuli. The scripts applied eight different angles of distortion (10°, 15°, 20°, 25°, 30°, 35°, 40°, anticlock-wise

along the x- and z-axis) to the joints between middle and distal phalanges of the index, middle and ring fingers of the subjects' 3D modelled right hand. Images for each distortion combination were rendered using Blender (see Figure 4.1). The levels of distortion for this experiment were picked based on pilot experiments and visual judgement of the experimenter. Distortions selected were 20° and 30° along the x- and z-axis. The 30° distortion was always used in the priming stimuli, and the 20° distortion was always used in the target stimuli. The reason behind this combination of prime/target distortion was to ensure that priming stimuli were having the desired effect, and the priming was raising detection above the no-priming levels.

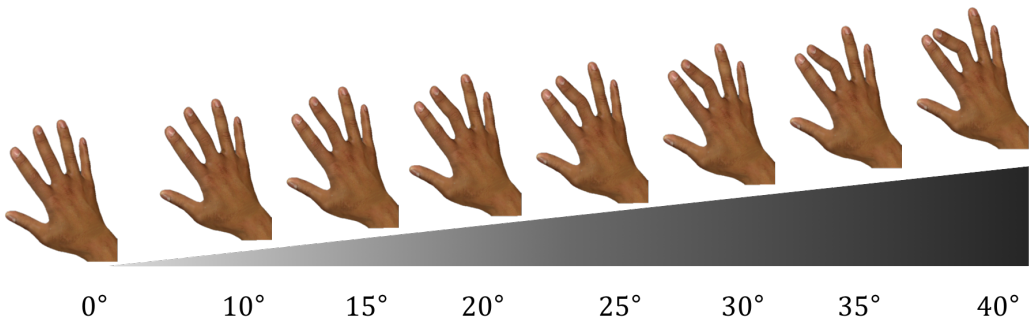

Figure 4.1: Depiction of the different images created for the pyschometric study to find different percentages of detection. Each finger was presented for 1 second in random fashion 4 times, and was always preceded by a white noise mask that jittered between 0.25s and 0.5s. Subjects had to respond within the 1s finger presentation in a 2 choice decision task.

To explore changes in the detection probability of different angles of finger distortions, and in particular to validate the choice of the 20° and 30° distortions, a short psychometric study was conducted after this experiment, but reported now for simplicity. Ten subjects viewed 8 previously collected hand models, with 7 angles of distortion applied to each finger. Each finger was presented for 1 second in a random fashion, 4 times, and always preceded by a white noise mask that jittered between 0.25s and 0.5s. Since distortion related responses are occurring more frequently, an extra 16 natural finger posture images were added

in order too many button presses in a row. This created a total of 272 finger presentation trials with the experiment lasting 6min14s. Only the dorsum view was investigated.

Subjects had to complete within the 1s of stimulus onset a 2 choice decision task (distortion or no distortion). To respond, subjects where instructed to press the left or right arrows of a keyboard. Button instructions were reversed half-way through the task. It was found that the 20° distortion had a detection rate of 60±0.52% and the 30° distortion had a detection rate of 75±0.076% (see Figure 4.2). Therefore,the initial choice of stimuli was justified however, using 15° would have lead to better representive of change level

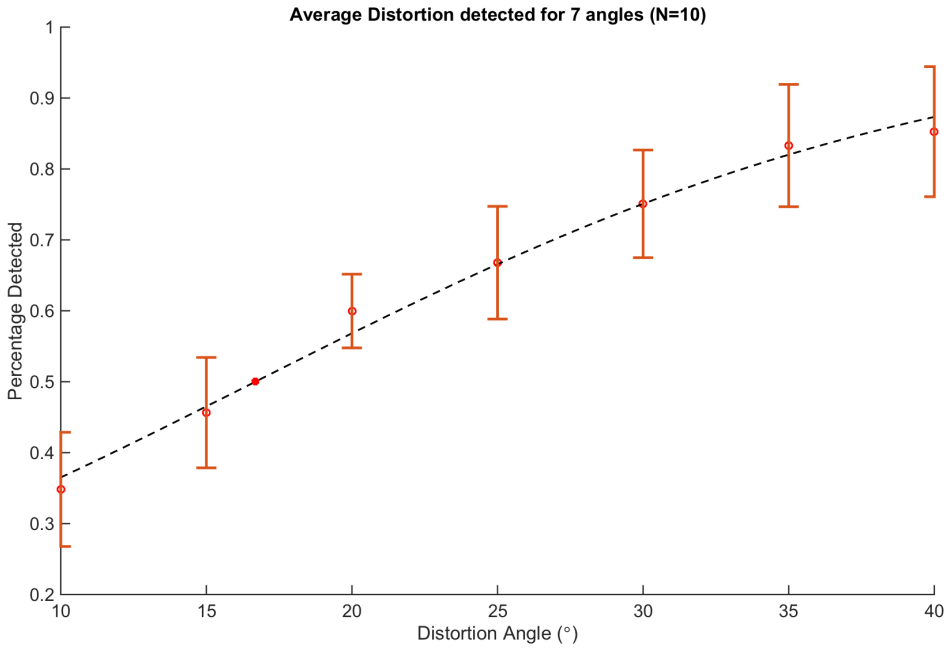

Figure 4.2: Results of the psychometric study conducted on different levels of distortion. Red dots represent individual points for each condition, and dashed line is an interpolation of those values using a psychometric sigmoid function. Accuracy to distortion identification at 10°= 34%, 15 = 45%, 20° = 60%, 25 = 66%, 30°= 75%, 35° = 83% and 40° = 85%. Red dot indicates 50% accuracy. Bars indicate the standard error of the mean.

Procedure. The design of this task was influenced by Cross et al. (2010), a fMRI study where a repetition paradigm was used in which subjects observed

static images of normal and contorted bodies, in new or repeated perspective, or in new or repeated configurations. For this experiment, different condition categories were presented as trials consisting of 3 events: a neutral hand posture (i.e. natural), followed by a prime, which could be a hand either of natural or distorted fingers in ego- or allocentric perspective, followed by the target which was always distorted aside from catch trials (where a natural hand was shown in a randomised fashion in 1/7 of the trials), see Figure 4.3. To remove effects of attention to specific regions of the screen, the position of the hand image was randomised to 0 or 2 cm along the x and y axis. A mask of white noise, with a blue fixation mark of size 2 cm, preceded each event in order to remove possible illusion of motion. Each hand stimulus was presented for 1 second, and the fixation mark duration was either 0.5 or 1 seconds.

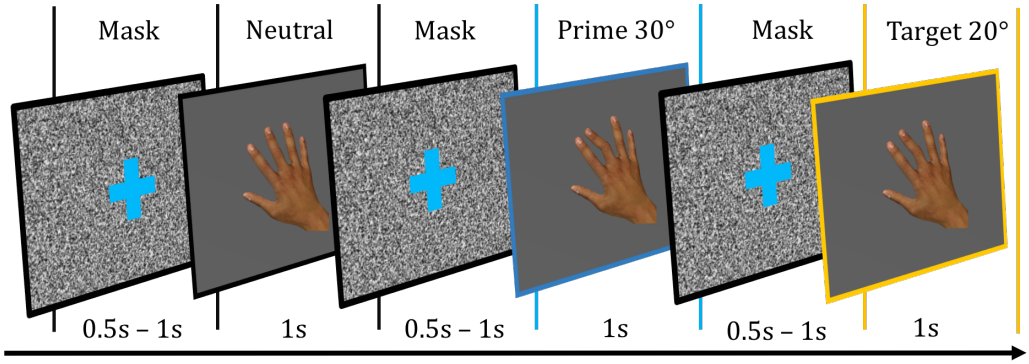

Figure 4.3: Depiction of a congruent primed trial. The target was the same picture as the prime but showing a distortion of 20° instead of 30°. In unprimed situations, the prime is natural and the distortion is random. For each event in the block the subject was instructed to press a button if distortion is detected or press a different button if not detected.

A 2x2x2 design was created (see figures 3 and 4): *distortion priming* (Unprimed, Primed) x *perspective of prime* (congruent, incongruent with target) x *perspective of target* (egocentric, allocentric); 16 trials per condition (*3events*8conditions) = 384 events, meaning the task took approximately 13 minutes to complete. The target, when distorted, showed the same type of 20° distortion as the prime 30° prime, and always presented on the same finger. This was done in order to ensure:

1) the image was not exactly the same but still of the same priming category; and 2) any carry over effects of priming would be easier to measure if the target is harder to detect.

After consenting to take part in the experiment, subjects were asked to sit inside an experimental cubicle 60 cm away from the experimental monitor. After being verbally instructed on how to complete the task, they engaged in two 2 minutes practice sessions with feedback indicating whether their response was correct, incorrect, or needed to be faster. After finishing the experiment, subjects were either given an inconvenience allowance or research participation credits.

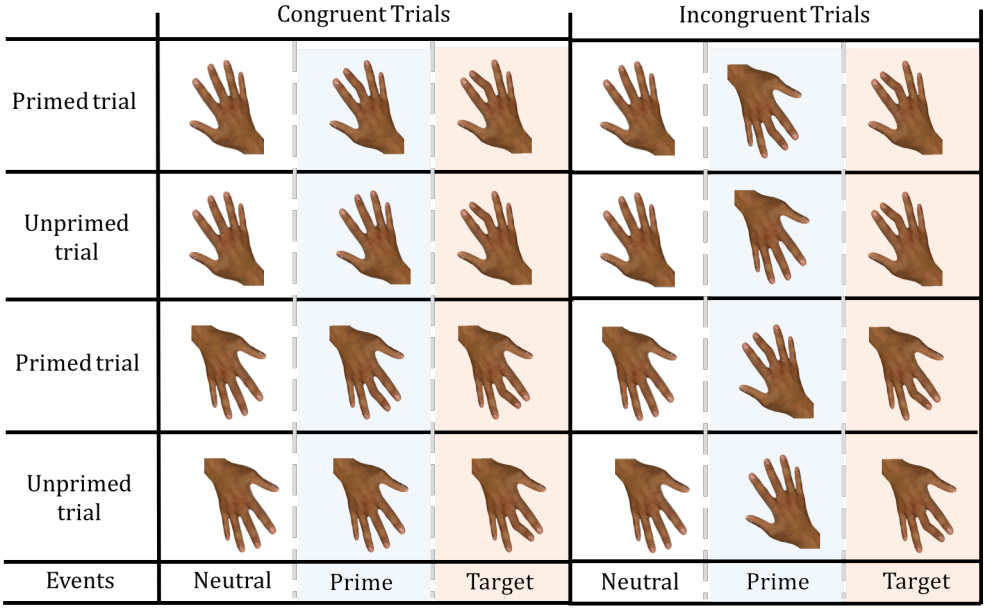

Figure 4.4: Design table of repetition priming. This structure also used for the fMRI experiment. Each row shows a prime and target events for primed and unprimed trial blocks. Each cell shows a hand image which follows the progression of the trial structure. Neutral events are not shown as they are not relevant for the analysis and overall design structure.

Analysis. In order to investigate priming effects of the finger distortions and perspective, a 2x2x2 *distortion priming* (Unprimed, Primed) x *perspective of prime* (congruent, incongruent with target) x *perspective of target* (egocentric, allocentric) ANOVA was conducted on reaction time and accuracy for the target event (refer to Figure 4.3 structure for trial structure). Reaction time analysis

was restricted to trials with responses during the presentation of stimulus (1000 ms) and after 200 ms (valid trials). Accuracy (acc.) was calculated as no. of correct responses/total trials. Bonferroni correction at α= 0.05 was applied to all follow-up t-tests.

4.2.1.3 Results

Reaction time analysis. The ANOVA (see Figure 4.5) identified a main effect of congruence, F(1,23) = 8.491, p = .008, on the RTs of distortion identification, such that congruent targets with the prime (mean±SE = $.670 \pm .009$), had faster reaction times than incongruent targets (mean±SE = $.694 \pm .010$). A main effect of distortion priming was also found, F(1,23) = 7.496, p = 0.012, such that targets that were primed with distortions ((mean±SE = $.672 \pm .080$), also had faster reactions times compared to unprimed ((mean±SE = $.692 \pm .011$). A significant congruence x Priming interaction was found, F(1,23) =8.117, p = 0.01. In order to investigate this interaction, conditions were averaged across perspective and a t-test conducted on congruent primed and unprimed stimuli (see Figure 4.6). Four two-tailed paired-samples t-tests were conducted between all conditions, and a significant difference was only found for the congruent primed vs. congruent unprimed comparison t(23) =-4.569, p <0.001, 95%CI = $-0.054, -.020$, such that congruent had significantely shorter reaction times (difference = $-.036 \pm 0.001$). This indicates that priming is having an effect on the speed of the response, although only in congruent trials (see Figure 4.6).

Accuracy analysis. An ANOVA was conducted on acc. and a main effect of congruence, F(1,23) = 5.209, p = .032, such that congruent primes (mean±SE = $.693 \pm .027$) elicited better detection of the distortion then incongruent primes

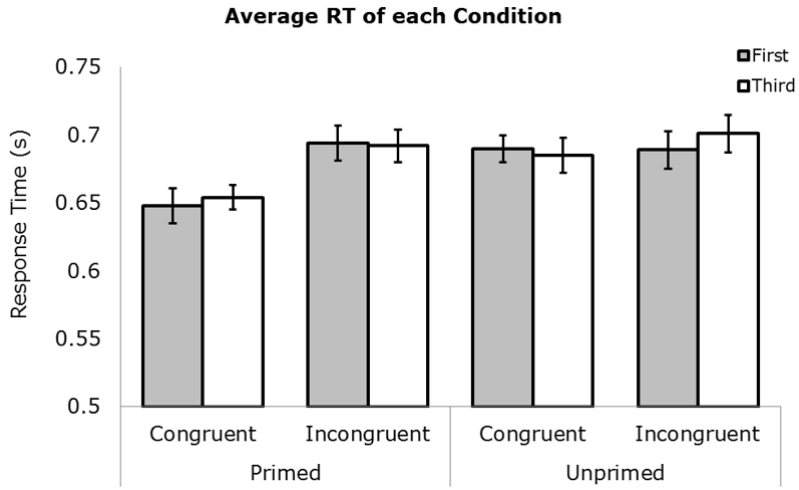

Figure 4.5: Bar graph showing the responses times for each condition. Only valid trials were included, that is trials where the responses were within the 1 s presentation window and after 200 ms. Error bars represents the standard error of the mean.

(mean±SE = .654 ± .032), and a main effect of perspective, F(1,23) = 13.675, p = 0.001, were found such that egocentric primes (mean±SE = .712 ± .031) than allocentric primes (mean±SE = .635 ± .030). A significant interaction between congruence x Priming, F(1,23) = 30.066, p <0.001, and perspective x priming, F(1,23) = 4.641, p = 0.042, was found (see Figure 4.7 and 4.8, left).

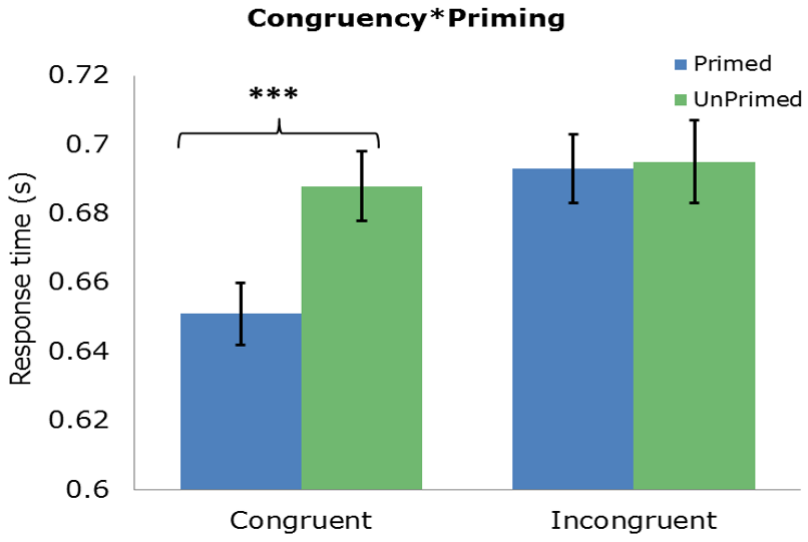

Figure 4.6: Results of collapsing the erspective conditions. The ANOVA indicates a significant difference between congruent conditions, such that priming had a significant facilitation effect on distortion identification. ***, p <0.001.Bars represent the standard error of the mean.

In order to investigate the interaction of priming and congruence, the per-

spective condition was averaged and four t-tests were performed across these collapsed conditions (see Figure 4.8). A significant difference was found between congruent primed (mean±SE = .747 ± .032) and unprimed conditions (mean±SE = .637 ± .031), t(23) = 3.643, p <0.006, such that when priming occurs in the same perspective as the target, detection of distortions is improved. A significant difference was found between incongruent primed (mean±SE = .608 ± .036) and unprimed conditions (mean±SE = .701 ± .035), t(23) = -2.973, p = 0.042, such that unprimed incongruent targets had better accuracy in the distortion identification task. Lastly, the t-test between primed incongruent and congruent showed that congruent primed targets had significantly better accuracy than primed incongruent targets [t(23) = 4.889, p <0.001] (see Figure 4.8, left).

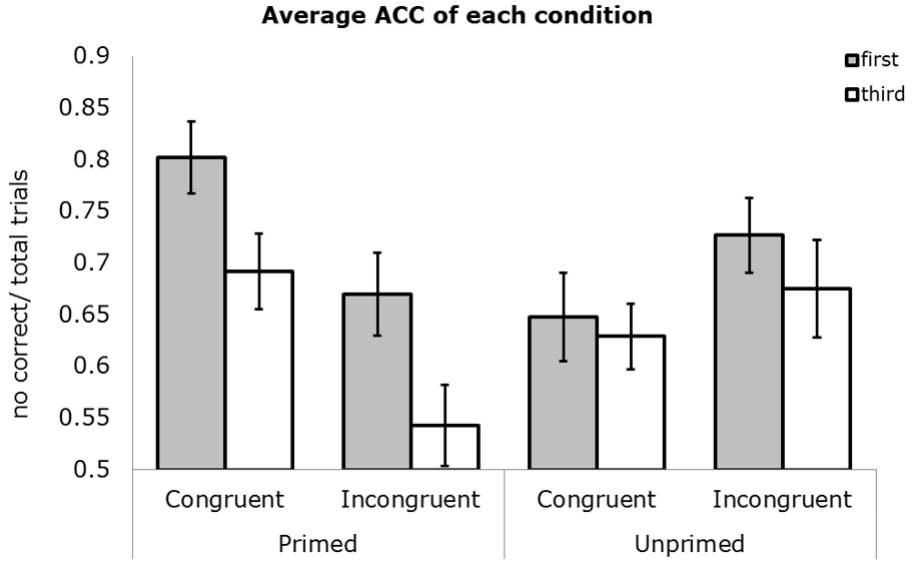

Figure 4.7: Bar graph showing the accuracy for each condition. Only valid trials were included, that is trials were the responses were within the 1 s presentation window and after 200 ms. Bars represent the standard error of the mean.

In order to investigate the perspective x priming effect further, congruence conditions were averaged and t-tests were conducted on primed and unprimed stimuli in each perspective. A significant difference, t(23) =5.450, p <0.001, error= .0217, was found between egocentric and allocentric perspectives such

that having the finger distortion in egocentric perspective facilitated distortion (mean±SE = .736±.033) detection for targets compared to allocentric (mean±SE = .687±.036). No other significant differences were found (see Figure 4.8, right).

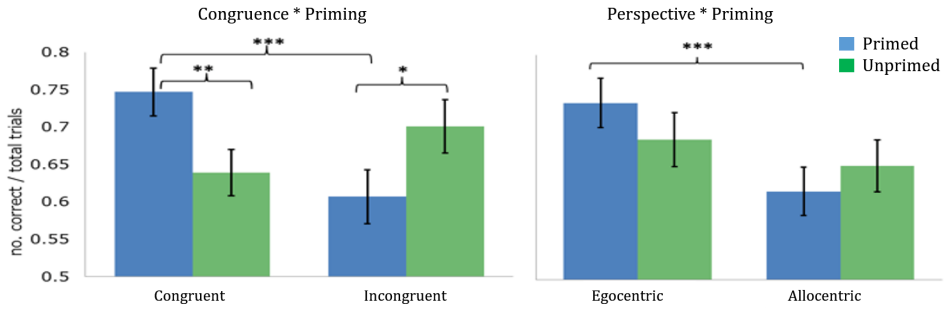

Figure 4.8: To the left, results of collapsing the perspective conditions. The ANOVA indicates a significant difference between congruent conditions, such that priming had a significant facilitation effect on distortion identification, but only in congruent condition. To the right, results of collapsing congruence the prime across conditions. Significant difference between targets in egocentric and allocentric, such that finger distortion in the former had better accuracy. * p <0.05, ** p <0.01, *** p <0.001. Bars represent the standard error of the mean.

4.2.1.4 Discussion

Results showed improvements of RTs and accuracy by finger abnormality priming. An interaction between congruence and priming was also observed such that congruent targets with priming elicited faster RTs and better accuracy compared to primed and unprimed incongruent targets, but also incongruent targets. The finding of slower RT suggests that subjects engage with the orientation of the hand in the priming event to determine whether or not it is distorted, creating a frame of reference in that perspective. Then, if the finger is primed by a distortion in an incongruent perspective, subjects mentally rotate the hand back to the frame of reference created by the prime in order to detect the distortion (which explains increase in RT and poorer accuracy). In other words, first subjects mentally rotate the observed hand to match the position with their own,

and then compare it with the known body schema of hand aspect to decide if there is an abnormality.

Note that this explanation is different to the one offered in section 2.3.1, where I suggested that the subject mentally rotates their own hand to match the observed (Parsons, 1994). The reason behind this alternative explanation, is that if the target and the prime are both in the allocentric perspective, distortion detection still occurs faster than in unprimed targets of the same perspective. A similar explanation can be offered from looking at the accuracy of targets which have been primed in incongruent perspectives; compared to the unprimed targets, the incongruent primed ones have significantly reduced accuracy, indicating the rotation mechanism proposed above. This should lead to prolonged decisions and be more prone to errors. It is likely, then, the RT results in the *Laterality of Hands Task* (see section 2.3.1) are also explained by this order of mental rotation processes.

These findings are a positive indication that priming alters the perception of the finger distortions and that finger abnormalities induce embodied simulation, at least behaviourally speaking. Furthermore, quite a few subjects anecdotally reported that when they were using their index finger to respond to the detection of a distortion in the same finger, they felt an interference effect that prevented them from responding as quickly as possible. This suggestion is in line with the embodied process proposed here, and an experiment comparing responses measuring performance of finger responses to perceived distortions on that same finger versus another (index versus thumb responses to observed distortion applied to index or thumb) could provide further evidence of an embodied simulation mechanism.

Another factor that could further validate the results of this experiment is is to vary the aspect of the hand ranging from a real hand, a minimal representation (such as the low-resolution bones I used in for the modelling of the hands in chapter 2, section 2.2), and non-hand stimuli such as chairs (as used in chapter 7) or tree branches as used in Taylor, Wiggett and Downing (2007); Taylor, Roberts, Downing and Thierry (2010).

In conclusion, assuming the correlation between priming and fMRI suppression, it is feasible that this design should be advantageous to an fMRI experimental design and lead to increased CNR.

4.2.2 fMRI Repetition Suppression

4.2.2.1 Introduction

Through the use of repetition priming in the previous section, I showed that observing distorted finger postures elicits a form of embodied stimulation. In order to confirm this assertion, I need to show activity overlap with the S1 areas that are responsive to direct tactile stimulation in order to demonstrate that the same neural structure underlying direct experience is also used for vicarious ones. Issues such as weak CNR, and voxel specificity to different perspectives are addressed here with an event-related repetition suppression design. This type of design benefits of being more sensitive to changes in suppression (Grill-Spector, Sayres & Ress, 2006), and because it presents a randomised order of stimuli, short-lag repetition effects are maximised, increasing the effect of suppression. Therefore, by achieving strong CNR, I aimed to map differential responses to the activity of egocentric and allocentric images of distorted fingers at the sub-region level of the S1.

If the *primed<unprimed* contrast elicits activity around the vicinity of the S1 hand area, then the study will acquire further data of finger specific somatotopy using vibro-tactile stimulation. If overlap is found between the contrasts and tactile-defined regions of interest, it would be possible to infer on whether observing finger abnormalities leads to overlapping S1 activity, and the existence of a embodied simulation mechanism that supports vicarious experience.

4.2.2.2 Methods

Subjects. Two right-handed subjects (1 female aged 20, and 1 male aged 27) volunteered to take part in this pilot study. No previous histories of psychiatric or neurological conditions were reported. This study received approval from the University of Nottingham Ethics Committee (ref:B/01/2011). Subjects provided written consent and were given £15 for the inconvenience.

Stimuli Procedure. For each subject a 3D hand model was created from photos taken few a days before the scanning, and three types of images were created, a normal hand posture, and distorted finger postures for index, and middle and ring fingers at 20° and distorted postures at 30° of distortions across the x- and z-axis. For more details see section 2.2.

In this study a similar stimuli sequence to the behavioural experiment was used: 2x2x2 *distortion priming* (Unprimed, Primed) x *perspective of prime* (congruent, incongruent with target) x *perspective of target* (egocentric, allocentric). Each condition trial was organised in 3 different events: Neutral + mask; Prime + mask; Target + Mask (see Figure 4.4 for trial structure, and see Figure 4.9 for example of new trial sequence). The duration of the hand stimuli was the same as the behavioural study, but the length of the mask varied between 1 and 1.5

seconds, such that the onset of a trial occurred at the start of a TR or inbetween TRs (at 50% of the interval between volume onsets). In order to have a trial length that was not repetitive whilst ensuring reasonable fMRI run duration, 58% of trials with a duration of 6s (mask and stimuli both 1 s), 22% trials with a duration of 6.5 s (one mask with 1.5 s duration, others 1 s), 11% with a duration of 7 s (2 masks with 1.5 s), and 6.6% with 7.5 s (all masks had a duration of 1.5 s) were presented to the subjects. In total per scanning run, for the first subject, 8 trials for each condition were presented (64 in total) plus 4 randomised catch trials in which there was no distorted finger posture; for the second subject, 5 trial blocks were presented (40 in total) per condition relevant trials plus 4 catch trial blocks in which there was no distorted finger posture.

In order to keep the task closely related to the behavioural one as well as maintaining the attention of the subject, a probing task was included in the design above. Four probes were inserted into the trial sequence such that they would only occur after a target was presented (see Figure 4.9). The probing block was indicated by a reduction in opacity of the target event stimuli, informing the subjects of the start of the probing trial. The opacity change would only occur at the end of 1 s and the more opaque stimuli was presented for an extra 0.5 s. Afterwards, a probe was presented for 4 s which asked the subjects to press a left or right button on a MR compatible response pad for their desired response. The probing message consisted of two words placed on either the right or left of the screen indicating which side button to press. For example, left button for "Distorted" and right button for 'Natural'. 'Distorted" and "Natural' label positions were pseudo-randomly allocated to each side with a 50% frequency.

Before entering the scanner, subjects were verbally instructed on how to

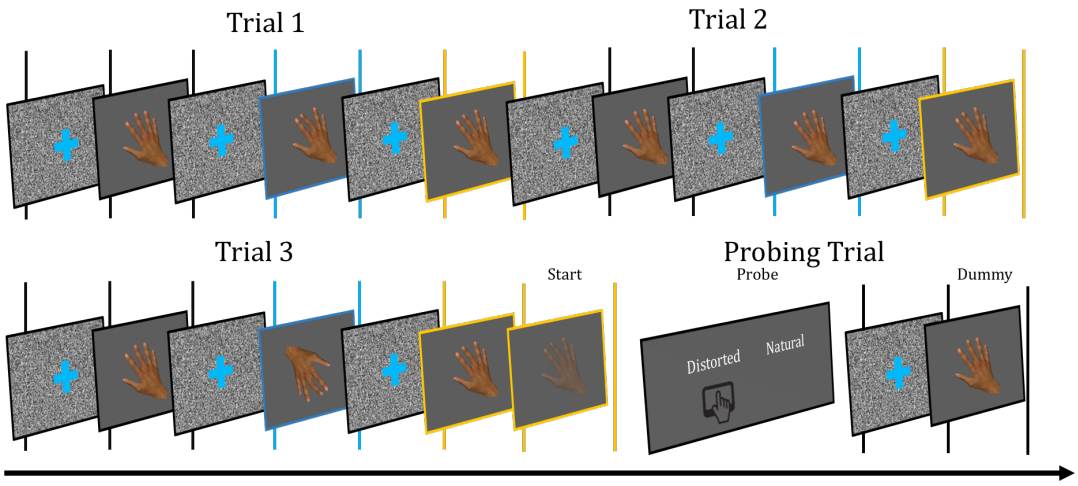

Figure 4.9: Depiction of the time line of 4 trials in the fMRI experiment. Trials 1 to 3 are normal trials for the conditions prime congruent, unprimed congruent, and primed incongruent. The probing trials starts with the reduction of opacity of the last target stimulus that lasts for 0.5 s. Then a message prompting a button response was seen and the subject had to indicate whether or not the last target was distorted or natural. This was followed by a white-noise mask, and then by a dummy stimulus that was always a hand with finger in the natural posture.

complete the task, and completed a 2-minute practice run where they had the opportunity to become familiar with the stimuli and the opacity changes. To avoid motor/somatosensory activity due to the button press, an extra dummy mask and natural hand posture was added after the question block in order to allow any button press related BOLD to scale down. Previous literature indicates that the hemodynamic profile for short sensory experiences are short-lived, lasting approximately 7-10 s (Rosen, Buckner & Dale, 1998). Therefore, by including the time after the button (average 2 s), the mask+dummy (2.5 s), and the events on the next block before the target (minimum 5 s), there is approximately 9.5 s to let the signal run its course. Due to this profile, combined with the event related paradigm, the effect of the button press should be negligible.

Data Acquisition. Data was collected on a Philips 7T Achieva system (Philips Medical Systems), using a volume transmit head coil and 32-channel receive coil (Nova Medical). To minimise head motion, foam padding was placed around the

subjects' head. Magnetic field inhomogeneity was minimised using image based shimming (see Poole & Bowtell, 2008; Sanchez-Panchuelo et al., 2010, for description in detail). High-resolution T_2*-weighted axial images (0.5 x 0.5 x 1.5 mm^3) were acquired with the same slice prescription and coverage as the functional data using a 2D-FLASH sequence (TE/TR = 10/906 ms, FA = 32°, SENSE factor = 2), allowing accurate registration with the whole head anatomical. A whole brain high-resolution T1-weighted anatomical data set was acquired using a Phase-Sensitive Inversion Recovery (PSIR) sequence (Van de Moortele et al., 2009; Mougin et al., 2016) for cortical segmentation and unfolding. The PSIR acquisition parameters where as follows: TE/TR = 3.9/12 ms, FA = 8°, 1mm isotropic spatial resolution, linear k-space phase encoding scheme, first train acquired at TI = 780 ms, second train acquired at TI = 2480 ms, 5000 ms cycle, total acquisition time = 4 mins 28 s. The first inversion time corresponds to the null point between grey and white matter, facilitating the segmentation of these two tissue types. Functional runs were acquired using T_2*-weighted, multislice, single-shot gradient echo EPI with the following parameters: TE = 25 ms, TR = 1.5 s, FA= 70°, field of view: 192mm x 208 mm in the right-left, anterior-posterior direction. A SENSE acceleration factor of 2.5 was used in the anterior-posterior direction and a multiband or simultaneous multislice factor of 2 included. This achieved 32 slices in subejct 1 and 22 slices in subject of 2 mm isotropic resolution. Brain volume was situated above the sylvian fissure. Each functional scan took approximately 9min × 4 runs or 5 min 20 s × 6 runs respectively for subject 1 and 2.

Data Analysis and Preprocessing Preprocessing All preprocessing, and analysis steps were conducted using mrTools (http://gru.stanford.edu/doku

.php/mrtools/) in MATLAB (The MathWorks, Natick, MA), and in-house scripts using FSL (https://fsl.fmrib.ox.ac.uk/fsl/, Smith et al. 2004). Functional data was realigned to the last volume (EPI reference frame) of the functional data set which was acquired immediately prior to the high-resolution anatomical T_2*-weighted FLASH data. All functional runs were detrended, high-pass filtered (0.01 Hz), and converted into percent signal change.

Statistics For each subject, functional data for target and prime events was modelled using a total of 12 regressors for each condition, and created by extracting their onset times: 8 regressors for the onsets of targets: Egocentric Congruent Primed (ECP), Egocentric Incongruent Primed (EIP), Egocentric Congruent Unprimed (ECU), Egocentric Incongruent Unprimed (EIU), Allocentric Congruent Primed (ACP), Allocentric Incongruent Primed (AIP), Allocentric Congruent Unprimed (AIU), Allocentric Incongruent Unprimed (AIU), 4 regressors for the onsets of primes: Egocentric Prime Distorted (EPD), Allocentric Prime Distorted (APD), Egocentric Prime Natural (EPN), Allocentric Prime Natural (APN). Each regressor was modelled by convolving a canonical HRF with a double-gamma function. A least-squares GLM was conducted and no spatial smoothing was applied. The following contrasts were calculated: all average, ECP<ECU, EIP<EIU, ACP<AIU, AIP<AIU, Primed (ECP + EIP + ACP+ AIP) <Unprimed (ECU + EIU + AIU + AIU). Additionally, the contrast Egocentric (ECP + EIP + ECU + EIU) <Allocentric (ACP + AIP + AIU + AIU) was computed. All statiscal comparisons were conducted using a one-tailed t-test which was corrected using false-discovery rate method (FDR, Benjamini & Hochberg, 1995).

4.2.2.3 Results

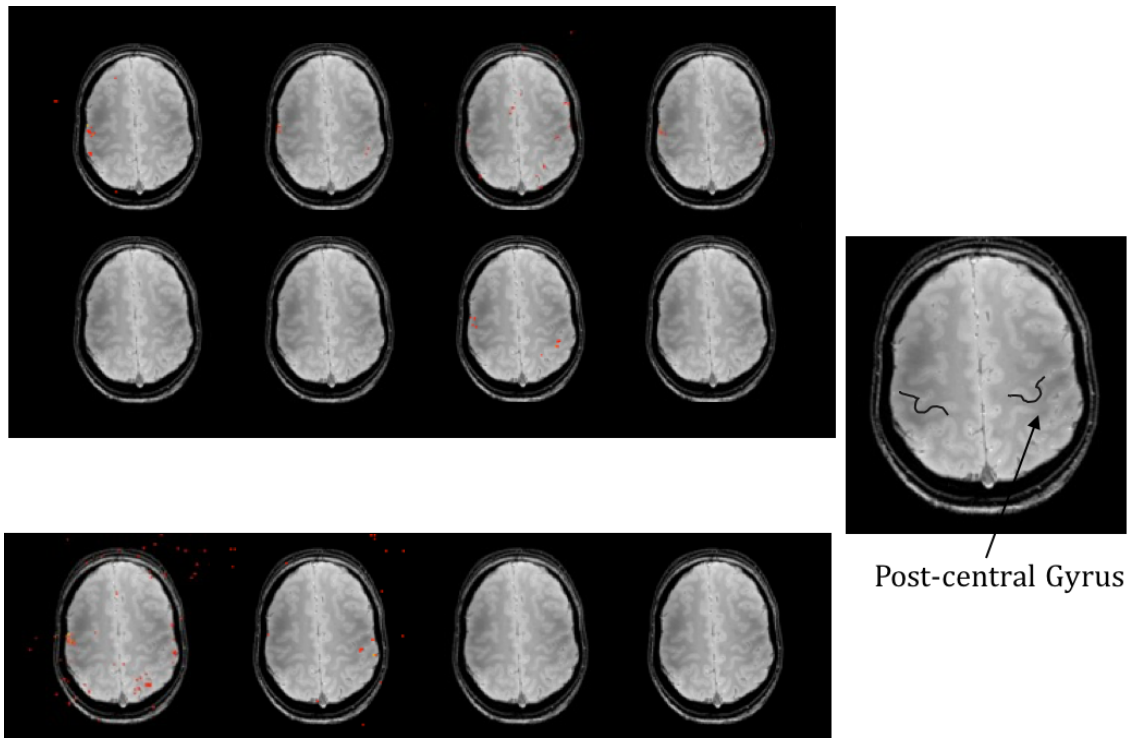

Figure 4.10: GLM results for subject 1 in neurological convention, and illustration of S1 inverted omega shape landmark (most right figure, black lines delineate M1 hand area). Top figure shows the results of the GLM for each regressor. Respectively, ECP, EIP, ECU, EIU, ACP, AIP, ACU, AIU. Bottom figure, GLM for the following contrasts, ECP <ECU AIP <AIU, Primed (ECP + EIP + ACP + AIP) <Unprimed (ECU + EIU + ACU + AIU), Egocentric (ECP + EIP + ECU + EIU) <Allocentric (ACP + AIP + ACU + AIU).

Only in subject 2 when compared to the null, condition specific regressors found activity on the primary somatosensory cortices. In subject 1, this was not apparent and further contrasts did not produce a significant activity (see Figure 4.10). For subject 2, activity was considerably stronger for allocentric conditions.

In several conditions there was significant activity at the supplementary motor (SMA) and bilateral motor areas (regions named based on visual landmarks). However, the activity patterns for AIU maps shows a considerable effect of motion as indicated by brain activity outside head (see Figure 4.11). Therefore, this regressor and its counterpart ACP were not included in the analysis. Aside from

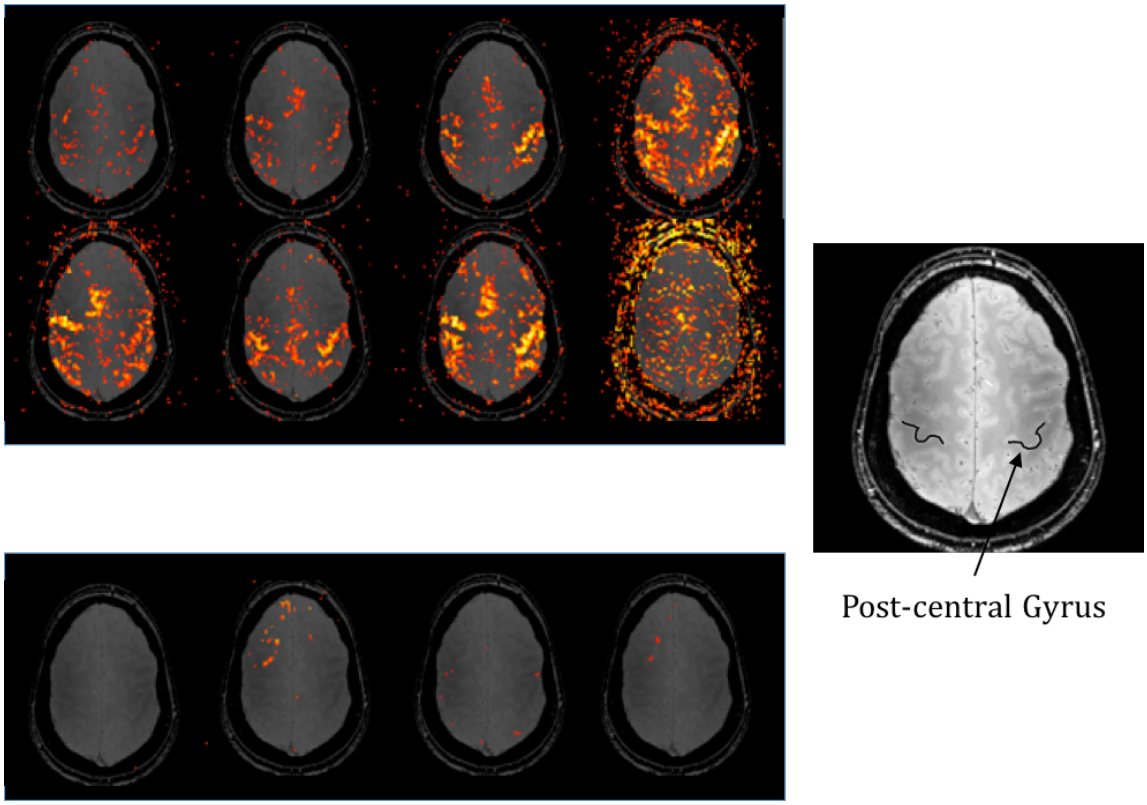

Figure 4.11: GLM results for subject 2 in neurological convention, and illustration of S1 inverted omega shape landmark (most right figure, black lines delineate M1 hand area). Top figure shows the results of the GLM for each regressor. Respectively, ECP , EIP , ECU , EIU , ACP , AIP , ACU , AIU. Bottom figure, GLM for the following contrasts, ECP <ECU AIP <AIU, Primed (ECP + EIP + ACP + AIP) <Unprimed (ECU + EIU + ACU + AIU), Egocentric (ECP + EIP + ECU + EIU) <Allocentric (ACP + AIP + ACU + AIU) .

AIP<AIU, which showed frontal activity, no significant activity was found.

4.2.2.4 Discussion

The single-subject GLM analysis provided weak to no results of interest. Indeed, it was observed that presentation of distorted finger postures lead to an increase in S1 activity when compared to chance. However, since no modulation was found for each of the contrast combinations, it is impossible to say that this design induced the desired effect. Data from both subjects does not permit straightforward interpretation: in subject 1, there was no significant effect of distortion priming, and in subject 2 strong movement artefacts were contaminating some of the conditions event after trimming trials and motion correction.

Other factors may have influenced the outcome of the two pilot experiments: In Grill-Spector, Sayres and Ress (2006) review of Repetition suppression, two methods of achieving suppression are outlined. First, blocking the repetitions and comparing the BOLD signal from the first presentation leads to a predictable reduction in activity and increased CNR. The disadvantage of this is that it may include new cognitive processes such as prediction, and whilst a suppression effect may be seen, other areas may show an enhancement effect. Secondly, event-related repetition similar to what was done here, works by randomising where the suppressing stimuli occurs and measuring the reduction in the BOLD response between primed stimuli and unprimed stimuli. On the other hand, this reduction can be considerably smaller than the one seen in blocked designs and therefore weak CNR is observed.

Alternatively, the stimuli may not have been salient enough, that is, the distortions may not be strong enough to elicit an embodied response by the subjects. The findings of the behavioural study suggest this is unlikely, since distortion detection was influenced by both priming and congruence of prime. Therefore, it is possible that a small change in the design of the task may have led to the lack of the repetition effects. In the behavioural experiment subjects had to respond to every single event, leading to an increase in attention demands and more engagement of the simulation mechanism as evidenced by significant differences between congruence and priming. The attention probe only occurred 4 times in the fMRI experiment, and therefore subjects may not have been sufficiently engaged with the task and therefore creating low motivation for embodiment.

In conclusion, regarding the fMRI pilot experiments: The event-related design that was modelled closely on the behavioural experiment did not yield the

expected repetition suppression patterns in the S1. Possible explanations range from, small effect size, technical factors such as subjects' movement to regionally specific response properties in S1, that generate inconsistent responses with repetition suppression. It was not realistic to resolve this matter in the current PhD project. Therefore in the subsequent chapter, I use a simple blocked-design approach to search for vicarious S1 activation during perception of hand postures.

Chapter 5

Images of Distorted Fingers Activate Posterior Somatosensory Cortex: An Ultra High-Field fMRI Investigation

5.1 Overview

In the previous chapter, using repetition suppression, I attempted to find somatosensory activity in response to the observation of finger abnormalities by comparing the activity of the primed distorted postures versus non-primed postures. The results of the pilot analysis where inconclusive due to a variety of reasons, this led me to develop a more simplified block design which offers larger CNR between conditions. This was done to address the question of whether em-

bodied simulation occurs during the observation of finger abnormalities. The aim was to understand the contribution of different S1 sub-regions to this behaviour. Here, subjects were presented with images of computer-generated 3D models of their own, and another subject's hand where postural distortions were applied to the fingers. Images of natural finger postures served as control stimuli. Brain activation patterns to stimuli presentation were measured using high spatial resolution fMRI at 7T. Regions-of-interest defining S1 sub-regions were generated from fMRI data in response to tactile stimulation of the digits of the hand using a travelling wave paradigm in combination with and restricted to, probabilistic cytoarchitectonic maps for Brodmann areas 1, 2 and 3. Results showed a consistent pattern of activation in the contrast *Distorted>Natural* finger postures in BA 2 overlapping with regions that are also active to direct tactile stimulation. This supports the proposition that embodied simulation exists in the S1, which is typically involved in first person experience, and that the posterior area of S1, i.e. BA 2, is likely involved in the representation of abnormal body schematic information. The contents of this chapter are adapted from a manuscript now under editorial review for Brain Structure and Function[1].

5.2 Introduction

The ability to vicariously experience what others feel is a mechanism which enables a range of socially relevant processes. This has been termed embodied simulation as it is a result of somatosensory recruitment of the observer in order to simulate the somatosensory event that is taking place (Gallese, 2005).

In order to investigate this phenomenon, I used images of hands (created from photos of individuals' actual hands, see Chapter 2, 2.2), as they have large

[1]Manuscript co-authors were Rosa-Maria Sánchez-Panchuelo, Susan Francis, and Martin Schürmann

topographical representations in the S1 (Penfield & Boldrey, 1937) making them ideally suited to explore potential activity overlap between visual and tactile induced responses (see section *Vicarious Activation in SI*). Distortions were applied to the fingers of the 3D hand models' fingers to make them look as if they were abnormally postured (see Chapters 2 and 4). Previous responses to these kind of stimuli were found in the lateral occipital cortex using MEG (Avikainen et al., 2003) and also in S1 and primary motor cortex (M1) using 3T fMRI (Schürmann et al., 2011). Studies using touch observation paradigms also suggest the simulative quality of the somatosensory cortices, in particular of posterior S1 areas such as BA 1 and 2. In light of these studies, a model has been proposed (see *Hierarchical Primary Somatosensory Cortex* and *Vicarious Activation in SI*) where involvement of the S1 in embodied simulation increases from anterior to posterior (BA 3 to BA 2) sub-regions depending on the type of stimulus (direct touch vs. vicarious representation).

This study aims to explore the involvement of the S1 sub-regions in the representation of abnormal body schematic information through observation of distorted finger postures and natural finger postures. I take advantage of the increased spatial resolution afforded by using ultra-high field (7T) fMRI to create highly specific S1 ROIs on an individual subject basis using tactile stimulation of each finger. Then, these ROIs are used to restrict analysis of activity related to observation of different finger postures, again, on an individual subject basis.

The following three hypotheses are predicted: 1) Distorted finger postures (vs. natural) will elicit more involvement of posterior S1 regions (BA 2); 2) Own hands will elicit more activity on the corresponding hand region, with distorted own fingers inducing more posterior S1 involvement; 3) Distorted finger postures

in egocentric orientation will elicit more activity in the hand region than in the allocentric orientation.

5.3 Methods

5.3.1 Subjects

Approval for the study was obtained from the University of Nottingham Medical School Ethics Committee, and all subjects provided full written consent for all parts of the study. Fifteen subjects completed the Empathy for Pain Scale questionnaire (see Appendix A, Giummarra et al., 2015). Question number 2 of this questionnaire asks: 'When you see a person who has recently had a surgical procedure in real (e.g. they have stitches or bandaged amputation stump) do you feel: ...', followed by 14 items, among them '... Bodily sensations (e.g. tingling)' and '... Bodily Pain (e.g. stabbing, throbbing, etc.)'. For these two items (the ten other items that were not analysed), subjects were instructed to respond on a 5-point Likert scale (1= strongly disagree; 5 =strongly agree). They were also instructed to answer 1 if the scenario elicited no vicarious sensation whatsoever, in order to avoid any confusion about what each scale point meant.

Five subjects who scored 2 or higher on at least one of the items Bodily sensations or Bodily pain (see table 5.1) participated in the fMRI experiment (all right-handed by self report, 3 female; mean$\pm$SD = 26 ± 3 years). The questionnaire served to ensure that the five selected subjects responded vicariously to the stimuli. The ten non-selected subjects reported 'no feelings' in the free-text answer to question 2, or that they would judge the scenario from 'a medical/neutral approach'.

Table 5.1: . Empathy for Pain scale results, for the subjects selected for the fMRI experiments. All responses on a 5 point Likert scale (1= strongly disagree; 5 =strongly agree).

	'When you see a person who has recently had a surgical procedure in real (e.g. they have stitches or bandaged amputation stump), do you feel:'	
	'Bodily sensations, (e.g. tingling)'	'Bodily Pain, (e.g. throbbing)'
Subject 1	2	2
Subject 2	3	2
Subject 3	3	1
Subject 4	3	2
Subject 5	4	3

5.3.2 Stimuli

Tactile Finger Stimulation (TF): For each subject, the fingertips of each hand were stimulated using 5 independent piezo-electrical devices (http://www.dancerdesign.co.uk; Dancer Design, St. Helens, United Kingdom) to deliver tactile stimulation at 50 Hz. Two fMRI runs using a travelling wave paradigm (where each digit of the hand is sequentially stimulated) were collected for each hand. In one of the runs the stimuli followed a forward order (digit 1 to 5), and in the second hand a reverse order (digit 5 to 1). Each finger specific stimulation consisted of a period of 4 s intermittent stimulation (a total of 0.4 s long bursts of 50 Hz stimulation alternating with 0.1 s rest). One full hand stimulation (across the 5 finger tips) was 20 s in duration and each run comprised 12 cycles, leading to a total acquisition time of 4 minutes per run (see Figure 5.1, and Sanchez-Panchuelo et al., 2010 for more details on this travelling wave procedure).

Finger Postures Observation (FP): Stimuli were images of 3D models of hands, computer-generated using Blender software, see section 2.2). The bone

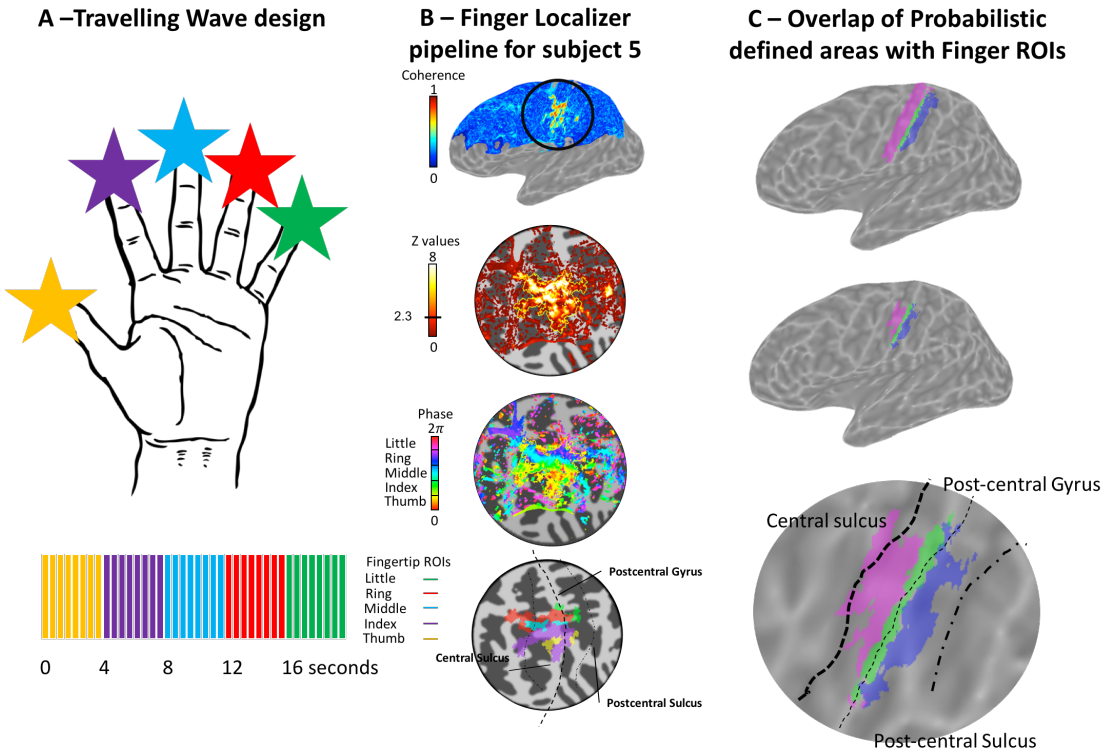

Figure 5.1: Example of the pipeline of analysis for the finger stimulation session to create fingertip ROIs to be used in the analysis of the distorted hand data. A – Timing of the travelling wave design. The finger tips of each subjects hands were stimulated sequentially. Each finger specific stimulation consisted of 4s intermittent stimulation (8 bursts of 0.4s blocks of 50 Hz stimulation alternating with 0.1 s gaps of no stimulation). Stimulation moved sequentially across the digits of the hand in a 20s cycle, which was repeated 12 times. B – Coherence, corrected p-values, phase, and finger ROIs displayed on the left hemisphere (top), and on flattened cortical maps (bottom 3 maps). Coherence values (middle top), were transformed into p-values (2nd map), and corrected using FDR to create a stringent finger specific response. To create the hand ROI, phase was divided into bins of $2\pi/5$ and for each bin, finger ROIs were defined and unified to create the hand region (4^{th} map). C – Top: Inflated right hemisphere with probabilistic Brodmann areas 3a + 3b (magenta), area 1 (cyan), and area 2 (red) acquired from Freesurfer recon-all routine. Middle – Brodmann areas overlapped with the finger ROIs defined in B, and in bottom Figure a zoomed in version.

structures controlling the wrist rotated by 1.5°, 1°, 8.3° (x, y, z) in order to mimic a similar perspective to that of viewing your own hand. A combination of clockwise and anticlockwise 40° rotations to the x-axis and anticlockwise rotations in the z-axis (either x: 0°/z: 40°, 40°/40°, -40°/40°, or 40°/0°) were applied to each finger (except the thumb) at the middle interphalangeal joint (between the intermediate phalanges and distal) in order to mimic an abnormality as they might occur after an accident (in total 16 distortions). Then hands were rendered with Blender camera presets (12:11 aspect ratio) with a focal length 35 mm, and

800 x 800 pixel resolution. Using this procedure, 7 individuals' hands (5 subjects for "own hand" stimulus, and an extra 1 female and 1 male hand for use as "other person's hand" stimulus) were modelled. Due to inter-individual differences in hand size and shape, manual adjustments were made in order to keep the ratio of hand to camera as similar between models as possible. Per hand, the procedure resulted in 16 images (4 per finger) of distorted finger postures (4 per finger) and 1 image of a natural posture. To create the allocentric perspective, images were rotated by 180° around the centre of the image. In order to hide the end of the hand model, as this may distract from the finger distortion, a Gaussian filter was applied to the centre of the image such that the edges of the images, and consequently the end of the model was blurred while the centre of the image remained visible. The other female or male hand model were rated unanimously by 8 individuals (not scanned) to belong to a specific sex category among a set of 14 hand models acquired for the experiment in Chapters 2 and 4.

The distorted postures fMRI paradigm consisted of a block-design of 20 s 'on' and 20 s 'off' period. Each 'on' block was of distorted finger postures, or natural postures, in ego- or allocentric orientation of the subject's own or another person's hand. 'Off' blocks consisted of a grey screen [RGB(64,64,64)] with a blue fixation mark (250x250 pixels, viewed at 10° visual angle). For the distorted blocks, for each finger, four different distortions were shown for 1 s, each followed by a grey screen which was shown for 0.25 s (16 postures per block). Each distortion, for a specific finger presentation, was randomised, as well as which finger shown (see Figure 5.2). The same stimulus timing applied to natural blocks, with an image of a natural posture shown 16 times. In a 500 s run, 12 'on' blocks were shown, out of which 8 were distorted blocks (own/other × ego-/allocentric, 2 blocks

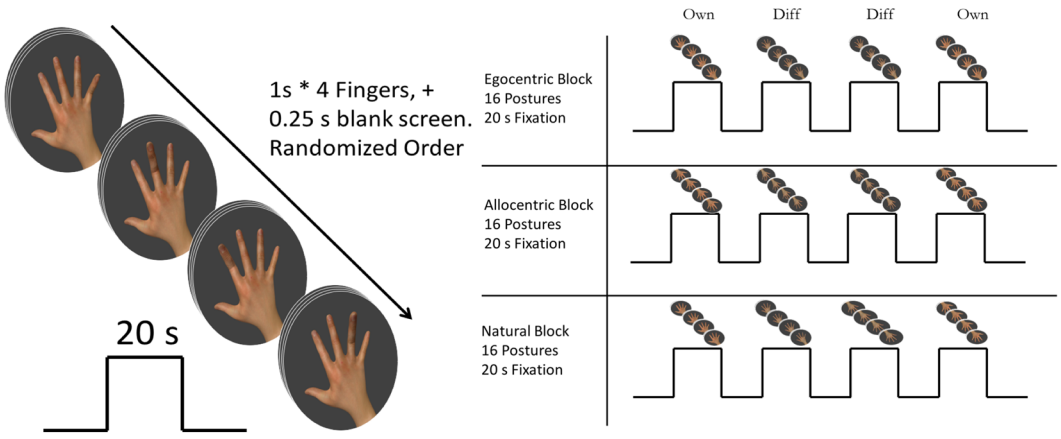

Figure 5.2: Left panel – Example of a distorted finger postures block. Each block lasted 20 s, starting with 4 different distortions presented for 1 s sequentially, then another 4 distortions for another finger, resulting in 16 stimuli for all four fingers. The order of distortions was randomised within each finger and between fingers. All stimuli were presented on a grey background. Right panel – Example of the progression of one full run consisting of pseudo-randomised Allocentric, and Egocentric perspectives of distorted finger postures and natural postures. Each run consists of 12 "on" blocks and 13 "off" blocks, resulting in a total duration of 500 s. In the distorted blocks, 16 distortions were shown as in the example in the left panel. In natural blocks, images of relaxed hands were shown. In order to track attention of the subjects, they were asked to count the number of opacity changes in the stimuli per run (accuracy >70% for all subjects). Run length was 500 s and four runs were conducted.

each) and 4 natural (own/other × ego-/allocentric, 1 block each). Within a run, the order of blocks was pseudo-randomised. Each subject completed four runs, separated by short breaks. The images of the hand were projected via mirrors to an MRI projection screen located at the front of the scanner bore. Subjects viewed the images on a grey background using prism glasses at 10° visual angle. In order to track attention, subjects were asked to count the number of times per run that they saw a change in opacity (100% to 60%) of the stimuli (1 subject 70%, 1 subject 80%, 3 subjects 100% correct count).

5.3.3 Data Acquisition

Two acquisition sessions for each experiment took place on different days. For both sessions the following acquisition methods apply. Data was collected on

a Philips 7T Achieva system (Philips Medical Systems), using a volume transmit head coil and 32-channel receive coil (Nova Medical). To minimize head motion, foam padding was placed around the subjects' head. Magnetic field inhomogeneity was minimized using image based shimming (Poole and Bowtell, 2008; see Sanchez-Panchuelo et al. 2010, for description in detail). High-resolution T_2*-weighted axial images (0.5 x 0.5 x 1.5 mm^3) were acquired with the same slice prescription and coverage as the functional data using a 2D-FLASH sequence (TE/TR = 10/906 ms, FA = 32°, SENSE factor = 2), allowing accurate registration with the whole head anatomical volume. In the first scan session, a whole brain high-resolution T1-weighted anatomical data set was acquired using a Phase-Sensitive Inversion Recovery (PSIR) sequence (Van de Moortele et al., 2009; Mougin et al., 2016) for cortical segmentation and unfolding. The PSIR acquisition parameters were as follows: TE/TR = 3.9/12 ms, FA = 8°, 1mm isotropic spatial resolution, linear k-space phase encoding scheme, first train acquired at TI = 780 ms, second train acquired at TI= 2480 ms, 5000 ms cycle, total acquisition time = 4 mins 28 s. The first inversion time corresponds to the null point between grey and white matter, facilitating the segmentation of these two tissue types.

Tactile Finger Stimulation session: For the four functional scans (2 forward and reverse for each hand), 26 axial slices spanning the primary somatosensory cortex were acquired using T_2*-weighted, multislice, single-shot gradient echo–echo planar imaging (EPI) with 1.5 mm^3 isotropic resolution (TE= 25 ms, TR = 2 s, FA = 75°, field of view: 192 mm x 192 mm in right to left, anterior to posterior directions). Each run took 4 minutes to acquire 126 volumes.

Finger Postures Observation paradigm session: Four whole-brain functional runs were acquired using T_2*-weighted, multislice, single-shot gradient echo EPI with the following parameters: TE= 25 ms, TR = 2 s, FA= 70°, field of view: 192mm x 208 mm in the right-left, anterior-posterior direction. A SENSE acceleration factor of 2.5 was used in the anterior-posterior direction and a multiband or simultaneous multislice factor of 2, achieving 52 slices of 2 mm isotropic resolution spanning the whole brain. Each run took 8 minutes and 20 seconds to acquire.

5.3.4 Data Analysis and Preprocessing

Preprocessing: All preprocessing, and analysis steps were conducted using mrTools (http://gru.stanford.edu/doku.php/mrtools/) in MATLAB (The MathWorks, Natick, MA), in-house scripts using FSL (https://fsl.fmrib.ox.ac.uk/fsl/, Smith et al., 2004). Surface reconstructions were performed using Freesurfer (http://surfer.nmr.mgh.harvard.edu/, Fischl, 2012), and probabilistic cytoarchitectural labels (Fischl et al., 2007) for Brodmann areas BA 1, BA 2 and BA 3 were extracted for each subject's segmented surface. The mrFlatmesh algorithm (Vista software, http://white.stanford.edu/software/), was used to create flattened patches of the cortical region surrounding the TF localiser. Functional data was realigned to the last volume (EPI reference frame) of the functional data set which was acquired immediately prior to the high-resolution anatomical T_2*-weighted FLASH data, which was previously aligned to the high-resolution whole head anatomical PSIR. All functional runs were detrended, high-pass filtered (0.01 Hz), and converted into percent signal change.

Alignment of Statistical maps and ROIs: Since the TF stimulation (right and left stimulation) data and FP observation data were acquired in different scan sessions and had different dimensions, they were aligned to a common anatomical reference (the whole head PSIR data set). This was done to allow the ROI acquired in the TF scan session to be imported into EPI space of the FP session, and to render the results on the surfaces of the flattened representations. To do this, first, the linear alignment (7 DOF) matrix was estimated between the PSIR whole-head anatomical and the anatomical T_2*-weighted FLASH data using an iterative, robust estimation method (Nestares & Heeger, 2000). Then, the alignment between the anatomical T_2*-weighted FLASH data and the EPI reference frame was estimated. Since 7T fMRI data is susceptible to field inhomogeneities that can cause geometric distortions, even if image-based shimming is used (Poole & Bowtell, 2008), non-linear alignment estimation using FSL's FNIRT algorithm was used Andersson, Jenkinson, Smith et al., 2007; see Figure 5.3).

In order to allow finger ROIs (defined from the TF scans) to be imported into the EPI space of FP scans, statistical maps for the TF were projected into the PSIR anatomical space. Then, each of the finger ROIs were unified and further divided into different S1 sub-regions using Freesurfer parcellations (see Figure 5.3B). The FNIRT algorithm was also run to align the T_2* anatomical image to EPI space for the FP scans (see Figure 5.3A, bottom panel) as the analysis depended on this alignment to calculate regional overlap (see Figure 5.3B). Warp coefficients for the T_2* anatomical to EPI transformation for the FP scans (previously aligned to the whole head) were applied to the finger ROIs' coordinate space, allowing for spatially accurate import into FP EPI space whilst accounting for distortions in both EPI spaces (Figure 5.3C). All the analyses were

conducted in the native space of the EPI scans, including activity overlap, the results shown in the 3D reconstructed cortical surfaces are only for visualisation purposes.

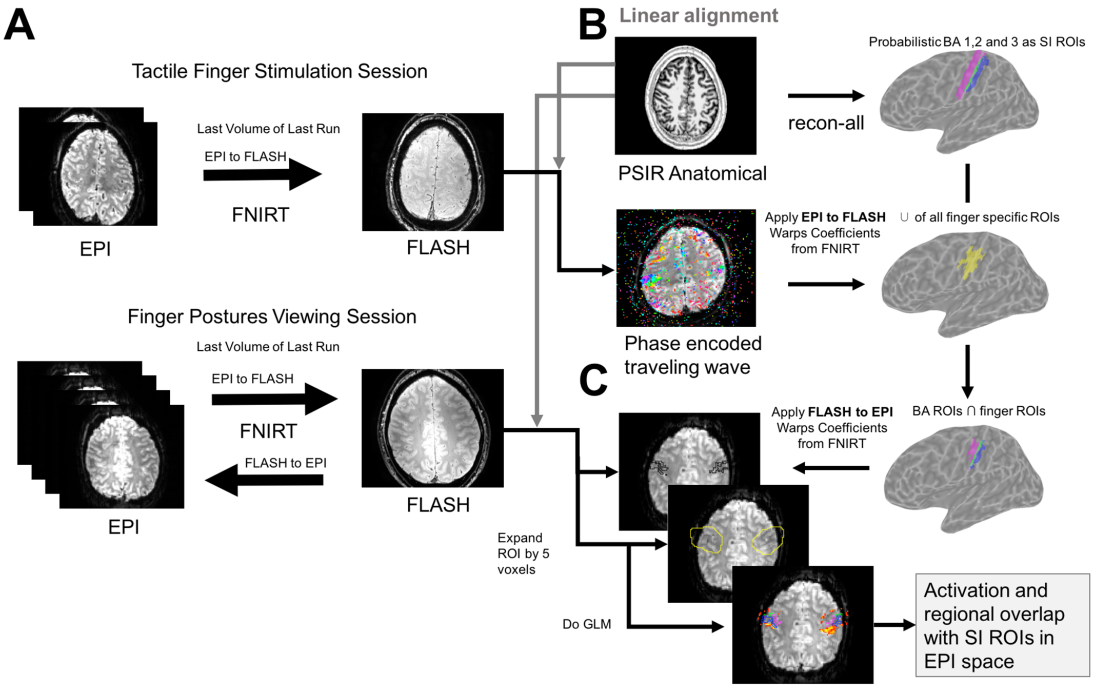

Figure 5.3: A – Top panel, flow diagram of the non-linear alignment of EPI scans to right and left hand stimulation to T_2*-weighted high resolution anatomical FLASH data, using the last volume of the EPI run as a reference. Bottom panel, flow diagram of non-linear alignment of EPI scans to T_2*-weighted FLASH. Since ROIs derived from the tactile finger stimulation were to be imported into this EPI scan space, I applied the same algorithm but now from FLASH to EPI. B – Top panel, the FLASH anatomical data for both sessions were linearly aligned to a common anatomical space (PSIR) in order to allow the projection of statistical maps, extraction of segmentations of BAs and easy import of ROIs from one scanning session to the other. In the bottom panel, the travelling wave results are seen in 3D surface, after applying warp coefficients created from the non-linear alignment. Phase maps were divided into the corresponding finger specific ROIs and then unified to create a larger ROI for the S1 to restrict analysis for the finger postures observation analysis, see figure 3B. C – Brain 3D surface shows the results of dividing the finger ROIs into three different S1 regions, magenta – BA 3, green – BA 1, and blue – BA 2. Using the warp coefficients from the finger postures viewing sessions, the ROIs were imported into the EPI space of this session in order to allow the definition of the analysis volume whilst maintaining precise control over the borders of the different sub-regions. Then, the overlap between the activity and the different sub-regions of the S1 was calculated.

5.3.5 Statistics

Tactile Finger Stimulation: The time series for the forward and reverse order travelling wave scans were combined by shifting both time series by -1 TR (to

remove the haemodynamic response function delay), time reversing the reverse order time series, and averaging both forward and reverse time series. Averaging the time series corrects for the haemodynamic response function delay in the estimation of the phase, resulting in a direct relationship between the phase value and the location of stimulation (see Besle et al., 2013). The phase, amplitude and coherence for each voxel were calculated by finding the best fitting sinusoid at the stimulation frequency using Fourier analysis (see section 3.2.6, *Travelling wave fMRI protocols*). To create a region of interest for each finger, the coherence values were converted into t-values using the formula $t = c \times \sqrt{(n-2)}/\sqrt{1-c^2}$, where c is the coherence and n is the number of time points in the series. The corresponding uncorrected P values were extracted and then corrected using step-up False-discovery Rate (FDR, Benjamini & Hochberg, 1995, 2006). An ROI for each fingertip was created by dividing the phase values into five equal bins spanning 2π, with each subdivision of $2/5\pi$ representing the preferred fingertip locations, and selecting continuous voxels that had a coherence threshold equivalent to $p<0.01$ (FDR corrected at $p<0.05$, see Figure 5.1 B; also refer to Sanchez-Panchuelo et al., 2010 for further details on this method). A whole finger area ROI was then created using the union of the fingertip specific ROIs.

Finger Posture Observation: The fingertip ROIs acquired for both the right and left hemisphere (see previous section) were imported to the FP session native space (see Alignment of Statistical maps and ROIs: and unified into a finger ROI), this was then expanded using a disc function by 5 voxels (Sanchez-Panchuelo et al., 2010) to capture other areas in the vicinity of the S1, such as the IPS, that play a role in the processing of abnormal postures (Chan & Baker, 2015). Then, unsmoothed S1 restricted data based on the unified finger ROIs was fitted using

a GLM ordinary least-squares for each block. Data was modelled using a boxcar convolved with the canonical HRF model with a total of 8 regressors for each condition - 2 (ownership: own, other) x 2 (perspective: ego, allocentric) x 2 (posture: distorted, natural). All estimate comparisons were FDR corrected. For each computed contrast (right-sided t-test) the number of voxels with $p<0.05$ in each S1 ROI (BA 1, BA 2, and BA 3) was calculated and converted into a percentage of overlap between ROIs and functional maps.

In order to explore the effects outside of the vicinity of the S1 a whole-brain GLM was conducted, and Distorted and Natural conditions where compared using a right-sided t-test (Distorted>Natural).

5.4 Results

Before directly addressing the hypotheses established regarding overlap, I first explored whether there was significant activity within the left and right hemisphere BA areas. For that purpose I extracted and average the betas for BAs 3,2, and 1 and run a 2 (Hemisphere) $\times$ 2 (Distortion) $\times$ 3 (BA) ANOVA (n=5). No significant main effects or interaction were found (see Appendix B.1).

To study the overlap of activation resulting from observing distorted finger postures with S1 sub-regions, BOLD estimates of each of 2 (ownership: own, other) x 2 (perspective: ego, allocentric) x 2 (posture: distorted, natural) conditions were calculated for voxels in the vicinity of the left and right S1. In order to address hypothesis 1, I computed the contrast of *Distorted>Natural* finger postures for each subject. All subjects showed significant differences in the posterior bank and fundus of the posterior central sulcus (PCS), along with activity extending into the posterior parietal cortex (PPC). Subjects 3-5 showed a difference in the pattern of activity which extended to S1 sub-regions. This effect was most

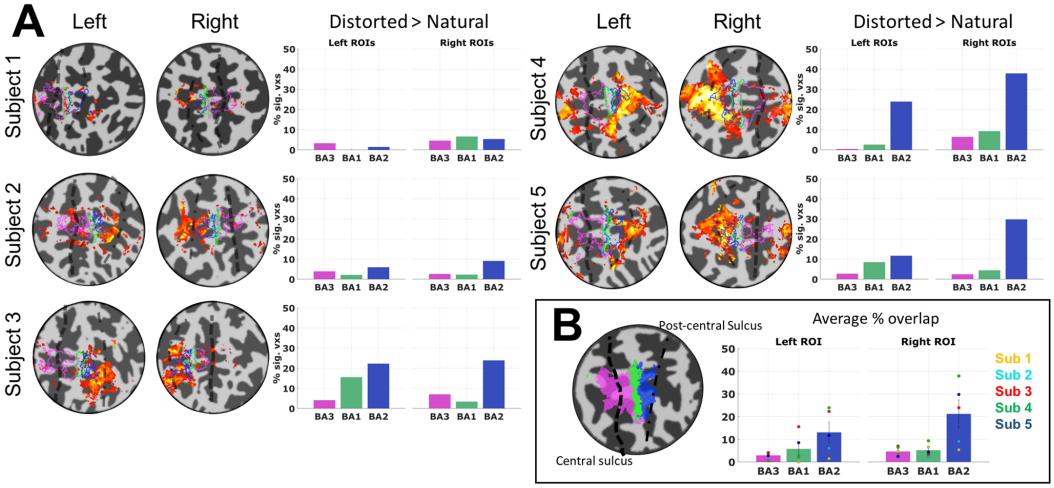

Figure 5.4: A – Flat maps, Individual subjects results of GLM analysis and t-test of Distorted (D) <Natural (N) finger posture on a flattened map in the vicinity of S1 for each hemisphere. Bar graphs, plot of the percentage of overlapping voxels $p<0.05$ (FDR corr.) of the D<N contrast with each S1 BA ROI created from Probabilistic labels, see Figures 2 and 3. From anterior to posterior direction, in magenta BA 3, anterior bank of the central sulcus to crown of the gyrus; in cyan BA 1, anterior lip to posterior lip of the Post-central gyrus; in blue BA 2, posterior lip of the post-central gyrus to anterior bank, to centre of the post-central sulcus. B – Flat map, left hemisphere of flattened example with the sub-regions divided finger ROI, dashed lines mark the central and post-central sulcus. Bar graph depicts the average percent overlap of the D<N contrast for each BA and hemisphere. Filled dots correspond to individual subject data.

pronounced in the BA 2 ROI (defined through functional localiser and atlas, see Figure 5.1 and 5.3 for ROI definition) as it showed the largest percentage overlap (defined as number of significant voxels in a ROI divided by total number voxels that constitute that ROI) across these subjects (see 5.4). The average percentage overlap (N=5) for *Distorted>Natural* was calculated in order to explore differences at a group level. These averages showed a larger right hemisphere (M= 21.21%, SEM = 6.15) involvement of BA 2 compared to the same area in the left hemisphere (M =13.06%, SEM= 4.42). The percentage of voxels active in response to distorted images was significantly different between left and right BA 2, $t(4) = 2.47$, $p = 0.03$. Table 5.2 summarises the size of the BA regions, and the number of voxels that passed the threshold for activity in response to *Disorted<Natural* in each S1 BA region.

To test hypothesis 2, I computed the estimates for *Own<Different*, and *Dif-*

ferent<Own, to address the overall effect of ownership, and then I calculated the estimates for *Own Distorted<Different Distorted* and *Different Distorted<Own Distorted*. The results for *Own<Different* suggest little involvement of the S1 in the representation of ownership of hand (see Figure 5.5). Similarly, the same can be said for Different<Own, however Subject 3 shows some involvement for the S1 across sub-regions, with a linear increase from 10% overlap at BA 3, to 20 % overlap at BA 1 and 35% overlap at BA 2 (see Figure 5.5). When investigating the effect of finger distortion on viewing hand ownership, only Subject 3 shows activity overlap (between 10% and 20% overlap) with S1 sub-regions in both hemispheres (see Figure 5.5).

Table 5.2: . Size of S1 ROIs (BA 3, BA 1, BA 2), and distortion-responsive voxels as absolute number and as % of ROI size (% overlap) in each hemisphere. Note largest % overlap in BA 2. Voxels were defined as distortion-responsive if they were significantly more active ($p<0.05$, FDR corrected) during the Distorted hands conditions compared to the Natural hands conditions. All values are averages (± standard error, SE) across 5 subjects.

Hemisphere	*Area*	*ROI size (±SE)*	*No. of distortion-sensitive vxs. (±SE)*	*Distortion-sensitive vxs. as % ROI size*
Left	BA 3	192.80±14.88	4.20±0.86	2.18
Right	BA 3	143.00±24.22	5.80±1.71	4.06
Left	BA 1	135.40±20.76	7.20±2.87	5.31
Right	BA 1	142.20±22.86	8.60±3.26	6.04
Left	BA 2	134.80±18.42	17.80±5.99	13.20
Right	BA 2	116.60±18.36	26.60±11.18	22.81

To address hypothesis 3, estimates for the following contrasts were calculated: *Egocentric Distorted<Allocentric Distorted*, and *Allocentric Distorted<Egocentric Distorted*. Then, the percentage overlap was calculated for each S1 sub-region. Whilst the average results indicate low percent overlap, for the first contrasts (see Figure 5.6), Subject 5 (cyan) has a marked response (30%) to distorted finger in the egocentric perspective in the right hemisphere. In contrast, Subject 2 (yellow), also has strong activity overlap with S1 sub-regions, but for the *Allocentric*

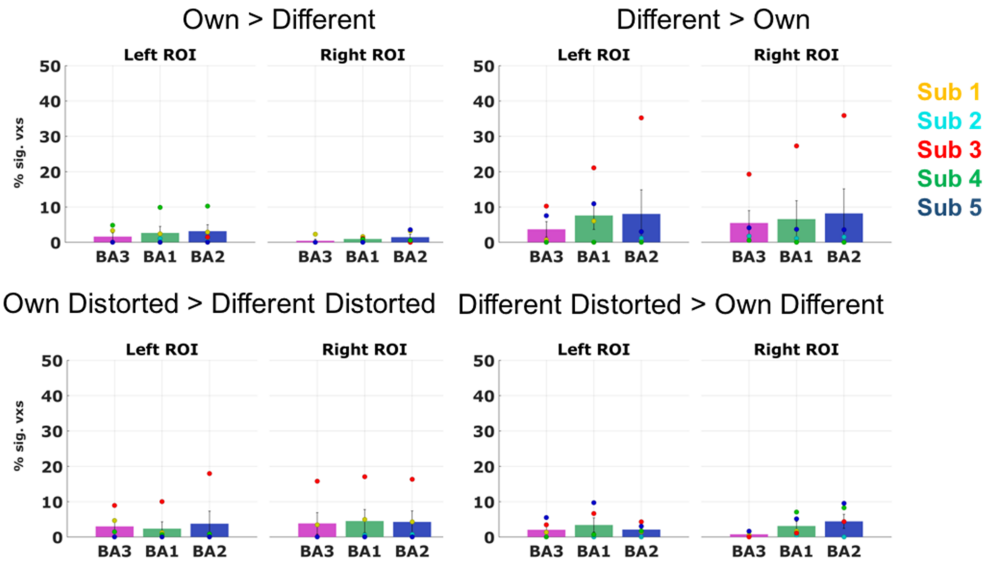

Figure 5.5: Bar graph of the average percent overlap for each S1 BA sub-region and hemisphere for contrasts regarding ownership of the hand viewed. Filled dots indicate individual subject overlap with previously defined ROIs. Subject 3 (red dot), shows larger S1 involvement for the different hand than own, perhaps indicating extra salience of an unfamiliar body part. When comparing the overlap of viewing own hand with distorted fingers versus different hand with distorted fingers, there is a difference with other subjects in S1 involvement, with ROI in the right hemisphere reaching approximately 20% overlap.

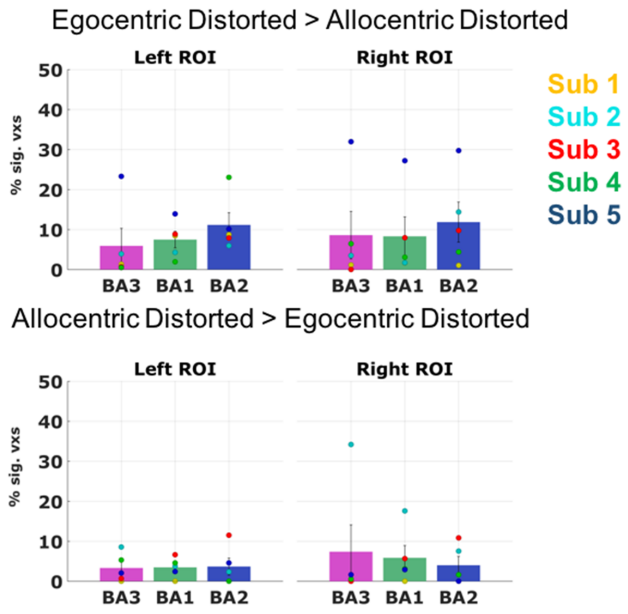

Figure 5.6: Bar graph of the average percent overlap for each S1 BA sub-region and hemisphere for the contrasts regarding perspective of the hand viewed. Filled dots indicate individual subject overlap with previously defined ROIs. Subject 5 (blue dot), shows larger right S1 involvement for distorted finger postures in *Egocentric vs. Allocentric postures*, perhaps indicating extra salience of an abnormal posture in a familiar perspective. Subject 2 (cyan dot),also shows larger right hemisphere involvement, but unlike Subject 5, the overlap of viewing distorted finger postures in the allocentric perspective elicited larger S1 involvement, but with more anterior S1 overlap.

Distorted<Egocentric Distorted contrast. In this case, the activity follows a linear decrease (35% to 10%) from anterior to posterior S1 in the right hemisphere (see Figure 5.6).

In order to investigate whether there an finger specific effects the betas within each of the finger specific ROI (created from the travelling wave paradigm) were averaged in those subjects show overlap above 18% in any of the defined BAs. The results of this were not clear from an initial visual inspection, and outside of scope of the hypothesis created here. For more details and results see Appendix B.2. The contrast between Distorted>Natural postures for the whole-brain GLMs, revealed significant differences in several areas involved in body perception and posture recognition (identified based on comparison with Desikan-Killiany Atlas available in the Freesufer package, Fischl, 2012) - lateral and ventral occipital cortex, IPS, superior parital lobule (see Figure 5.7). As this was not the focus of this chapter, it is only reported here to allow for further comparisons with other results reported in this thesis.

5.5 Discussion

Using ultra-high field 7T fMRI, it was demonstrated that the mere observation of distorted finger postures activated the posterior hand area of the primary somatosensory cortex in 3 out of 5 subjects. The combination of a tactile localiser along with probabilistic cytoarchitectonic atlases for the different sub-regions adds to the specificity of the result observed. This is consistent with the proposal that posterior regions of the somatosensory cortex are part of an embodied simulation mechanism that allows the retrieval of pre-existing body related information in order create vicarious experience of a certain outcome (Keysers et al., 2010; Damasio, Everitt & Bishop, 1996). This assertion is further supported by

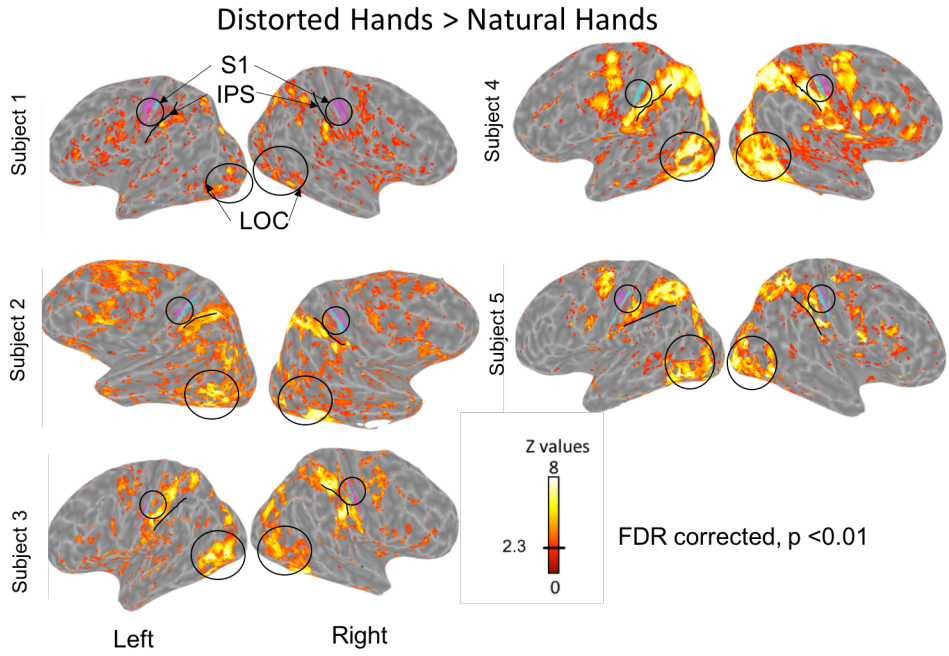

Figure 5.7: Results of a whole-brain positive t-test testing Distorted >Natural on a individual subject basis. Statiscal maps are marked by circles and lines to highlight areas of interest such as S1 , IPS and LOC. All maps were corrected using FDR at p<0.01.

studies investigating touch observation, where posterior regions of the somatosensory cortex (BA 2/1) also show significant activation (see *Vicarious Activation in SI*), and is consistent with findings in multisensory integration research where visual information pertaining to roughness can induce somatosensory activity (Sun, Welchman, Chang & Di Luca, 2016); and furthermore, PPC and posterior S1 activation is consistent with macaque studies investigating changes in body schema representations due to task demands (Iriki et al., 1996). Lastly, this study also offers comparable results to those of Schürmann et al. (2011), where the *Distorted<Natural* contrast elicited right hemisphere specific activation in both motor and S1 cortices. The stimuli also varied in terms of hand perspective (ego- vs. allocentric) and ownership (own vs. other hand) but related differences were inconsistent. However, Subject 2 showed overlap within the S1 sub-regions, but did not appear because the results was highly specific to the Egocentric

distorted perspective, and this effect was lost in the averaging.

Although the hypothesis for an embodied simulation mechanism was developed to explain somatosensory involvement of touch observation (Keysers et al., 2010) or actions/goal oriented behavior (Gallese, 2005), here I demonstrate that, given the overlap between the tactile and visual activity, observing body abnormalities (as in Avikainen et al. 2003, Schürmann et al. 2011) triggers a similar process and therefore the first aim (step) of the thesis is tentatively achieved as only 3 subjects showed overlap above 18%. This criterion based on a previous study by Keysers and Gazzola (2009), in which they found the percentage overlap of voxels used during action execution and action observation (n=16). Their average value was 18% therefore, this also applied here as a threshold. However, in the future, a more elaborate analysis is necessary to derive a data driven threshold. A value of less than 18% may still be above chance because I have decided the cut-off externally to this data. A permutation based approach would prove to be more useful to fully elucidate on an actual chance level of overlap. By repeating the GLM procedure several times (e.g. 1000 times) whilst randomising the regressor labels for each condition, and then calculating the overlap, a normal distribution of the overlap can be found. Then, only the overlap percentages that fall within top 5% of the distribution can considered as significant overlap.

However, these results point to a potential mechanism that depends on a tight interaction between parietal and somatosensory areas, because the PPC is the locus for integrating visual and sensory information (Gallese & Lakoff, 2005; Bolognini, Rossetti, Fusaro, Vallar & Miniussi, 2014) and S1 contributes to the creation of a vicarious response. In this study, a consistent finding is the involvement of the posterior parietal cortex bilaterally, and the caudal part of the

postcentral sulcus. The former area contributes to the processing of limb posture and position, the retrieval of motor schemas, and the combination of multisensory information to develop senseful movements (Kalaska, Scott, Cisek & Sergio, 1997). For example, using light-point displays of walking models, increased gamma oscillatory activity was observed in parietal areas (Pavlova, Lutzenberger, Sokolov & Birbaumer, 2004). The involvement of this region is, therefore, implicated in the recognition of biological plausibility of certain actions and postures, retrieval and binding of body schemas and visual information. In this study, two subjects did not show activity overlap with S1 but showed PPC involvement (as well as the other three subjects who did show overlap). This may represent only a retrieval and comparison of schematic information below somatosensory engagement threshold. This suggestion is supported by Bolognini et al. (2014), where paired-pulse TMS over PPC and S1 was applied during observation of touch in congruent or incongruent locations with actual touch. Tactile acuity error increased for paired stimulations over the PPC-S1 and S1 alone, but not for premotor-S1 during incongruent touch observation. This result is explained as a consequence of increase in intracortical activity of the PPC and S1 leading to the experience of phantom touches, likely derived from the combination of incongruent visual input to tactile experience.

One particular concern during the design of this study was how to demonstrate that the overlap between visual and tactile representation was real. In Chan and Baker (2015) the role of the S1 in the embodied simulation mechanism is questioned. The authors explain that inconsistencies in the manual labelling of the S1 (and its sub-regions) and overly liberal ROI size led to the inclusion of non-somatosensory areas in previous studies (such as Schaefer et al., 2012; Kuehn

et al., 2013 and 2014). In turn, this led to overestimation of the involvement of the posterior S1 sub-regions (namely BA 2) and in fact it is posterior parietal cortex involvement that is being reported. Therefore, here it was especially important to have an accurately defined hand region and S1 sub-regions, as the answer to the main research question of this thesis relies on good localisation of the somatosensory response.

A potential confound is that the several realignment steps could have added error to the transfer of the ROI between functional sessions, and activity from non-S1 regions may have smeared into the ROI. However, in both sessions a high-resolution anatomical T2* scan was acquired be to used an intermediate alignment step between functional scans and the PSIR scan, which was going be inflated and flatten. The use of this extra anatomical (T2*) scan allows for whole-head robust multi-resolution alignment with error<1mm (Nestares & Heeger, 2000). This in combination with non-linear registration, which shows similar error levels (Andersson et al., 2007), means that the realignment steps would have induced minimum amount smear between and within sessions. Another related concern is the distribution of large draining veins across sulci and gyri (Turner, 2002). Whilst the contribution of noise arising from intra-vascular signals in negated due to the use of gradient-echo scanning, at 7T extra-vascular contribution are potential concern (Yacoub et al., 2001). In order for this to be an issue, the vasculature at the BA2 and post-central gyrus must be different than vasculature at the IPS. While, I do not have vein maps to prove this, to my knowledge there has been no study demonstrate the existence of such a difference empirically. Recently, however, a study investigated the temporal dynamics the HRF in the cortex and found that, for similar type of stimuli, the HRF remains extremely

similar in 77% of the cortex (Taylor, Kim & Ress, 2018). Remaining percentage reflects the fact that larger veins, will have different HRFs due their anatomy (i.e. take longer to reach peak due larger volume), therefore the results here obtained are unlikely to have been affect by their drainage. In the future, however, vein maps should be created in order to observe the distribution of veins and explore the possibility of overlap with the signal.

Although bilateral overlapping activation is seen, there is greater voxel involvement in the right-hemisphere BA 2. This is at first an unexpected result as the hands shown here were right hands, and therefore one would expect predominantly left (contralateral) involvement. The current result is, however, not as unexpected as it may seem. Indeed, the result adds spatial specificity (within S1) to earlier findings of right-lateralized somatosensory and motor area activation in response to distorted finger postures (Schürmann et al., 2011). However, I postulate that right-hemisphere involvement may be reflective of the particular salience of the stimuli, related to visuospatial and/or emotional processing. Distorted postures demand increased visuospatial processing to infer three-dimensional structure from two-dimensional images, a right-hemisphere dominant process (Bowers & Heilman, 1980; Corbetta & Shulman, 2002). The emotional contents of distorted finger images were confirmed in unpleasantness ratings given by participants of an earlier study (Schürmann et al., 2011). Right-hemisphere dominance for processing of emotional stimulus contents is evident from studies of patients with right somatosensory cortex lesions and impaired recognition of fearful facial expressions (Borod et al., 1998). Importantly, such deficits are not seen is patients with lesions in the left somatosensory cortex (Adolphs, Damasio, Tranel, Cooper & Damasio, 2000). Like distorted fingers, fearful faces contain socially relevant

information and are likely to create a somatosensory representation in the observer's brain in order to re-create the others' sensations, and therefore prompt embodied simulation.

The use of questionnaires, although not crucial for the interpretation of the results, was important to identify subjects that may have a somatosensory experience to the stimuli. Also, subjects were experienced in participating in fMRI experiments in order to minimise issues related to head motion. This goes against typical random sampling of the population, but since I aimed to demonstrate this effect on a single-subject basis, it was important to ensure high quality of the data. Thus, one crucial limitation is the number of subjects studied. This type of research will benefit from a larger cohort of subjects, and in particular investigating correlations with questionnaires pertaining to body awareness, empathy, and perspective-taking to further elucidate this mechanism. Another aspect is that, given questionnaires are subjective, it is impossible to be sure that they provided an accurate measure of how much a subject would engage with stimuli. Another limitation is related to the fact that the natural postures did not change in aspect, unlike the distorted finger postures, which changed every 4 seconds. This could have lead to an adaption mechanism which can lower BOLD signal (Grill-Spector, Henson & Martin, 2006). A potential fix to this would be either to highlight the finger with a different colours, or have the fingers in the natural conditions shown in natural postures. Having considered this, it is still interesting that visual presentation of a (distorted) finger may lead to involvement of the somatosensory hand areas (BA 2). This could still point towards and embodied simulation mechanism underlying observed body parts. In the future, it would be interesting to investigate whether a similar effect can be achieved by study-

ing the overlap between tactile and visual stimulation of other body part, say the face. Significant overlap between tactile and visual presentation of stimuli in somatosensory face areas would further add weight to the tentative findings reported here.

In conclusion, significant activity differences in the observation of distorted finger postures, compared to natural, were seen in posterior S1(BA 2), identified with overlapping activity between the probabilistic cytoarchitectonic maps and the finger specific ROI acquired from functional imaging data of direct tactile stimulation. This supports the proposition that embodied simulation exists at the S1, which is typically involved in first person experience. Furthermore, this study expands current literature by demonstrating that the S1 is likely involved in the representation of body schematic information. Lastly, larger right hemispheric involvement is congruent with previous findings relating to the affective visual processing of body and facial expression through somatosensory simulation of the stimuli.

Chapter 6

M-EEG Primer

6.1 Overview

In this section I offer a short primer regarding the basic biological and physical underpinnings of magnetoencephalography (MEG) and electroencephalography (EEG) techniques which are used to explore steps 2 and 3 of this thesis. This is followed by relevant methods for pre-processing data, averaging evoked-responses, and localising the source of data.

6.2 Signal Generation of EEG and MEG

The electrical activity generated by neuronal firing can be detected by electromagneto sensitive machines. EEG can detect this electrical activity using electrodes placed on the scalp, and detect the oscillations of produced by the firing of the neurons. MEG, uses SQUIDs (superconducting quantum inference devices), and detects these responses using the small magnetic fields (in the order of femto Tesla) generated.

Both EEG and MEG have the same celluar basis: changes in membrane potentials. Such changes occur either as action potentials (APs) or postsynaptic

potentials (PSPs), forming the basis of brain and body communication. APs are very short (1 ms), and occur when the membrane potential reaches a specific threshold (typically -55 mV, compared with a resting membrane potential of typically -70 mV) at the axon hillock, inducing cell depolarisation across the axon, followed by re-polarisation of the membrane, creating a current quadrupole (see Figure 6.1A). Because of their opposite directions, the dipoles are virtually invisible to the EEG and MEG. To understand why this is the case, first consider that a quadrupole current falls off as $1/r^3$, where r is the distance from the cell body. In contrast, PSPs at dendrites polarise neurons in one direction, towards the cell body, forming a dipole with current falling off as $1/r^2$ (Fig. 6.1 B). This is the main source of the EEG and MEG signal - current dipoles that arise in post-synaptic firing in apical dendrites (see Figure 6.2A).

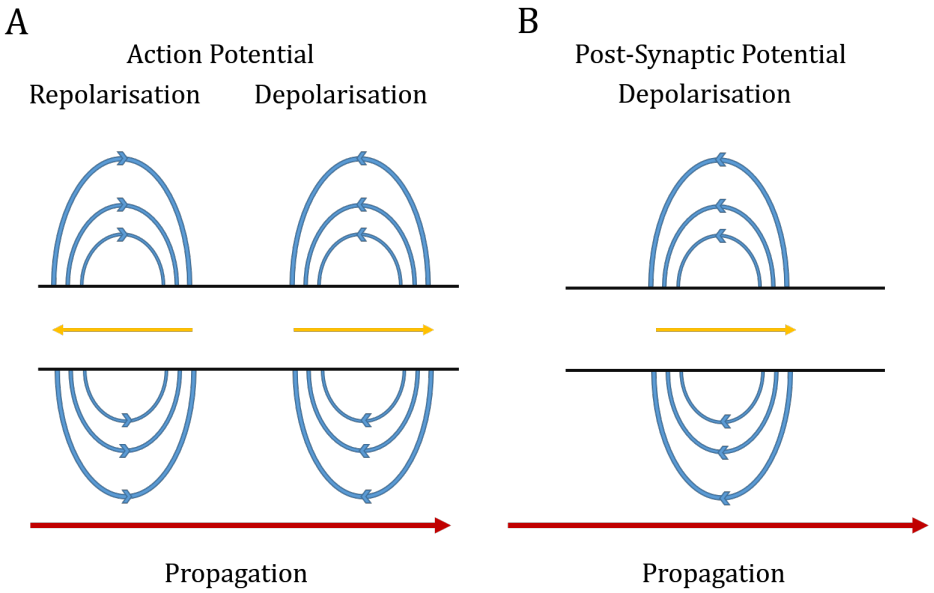

Figure 6.1: Schematic representation of a quadrupole (A) and dipole (B) inside a an axon or dendrite respectively. The red arrow indicates the propagation of the signal, the yellow arrow represents the intra-cellular current, and blue arrows the extra-cellular currents induced by the in- and out-flow of ions.

Individually, and compared to APs, the signal of a single post-synaptic potential (PSP) is too small to be measured (see Figure 6.3A and B). However,

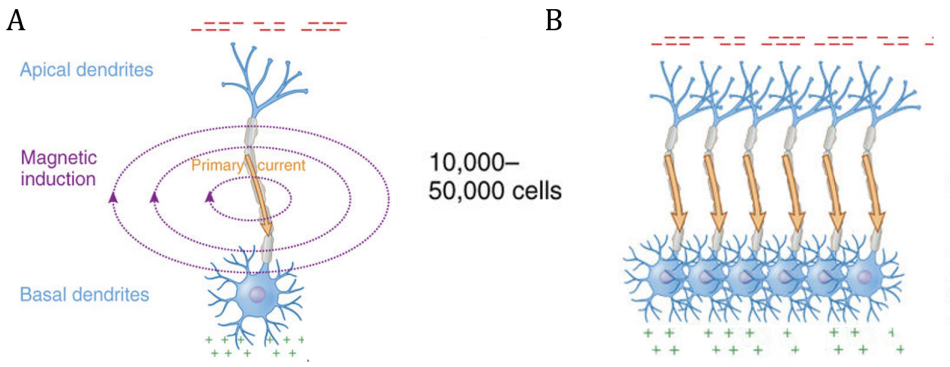

Figure 6.2: A) representation of a pyramidal neuron depicting the direction of the primary current and the magnetic field that it induces. B) visual representation of several pyramidal neurons firing at the same time. Extracted and adapted from Baillet (2017).

pyramidal neurons have certain biophysiological characteristics that allow them to be measured. First, columns of pyramidal cells create an open field where dendritic dipoles are polarised with similar alignment, creating pairing of positively charged particles in one side (cell bodies), and negatively charged particles in the opposite side (apical dendrites, see Figure 6.2B). In order for the signal to summate, thousands of nearby columns of dendrites' PSPs must fire within 10 ms of each other after synaptic input, in order to produce a signal that is measurable at the scalp (see Figure 6.3C). Apical dendrites of pyramidal cells in the cortex fit these conditions, and contribute the most to the M-EEG signal. In addition, they have perpendicular alignment to the cortex surface (see Figure 6.4) allowing the microscopic currents formed in PSPs to add together, generating a net current that is detectable.

6.3 EEG versus MEG

The difference between EEG and MEG techniques arises from the fact that they measure two different types of dipole. EEG measures and detects the net voltage created from the extracellular return current dipoles arising from a primary current travelling inside a dendrite (Figure 6.2A). As these extracellu-

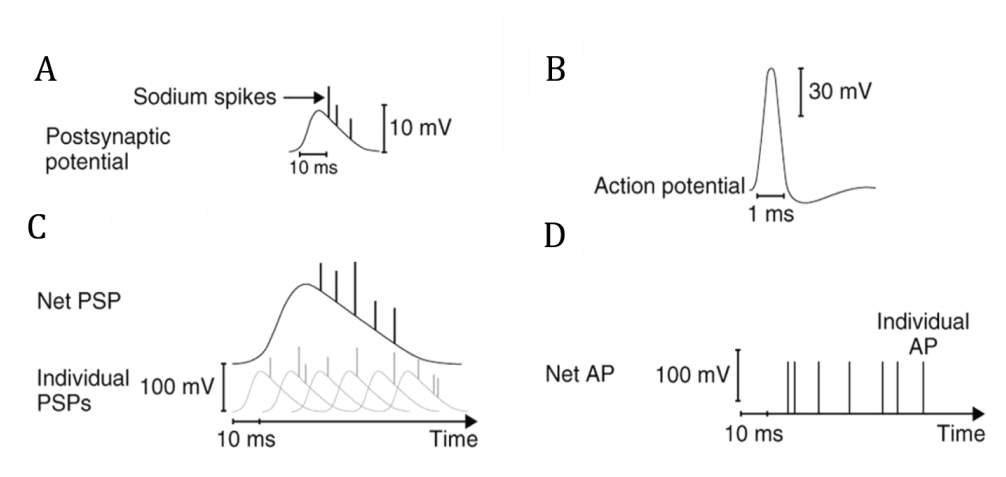

Figure 6.3: A) graph representing a single postsynaptic potential, and B) an action potential. Note the difference in timing and amplitude; Action potential quicker but larger amplitude. C) shows the net current of thousands of postsynaptic potentials firing which are able to summate, and far exceed the amplitude of action potentials in D). Extracted and adapted from Baillet (2017).

lar currents are situated in a conductive medium [e.g cerebral spinal fluid (CSF)], some of the negatively charged particles travel from the negative side to the positive side of the dipole, thus creating a radially oriented dipole (6.2B). Due to the physical properties of electromagnetic induction, any current loop within a system, such as an intracellular dendrite current, will induce a tangentially oriented magnetic field which is detected by MEG (purple lines, Figure 6.4). Consequently, in these two dipoles' orientation lies the difference between the two brain imaging techniques.

In Figure 6.4, the importance of this effect is demonstrated; a sphere, as a model of a head, shows that radially oriented return currents are symmetric with respect to the corresponding volume currents, consequently not producing magnetic fields outside the sphere (Hämäläinen, Hari, Ilmoniemi, Knuutila & Lounasmaa, 1993). On the other hand, tangentially oriented dipoles associated with volume currents are not symmetric, and therefore produce a magnetic field outside of the head. If all dipoles are at the centre of the sphere, i.e., have deep sources (see Figure 6.4C), then all dipoles are radially oriented, as they

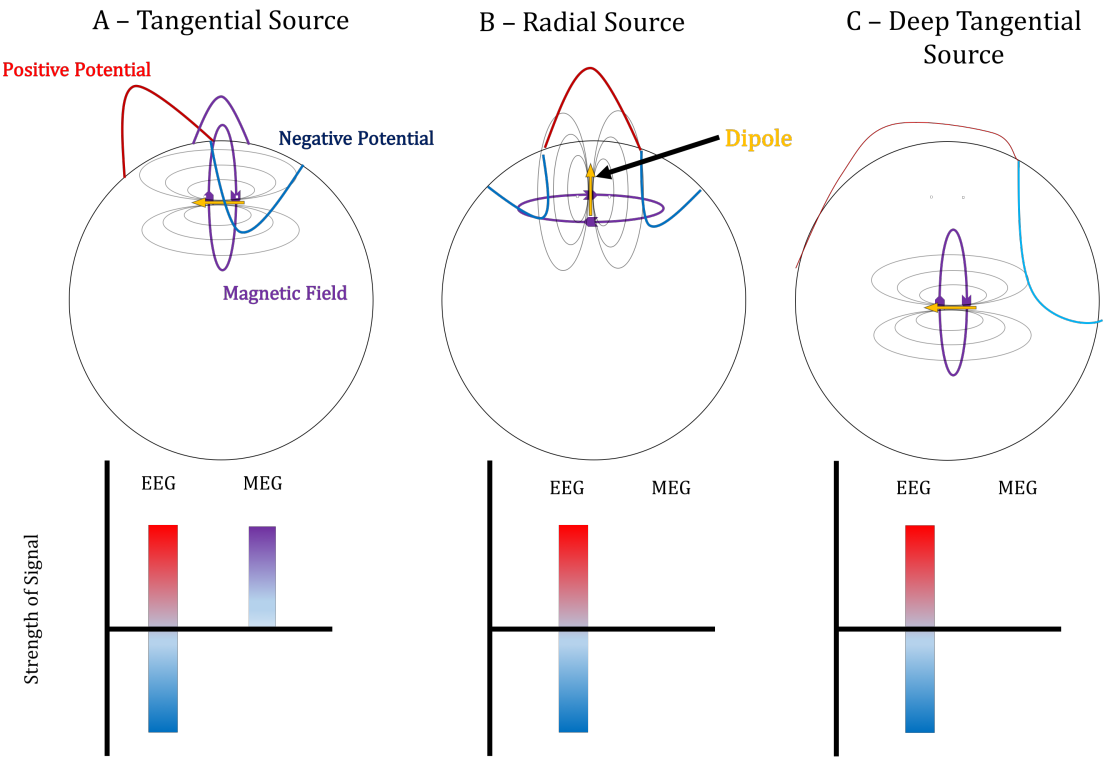

Figure 6.4: Top (A,B,C), a spherical representation of three different types of dipoles occurring from neuronal activity. Bottom, corresponding EEG and MEG signal strength (not to scale).

are equidistant from the sphere's surface. Superficial and tangentially oriented dipoles produce a magnetic field that goes outside of the sphere.

Another point to consider using this spherical model, is that the head consists of CSF, bone, air, and skin, all of which contribute to the dispersion volume currents created in the brain. The magnetic fields created by intracellular currents are blind to these tissues. Consequently, it can be said that the source of the MEG signal is the apical pyramidal neurons located in the cortex that have a tangential orientation. This means that MEG measures activity mostly from sources located in sulci (see Figure 6.5 cortex representation). EEG, is better suited to detect currents in the convexial cortex (from apical dendrites in gyri) close to the scalp (i.e., electrode), but suffers from the signal dampening and smear caused by non-brain tissues. However, because of this EEG can detect both radial and tangential dipoles, and signals from deeper sources.

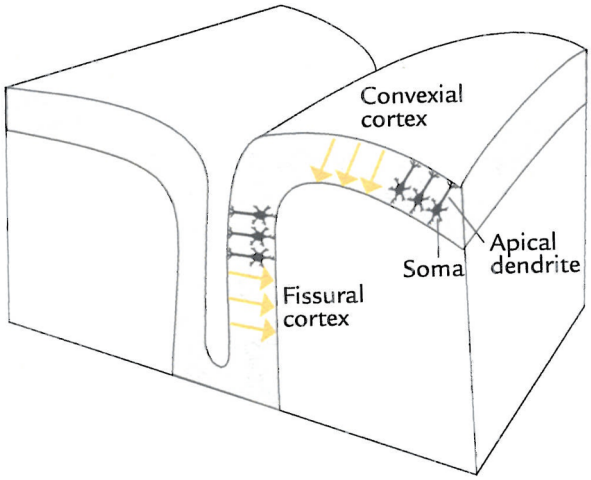

Figure 6.5: Schematic representation of the cortex showing the perpendicular nature of apical dendrites of pyramidal neurons, which are the basis of the M-EEG signal. Extracted from Hari and Puce (2017), page 10.

6.4 Measurable Effects

EEG and MEG measure signals rich in temporal information about brain activity that underlie a wide variety of effects. Classically, these are divided into evoked responses, spontaneous rhythms, and induced responses.

6.4.1 Evoked Responses

Event-related potentials (in EEG) or fields (in MEG) are responses locked to the onset (or offset) of a stimulus or response resulting in a spike in the voltage or magnetic field strength. Most commonly, these are used to research visual, auditory, or somatosensory processing, as these stimuli produce strong and highly stereotypical responses across populations. This phenomenon allows the time-locked single trial responses to accumulate and enhance the SNR to a particular stimulus (6.6A). In order to extract meaningful measures out of the averaged time course, studies typically use baseline to peak amplitudes, area under the curve, or difference waveforms (see Figures 6.6B and C). These help quantify the shape of the responses and understand the underlying cognitive process creating

that shape. For example, broadly speaking, exogenous responses are automatic and controlled by the physical characteristics of the brain, occur within 100 ms of the onset, and are modality specific. Endogenous responses, occur later (>100 ms) and typically reflect some task-relevant processing such as categorisation, attention, or refreshing working memory.

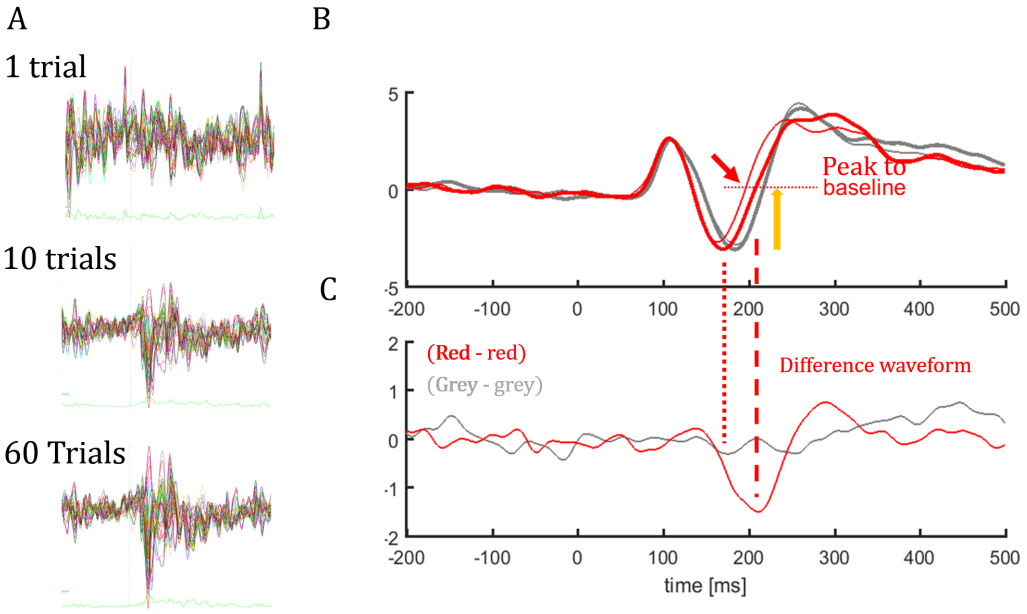

Figure 6.6: A) depiction of the sharpening of evoked-responses after averaging increasing numbers of trials across 64 EEG channels. The green line is a visual indication of the temporal SNR. B) average responses to four different conditions (Red/red, heavy/thin red line, and Grey/grey with the yellow line showing the baseline-to-peak measure, and in C) the corresponding difference between the red and grey conditions, i.e. the comparison of the difference waveforms.

6.4.2 Spontaneous Rhythms and Induced Responses

Spontaneous rhythms refer to oscillatory signals that underlie on-going brain activity. As explained first by Berger (1929), oscillations between 8-13 Hz in the occipital cortex of the human brain could be attenuated by visual stimuli. Since then, the full spectrum of the underlying oscillations of the brain have been explored and categorised into different ranges depending on the correlations

behaviour with oscillation changes (see Figure 6.7B). Unlike evoked responses, these cannot be averaged as they are not precisely onset locked. Instead, the analysis of these responses depends on frequency decomposition methods (such as Fourier analysis) in order to analyse the power or onset of certain frequency bands. This frequency decomposition can be averaged on a trial-by-trial basis and then analysed with classical parametric or non-parametric statistics to find differences between conditions (see Figure 6.7B). These type of responses are induced effects, and reflect attenuation or augmentation of oscillatory activity after stimulus or response onset or offset across a number of bands. Examples of this are alpha band attenuation after visual stimuli, as demonstrated by Berger (1929), or beta rhythm attenuation (and rebound) after somatosensory stimuli (see Pfurtscheller & Lopes da Silva, 1999 for review). Underlying this effect, Donner and Siegel (2011) put forward that excitatory neurons trigger GABAergic interneurons, which in turn inhibit neural oscillations leading to the suppression and rebound observed in response to a wide variety of stimuli. One of the most common ways to investigate this effect is to measure the amplitude envelope of a certain band across time (see Figure 6.7C), resulting in a *Power* measure of neurons acting in synchrony.

6.5 Source Localisation

6.5.1 The Forward Problem

This refers to the attempt of estimation of the electrical or magnetic field potentials outside the head from known primary currents inside the head. Due to the complex inhomogeneity issues surrounding the EEG signal, and since no source localisation of the EEG was attempted in this thesis, this section only

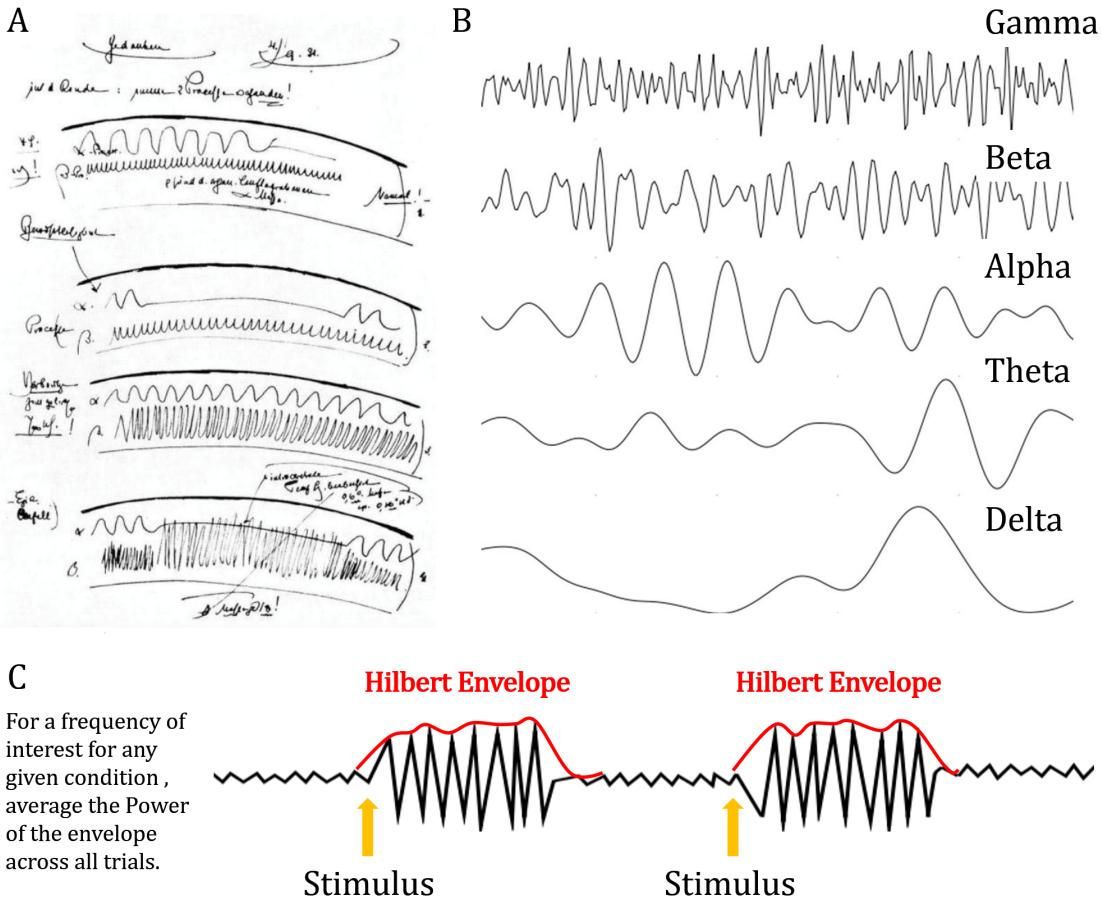

Figure 6.7: A) capture of Hans Berger's notes for the first EEG data collection. B) schematic of different wave frequencies discovered since then. C) schematic of the measurement of an induced response using Hilbert envelope to calculate the power of a given frequency band. Time course and amplitudes not to scale.

relates to MEG source localisation.

To solve this problem, it requires calculating the magnetic field outside of the head from a known electro-magnetic distribution inside the head (see Figure 6.8A). In order to achieve this, one must first approximate the head shape into a well-known shape, such as a sphere (Hämäläinen et al., 1993). This is particularly well-suited for MEG as volume currents (only intracellular) do not contribute to the generation of the magnetic field. Although, this is the classical method in which magnetic field distributions are estimated, it leads to drop-off signal from ventrally oriented sources, deep sources, or areas of the brain that are not very

spherical (Huang, Mosher & Leahy, 1999). Since, I am interested in areas that can be quite ventral (such as the fusiform gyrus), for the purposes of this thesis I use an overlapping spheres (see Figure 6.8B) approach. This uses a sensor-weighted sphere at each MEG sensor in order to model the underlying currents and associated magnetic fields (Huang et al., 1999).

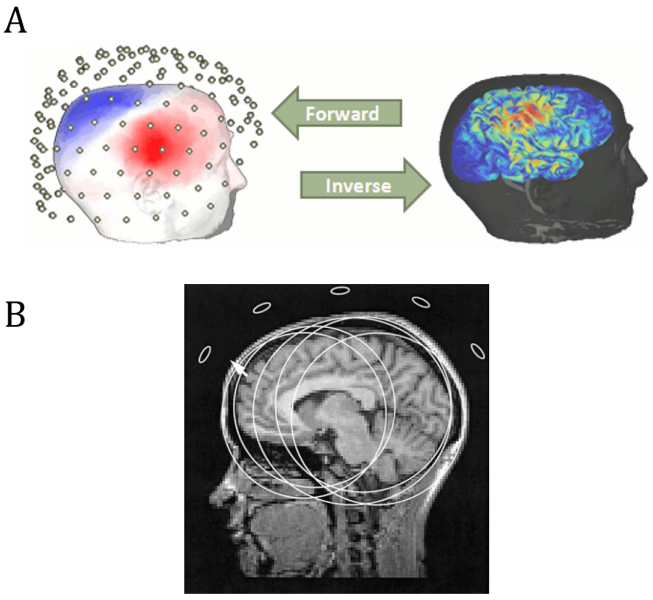

Figure 6.8: A, Depiction of the Forward and Inverse Solution (from http://neuroimage.usc.edu/brainstorm/Tutorials/SourceEstimation. In the left, it shows the amplitude and orientation of the magnetic dipole. In the right, it shows the strength of the estimate of the source in A. B, schematic representation of the overlapping spheres model, extracted from Huang et al. (1999).

6.5.2 The Inverse Problem

The inverse problem refers to the estimation of the distribution of the volumetric currents inside the brain from the magnetic field that is measured outside of the head at different sensors. This problem is ill-posed, as there is an infinite number of source activity patterns that could generate the same sensor topography. Understanding where those sources are is a complicated topic and it requires a few assumptions to be made. First, it requires the forward solution

to compute the field from the dipole at any given location with any given orientation. Then, a leadfield, or head model, to explain the given currents, and a volume or surface representation of the brain to compute the source estimate that explains the observed topography the best. In order to estimate the source, a small number of equivalent current dipoles over an *a priori* region-of-interest can be applied to measure amplitude changes over time in that region; or a distributed grid of several dipole models that sample the cortex (or brain volume) to allow the estimation of the amplitude across different areas of the brain. The first approach is often ideal to measure responses to strong sensory input at earlier latencies, where a well-known number of brain regions are involved. However, the distributed approach allows one to capture spatio-temporal dynamics across different regions of the brain, and develop a wider understanding of the processing strategies underway at each moment in time.

In this thesis, I use minimum norm estimates (MNE) imaging where anatomical constraints are imposed in order to restrict the source of the signal to the cortical surface (as the neurons that are visible to the MEG are located here), therefore reducing the number of solutions for the ill-posed problem (Hämäläinen et al., 1993). To estimate the sources using this technique, first the distributed current source density image at each time point is calculated until the best fit to the data is obtained, given a specific forward model. Then, the ill-posed problem is solved by applying a linear regularisation term (e.g., Tikhonov regularisation) to find the least-squares solution that offers the minimum energy norm whilst accounting for the noise in the MEG system (Hämäläinen et al., 1993; Huang et al., 1999). Therefore, a noise covariance matrix must be recorded directly from the sensors in order to estimate the sources successfully. One of the issues that arises

from using this techniques is that MNE generates low-resolution estimates that are wide-spread and span over multiple structurs of the brain as a consequence of the depth variation in terms of the sources. For instance, current density maps place activity sources in superficial regions of cortex, and signal strength and resolution drops at deeper areas such as the fundus of a sulcus (Dale & Sereno, 1993). In order to address this issue, I use a normalisation technique developed by Dale et al. (see Dale & Sereno, 1993; Dale et al., 2000) in which the noise-covariance and a linear kernel of the inverse solution are used to calculate the noise variance of the sensors. Then, at each dipole, current density value is normalised by the square root of these variance estimates. Therefore, this is similar to calculating the standard deviation of signal from the noise - with positive or negative polarities indicating the orientation of the flow (Dale et al., 2000). As a result, this reduces the spread of activity because each cortical dipole is compared to a constant noise value (Dale & Sereno, 1993).

6.6 Instrumentation

6.6.1 The EEG system

In experiments 1 and 2 of chapter 7, a EEG system was used to measure the evoked electrical activity in response to visual stimuli. Because of artifacts from electrical mains, a Faraday-cage (2.5 $\times$ 2.3 $\times$ 2.3 m) quiet room at ambient temperature was used.

In this thesis, I used a 64-channel Active-Two acquisition system (BioSemi, Amsterdam, Netherlands), sampled at 1024 Hz, and digitised at 24-bits (see Figure 6.9). This system uses a two electrode ground system which replaces the traditional reference/ground system of electrodes by creating a common mode

voltage for any given subject. The *Common Mode Sense* (CMS) active electrode and the *Driven Right Leg* (DRL) passive electrode complete a feedback loop that allows the impedance of the passive electrode to be reduced. Furthermore, it allows the subtraction between other electrodes and CMS to generate better SNR compared to regular systems as the common mode is subtracted from the digital data instead of the analog circuitry, leading to reduction of noise and electrode drift (see https://www.biosemi.com/faq/cms&drl.htm). Because of this, BioSemi systems allows for reference-free recordings, and only at pre-processing stages were the time series of the electrodes referenced to an all-electrode average.

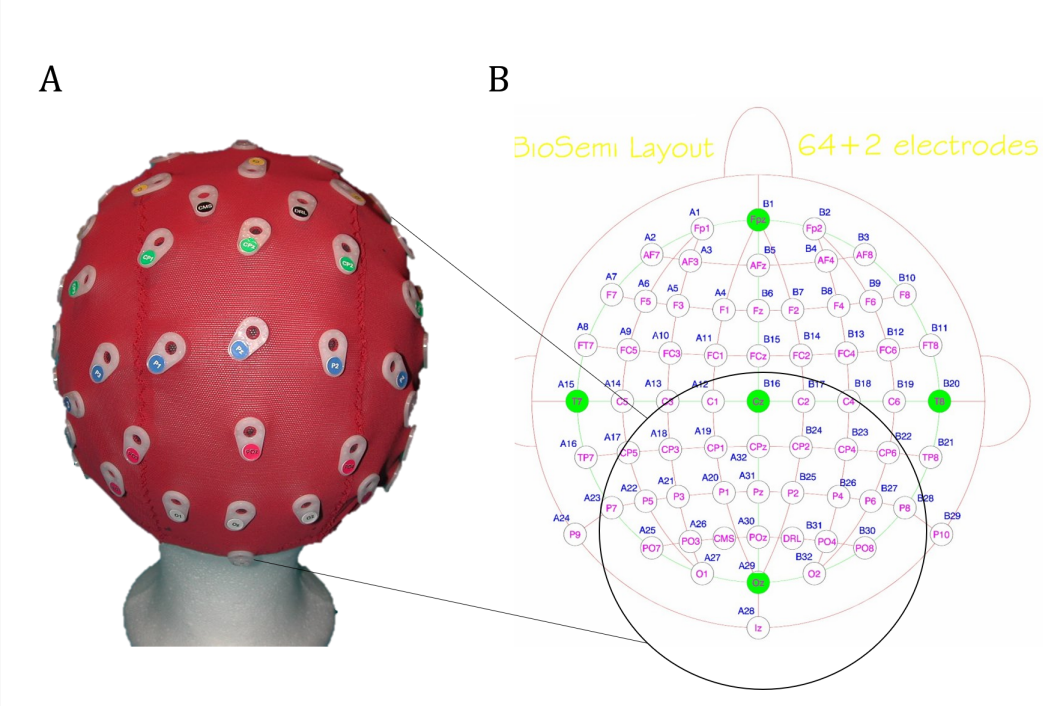

Figure 6.9: A) Photo example of a medium sized Biosemi electrode cap from an anterior view. B) 2D schematic of the electrode layout used in EEG experiments 1 and 2 in chapter 9), anterior aspect on the top.

In order to measure eye movements and blinks, which severely contaminate the data with muscle artifacts, an additional 6 Ag/AgCl electrodes were placed at M1, M2, F9, F10, T9, T10. Data were collected using ActiView 7.0. In order

to segment the data into different trial epochs, digital triggers were sent and received using a Cedrus Stimtracker via a fibre-optic cable.

In order to measure electroencephalographic activity, electro-conductive gel is often used in order to form a conductive bridge between the scalp and the electrodes. Subjects were always asked to come with dry and gel free hair, as the Ag/AgCl electrodes used must be embedded in a specific type of electro-conductive layer to create a current flow that is related to neuronal activity. If water is present, the current from the scalp will disperse across all electrodes, making the EEG system behave as if it is one single electrode. If any other type of gel (outside of the recommendations) is present, then ionic interactions between the silver ions in the electrodes and the gel can lead to unpredictable current flows that may not be representative of actual brain activity.

6.6.2 The MEG system

A whole-head 275-channel CTF Omega 2000 MEG system (CTF Systems, Inc., VSM MedTech, Coquitlam, British Columbia, Canada), was used to acquire the data in Chapter 8. This system consisted of gradiometer pick-up coils lining the helmet of the MEG, connected to superconducting quantum interference devices (SQUIDS) located in the body of the MEG (see Figure 6.10A). The SQUIDS allow the small magnetic fields generated from neuronal activity (≈ 100 fT, i.e. one part in 10^8 of the Earth's magnetic field) to be detected. Due to this extreme sensitivity, the MEG is inside a magnetically shielded room.

SQUIDs must have a core temperature of $\approx 270°$C in order to preserve superconductive properties that allows current to experience close to zero resistance going through a circuit (Hämäläinen et al., 1993). The SQUIDs and gradiometers create a current loop where the magnetic field changes generate current to run

through the system. Because SQUIDs contain materials that create Josephson Junctions (layers of resistant material), whenever there is a big enough change in the current, there is a voltage drop across this junction, and a feedback current is generated to offset this drop (see Figure 6.10B). This current is the measured output and the basis of the MEG signal.

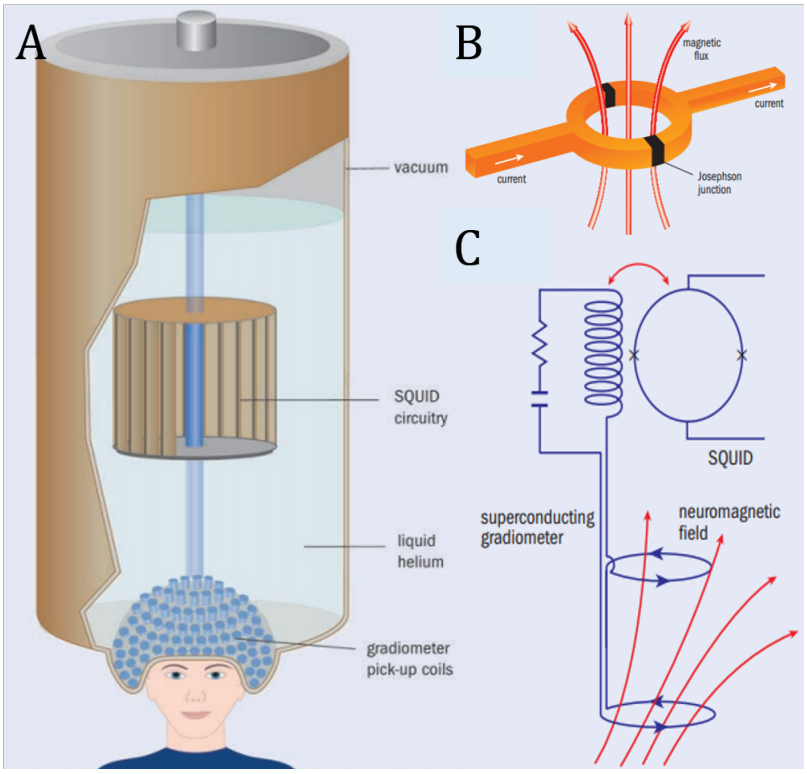

Figure 6.10: A) schematic of the CTF MEG system at the University of Nottingham. B) diagram of a SQUID with Josephson junctions, which induces current changes as magnetic flux goes through the system, creating the signal of the MEG. C) diagram of a circuit gradiometer with two opposing coils coupled with a SQUID. The red line show a neuromagnetic field, which varies with distance. This generates a net current which travels in the gradiometer circuit and then inducts a current flow in SQUID. Extracted and adapted from Brookes and Singh (2013).

Even in a magnetic shielded room, magnetic interference is present from sources other than the brain. Axial first-order gradiometers, such as the ones present in the CTF MEG system (see Figure 6.10C) used in this thesis, minimise the effect of such interference. In these devices, an opposite (compensation coil) wired loop is connected to the pick-up coil. The compensation coil generates an opposite net flux to that of the pick-up coil. As the pick-up coil is closer to the

neuronal sources, the magnetic field will decay between coils in the order of $1/r^2$, and generate a current only at the pick-up coil (see Figure 6.11). For magnetic sources related to noise, typically from sources far away from the head, field decay between coils will be 0 or very small. This means that they will generate similar levels of current at both coils, and because they generate opposite currents, the noise will cancel-out. Further improvement of noise cancellation can be achieved through the use of synthetic third-order gradiometers which use 29 sensors in the MEG as a reference array (Hämäläinen et al., 1993). This ensures that all the sources of magnetic noise are detected and subtracted from the data (see Figure 6.10C).

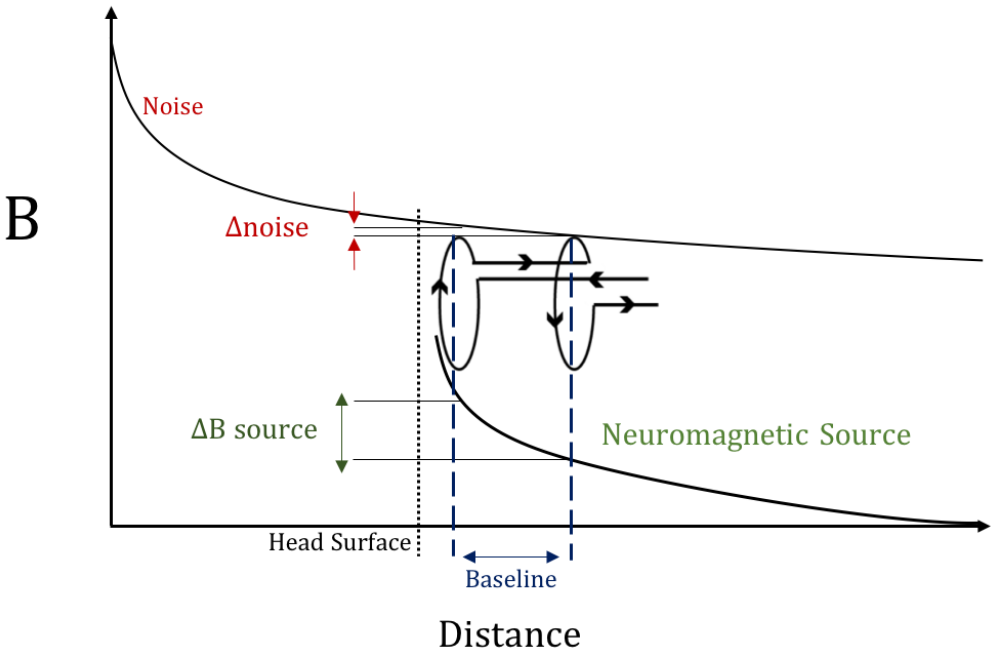

Figure 6.11: Illustration of the differential magnetic field (B) created by noise and neuromagnetic sources, and highlights the differences in signal drop-off with distance from the neuromagnetic source.

6.7 Subject Co-registration

6.7.1 Head Localisation

One disadvantage of MEG compared to EEG, is that the head of the subject is not attached to the sensors. In EEG, the electrodes are placed in the cap that moves with the subject, therefore each electrode is always in the relative position to each and to a patch of scalp. In MEG, this is not the case; the head is free to move, even using foam padding. This creates serious issues with co-registration of the sensors to the individual subject's anatomy (see Figure 6.12). In order to circumvent these issues, head localisation coils along with a 3D shape digitiser (Polhemus 3SPACE^{TM} FASTRAK®, Colchester,Vermont, USA, http://polhemus.com) are used. For each subject, approximately 500 points of the scalp, eye-sockets, and nose bridge were digitised prior to MEG data collection. After the prepossessing stages of anatomical data (i.e., MRI cortical segmentation), the skull and brain were co-registered to the sensors, first using manual alignment and then an iterative closest point algorithm (part of the Fieldtrip/Brainstorm toolboxes) was used to refine the head registration between the sensors and the anatomy. In the MEG experiment, T_1-weighted MPRAGE anatomical scans from either 3T or 7T were used depending on availability.

6.7.2 Freesurfer sphere registration for group analysis

In order to conduct group analysis of the MEG data on a source level, subjects' individual anatomy must be co-registered to a common space. Wide-spread volumetric approaches such as those outlined by Talairach and Tournoux (1988) are often used to co-register individual anatomies to template anatomies. However, they treat the cortex as a 3D structure which leads to substantial estimation

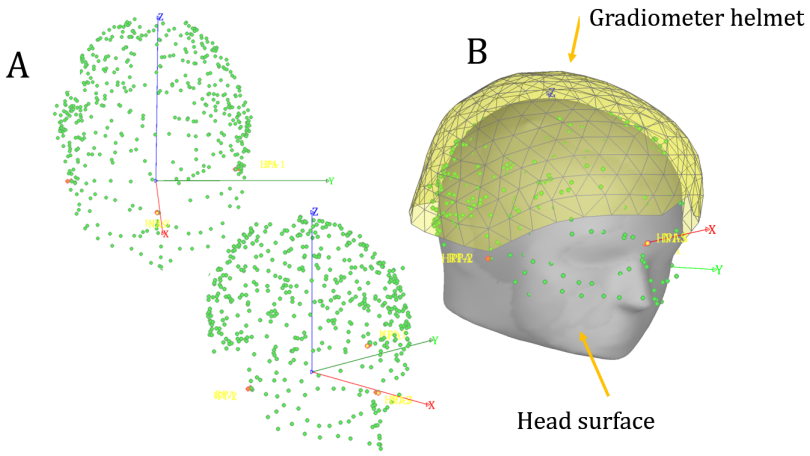

Figure 6.12: A, digitised 3D points using the Polhemus system. B, Head-surface, digitised points and sensors aligned to individual anatomy.

error in the distances between two points in the cortex (Fischl, Sereno, Tootell, Dale et al., 1999).

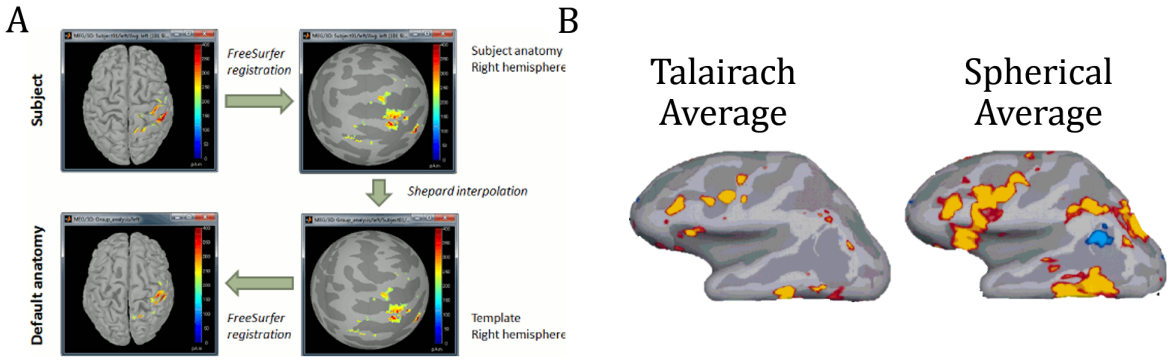

Figure 6.13: A, diagram of morphing algorithm used to match individual cortical anatomies to a template anatomy, extracted from http://neuroimage.usc.edu/brainstorm/Tutorials/CoregisterSubjects. B, Example of averaging of 20 subjects using a Talairach procedure or the spherical procedure in, and image extracted from, Fischl et al. (1999).

Several studies have demonstrated that this method is ill-suited to handle anatomical variability that is often seen between individuals. Using an approach that treats the cortex as a 2D cortical sheet achieves a better representation with the underlying sources that contribute to the MEG signal. Therefore, I use a registration technique that relies on the 3D reconstruction of the cortex using

Freesurfer algorithms (see 3D Cortical Flattening and Surface Based Atlas). This uses inflation of the 3D individual subject anatomy into a sphere, allowing the preservation of anatomy whilst adapting for relative size. Then, an interpolation algorithm (see Figure 6.13A) is applied to the individual subject sphere and a template, and they are aligned by minimising the squared difference of the convexity between individual spheres, followed by minimisation of the metric distances - which distorts or restrict distortions of individual anatomies to increase the correlation with the template and to account for individual variability.

Chapter 7

Lateral Occipital N1 Responses to Hands and Distorted Fingers.

7.1 Overview

In this chapter I describe two experiments that used occipito-temporal event-related potentials (ERPs) as response correlates of activation in the extrastriate body area (EBA). The purpose of these experiments was to address step 2 in the thesis: to determine whether abnormal finger postures are detected early in the visual processing stream, which could potential underlie a trigger for an embodied response as demonstrated in Chapter 5.

The first experiment assesses whether ERP differences exist between hands and whole bodies in order to find a suitable component for the investigation of distorted hands postures in Experiment 2. As a secondary aim, attempts are made to replicate lateralisation effects of EBA involvement in fMRI studies showing left hemisphere dominance in this occipital region. Results showed that

already at N1 latency of ≈ 170 ms, hand-related ERP patterns manifest in two results: 1) significant differences in amplitude for images of hands versus bodies in occipito-temporal N1 responses; 2) left lateralisation of responses to images of hands, and also of the difference waveforms (hands minus bodies), quantifying hand-related responses.

In the second experiment, I investigated if distorted finger postures modify the biologically specific processing mechanisms underlying the N1 response to hands (justified by the results of Experiment 1). Subjects viewed computer-generated images of hands (distorted and natural), and as a control, images of chairs (distorted and natural). Stronger N1 responses were found for distorted hands and were absent for distorted chairs. N1 modulation was robustly right-lateralised (unlike Experiment 1), and could reflect distorted hands as emotionally laden stimuli (Schürmann et al., 2011). These results are in line with enhanced visual processing of hands as highly salient body parts, with distortions engaging neural resources that are especially sensitive to biological stimuli and may underlie the start of embodied responses, as introduced in Chapter 1: *Viewing Bodies*.

The results of Experiment 1 have been published in *Neuropsychologia*, Santo, Maxim and Schürmann (2017) and Experiment 2 in *Scientific Reports*, Santo, Chen and Schürmann (2017).

7.2 N1 Responses to Non-Distorted Images of Hands

Hands, much like faces, communicate a wide variety of social and cognitive information. Hand and body postures work together to emphasise and express language and emotions. Pointing gestures are a good way to orient attention, leading to an increased focus on hand postures during observation of arm movements (Matarić & Pomplun, 1998). Crucially, from a young age, as early as 3

months, there is intense practice of different hands postures (D'Entremont, Hains & Muir, 1997), and greater attention to others' hand gestures rather than relying on gaze only for orienting attention (Langton, Watt & Bruce, 2000; Yu & Smith, 2013). This suggests that hands play an important role in social and cognitive development, therefore may enjoy some form of 'special' processing like faces (McKone, Kanwisher & Duchaine, 2007). Indeed, fMRI studies seem to support this assertion with findings of a double dissociation of responses between hands and bodies in the left lateral occipital cortex (LOC, Bracci et al., 2010; Weiner & Grill-Spector, 2011; Bracci et al., 2012).

While the visual processing of bodies has been studied in fMRI and electrophysiology (as explained above), research questions regarding hand-related occipito-temporal responses have so far only been addressed in fMRI (for example, Op de Beeck et al., 2010; Bracci et al., 2010 and 2012, Orlov et al., 2014), with the exception of Taylor et al. (2010), which did not formally test amplitude differences to hand-related responses (but grand average waveforms show large left hemisphere LOC amplitudes). As a control condition, images of whole bodies were included, which are known to elicit N1 responses that have been linked with EBA activation (Thierry et al., 2006; Taylor et al., 2010). To ensure that N1 responses to bodies were comparable to findings in earlier work, images of faces and objects were also included as reported in earlier studies (Thierry et al., 2006). Consequently, I assessed hand-related ERP responses (versus bodies), and tested the difference in laterality effects between hand and body conditions. This experiment served as the first stage of investigation of LOC (or EBA) involvement in the triggering of an embodied response, and helped to narrow down ERP components sensitive to hands to facilitate research in Experiment 2.

Based on previous fMRI studies, and guided by grand average waveforms in Taylor et al. (2010), I predicted the following: 1) Occipito-temporal electrodes will show different N1 amplitudes for hands compared with bodies; 2) this amplitude difference will be stronger in the left hemisphere compared to the right hemisphere; 3) underlying this hemispheric difference is an asymmetric response to hands: left N1 to hands will be more negative than right N1 to hands.

7.2.1 Methods

Subjects. A total of 33 subjects (24 female), with age mean±SD= 24.4 ± 3.4 years participated in this experiment. Subjects were right-handed, with no history of neurological or psychiatric problems nor drug abuse (all by self-report). This experiment was approved by the ethics committee of the School of Psychology, University of Nottingham (Ref: 692R).

Stimuli and Procedure. Subjects sat approximately 60 cm from the screen and stimuli were resented on a ViewPixx3D (VPixx Technologies, Saint-Bruno, QB, Canada) presentation monitor (1920$times$1080 pixels, 23.6 in., 120 Hz refresh rate, 1 ms pixel response time). Subjects viewed images of hands, bodies, faces, and objects.

Images were shown at 4° of visual angle, consisting of 250 × 250 pixels. Images of hands, bodies, and faces were as in bracci2010dissociable, and used with the authors' permission. Face images portrayed 18 female and 18 male individuals in neutral expression with gaze diverted. Images of the hands consisted of 36 hands of both sexes (not identifiable from pictures), 14 in palmar view, 19 in dorsal view and 3 viewed from the side. Of the 36 hands (15 left), 21 were in passive/relaxed positions, and 15 suggested a form of grasp or action. Images

of bodies had the heads removed, bodies were all clothed and the set consisted of 18 female and 18 male models. Images of objects were acquired online from http://www.cogsci.nl/ stimulus-sets and consisted of 20 man-made objects (e.g., bag, button, fork, candle) and 16 natural objects (e.g., flowers, leaf, sea-shell, peanut). In total 36 different fully desaturated (black and white) images per category were presented three times. Stimulus order was pseudo-randomised in order to allow images to be repeated for purposes of a 1-back task. Each image was presented for 200 ms, immediately followed by a fixation point of jittered duration (randomised, either 1000, 1200, or 1500 ms, see Figure 7.1). During the presentation of these images, subjects were instructed to press a button on a Cedrus Response pad (4^{th} generation, Cedrus Corporation, San Pedro, CA, www.cedrus.com) whenever they saw an image that was identical to the preceding image (1-back task). In total 432 stimuli were presented (4 categories $\times$ 36 images $\times$ 3 repeats), excluding 5% repeated 1-back trials and in total this task took approximately 12 minutes to complete.

Data Acquisition. Data was acquired using the EEG equipment and explained in Chapter 6: *The EEG system.*

Signal Processing. Signal processing was performed in Matlab (The MathWorks Inc., Natick, MA) using Fieldtrip (Oostenveld, Fries, Maris & Schoffelen, 2011) and EEGLAB (Delorme et al., 2011) routines. Due to active electrodes (see *The EEG system*), the BioSemi systems allow for reference-free recordings, and only at the pre-processing stages were the time series of the electrodes referenced to an all-electrode average. Data were band-pass filtered between 0.4 and 35 Hz followed by a visual search (blind to condition) to identify obvious bad trials

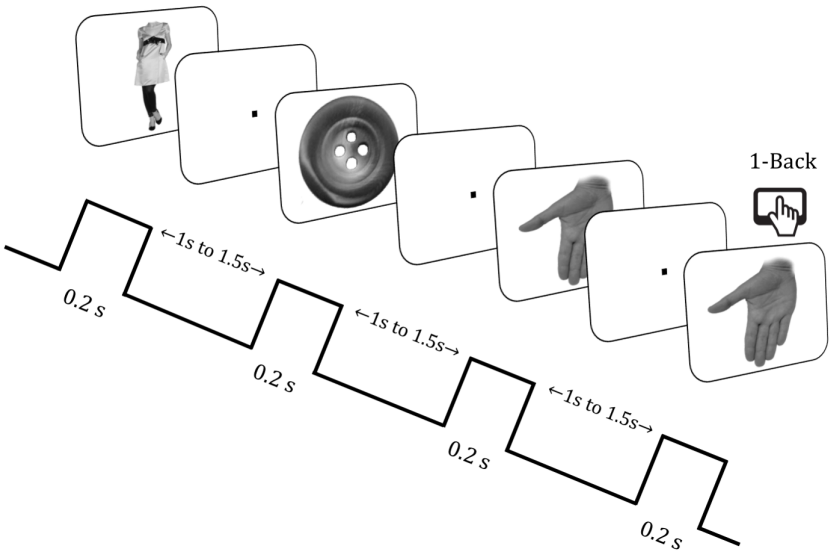

Figure 7.1: Experimental design.Each trial consisted of 0.2 s presentation of a stimulus of one of the four categories, followed by a fixation mark (inter-stimulus interval either 1 s, 1.2 s, or 1.5 s). The schematic image of the hand pressing a button indicates a valid 1-back target (this occurred in 5% of trials).

based on typical artifact waveforms (as described for example in Hari & Puce, 2017, Chapter 8). Such trials were removed from the dataset. A plot of trial by variance was created to identify which trials had largest variance. Those that had standard deviations >5 z-values were removed from the data (Bigdely-Shamlo, Mullen, Kothe, Su & Robbins, 2015). ERP data for each trial was collected, baseline corrected and averaged for each participant, with an epoch length of -200 ms (from stimulus onset) to 500 ms (post-stimulus onset). Subsequently, segmented trials were put through an independent component analysis (ICA) using the algorithm runica (see Makeig, Jung, Bell, Ghahremani & Sejnowski, 1997), allowing for blind separation of the underlying component topographies. The results of the ICA were then put through an automatic artifact rejection algorithm (MARA, Winkler, Haufe & Tangermann, 2011) to flag topographies containing blinks, vertical or horizontal eye movements, muscle activity, and other noise-related artefacts. This algorithm is a linear classifier that rates different fea-

tures of the topographies and provides a classification of 'reject' (for noise and outliers) or 'accept'. Even though MARA is a robust method, some artifacts can escape rejection, for example blinks that are highly correlated with stimuli presentation. Therefore, this step was complemented with visual inspection to validate the classification, searching for well-known artifact topographies (see examples in Jung, Makeig, Humphries et al., 2000 and in Jung, Makeig, Westerfield et al., 2000). After these steps, trials were sorted by condition and averaged, resulting in 4 averaged waveforms per subject (hands, bodies, faces, objects).

Event-related Potential Analyses. In order to explore the hypotheses outlined above a mass-univariate approach was taken as it requires fewer a priori assumptions, and allows one to find smaller differences between conditions that extend across time as opposed to selecting a single value from a time-window (for review, see Groppe, Urbach & Kutas, 2011). Using Fieldtrip functionalities, to address hypothesis 1) a mass-univariate two-sided t-test was conducted across all time points and electrodes, for each individual subject average for the contrast hands $\neq$ bodies. For hypothesis 2), first the difference for each electrode across all time points between hands and bodies was calculated, generating one single topography of the difference for each time point. Then, the resulting topography was split into right and left hemispheres, and the right hemisphere electrodes were assigned to the corresponding position of the left hemisphere - so that for example, P8 is now P7 - effectively flipping the right hemisphere topography to the left. This allowed direct comparison between right and left electrodes. Following this flipping procedure, a one-tailed mass- univariate t-test was conducted to directly test for left-lateralised hand-versus-body differences. To test hypothesis 3), the same flipping procedure was performed as above, but now using

the waveforms for the hand condition. The electrodes in the right hemisphere were assigned to the left, and a one-tailed mass-univariate t-test was conducted to directly test for left-lateralised brain responses to hand images. A Monte Carlo distribution (N = 2000) of t-statistic for each comparison was obtained to define the critical t-value on the tested sides of the distribution. Then, multiple comparisons were further corrected using a threshold-free clustering algorithm as implemented in Fieldtrip (Oostenveld et al., 2011) to find significant time points where the maximum cluster t-statistic survived the threshold (cluster alpha = 0.05, minimum neighboring channels = 2). Latencies were extracted based on the most negative waveform within a time interval of 150–200 ms within P7, P9, PO7, PO3, and P8, P10, PO8, PO4 as electrodes of interest (closely matched to electrodes studied in Thierry et al., 2006) and tested for differences in a repeated measures ANOVA using SPSS (IBM, Armonk, NY).

Outlier subjects were identified based on two criteria. First, individual subjects' condition-specific averages were visually inspected (blind to the condition) in order to find atypical waveforms. Those that did not show clear waveforms in all 4 conditions above the baseline were removed. This was done so that mean ERP waveforms are not grossly contaminated by non-brain signals such as muscle activity, eye movements, impedance fluctuations, or amplifier blocking which can alter follow-up analysis at a group level (Hari & Puce, 2017). This resulted in the removal of 2 subjects from further analysis, leaving 31 subjects. Second, in order to remove those subjects that were paying enough attention to the task, as this can influence the amplitudes of the ERPs (Parks, Gannon, Long & Young, 2016) behavioural performance in the 1-back task was assessed in terms of accuracy = hits/ (hits+misses) * 100. Subjects with accuracy below 80% were also removed.

This led to the removal of 3 further subjects, leaving 28 subjects.

7.2.2 Results

7.2.2.1 Behavioural Results

Accuracy analysis of hits and misses on the 1-back task (N = 28, after removal of outliers) resulted in a mean accuracy of 95.5% with SEM of 1.3%.

7.2.2.2 ERP Waveforms and N1 Peak Latencies

Typical ERP waveforms were present in all subjects (N = 28): P1, N1 (N170/N190), and P2 as seen in grand averages (see Figure 7.2). N1 latencies (as means over P7, P9, PO7, PO3, and P8, P10, PO8, PO4) were 167 ms (SD = 8 ms, min/max = 151/186 ms) for faces, 173 ms (SD = 10 ms, min/max = 153/194 ms) for bodies, 174 ms (SD = 10 ms, min/max = 152/188 ms) for hands and 174 ms (SD = 10 ms, min/max = 151/ 190 ms) for objects [$F(1,27) = 13.73$, $p < 0.001$, repeated-measures ANOVA]. In post-hoc t-tests (two-sided, Bonferroni-corrected), latency differences were significant for faces versus bodies ($p < 0.001$), faces versus hands ($p < 0.001$), and faces versus objects ($p < 0.001$), also bodies versus objects ($p = 0.036$). No other comparisons resulted in significant differences (all $p > 0.05$).

For bodies, the overall waveforms of grand average responses, including relative amplitudes and latencies compared with faces and objects, were highly similar to responses in earlier work (Thierry et al., 2006). Beyond this initial comparison, faces and objects are not directly relevant to the research questions and will not be analysed further.

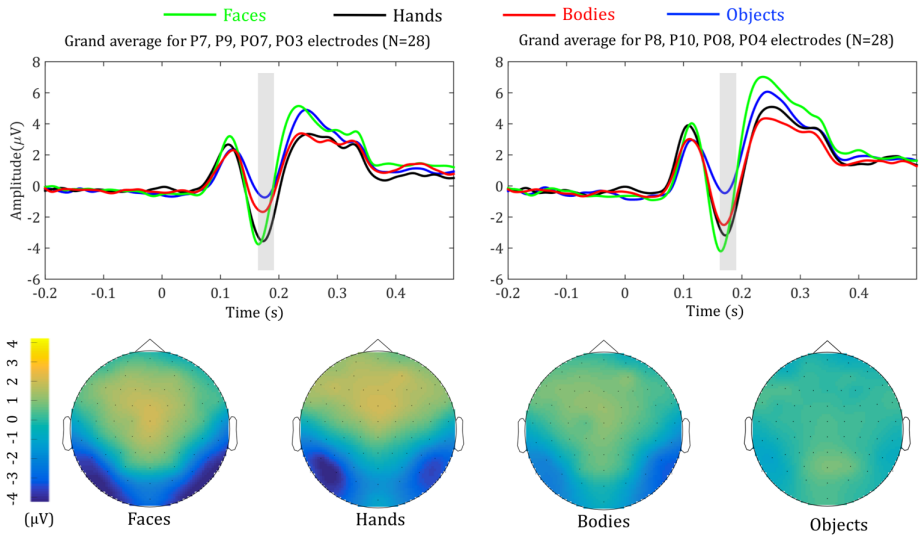

Figure 7.2: Top panel: Grand average event-related potential waveforms (N = 28 subjects) for each viewing condition, averaged across P7, P9, PO7, PO3 (left hemisphere) and P8, P10, PO8, PO4 (right hemisphere). The N1 elicited by faces peaked approximately at 167 ms, other conditions elicited significantly later peaks – hands, 174 ms; bodies, 173 ms; objects, 174 ms (averaged across above-mentioned electrodes). Each waveform was baselined using a 200 ms pre-stimulus interval. Stimulus duration 200 ms. Bottom panel: Averaged topography for each condition over greyed-out area (160–190 ms) in waveform plots.

7.2.2.3 Responses to Hands Differ from Responses to Bodies

A mass univariate dependent samples two-tailed t-test for hands ≠ bodies was performed in the time period of 0–400 ms. Permutation tests established critical t-values= ±2.052. Significant amplitude negativity difference ($p < 0.001$) between hands and bodies was found over the parietal, occipito-temporal and parieto-occipital electrodes in the time period of 75–275 ms after stimulus onset (see Figure 7.3). In these electrodes, this difference was observed in P1, N1, and P2 peaks of the waveform. Out of the eight electrodes of interest, six (P7, P9, PO7, PO3, and PO8, PO4) showed significant differences between 125 and 275 ms. Here, I just report the condition-specific difference in the N1 latency range to which the research questions are related. Maximum difference of the N1 occurred at 174 ms.

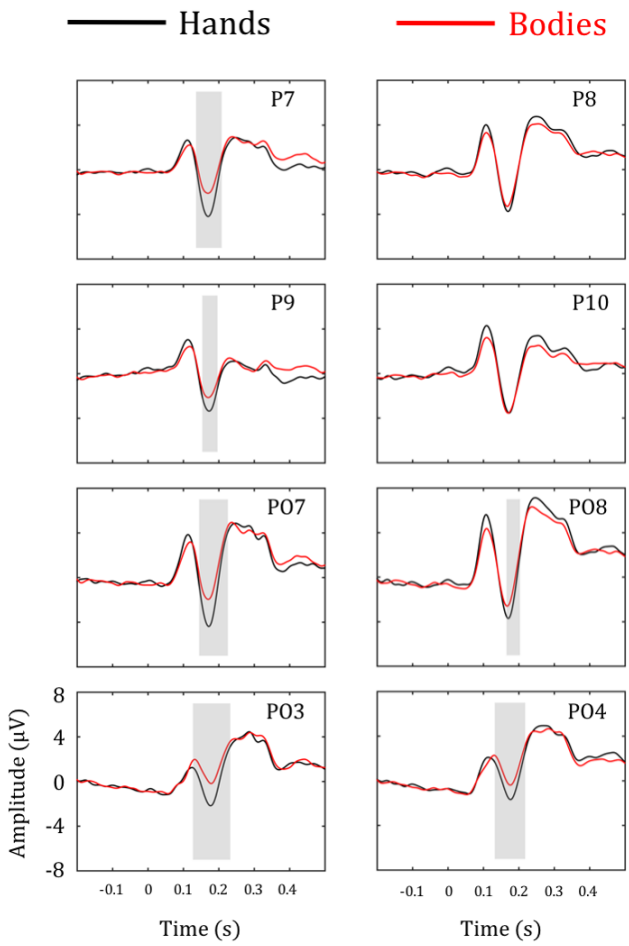

Figure 7.3: Grand average event-related potential waveforms (N = 28 subjects) for the electrodes of interest (P7, P9, PO7, PO3, and P8, P10, PO8, PO4) similar to (Thierry et al., 2006) for the observation of hands (black) and bodies (red) images. The grey panel indicates areas of significant difference ($p < 0.001$) between conditions calculated using a mass-univariate t-test between waveforms.

7.2.2.4 Hemispheric Dissociation of Responses to Hands and Bodies

In order to investigate hemispheric dissociation of the hand and body stimuli, first a difference wave ($hand - body$) was calculated for each electrode and each subject (see Figure 7.4, note that more negative amplitude in the difference waveform indicates stronger responses to hands than to bodies).

To compare the amplitudes of difference waves from left versus right hemisphere electrodes, a mass-univariate dependent samples one-tailed t-test was per-

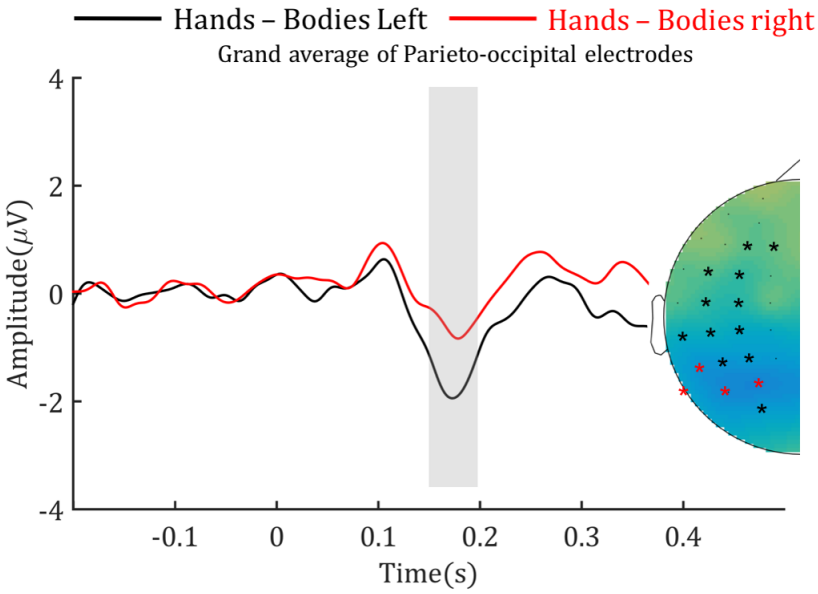

Figure 7.4: Grand average waveforms (N = 28) for the difference in amplitude between hands and bodies on the right and left hemispheres, averaged over P7, P9, PO7, PO3 and P8, P10, PO8, PO4. The difference between conditions is larger on left hemisphere (black line) versus right hemisphere (red line). Over both hemispheres, the difference waveform is negative, indicating stronger responses for hands versus bodies (see Figure 7.3). To test the significance of the difference between hemispheres, the difference-wave topography was flipped (see Section 7.2.1) and a mass-univariate t-test was conducted between the left hemisphere electrodes and the right-flipped hemisphere electrodes. Electrodes with significant hemispheric differences ($p<0.05$) are highlighted with asterisks (with red asterisks corresponding to the waveform display) superimposed on the topography of the hemispheric difference-waveform [$Left(hands–bodies)–Right(hands–bodies)$]. Colour scale same as in Figure 7.2. Significance for $Left(hands–bodies)–Right(hands–bodies)$ was observed in the time period of 142–199 ms. This time window, depicted in grey in the waveform display, was established as the common time window of significance across the parieto-occipital electrodes used for the grand-average plot.

formed in the time period of 0–400 ms and a critical t-value=-1.703 was. Significant differences (p = 0.036) were found in parietal, parieto-occipital, occipito-temporal and central electrodes in the time window of 140–278 ms. In occipito-temporal electrodes this difference started at N1 latency but did not extend to P2 latency (see Figure 7.4). The maximum difference at PO7 where the *hands − bodies* amplitude difference was of 2.45 μV.

7.2.2.5 Left N1 to hands more negative than right N1 to hands

The last aim of the study was to investigate whether responses to hand stimuli are lateralised to the left hemisphere. A mass-univariate dependent samples one-tailed t-test on the amplitude between left and right hemisphere was performed in the time window of 0–400 ms. The results showed that an early left versus right difference was seen in PO7/8 and P7/8 electrodes starting at 174 and 183 ms respectively, which is the time corresponding to maximum N1 amplitude for hands. This difference then continues into P2 latency and is also seen in C5/6, CP5/6, TP7/8, P9/10, P5/6, P3/4, PO3/4, and O1/2 electrodes from 205 ms (see Figure 7.5).

7.2.3 Discussion

This experiment aimed to find hand-related features of the occipito-temporal waveforms using images of the hand and of bodies for comparison. In line with ERP predictions, the results of this experiment were three fold: 1), a significant topographical difference between responses to hands and bodies at the N1 latency was observed; 2) when comparing the waveform difference between hemispheres, the difference between hands and bodies was larger in the left than in the right hemispheres; 3) a significant lateralisation to the left was also found starting

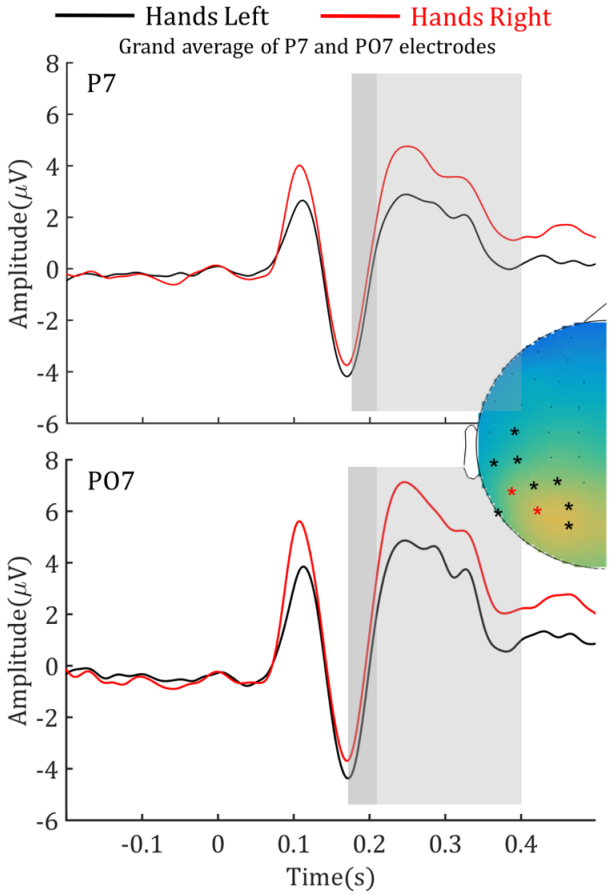

Figure 7.5: Grand average event-related potential waveforms (N = 28) for left (black) and right (red) hemisphere for the viewing of hand stimuli for electrodes P7/P8 and PO7/PO8 (red asterisks on the topography for P7 and PO8). To find the difference between hemispheres, the waveform topography was flipped and a mass-univariate t-test (flipped versus original) was conducted on the left hemisphere electrodes. Asterisks superimposed on the topography indicate significant differences between left and right hemisphere responses to hands ($p < 0.05$). Colour scale same as in Figure 7.2. The results showed a significant difference between hemispheres starting at 183 ms for P7 versus P8 and at 174 ms for PO7 versus PO8 (darker grey, on the waveform plots, and red asterisks on the topography) exclusively, overlapping with the N1 component. Later significant differences were observed in other electrodes (black asterisks, starting from 205 ms ending at 400 ms), indicated by the lighter grey.

at the N1 latency for responses to hand stimuli. These were stronger in the left than in the right hemisphere. These findings suggest that different body parts have specific regions of the cortex dedicated to their encoding that starts at the N1 latency, and this complements previous fMRI findings indicating a left hemispheric lateralisation of visual processing of hands (Bracci et al., 2010; Orlov et al., 2010; Bracci et al., 2012).

As the current experiment specifically compares hands with a semantically

matched control condition (bodies), it goes beyond earlier research reporting responses to observed hands in MEG (such as Avikainen et al., 2003) and EEG (such as Möhring, Shen & Neuhaus, 2014). These studies found lateral-occipital responses to hands (with latencies of less than 200 ms, in line with our results), but non-hand controls were not required, due to the intended comparison between different hand postures or gestures. Furthermore, our result of stronger responses to hands than bodies are congruent with the findings from fMRI research. An fMRI study compared voxel specificity to faces, non-body parts, torsos and hands, reporting hands versus torsos as the strongest between-categories difference (Op de Beeck et al., 2010). This difference led to distinct topographical representations with hand representations overlapping more with extrastriate areas, and torsos more represented in the ventral areas of the occipito-temporal cortex and fusiform area. Furthermore, Orlov et al. (2010) demonstrated cortical activation with well-defined borders after visual presentation of different body parts. Along side this evidence, the current study showed a significant difference in N1 amplitude between whole body viewing and hand viewing suggesting larger neuronal populations and/or stronger involvement of specific neuronal regions for hands. This prompts the use of the N1 component for investigating distorted hand postures in the following EEG experiment in Section 7.3.

The result of different hemispheric involvement in visual processing of hands - as stronger hand-related responses (versus whole bodies) in left hemisphere, and as left laterality for responses to hands is in line with fMRI results: In Bracci et al. (2010) it was shown that hand viewing has a dedicated processing region on the left. These results and the complementary electrophysiological data here, converge on left lateralisation of occipito-temporal responses to hands.

This result matches the N1 responses to hands in Taylor et al. (2010). In the grand averages of their study, responses were stronger over the left hemisphere, but lateralisation was not tested for significance. In contrast, this contains a direct statistical test of response laterality. Not directly related to the main research questions, it is interesting to note that in contrast with fMRI results in Bracci et al. (2010), right hemispheric occipito-temporal ERP responses are not stronger for bodies than for hands (neither in Taylor et al. (2010) nor in the current study). To interpret this disparity, it is important to notice that fMRI, in comparison with ERPs such as N1, captures activity in a much broader time window after a stimulus, in particular when stimuli of one category are grouped together in a block design, unlike the random order of stimuli in ERP studies. The disparity could therefore hint at different temporal dynamics of responses to hands versus bodies, a topic of interest for future studies, but also points towards an N1 sensitivity to observed hands. This point makes the N1 particularly suited for the investigation of distorted finger postures in the next experiment.

Whilst complementing fMRI results of hand-specific visual brain areas, this is the first electrophysiological study to empirically demonstrate a laterality effect of observing hand stimuli which suggests a specialisation of the left hemisphere to hand perception. Therefore, it would be interesting to investigate whether this laterality is replicated when observing distorted finger postures, which have a laden emotional quality and therefore likely to be right lateralised (Schürmann et al., 2011). As an added outcome of this research, the occipito-temporal N1 could be used to investigate whether this lateralisation effect remains true for the observation of other body parts, especially ones involved in motion (i.e., those body parts that have larger degrees of freedom for movment).

A potential confound to consider is the that the exclusion of subjects may have biased the results. In Parks et al. (2016) this potential source of bias is addressed by bootstrapping the SNR of each subject and achieving a normal distribution of 'good' SNR and only those that are above an arbitrary threshold are included for statistical analysis. In this study, I used visual inspection of the ERP wave formations, blind to conditions categories, to investigate whether or not they showed the typical P1,N1,P2 arrangement that should be observed in these type of ERP studies. For a variety of reasons some subject may not show measurable waveforms, and visual inspections in the traditional (Hari & Puce, 2017), albeit slightly subjective, method of subject inclusion. Given, the size of the sample of this study, I can still be certain of results reported here, however, in the future it is important to consider more objective methods for subject inclusion.

In conclusion, the occipito-temporal N1 may be an important tool for investigating social processes which may involve hand postures (such as in following experiment), and/or observation of action and pain, providing new insights in social neuroscience at lower cost, and of easier access than fMRI.

7.3 N1 Responses to Images of Distorted Fingers

In the previous experiment, results showed that observing images of hands not only influenced the amplitude of N1, but also its lateralisation. This effect manifested in two ways: first, hand images elicited larger amplitudes compared to whole bodies, and second these effects were also lateralised to the left hemisphere. Based on these results, the N1 evoked component is the ideal candidate as a measure of the impact of finger distortions in early visual processing of observed bodies.

The current experiment aimed to assess the role of lateral-occipital brain areas as nodes of interest (see Chapter 1, 1.3) in the network of embodied simulation using the N1 ERP component as a correlate of LOC (or EBA) activity. As explained in Chapter 1, 1.4, lateral occipital and fusiform areas are sensitive to images of body parts, according to brain imaging studies (Downing et al., 2001; Peelen & Downing, 2005; Thierry et al., 2006; de Gelder et al., 2010), however, N1 responses to faces and whole-body postures also vary with emotional expression (Eimer & Holmes, 2007, Borhani et al., 2016). Although of a different quality than fearful body postures, images of distorted fingers are emotionally laden, in that they can make an observer feel uneasy, and this could lead to stronger N1 responses. This effect could also be due to the novelty of the distorted hands which requires increased visuospatial attention. To separate between emotional contents vs. novelty and visuospatial processing (which may lead to stronger N1 responses), it is necessary to introduce additional control stimuli that match in terms of novelty and visuospatial processing while lacking the emotional contents of distortion applied to hands as biological stimuli. In certain orientations, the back of the hand and four fingers (except thumb) are compellingly similar to the backrest and four legs of a chair[1]. Here, they were used as control stimuli, and to match to distorted hands, the same distortion script (see Chapter 2: Stimuli Creation) was applied to the chairs' legs. Figure 7.6 gives examples of all stimulus categories. Adding these control stimuli goes beyond earlier research, where analyses were limited to comparisons between distorted and natural fingers, as these studies aimed to facilitate detection of distortion-related activation.

The current study using occipito-temporal N1 responses to images of *hands*

[1]In fMRI studies in search of activation sensitive to images of hands, chairs served as non-biological controls (Bracci et al., 2010, 2012; Zopf & Williams, 2013).

versus *chairs* in *distorted* versus *standard* configuration addressed: whether the N1 is sensitive to biological abnormalities; and, because of the finding of right-lateralised S1 activation in the *distorted hands* condition in the fMRI experiment in Chapter 5, it investigates whether the right-left asymmetry occurs at the early latency of the N1 response. As Experiment 1 showed significant differences at the N1 latencies, the search can be limited in terms of electrode locations and response latency windows sensitive to the N1 response. Perspective factors (hand images all egocentric) was not added to this experiment in order to minimise the number of conditions, and because no clear difference between perspectives were found in the earlier fMRI study. Consequently, based on previous findings it was predicted: 1) N1 responses to distorted hands will be stronger than to natural hands; and the difference between distorted and standard will be stronger for hands than for chairs; 2) the distortion-related response to hands (established in the distorted vs natural contrast) will be stronger in the right hemisphere (relative to left).

7.3.1 Methods

Subjects. A total of 15 subjects (11 female), of age mean±SD = 24.80 ± 3.62 years, all right-handed by self-report and with no history of neurological or psychiatric problems nor drug abuse, also by self-report, participated in this experiment. In preparatory analysis, data from one participant was indenfied as an outlier (see below). Informed consent was obtained from all participants. The study was approved by the ethics committee of the School of Psychology (University of Nottingham) and performed in accordance with the declaration of Helsinki.

Stimuli and Procedure. Stimuli comprised of the 48 images of only right hands (24 distorted, 24 standard, i.e., natural). Hand images were complemented with 48 images of chairs (24 distorted, 24 standard). Hand stimuli were created as in Chapter 2, 2.2, however, an extra desaturation step was added to remove differences in colour between hand and chair images as this may be a potential confound for ERP amplitudes. Chair stimuli were created using method similar to that outlined in Chapter 2, Section 2.2. Please refer to Appendix C, or Santo, Chen and Schürmann (2017) supplementary material, for more information on how the chairs were created.

Stimulus size, presentation duration, ISI, and viewing equipment were the same as used in Experiment 1. See Figure 7.6 B for a schematic of the experimental time-line. In order to keep participants' attention, a small number of images was superimposed with a white shadow (100 x 100 pixels, opacity ratio 0.6). The number of shadows that would appear was randomised between 8 and 16 per run. Subjects were informed of the minimal and maximal number at the beginning and instructed to respond with a button press upon detection of a shadow and to keep a mental count of how many shadows they saw. Before the start, they completed two minutes of practice. At the end of each experimental run (5 in total), they were asked how many shadows they counted.

Data Acquisition and Signal Processing. Data was acquired using the equipment and as explained in Chapter 6 *The EEG system.* For signal processing see section 7.2.1. After these steps trials were sorted by condition and averaged, resulting in 4 averaged waveforms per subject (distorted fingers and chairs, and natural (or standard) hands and chairs).

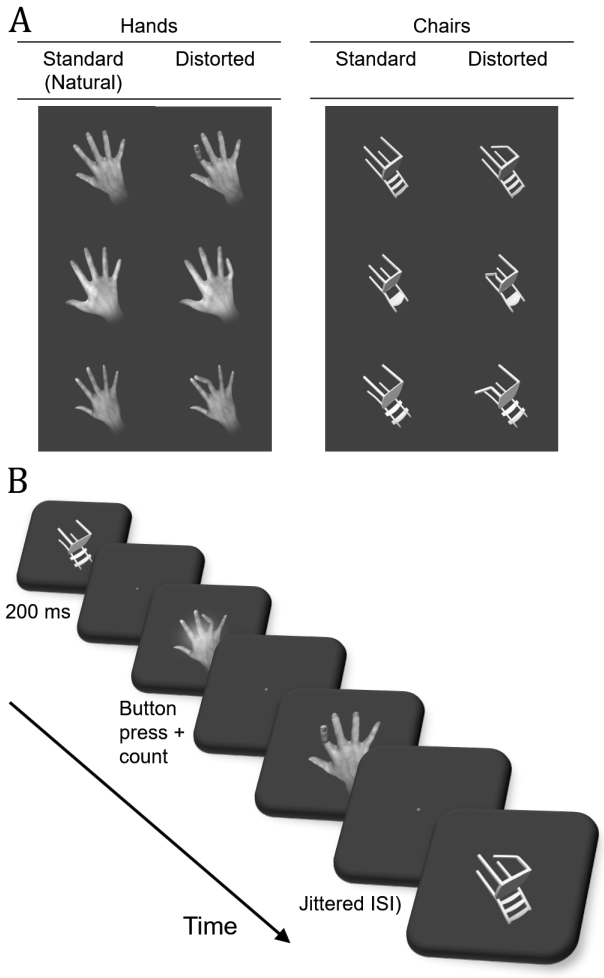

Figure 7.6: Stimulus setup. A) Stimulus categories, 3 (out of 6) exemplars per category, each in natural and distorted configurations. Stimuli computer-generated using the protocol developed in Stimuli Creation. B) Stimulus time-line. Stimuli not shown to size (actual size 4° of visual field).

LOC N1 analysis. For each hemisphere, three electrodes overlying lateral occipito-temporal cortex were chosen for analysis: P7, P9, PO7, and P8, P10, PO8 (complementary locations to Thierry et al., 2006). This selection was based on the above experiment of N1 responses sensitive to images of hands and on an older study of N1 responses to whole bodies (Thierry et al., 2006). N1 amplitudes were extracted based on the most negative waveform within a time period of 150 to 200 ms for each of the 6 electrodes, using a baseline of −200 to 0 ms. One participant's data was classified as an outlier (outside 2 SD in multiple electrodes), therefore these data were removed from further analysis. This is different

from experiment 1 because in the current experiment the criteria was based on peak values rather than the standard deviation of within the trial as it was in experiment 1. The remaining 14 subjects' amplitude data underwent a within-subjects repeated measures ANOVA with factors of stimulus type (hand, chair), configuration (distorted, standard), and hemisphere (left, right), using data averaged across 3 electrodes per hemisphere. A second analysis step was performed by conducting an ANOVA of N1 peak latencies with the same 3 within-subject factors as above, using data from P9/P10 electrodes of maximal N1 amplitudes. Then, difference waveforms (distorted-standard) were analysed. Peak amplitudes of difference waveforms were measured in a time window of 150 to 250 ms (defined on the basis of visual inspection and therefore different from the time window for latencies in per-condition waveforms, see Figure 7.7) against a baseline of -200 to 0 ms. As measures of effect size, Cohen's d for t-tests and η_p^2 were calculated for ANOVAs (Lakens, 2013).

7.3.2 Results

7.3.2.1 Behavioural Results

As EEG data acquisition was split into 5 runs, each subject reported 5 mental counts of stimuli with superimposed shadows: On average, mental counts were correct for 4 out of 5 runs (across 5 participants for whom data were available, see Methods). Erroneous counts included too low and too high counts. The 5 individual subjects' total shadow counts were as follows: 53 (error + 1, relative to actual number of 52), 54 ($\pm$0), 62 ($\pm$0), 64 (-2) and 62 (-2). Overall, these data suggest attentive performance on a task that was not too easy and unrelated to the stimulus categories of relevance to the research questions.

7.3.2.2 ERP results

Figure 7.7A shows ERPs from an example location (P10), illustrating stimulus-type and configuration-related ERP differences. The hypothesis-driven analysis focused on amplitudes and waveform shapes at N1 latency as relevant correlates of LOC involvement. In the article (Santo, Chen & Schürmann, 2017) published as result of this work, exploratory analysis in latency windows before and after N1 are included but were not relevant for the purpose of this thesis. Overall, we studied amplitudes of P1 peaks (see Appendix C, or article), amplitudes of N1 peaks (see section *LOC N1 Amplitudes* below), the overall shape of N1 peaks in search of potentially prolonged responses (see section *Shape of the N1 Peak* section), and amplitudes in a broad window of 250 to 500 ms to capture response components later than N1 (seen appendix C, or article).

7.3.2.3 LOC N1 Amplitudes

The grand average over 3 electrodes per hemisphere (P7, P9, PO7, and P8, P10, PO8), N1 amplitudes and latencies are given in Figure 7.8. Because responses to distorted stimuli were to be compared with responses to standard (natural) stimuli, the first analysis step was a t-test across standard stimuli comparing hand versus chair responses (averaged across hemispheres). No differences were found, $t(13) = 0.267$, $p = 0.794$, Cohen's $d = 0.07$, thereby justifying the choice of standard stimuli as a baseline for comparisons with distorted stimuli.

In the main ANOVA on N1 amplitudes, no main effects were found to be significant (stimulus type, configuration, hemisphere, see table 7.1), but a significant stimulus type $\times$ configuration interaction was found, $F(1,13) = 7.009$, $p = 0.020$, $\eta_p^2 = 0.350$. This reflected a distortion effect of opposite direction

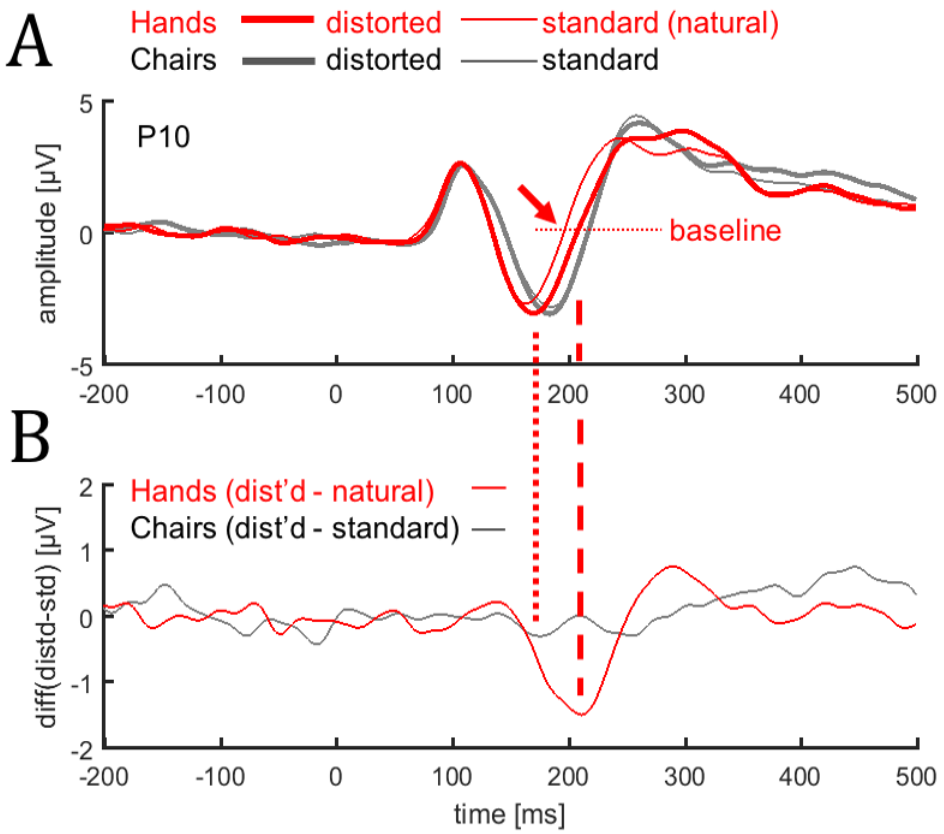

Figure 7.7: A) grand-average (N=14) time courses of ERPs at P10 to illustrate condition-related differences in the main analysis. Lines for hands are in red and chairs in black; for distorted, in heavy lines and for standard configurations in thin lines. Negative peaks in 150–200ms time window seen in all conditions. Arrows: For distorted hands, broader peaks (relative to natural hands). B) Difference waveforms, *distorted - natural hands* and *distorted - standard chairs*, calculated from corresponding curves in panel A, amplitude in μV but scale different from panel B. The peak of the difference waveform reflects a delayed return to baseline in the per-condition-waveform (dashed vertical lines).

for hands versus chairs, such that distortion increased the N1 peak amplitude in hands and decreased it in chairs. A significant configuration $\times$ hemisphere interaction, $F(1,13) = 13.879$, $p = 0.003$, $\eta_p^2 = 0.516$, was also found showing effects of opposite direction in left and right hemisphere. No other interactions were significant (see Table 7.1).

Table 7.1: ANOVA, all conditions, N1 amplitudes in per-condition waveforms (complementary with Figure 7.8), all factors within-subjects.

Effect	df	F	p	η_p^2
stimulus type (hand, chair)	1,13	1.582	0.231	0.109
configuration (distorted, natural/standard)	1, 13	0.001	0.970	0.000
hemisphere (left, right)	1,13	0.020	0.889	0.002
stimulus type × configuration	**1,13**	**7.009**	**0.020**	**0.350**
stimulus type × hemisphere	1,13	1.760	0.207	0.119
configuration × hemisphere	**1,13**	**13.88**	**0.003**	**0.516**
stimulus type × configuration × hemisphere	1,13	0.583	0.459	0.043

To facilitate the interpretation of the stimulus type × configuration interaction, two follow-up ANOVAs were performed. The first was for hands only, and a trending main effect (defined as p <0.1) was found for configuration, F(1,13) = 3.624, p = 0.079, η_p^2 = 0.218. This demonstrated a higher N1 amplitudes for distorted hands. In the second ANOVA, for chairs only, the only significant result was a configuration × hemisphere interaction, F(1,13) = 5.859, p = 0.031, η_p^2 = 0.311, which reflected lower N1 amplitudes for distorted chairs in the left hemisphere and not of immediate interest to the research question (see Figure 7.8).

7.3.2.4 Shape of the N1 Peak

Difference waveforms (distorted – natural, example in Figure 7.7B) served to identify potential condition-related differences in N1 response that were not captured in the analysis of peak amplitudes. These were computed for hands, the condition of interest, and also for chairs as the control condition. For each

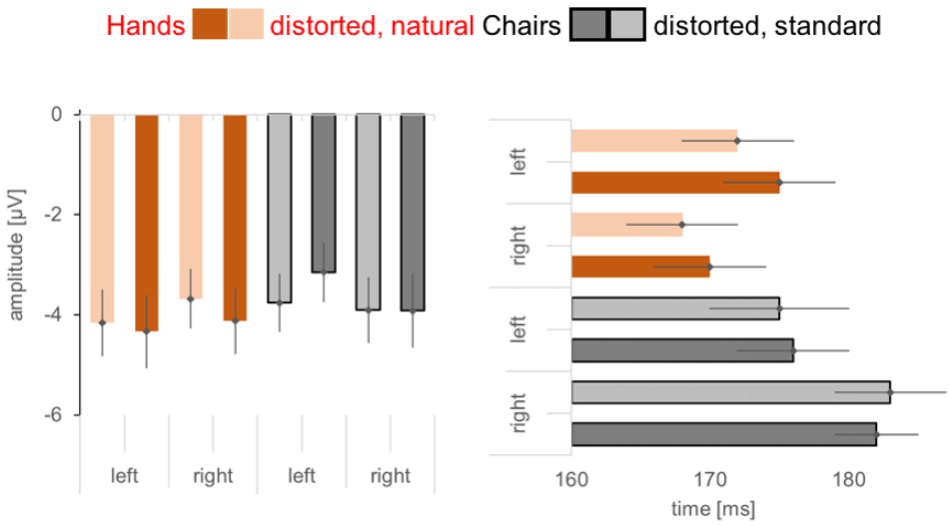

Figure 7.8: N1 amplitudes and N1 latencies, separated by stimulus type. Left bar graph shows N1 amplitudes for each of the stimulus conditions (mean ± SEM). Right bar graph shows N1 latencies for peak N1 amplitudes (mean ± SEM). Along the x-axis, latency in ms (relative to stimulus onset at 0ms)

of the 6 electrodes, difference waveforms are shown in Figure 7.9A, with clearly defined peaks for hands. Peak difference amplitudes for hands (averaged across all 6 electrodes) were significantly different from zero, $t(13) = 4.832$, $p < 0.01$, $d = 1.29$. For chairs, no clear peaks were observable, $t(13) = 0.360$, $p = 0.725$, $d = 0.10$. Consequently, further statistical analysis of difference waveform amplitudes was limited to the hands condition. In line with visual inspection for Figure 7.9A, a t-test demonstrated hemispheric differences, $t(13) = 2.755$, $p = 0.016$, $d = 0.74$, for amplitudes averaged across 3 electrodes per hemisphere. To further illustrate the effect underlying the grand-averages, Figure 7.9 B shows subject-by-subject peak amplitudes of difference waveforms in the 150-250 ms period. Negative difference waveforms (indicating stronger negative-amplitude responses to distorted vs natural hands) were present for 11 out of 14 subjects in the left hemisphere and for 13 out of 14 subjects in the right hemisphere. Amplitudes were lower for right (vs left) hemisphere in 9 out of 14 subjects.

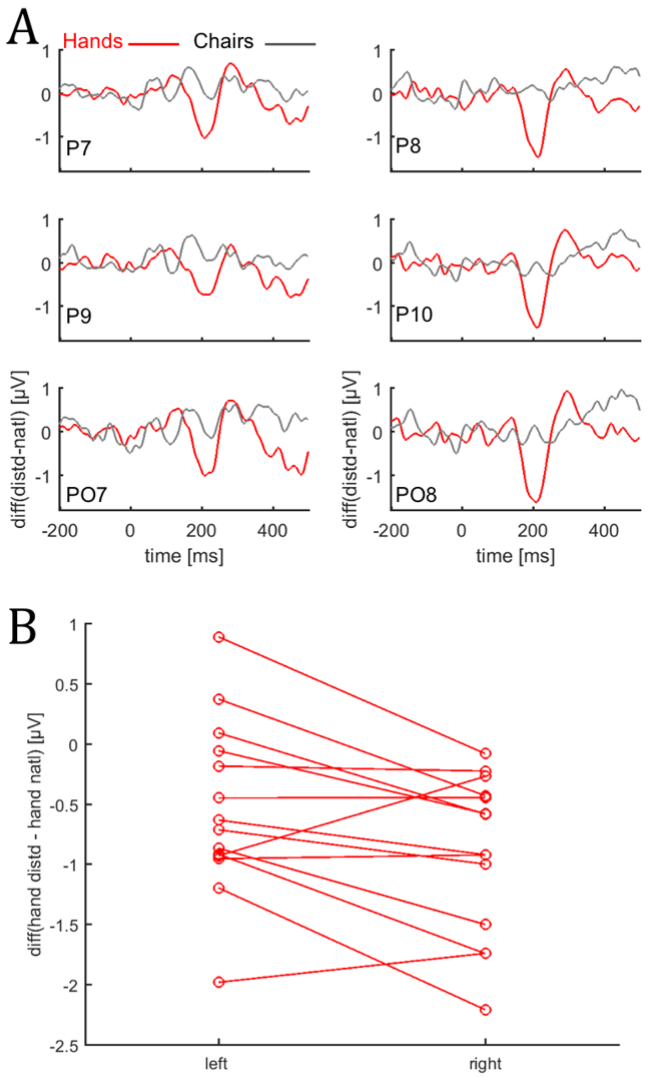

Figure 7.9: A) Grand averages (N=14) for electrodes P7, P9, PO7, (left hemisphere) and P8, P10, PO8 (right hemisphere) of the difference waveforms: distorted – natural for hands (red) and distorted – standard for chairs (black). Across all electrodes, difference waveforms for hands – but not for chairs – show negative peaks in 150–250ms latency range. B) Peak amplitudes of difference waveforms for hands, averaged across 3 electrodes per hemisphere. For 9 out of 14 subjects, distorted – natural differences are larger (more negative) in right (relative to left) hemisphere, t(13)=2.755, p=0.016.

The difference in waveforms, peaking ≈ 40 ms later than N1 latency (as in Figure 7.7A and B), do not reflect N1 peak amplitude differences but rather changes in the shape of the N1 wave. In the 3 right-hemisphere electrodes, the N1 peak for distorted hands was wider than for natural hands, with a later return to baseline (illustrated in grand averages of Figure 7.7 A for P10 example, see

arrow). To establish whether this difference is statistically significant, the time of return to baseline (time from maximum peak amplitude to 0) was measured from electrodes P9 and P10 where N1 peaks were best defined. Times of return to baseline were obtained in 11 out of the 14 subjects studied (in the remaining 3 subjects, no negative N1 amplitudes). One subject's data were identified as an outlier. An ANOVA on the remaining 10 subjects' data yielded a main effect of configuration, $F(1,9) = 20.451$, $p = 0.001$, $\eta_p^2 = 0.694$, and, as a trend, a configuration × hemisphere interaction ($F(1,9) = 4.087$, $p = 0.074$, $\eta_p^2 = 0.312$). For P9, the return to baseline was at 217 ± 10 ms (mean ± SEM) for distorted versus 212 ± 10 ms for natural hands (paired samples t-test: $t(9) = 2.771$, $p = 0.022$, $d = 0.87$). For P10, the return to baseline was at 202 ± 5 ms for distorted versus 193 ± 5 ms for natural hands, $t(9) = 4.930$, $p = 0.001$, $d = 1.56$. The delays for P9 and P10 indicate a prolonged response beyond what could be explained by the difference in peak latencies, consequently at least for P9 and P10, a delayed return to baseline (in responses to distorted vs natural hands) underlies the peaks in difference waveforms (distorted – natural). The longer delay for P10 than for P9 (9 vs 5 ms, $p = 0.074$ for configuration × hemisphere in ANOVA above) is in line with larger difference waveform amplitudes for right versus left hemisphere ($p = 0.016$, see above). Thus, the difference waveforms indicate prolonged activation (broader negative peaks), in response to distorted compared with natural hands.

7.3.3 Discussion

In this experiment, I aimed to show that N1(N170/190) ERP component indicates the start of the involvement of an embodied simulation network, by demonstrating differential activity profiles for biological relevant abnormalities

compared to non-biological ones (i.e., distorted hands vs. chairs). Here, three particular findings support this assertion: 1) stronger N1 responses to distorted stimuli were observed only for hands, as opposed to non-body-part images of comparable geometric structure and visual complexity; 2) modulation started remarkably early, from 170 ms post stimulus, affecting N1 as an ERP component that has been linked with activation of EBA. Distortion-related N1 modulation was visible as a broadening of the N1 peak, suggesting prolonged activation of the EBA (in line with the speculations in section 1.3 and 1.4); 3) N1 modulation for distorted versus normal hands was present over both hemispheres but strongly right-lateralised.

Despite the good match between hand and chair stimuli, could it be possible that with the unfamiliar (rotated) chair stimuli subjects did not detect distortions as easily as in highly familiar hands? We used chairs rotated into an orientation where backrest and legs resemble the back of the hand and fingers. Distorted chair legs corresponded to distorted fingers. Consequently, chair images were comparable to hands in geometrical configuration and complexity. However, for chairs the rotation resulted in an unfamiliar perspective, as opposed to the highly familiar first-person perspective for hands. Any effect of unfamiliar perspective should have been small, because subjects viewed a number of practice stimuli before the experiments, and all chairs were deliberately shown in a single perspective across 480 trials. In that case one could expect similar distortion-related activity for chairs (as for hands) but weakened and/or delayed. However, N1 peaks did show sensitivity to distortion in chairs at the same latency as for hands but with different direction and topography (reduced responses in left hemisphere). Furthermore, across hands and chairs, distorted stimuli were carefully matched in

terms of how conspicuous the distortion was. However, unlike distorted hands, distorted chairs were not associated with stronger N1 responses. Stronger responses to distortion in the hand condition only, suggests neural circuits that are activated when distortion is seen in biologically relevant stimuli (as seen in Figure 7.8). Such circuits could underlie the high perceptual salience of distorted hands in social perception, as discussed in this thesis introduction (see section 1.4).

Through measurement of a predefined ERP component (N1), the current study extends previous MEG findings where distortion-related activation was found in bilateral occipital areas starting only from 260 ms after stimulus (Avikainen et al., 2003). This N1 latency is consistent with the modulated ERP at 190–230 ms latency to viewed hands or whole-body images with lower arm or thumb rotated into impossible positions - however, hand images were not analysed separately in that study (Overney, Michel, Harris & Pegna, 2005). The body-sensitive N1 peak targeted here through choice of electrodes and latency window, has been linked with EBA activation based on ERP source analysis (Thierry et al., 2006) and comparison with fMRI data (Taylor et al., 2010), but more importantly it was driven by the results of the first experiment in this chapter. These results, therefore, suggest a distorted finger related modulation that manifests itself as a broadened N1 peak, starting only after peak latency which could have led to prolonged EBA activation.

This study deliberately avoided any task-related attention to distortions. To perform the task, subjects had to be attentive across all stimulus categories as task-relevant stimuli were randomly distributed in the stimulus series, across all stimulus categories.

The observed lateralisation to the right hemispheres, is in line with the fRMI

study by Schürmann et al. (2011). For right hands viewed in the first-person perspective (as in current study), the fMRI study found distortion-related sensorimotor activation with right hemisphere dominance. Furthermore, right-lateralised N1 responses are in line with right lateralised EBA activation in an earlier fMRI study (Costantini et al., 2005) with observation of videos showing impossible (vs possible) finger movement of the right hand. Right-lateralised EBA activation was also found for contorted whole-body postures, using fMRI (Cross et al., 2010). Therefore, the current N1 responses provide timing information that is lacking from these fMRI studies.

In conclusion, these results indicate privileged visual processing of hands as highly salient body parts, with distortions engaging EBA resources that are especially activated for biological stimuli in social perception. Such activity was found from 170 ms after stimulus onset in a hypothesis-driven latency window and choice of electrodes, at an earlier stage than MEG-measured responses to distorted fingers (Avikainen et al., 2003).

7.4 General Discussion

These two experiments provided evidence that the occipito-temporal N1 ERP is sensitive to depiction of hands including biologically salient abnormalities in the observed body, in line with other studies investigating body-related N1 modulations (Overduin & Servos, 2008; Meeren et al., 2008; Borhani et al., 2015; Groves et al., 2017); thereby reinforcing the idea that the N1 is indeed also responsible for gauging biological plausibility of the stimuli. However, one crucial discussion point was purposefully left out from both experiments: the asymmetry in laterality of responses to stimuli is intriguing and requires discussion in tandem, therefore it is addressed here for the sake of brevity and clarity.

In Experiment 1, a key question remained to be addressed: why is the left LOC more responsive to hands? A potential answer lies in that the brain processes involved with the representation of hands in the left occipito-temporal cortex may support a synergetic relationship between somatomotor regions and vision. Structural proximity within the same hemisphere, may facilitate sensory integration allowing precise information about grasp, tool use and posture to be represented in the cortex. Therefore, the large hand representation in the left hemisphere may be linked to hand use as all our subjects were right-handed (like in the fMRI study that found left hemisphere hand-responsive clusters, Bracci et al., 2012). For example, the motor properties of body parts influence their representation in lateral occipital cortex, which does not follow a 'nearest neighbour rule' (as in somatosensory cortex), as found using fMRI (Orlov et al., 2010): body parts that have wider range of movements largely overlapped with areas of visual motion processing (such as hMT+), and those that are restricted (e.g., trunk) had more ventral locations within the lateral occipital cortex. In addition, ROIs showing upper limb preference also produced the largest clusters of activation. In Bracci et al. (2012) it was demonstrated that hand and tool regions of the left LOC responded similarly and were functionally connected.

Another reason for the left lateralisation could be that the static images of hands benefit from motor-related attention. In everyday life, attention to hands is mostly attention to motor acts – those which an individual performs with her own hands, or those which an individual observes others perform with their hands. For example, in cueing tasks faster reaction times are elicited when the probe is placed closer to the responding hand (Reed, Grubb & Steele, 2006; Morrisey & Rutherford, 2013). Infants have a stronger reaction to observed actions

conducted with the hand than those with a non-hand control object (Saxe and Carey, 2006), and infants of two years will engage in imitation of hand postures, even when there are no bodies or faces present (Slaughter, Nielsen & Enchelmaier, 2008). Motor-related attention, in turn, has been linked with left parietal cortex activation (Rushworth, Krams & Passingham, 2001). Related left lateralisation has been found for motor-planning networks (Buxbaum, Johnson-Frey & Bartlett-Williams, 2005) and for activity during integration of proprioceptive information with observed congruent and incongruent limb postures (Limanowski & Blankenburg, 2016).

In the second experiment, the N1 modulation in the distorted fingers condition, although present over both hemispheres, was robustly right-lateralised. This finding is remarkable because response to normal hands was left lateralised in Experiment 1, and in the current experiment all hands presented were shown as right hands for which a stronger left-hemisphere (contralateral vs ipsilateral) activation could be expected. Therefore, this raises the question - could the distortion-modulated N1 be driven by feedback from the amygdala (activated in fMRI responses to distorted hands in Schürmann et al., 2011)? Such feedback was hypothesised for the distortion-related activity from 260 ms by Avikainen et al. (2003). Even at the early N1 latency, amygdala feedback would be conceivable, given that at even earlier latencies (from 74 ms), amygdala responses to socially relevant stimuli (fearful faces) were recently observed in human intracranial data (Méndez-Bértolo et al., 2016). Also, amygdala damage affects ERPs to fearful faces from 100 ms post-stimulus (Rotshtein et al., 2010). Alternatively, another explanation would rely on the demand for visuospatial processing as the subject constructs a three-dimensional representation of the observed hand from two-

dimensional images. Visuospatial processing is known to be a right-hemisphere-dominant brain process (De Schotten et al., 2011). However, right-hemispheric responses to the chair stimuli were not distortion-sensitive even though they were carefully matched for geometric complexity. A better explanation of right hemisphere lateralisation would be that images of hands (and perhaps other body parts) may have an alternative processing route, that is not motor/action dependent, and instead follows a similar route as emotional faces. In earlier studies (Avikainen et al., 2003; Schürmann et al., 2011), subjects rated static images of distorted hands or videos of biologically impossible hand movement as unpleasant, and negative emotional stimuli require right-hemisphere processing (see Najt, Bayer & Hausmann, 2013; Shobe, 2014 for review). The link between emotional contents and stronger N1 responses is tentative and requires further support, for example from an experiment that would include rarely seen, but not distorted hand postures in an additional condition. The aversive quality of distorted hands may induce a response that shares neural resources with processes of aesthetic judgement of body postures, with such judgements being impaired after virtual lesions to right EBA (Calvo-Merino, Urgesi, Orgs, Aglioti & Haggard, 2010). The right lateralisation effect of the N1 to the distorted fingers condition could suggest an EBA processing step that co-occurs with distortion-related activation in sensorimotor areas in fMRI (also right-lateralised, see Schürmann et al., 2011). This could be interpreted as a correlate of embodied simulation within a network responding to observed bodily distortions. This suggestion aligns itself with the results of the fMRI study in Chapter 5, and with the discussion outlining the lateralisation effect.

In conclusion, the results of these experiments demonstrate the privileged

visual processing of hands as highly salient body parts, with distortions engaging EBA resources that are especially activated for biological stimuli in social perception. Further studies are needed to establish if distortion-related EBA activation starts before sensorimotor activation (bottom-up processing), simultaneously with sensorimotor activation (potentially driven by a third site of activation), or after sensorimotor activation (as in a top-down process). In the next chapter, I attempt to develop this network using MEG to investigate the temporal dynamics of such a responses and to bridge the results here outlined with those from the fMRI study (Chapter 5).

Chapter 8

Spatio-temporal Dynamics of Embodied Simulation: MEG Investigation of the Observation of Distorted Fingers

8.1 Overview

In this chapter I aim to integrated the findings from the fMRI experiment in Chapter 5 (involvement of posterior S1) with the results of the EEG experiments in Chapter 7 [right-lateralised lateral occipital cortex, (LOC), involvement]. To accomplish this I use MEG to measure magnetic evoked-responses, which has the benefit of providing moderate spatial resolution and high temporal resolution. Fifteen subjects conducted a similar experiment as the EEG in experiment 2 of

Chapter 7; observation of distorted/standard chairs and finger postures. In order to localise the source of the activity in the different conditions, minimum-norm estimates source localisation was used. Source estimates differences were investigated to understand the temporal evolution of brain responses to distorted fingers and chairs. The result of the t-test *Distorted Hands − Standard Hands* showed significant differences over lateral occipital cortex within the 80-120 ms window, fusiform gyrus (FFG) and occipito-temporal junction (OTJ) before 250 ms past stimulus onset. In addition, significant differences were found in the time interval of 270 - 400 ms over areas that overlap with supramarginal gyrus (SMG), intraparietal cortex (IPS), postcentral sulcus (PCS), secondary somatosensory cortex (S2) and pre-motor cortex (PM) using Desikan-Killiany atlas. Interaction test revealed that the early difference (80-120 ms) may arise from small effects or visual differences between conditions, however, it showed that the right Parietal areas post 250 ms of stimulus presentation are significantly involved in the processing of distorted fingers. The temporal evolution of these responses fits with previous findings from the literature, and complements both EEG and fMRI studies indicating that a trigger of an embodied response may start as early as 100 ms of stimulus onset.

8.2 Introduction

In previous chapters, I used brain imaging techniques that were limited by their spatial (EEG) or temporal resolution (fMRI). EEG can show well resolved responses in time across different electrodes, but has poor spatial resolution. fMRI, especially at 7T, can resolve activity spatially very accurately using the BOLD response, which takes $6s$ to peak, but has poor temporal resolution. However, a complex mechanism such as embodied simulation will likely start at early

stages of visual processing (as demonstrated in Chapter 7) and have an intricate spatio-temporal profile, arising from the involvement of a variety of brain regions.

The first study to investigate the spatio-temporal profile in response to the observation of distorted fingers was conducted by Avikainen et al. (2003). In this MEG study they compared source estimates in the LOC between the observation of distorted fingers and that of natural finger postures. They found significant differences from 250 ms onward in pre-defined regions overlapping with the bilateral LOC. Whilst this demonstrated that biological abnormalities were represented in the visual cortex it did not provide more information about other brain areas; and, since it used a large region of interest, small differences that may occur earlier in time in the visual processing stream may not be detected.

Other M-EEG results point towards a more complex interaction between bottom-up and top-down mechanism involved in the processing of such stimuli. For instance, in an MEG study of the inversion effect of images of faces and bodies, results showed category specific responses to inversion of the images within 100 ms of stimulus onset (Meeren et al., 2008). Other studies using images of faceless body postures of fearful or neutral valence, showed significant differences at similar latencies for the P1 ERP component (Van Heijnsbergen, Meeren, Grezes & de Gelder, 2007). Differences between these conditions were localised to the right parietal cortex, including regions such as the IPS and PCS (Meeren et al., 2016).

These findings suggest an earlier ability to categorise the human body, however, the ERP findings reported in Chapter 7 suggest that a biological abnormality is categorised slightly later, at latencies from 160 ms onward. Indeed, studies comparing N190 amplitude responses of low versus high alexithymia sub-

jects, showed considerably larger emotional body posture modulation with fearful postures having larger N1 negativity than happy ones (Borhani et al., 2016). A recent study offers a potential explanation by demonstrating different body processing stages occur at different times. Groves et al. (2017) showed that female subjects diagnosed with eating disorders (ED) had earlier P1 peak latency to viewing male and female bodies in comparison to controls. In addition, they found that viewing female bodies elicited significantly more negative amplitudes versus male bodies. This highlighted that different body related information is being processed at different times – for instance detection of a body occurred at the P1 latency, but more specific information such as gender, occurred later, approximately at the N1 latency (150 to 200 ms).

The combination of these results demonstrate that the processing of visual information pertaining to the body starts within the first 100 ms (Van Heijnsbergen et al., 2007; Meeren et al., 2008, 2016), and processing of all of its relevant features starts shortly after but extends past 250 ms (Avikainen et al., 2003) from stimulus onset. Therefore, in this chapter I study the spatio-temporal profile of the observation of highly salient body parts, such as distorted fingers, and compare it to control images of natural hands and chairs in similar configurations.

In order to support the existence of a link between body perception and embodied simulation, activity in the areas related to somatosensory processing must follow activity in the visual areas. This is because the visual information regarding the finger distortions is processed in the LOC, and given the onset of this difference (as shown in Chapter 7, exp. 2) the embodied simulation of an observed stimulus will likely have to depend on the visual areas being able to discern the different between natural and distorted postures.

The temporal profile of vicarious somatosensory activation using MEG is scarce and warrants more investigation. However, from a few studies a time interval of interest can be established. For example, the mu-rhythm, for which the suppression is representative of somatosensory involvement, starts during a 200 - 300 ms time window after tactile stimulation (Pfurtscheller & Lopes da Silva, 1999; Cheng, Yang, Lin, Lee & Decety, 2008; Hari & Puce, 2017). Chen et al. (2009) showed sustained right insular involvement from 190 ms after observing emotional faces. Lastly, Pihko et al. (2010) showed S1 involvement after 200 ms from observation of touch. Therefore, if distorted hands elicit somatosensory engagement, this should occur approximately 200 to 300 ms after stimulus onset.

In line with the Experiment 2 in the previous chapter (section 7.3) it is predicted: 1) the first significant differences will occur between distorted hands and chairs, and distorted hands and natural hands within the 150 to 200 ms period; 2) In line with previous MEG studies, sustained activity in visual areas (localised to ventral areas of the LOC and FFC) will go beyond the typical 170(90) ms (N1) peak responses, and will extend to, and maybe past, 250 ms from onset, and will be right lateralised; 3) differential involvement of the right intra-parietal sulcus in processing will occur within 100-200 ms of stimulus onset and will be right lateralised, as seen in Meeren et al. (2016); 4) based on studies investigating somatosensory activity using MEG, it is predicted this will occur from 200 ms onwards and be right lateralised (based on fMRI results in Chapter 5).

8.3 Methods

8.3.1 Subjects.

A total of 15 subjects (8 female), of age mean±SD = 23 ± 5 years, all right-handed by self-report and with no history of neurological or psychiatric problems nor drug abuse, also by self-report, participated in this experiment. Informed consent was obtained from all participants. The study was approved by the ethics committee of the School of Psychology (University of Nottingham) and performed in accordance with the declaration of Helsinki. During data acquisition, two subjects were removed due to excessive head motion (head movement exceeding 5 mm), and one subject due to technical difficulties during data acquisition (unknown source of noise contaminating the data). In preparatory analysis, data from 1 subject was identified as an outlier and subsequently removed. The threshold for removal was if more than 50% of trials (blind to condition) were removed (z-value>5) during preprocessing of data. All reminding subjects had a trial removal percentage of <30%.

8.3.2 Stimuli and Procedure.

Subjects laid in a supine position while stimuli of hands and chairs were presented to them via a projector and mirror system, displaying the image on a MEG compatible screen approximately 50 cm away from the subjects' head. Stimuli comprised of 48 different images of right hands (24 distorted, 24 standard, i.e., natural). Hand images were complemented with 48 images of chairs (24 distorted, 24 standard). 16 repeated images were selected at random from each category, and were added to the stimulus list to ensure sufficient number of trials per condition. Thus, 64 images where presented per condition. Chair and hand

stimuli were created using the method outlined in Chapter 7 Experiment 2 (see Section 7.3.1). Also please refer to Chapter 2, Section 2.2 and Appendix C, or Santo, Chen and Schürmann (2017).

Stimulus size and presentation duration were the same as described in Chapter 2, Experiment 1. Inter-stimulus interval was 1200 ms 50% of the time, 1700 ms 25% of the time, and 2000 ms 25% of time. See Figure 8.1 for a schematic of the experimental time-line. In order to keep participants' attention the same white shadow counting task used in Chapter 7 experiment 2, was used here. Before subjects entered the shielded room with the MEG scanner, they had the opportunity to complete a short practice run. Button press responses were done using their left hand on a MEG compatible bimanual fibre optic response pad (Current Designs Inc., PA, USA). Trials containing the white shadow were recorded but excluded from further analysis.

Data Acquisition. MEG data was acquired using the equipment described in Chapter 6, Section 6.6.2, and head shape, anatomical MRI, and co-registration as explained in Section 6.7 of the same Chapter. The MEG sampling rate was 600 hz.

Signal Processing Signal processing was performed in Matlab (The MathWorks Inc., Natick, MA) using Fieldtrip (Oostenveld et al., 2011) and Brainstorm (Tadel, Baillet, Mosher, Pantazis & Leahy, 2011) routines. Data were first downsampled to 300 Hz, band-pass filtered (Butterworth, order 4, 0 phase shift) between 0.01 and 40 Hz, followed by a visual search (blind to condition) to identify obvious bad trials based on typical artifact waveforms (as described for example in Hari & Puce, 2017, Chapter 8). Such trials were removed from the dataset.

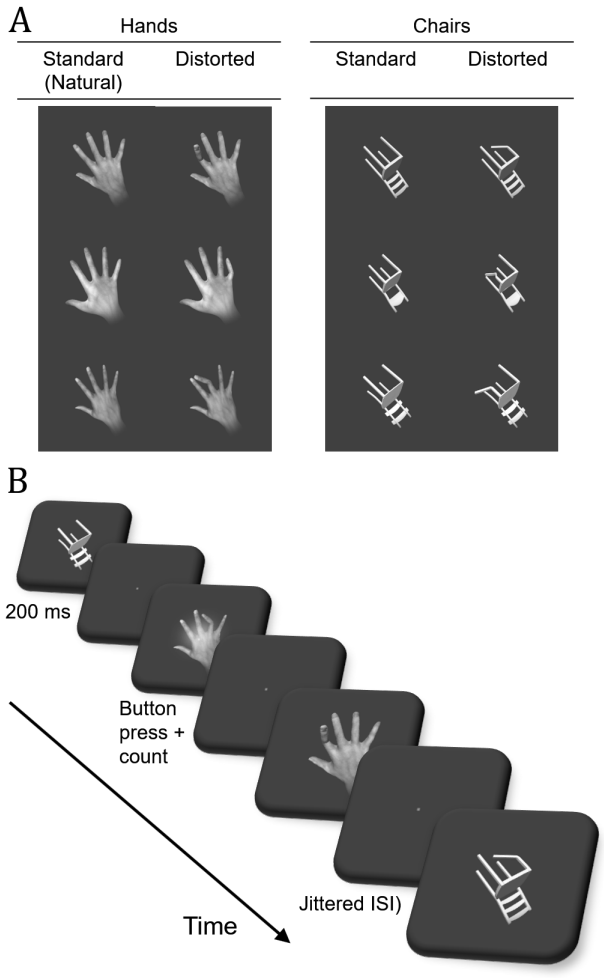

Figure 8.1: Stimulus setup. A) Stimulus categories, 3 (out of 6) exemplars per category, each in natural and distorted configurations. Stimuli computer-generated using the protocol developed in Stimuli Creation. B) Stimulus time-line. Stimuli not shown to size (actual size 4° of visual field).

A plot of trial by variance was created to identify which trials had the largest variance. Those that had standard deviations >5 z-values, were removed from the data. Data for each trial was baseline corrected (-500 to 0 ms) and averaged for each participant, with an epoch length of 1700 ms, -500 ms before stimulus onset to 1200 ms past onset. Subsequently, segmented trials were put through an independent component analysis (ICA) using the algorithm runica (see Makeig et al., 1997), allowing for blind separation of the underlying component topographies. This analysis searched for well-known artifact topographies (see examples in Jung, Makeig, Humphries et al., 2000 and in Jung, Makeig, Westerfield et al.,

2000). After these steps, trials were sorted by condition, resulting in 4 categories of waveforms per subject: *Distorted Hands* and *Chairs*, and *Standard Hands* and *Chairs*.

Source Localisation To estimate the source strength of the evoked-field responses to the stimuli, minimum norm estimates (MNE, Hämäläinen et al., 1993) were calculated for the head model, generated with the overlapping spheres approach (Huang et al., 1999), using Brainstorm software (http://neuroimage.usc.edu/brainstorm).

As explained in Section 6.5.2, in order to normalise the MNE solution, and account for depth variability, a noise-covariance matrix was calculated from a pre-stimulus interval of -500 ms to 0 ms (Dale et al., 2000) and applied to the estimates. This generated a dynamic statistical parametric map (dSPM), with a F-distribution under the null-hypothesis. These estimates were constrained to the cortical surfaces derived from Freesurfer (Fischl, 2012) on an individual subject basis. Also, for each subject this procedure was applied for each trial of each condition, and the dSPMs for each trial were averaged generating a dSPM average per condition per subject. Each average was weighted based on the total number of trials per condition in order to allow for pooling of subjects: For each condition the following is applied wmean = sum(nAvg(c)* M(c))/sum(nAvg(c)), where c is any given condition, nAvg is the number of trials in that condition, wmean is the weighted mean and M is the arithmetic mean. To conduct group analysis at a source level, each of the subjects individual cortical surfaces were deformed (see Section 6.7.2) and registered to the ICBM MNI152 template (Lancaster et al., 2007). In Brainstorm, this template consists of 7,500 dipoles per hemisphere (one dipole per vertex, Tadel et al., 2011). Once each subject's average dSPM

data was registered to the template, it was then spatially smoothed using a full width at half maximum Gaussian kernel of 3 mm (with MRI template resolution of 1 mm isometric).

Statistics A mass-univariate t-test with Monte Carlo clustering procedures, as implemented in Experiment 1 of chapter 7, was not conducted on a time point * dipole basis due to lengthy computation and processing power requirements to complete enough permutations. Instead, to explore the hypothesis outlined above, contrasts of interest were first calculated by subtracting the average dSPMs between conditions for each subject. Then, a whole-brain mass-univariate Student's t-test was performed against the baseline period (-500 to 0 ms) and compared to the post-stimulus onset interval of 0 to 500 ms. Multiple comparisons were corrected at $p<0.01$ using False-Discovery rate correction.

An additional statistical comparison procedure using the Monte Carlo approach (Oostenveld et al., 2011) was conducted on the average dSPM of the main contrast of interest (Distorted Hands>Standard Hands) inside anatomically defined regions using the Desikan-Killiany atlas (Desikan et al., 2006). This expands on the previous analysis by formalising with an objective location, the difference in the contrast of interest (*Distorted hands>Standard Hands.* For this, a random sampling distribution (N = 3000) of the t-statistic for this contrast was obtained to define the critical t-value on the positive side of the distribution. Then, multiple comparisons were further corrected using a threshold-free clustering (only across time points since large ROIs were used) algorithm as implemented in Fieldtrip (Oostenveld et al., 2011) to find significant time points where the maximum cluster t-statistic survived the threshold (cluster alpha = 0.05).

8.4 Results

All subjects reported correct detection of the white shadows within ±2 of the target value (always 10). The purpose of this was to ensure that subjects were paying sufficient attention to the images.

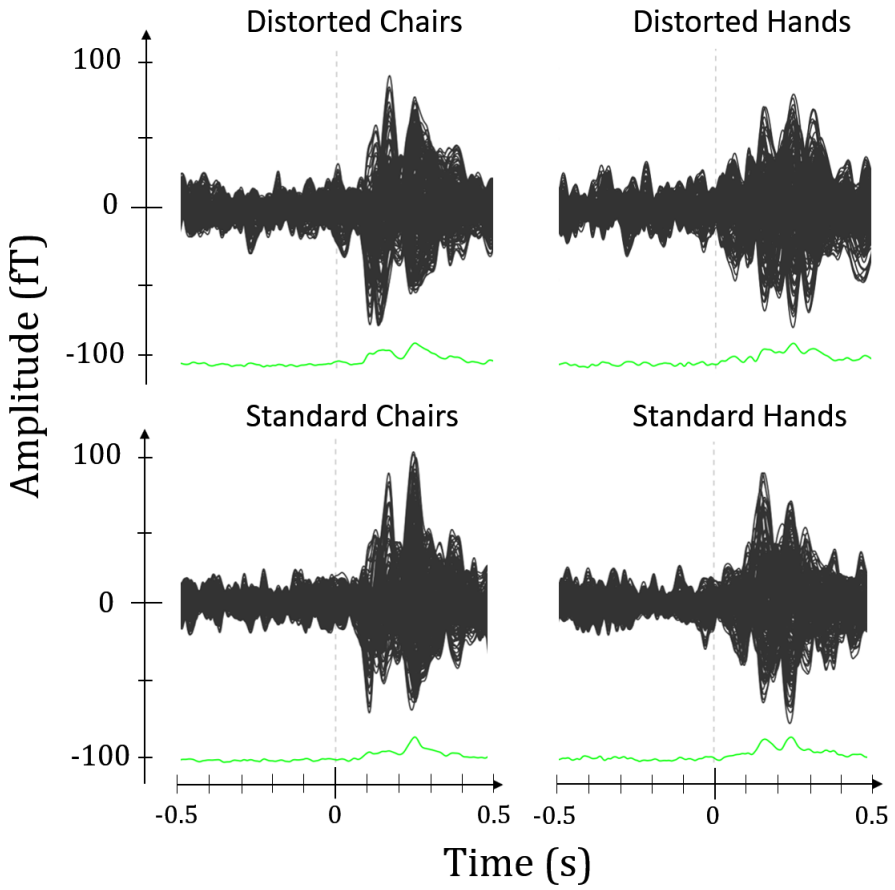

Figure 8.2: Grand-average of the sensors for each condition in the period of -500 to 500 ms from stimulus onset. Green line shows the global field, which is a measure of temporal stability of sensors.

The waveform average across MEG sensors of each of the conditions showed the typical pattern of response. M1, M170, and M2, identified using the global field potential peak (the standard deviation of the sensors across time) and were observed in all conditions, see Figure 8.2. Source localisation to approximate times of these peaks is seen in Figure 8.3. This figure shows consistent activity

of the visual areas across all conditions, fusiform and middle temporal gyrus. In the later time windows the distorted hands conditions shows increasing source strength over the parietal cortex and somatosensory areas.

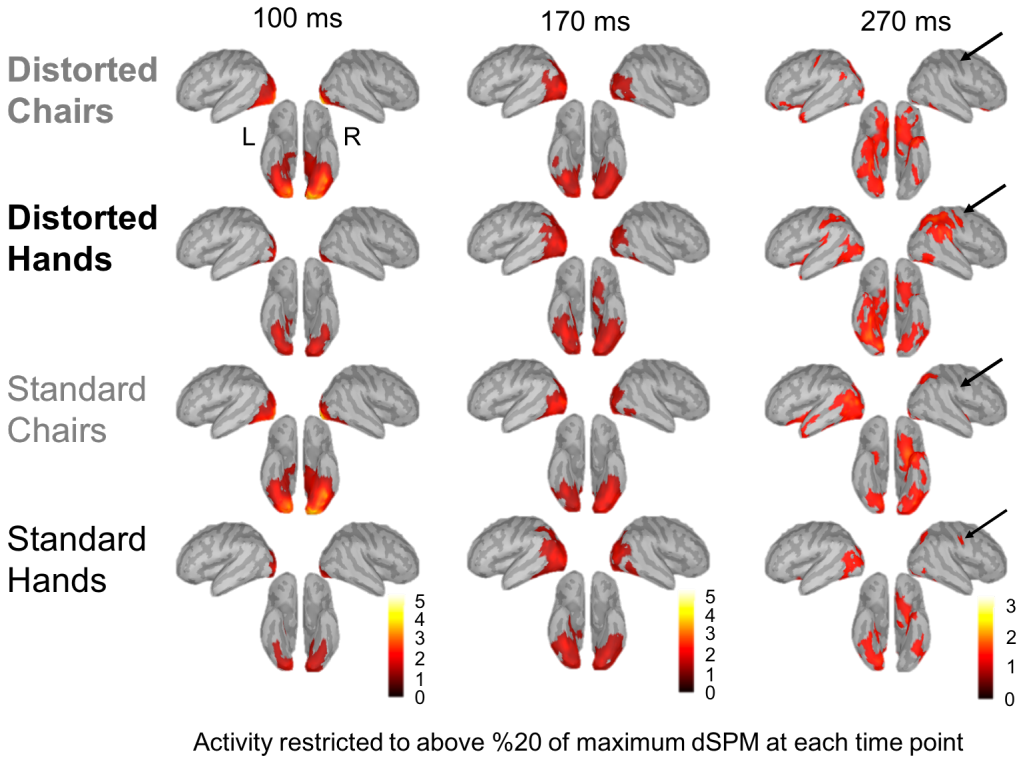

Figure 8.3: Grand-average (N=10) of the source dSPM for each condition in time points of interest identified from the sensor grand-average inspection. Please note the activity has been restricted to show only areas of activity thresholded above 20% of maximum dSPM value in that time point. Another restriction is it only shows activity patterns that are larger than 20 vertices in order clarify the visualisation of the grand averages. Please note, in later latency, the use of a different scale, and that Distorted Hands conditions shows a large cluster of activity over the parietal cortex.

8.4.1 Impact of stimulus configuration between Hands and Chairs

To investigate the effect of distortion between hands and chairs, for each subject the dSPM values in source space were subtracted from the distortion conditions, such that for each subject a difference source estimate was created. This created the contrasts *Distorted: Hands - Chairs* and *Standard: Hands - Chairs*. The results of the mass-univariate positive t-tests for these contrasts against baseline are summarised in Figure 8.4. Significant differences at $p<0.01$

(FDR corrected) compared with the baseline period were found for the *Distorted: Hands - Chairs* contrast in left and right lateral occipital cortices within the time interval of 100 to 200 ms. Furthermore, insula activity was observed from

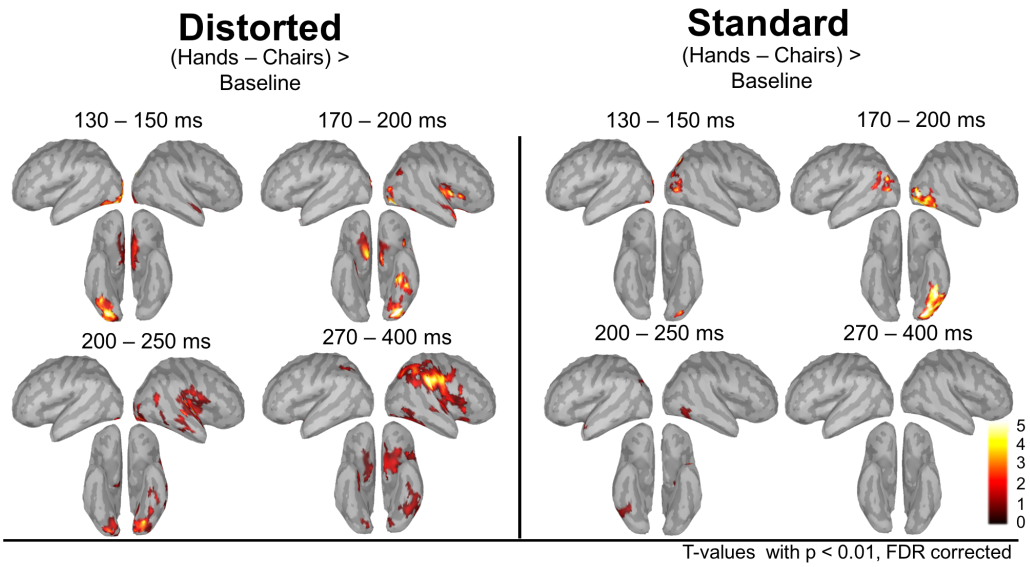

Figure 8.4: Results of the t-test (Hands – Chairs) >Baseline. The figure shows t-values averaged over time windows which showed consistent results based on visual inspections of the results.

170 ms of stimulus onset and persisted, albeit with weaker strength, to 400 ms. From 200 ms onward, the left and right lateral occipital cortex show significant differences which decline with time, and from 270 ms this activity disappears and right fusiform and middle temporal gyrus differences are found. From 270 ms differences are seen in a large right hemispheric cluster overlapping with the IPS, SMG, post- and pre-central sulcus, and insula.

8.4.2 Impact of stimulus type between Distorted and Standard stimuli

The results of a mass-univariate positive t-test for the contrasts *Hands: Distorted - Standard* and *Chairs: Distorted - Standard* against baseline are summarised in Figure 8.5. The *Chairs: Distorted - Standard* comparison elicited a

very small and short lived significant difference over the right lateral occipital cortex in the time window of 150-190 ms, and over part of the motor and pre-motor area, of the right hemisphere. However, the *Hands: Distorted - Standard* comparison elicited a more complex significance pattern involving a number of regions starting from 80 ms. Significant differences for this contrast were ob-

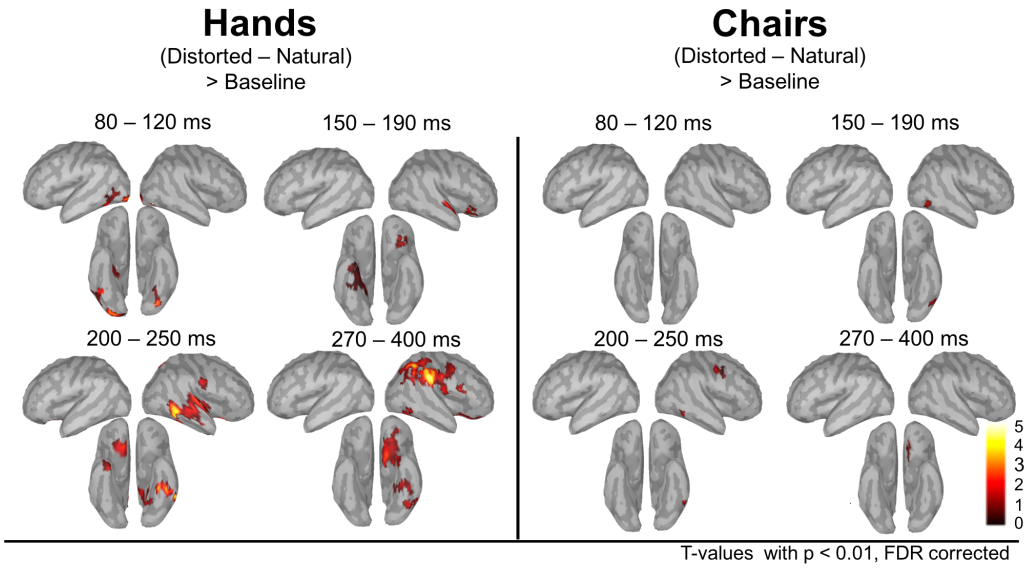

Figure 8.5: Results of the t-test (Distorted – Natural) >Baseline. Figure shows t-values averaged over time windows which showed consistent results based on visual inspections of the results.

served at ventral areas of left and right lateral occipital cortex, and at the ventral temporal-occipital junctions of the left hemisphere. In the time window between 150 and 190 ms, weak or short lived differences were in ventral areas of the brain. In the time window of 200-250 ms, significant differences were found in areas overlapping the right fusiform, right middle, and superior temporal gyrus, posterior insula, and S2. Lastly, in the time window of 270 to 400 ms, areas in the right parietal cortex overlapping with intra-parietal sulcus, post-central sulcus, supramarginal gyrus and S2. Also, outside of the parietal cortex, parts of the ventral pre-motor cortex and pars opercularis also showed significant differences to baseline.

8.4.3 Interaction between distortion and stimulus category

To investigate the interaction effect of distortion between hands and chairs, the difference between the contrasts *Distorted: Hands - Chairs* and *Standard: Hands - Chairs* was calculated, and a mass-univariate t-test was conducted on this difference. To simplify this is referred to as D(H-C) - S(H-C). Results showed that significant differences started from 130 ms over right inferior temporal gyrus area, and at a later stage this area showed bilateral activation. During 250 - 300 ms activity persisted but was only located in the right hemisphere, and significant differences were observed in the right parietal cortex overlapping with intra-parietal sulcus, post-central sulcus, supramarginal gyrus and S2. No significant differences were observed before 130 ms.

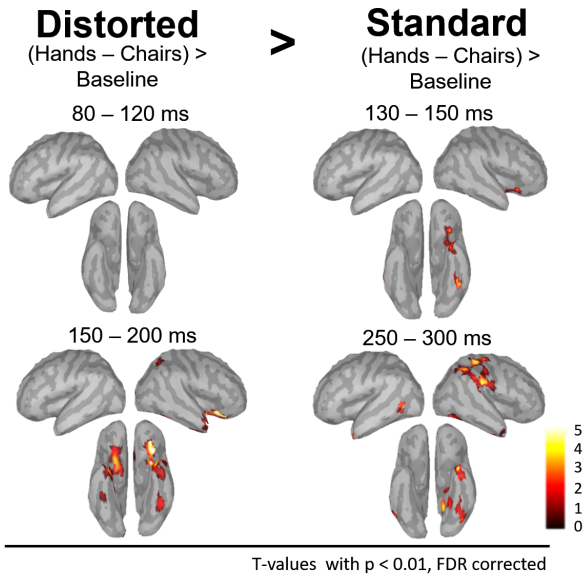

Figure 8.6: Results of the t-test D(H-C) - S(H-C)>Baseline. Figure shows t-values averaged over time windows which showed consistent results based on visual inspections of the results.

8.4.4 Atlas based Analysis

The *Hands: Distorted - Standard* >baseline, is the contrast of interest as it provides direct evidence of the finger distortion effect in observed hands. This

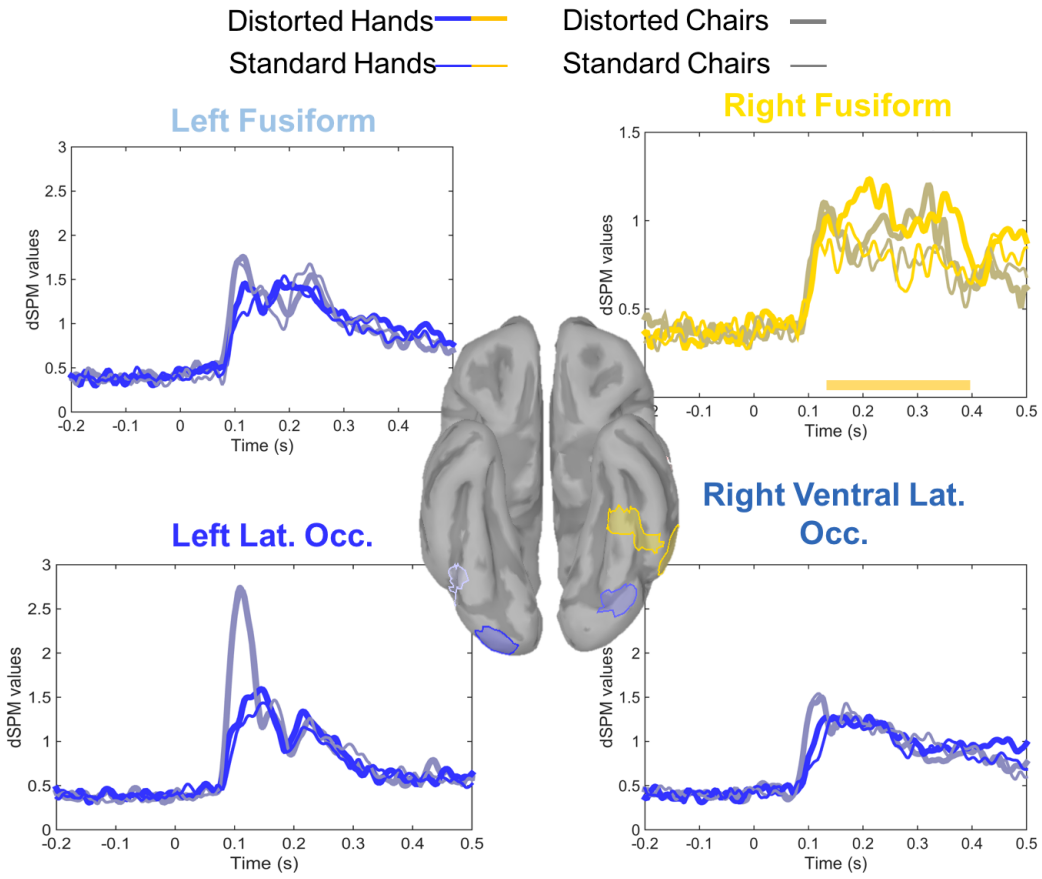

Figure 8.7: Depiction of the grand-average time series for the ROIs defined using the Hands (Distorted – Natural) >Baseline t-test result (as seen in Figure 8.5 left panel) that showed significant differences within 200 ms of stimulus onset . This is shown for visualisation purposes, no statistical analysis. Please note, that the yellow line over x-axis in the right fusiform plot is highlighting sustained activity over that period of time.

contrast was used as the basis from which to create ROIs which illustrate the time course of the significant effect. Figure 8.7 shows the time course across all conditions for the ventral areas in the visual and temporal cortices which showed significant differences between 80 and 200 ms. In Figure 8.8, time course across all conditions for the ROIs that showed significant differences in period of 200 to 400 ms is shown.

In order to confirm the results above, an atlas based analysis was conducted using the anatomical regions defined in the Desikan-Killiany atlas (Desikan et al., 2006). For this, dSPM values were averaged within each of the 68 regions at each

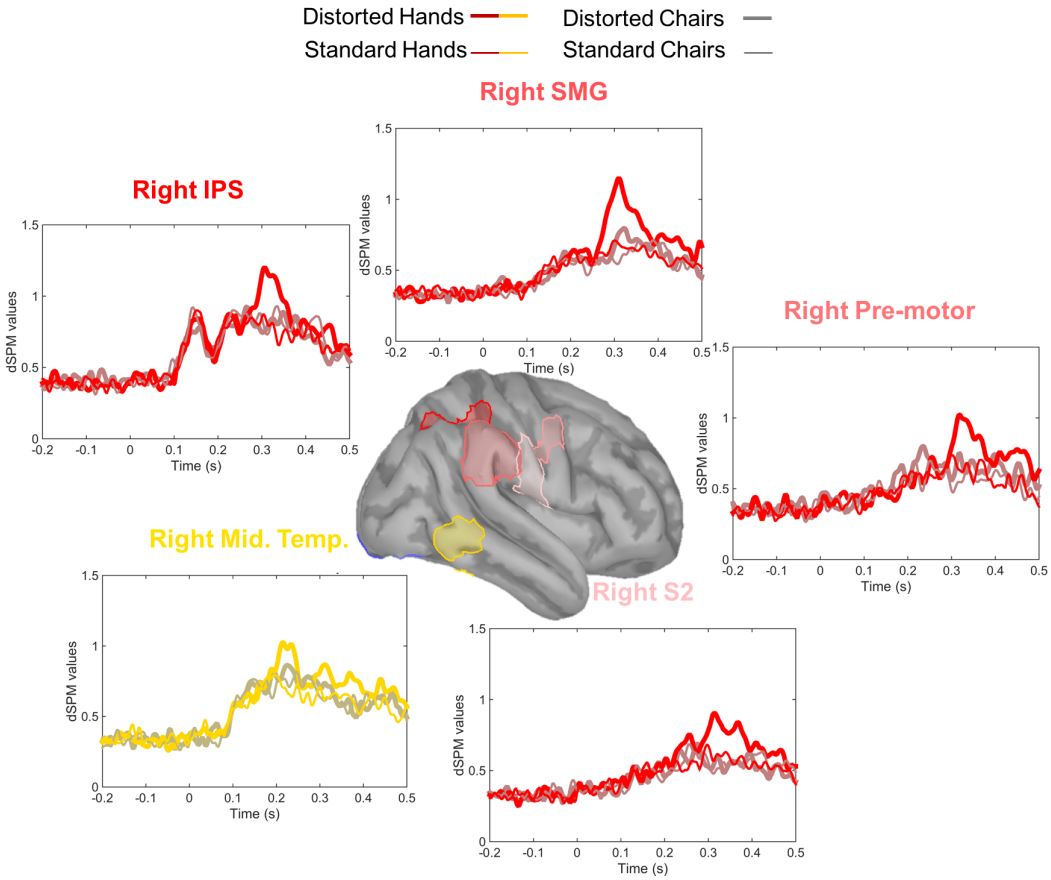

Figure 8.8: This is a continuation of Figure 8.7. Average dSPM time course for all conditions for ROIs created on the basis of the significant differences before 200 ms of the *Hands: Distorted - Standard*>baseline contrasts (as seen in Figure 8.5 left panel).

time point. Then, a paired-samples t-test was conducted between the dSPMs for *Distorted Hands*>*Standard Hands*. Results showed significant differences between these conditions in the right hemisphere for the following ROIs: fusiform gyrus, p = 0.036; inferior temporal gyrus, p <0.001; pars opercularis, p = 0.023; post-central sulcus, p = 0.010; supramarginal gyrus, p = 0.016. See Figure 8.9 for visualisation of the length of these significant differences.

In summary, this analysis revealed anatomical overlap between the fusiform and temporal areas but only from 300 ms of stimulus onset. However, significant difference were found in similar time-windows as the whole-brain analysis for the supramarginal gyrus, post-central sulcus, and pars opercularis parcellations.

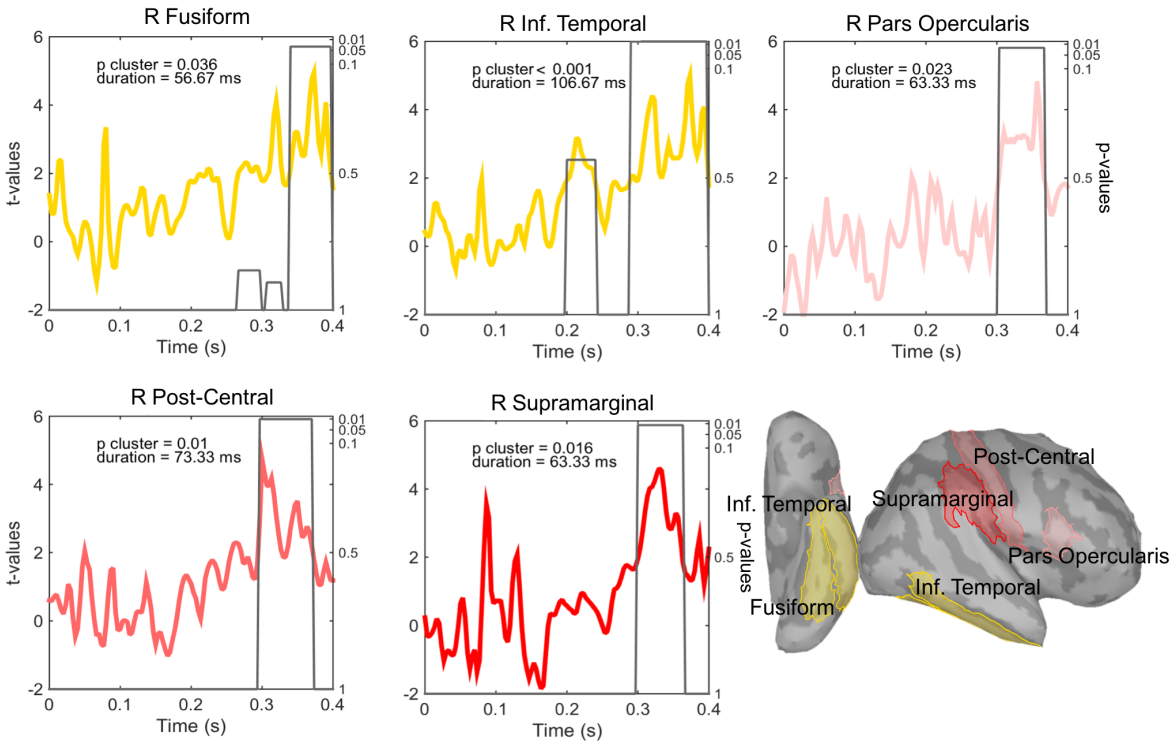

Figure 8.9: Results of the atlas-based analysis using an atlas based approach. The left y-axis depicts the t-value for the paired samples t-test of *Distorted hands>Standard Hands*. The right y-axis corresponds to the p-values of each time time point. Bottom right figure shows the colour-coded brain regions that showed significant differences for this contrast. Significant differences between conditions are observed from 300 ms after stimulus onset. These five regions were significant out of 68 analysed.

8.5 Discussion

This chapter aimed to establish the spatio-temporal dynamics of the brain regions supporting embodied simulation. In line with hypothesis 1), differences between hands and chairs were observed within the first 200 ms of stimulus onset. Similarly, however of weaker strength, significant differences between distorted and standard hands were also observed in the occipital and fusiform areas, but occurred earlier than expected. However, the lack of an interaction effect within this time window may suggest that the differences within 120 ms from stimulus onset may reflect processing of the different type of stimuli. Both of the hand condition related contrasts (left panels in Figures 8.4 and 8.5) support hypothesis

2), as differences were localised to ventral areas of the LOC and FFC, and were later than the typical latency of the N1 response observed in the EEG experiments in this thesis. The results of the atlas based analysis, while not confirming significant differences before 200 ms, provided converging evidence for the later involvement of these areas. In hypothesis 3), it was predicted that the intraparietal sulcus would show differential involvement of the processing distorted hands. This was not confirmed (see Figures 8.6 and 8.8, right IPS plot) at in interval between 100 and 200 ms. However, and supporting hypothesis 4), the IPS and other regions involved in the processing of somatosensory information showed significant differences between the distorted hands and chairs conditions, and standard hands condition. The following sections of this discussion will explore each of these findings and contextualise them chronologically.

8.5.1 Differences between 80 and 130 ms

Early significant differences (between 80 and 130 ms) between hand configuration conditions (simplified here as DH-SH) are in line with EEG studies' findings of rapid perceptual detection of emotional body postures at the occipital-temporal electrodes (Meeren, van Heijnsbergen & de Gelder, 2005; Van Heijnsbergen et al., 2007). The convergence of these findings point towards a processing route where, even at earlier latencies, biological salience is decoded from the observed stimuli and represented in the visual cortex. Such an effect was not observed in any of the other comparisons (see Figure 8.4 and 8.5) and significant differences were only found slightly later (between 130 and 250 ms, discussed below). This is particularly striking, because the DH-SH test is specifically aimed at testing the effect of the distorted finger only. The image of the hand in a natural configuration is exactly the same as in the distorted configuration, except for the abnormality.

Therefore, this suggests that the biological abnormality is being detected very early in the 'embodied simulation time-line', and that these areas are the trigger of such a response. However, the results of interaction test of D(H-C) - S(H-C) do not show differences within this time window. This findings raises the potential issue that the observed finding is related to differences between hand categories visual aspect rather than the distortion itself (Rossion & Jacques, 2008). The fact that from 130 ms onwards the effects starts to show, may suggest that this difference has a small effect size that and not detected by this statistical approach.

Another interesting response is the large peak (over 80-120 ms) for the chairs observation condition (see Figure 8.7). Even though not tested or predicted from previous literature, or from previous findings in this thesis, such a large response (compared to the responses to hands) warrants mention. No significant differences were found (right panel, Figure 8.5) between distorted and standard chairs. Therefore, this could have arisen due to the contrast between the background colour and the chairs in the MEG room. Even though efforts were made to maintain the same colour aspect between conditions, images were were projected onto the MEG screen from outside the shielded room using several mirrors. This resulted in slight loss of contrast and the edges of the images becoming slightly blurry. Given that the hand images have softer edges than chairs, the perceived contrast may have changed, inducing this difference in peaks. This claim is supported by ERP literature on psychophysics and perceptual attention, as the responses over this latency are very sensitive to the physical characteristics of the stimuli (for examples see Luck, Woodman & Vogel, 2000; Nakashima et al., 2008; Rossion & Jacques, 2008; De Cesarei, Mastria & Codispoti, 2013). Furthermore, due to the choice of conditions, with distorted and standard stimuli for hands as well as

for chairs, any difference in contrast would not have affected the comparisons of interest (i.e., the comparisons between distorted and natural hands, and between distorted and standard chairs).

8.5.2 Differences between 130 and 250 ms

Significant differences over the interval of 150 to 250 ms were found for the contrasts investigating the effect of distortion between stimulus categories (*Distorted Hands - Distorted Chairs, Standard Hands - Standard chairs*, DH-DC and SH-SC respectively). The location of these differences occurred in regions of the brain typically associated with the N170(90) and P2 ERPs, and demonstrate a general effect of stimulus type in the EEG literature.

In the time window of 130 and 150 ms, significant differences were seen for the contrast DH-DC, but not seen for the SH-SC contrasts. The results of the interaction effect between tested conditions [i.e., D(H-C) - S(H-C)], does not confirm this finding but a significant difference is found in the right inferior temporal gyrus. A potential explanation for this effect could be that the observed finger abnormalities are processed first in the visual processing stream. This suggestion is supported by studies showing that coarse processing of biologically relevant stimuli such as (emotional) bodies or faces occurs within the P1 peak latencies (Meeren et al., 2005; Van Heijnsbergen et al., 2007; Nakashima et al., 2008). Another study that used static images of hand insults suggested that this effect is related to top-down influences due to existing knowledge about the observed body, as differences between neutral and insult gestures were found at the P1 latency (Flaisch & Schupp, 2012). This study's finding is relevant to the stimuli used here, since they are both emotionally laden, but with an obvious semantic difference.

Another interesting result observed in the 170-200 ms interval is the posterior dorsal insula involvement in the DH-DC contrast. The insula is often acknowledged as a centre of proprioception (Craig, 2002a). This finding suggests that the distorted fingers response observed in the insula may represent the first stage of embodied simulation (as defined in Section 1.1)- the creation of a wide-spread and intrinsic response. Another congruent piece of evidence is that insula activity has been reported in studies investigating vicarious observation of (pleasant or otherwise) touch among other somatosensory areas (Keysers et al., 2004; Keysers & Gazzola, 2009; Keysers et al., 2010; Björnsdotter & Olausson, 2011; Schaefer et al., 2012). Indeed, in the Keysers et al. (2010) model (see Figure 1.3) the insula is one of the major areas observed in the vicarious representation of touch, and consequently likely to be part of the embodied simulation network that I am attempting to establish in this thesis. Lastly, anecdotal reports from subjects that took part in experiments in this thesis, often mentioned a visceral, or 'gut' reaction, for which the brain region supporting such a response may be the insula. This response was not observed in the interaction contrast. If distorted hands observation was recruiting the insula to generate a visceral reaction then one would expect a significant difference in this contrast contrast; however, this was not found. This may be related to varied intensity of the visceral response to the observation of standard hands and distorted hands between subjects. The argument about insula recruitment, however interesting and congruent with previous research, should be taken tentatively.

8.5.3 Differences between 270 and 400 ms

Since the significant differences were observed within 250 and 300 ms interval for the interaction effect. This finding was further investigated with the

contrasts DH-SH and DH-DC. Since there is quite a lot of time overlap between this contraststst I will only explain these results in the context of the DH-SH as discussion points will overlap. In the DH-SH contrast significant differences were found over the inferior and middle temporal gyrus, and fusiform gyrus from 200 to 400 ms of stimulus onset. Such a response is in line with predictions of sustained involvement of the body processing areas. This result is supported by an ERP study showing significant differences between body inversion (Stekelenburg & de Gelder, 2004) in the latencies corresponding to P2 and other later components. One study used words that describe the visual appearance of the bodies negatively (e.g., fat), and subjects that experienced ED showed significant differences (compared to neutral words) over lateral occipital electrodes in this peak's latency (Gao et al., 2011). Another study using subjects with ED, also reported similar effects of viewing male or female bodies (Groves et al., 2017). Supporting these results, the atlas based analysis showed significant differences for the $DH > SH$ comparison in the fusiform gyrus and inferior temporal gyrus. These findings, together with the literature, confirm the sustained activity observed for the distorted hands condition. Therefore, this could be interpreted as the result of continuous reappraisal of the observed image necessary to achieve fine grained processing of the salient distortion. Alternatively, and given that this difference co-occurs with the right IPS, a region involved in the retrieval of body schemas (Iriki et al., 1996; Ishida, Nakajima, Inase & Murata, 2010), the sustained activity could reflect a template matching process. This explanation is in line with the results from Möhring et al. (2014), where ERPs for static images of the gestures in the rock-paper-scissor game, were source localised to the left IPS at 250 ms from stimulus onset. The lateralisation difference observed between the results

here and the results in Möhring et al. (2014) could potentially highlight a cognitive processing route (left IPS) and a visuo-spatial, potentially emotionally-laden processing route.

The involvement of the SMG, pre-motor cortex and pars opercularis is an interesting finding as these regions are often found active in response to a variety of social-related tasks or during action observation. For instance, the pars opercularis is often reported in studies related to hand action observation (Murata et al., 1997; Rizzolatti, Fogassi & Gallese, 2002; Gallese, 2005; Baumgaertner, Buccino, Lange, McNamara & Binkofski, 2007). The SMG, in pariety with the pre-motor cortex, is reported during the observation of fearful bodies postures (Grezes, Pichon & De Gelder, 2007). Furthermore, these regions are also active during tasks that require integration of sensory modalities and body schemas such as pantomime of objects using body parts (Ohgami, Matsuo, Uchida & Nakai, 2004), or social perspective shifting (ego- to allocentric) tasks (Silani, Lamm, Ruff & Singer, 2013). Other studies investigating multisensory integration of visual and proprioceptive information report activity in the same brain regions observed in this time window. For example, tactile stimulation of the right hand when placed in unusual positions (e.g., across the midline of the body toward the left side of the body) leads to increased activity of the left SMG, S1, premotor cortex, and ventral IPS compared to normal positioning (right side of the body). A recent meta-analysis investigating peripersonal space and body ownership also implicates these regions as control centres of multisensory integration (Grivaz, Blanke & Serino, 2017). It must be noted that many of these studies report left-lateralised responses of areas, however the right lateralisation seems to be consistent with the previous assertion of a visuo-spatial and potentially

emotionally-laden processing route.

8.5.4 Atlas Based Analysis

Based on this literature, the findings of this experiment demonstrate that observing distorted fingers elicits involvement of the areas serving multisensory integration. As defined in Section 1.1, in order for the observation of fingers to become embodied through simulation, somatosensory areas must also show involvement. In line with this statement, the results of both whole-brain and atlas based analysis, show involvement in areas that are involved in somatosensory processing. For example, a cluster of activity in the DHcontrast was found in the anatomical regions that can be identified as the S2 (Eickhoff, Schleicher, Zilles & Amunts, 2005). This region is involved in the processing of touch, and painful stimulation and shows some evidence of topigraphic organisation (Eickhoff et al., 2005; Hinkley, Krubitzer, Nagarajan & Disbrow, 2007; Wasaka & Kakigi, 2012). Studies investigating somatosensory monitoring of tactile responses report S2 activation when subjects are presented with unexpected stimuli (e.g, unexpected touch, or unexpected visual feedback of a movement, Chen et al., 2008; Wasaka & Kakigi, 2012). These results prompt the suggestion that subjects may see the finger abnormalities as uncommon stimuli, and this triggers the integration of sensory information available to schemas related to the hand. This integration suggestion is supported by findings where more than one modality of stimulus is presented simultaneously. For example, Gazzola, Aziz-Zadeh and Keysers (2006) looked for brain regions that were both active when an action was executed, and when the same action was heard. Common areas included parietal clusters outlined above, but also included the S2. This finding further reinforces the idea that S2 is involved in supporting the somatomotor integration necessary for

somatosensory discrimination, and based on its onset of activity there seems to be a temporal hierarchy of processing with the S2 only being active at a later period.

The results of the Atlas based contrasts $DH > SH$, reinforce the findings and explanation above by means of a significant difference in the PCS. This is a large area in the cortex and the differences observed can perhaps be explained by the overlap of activity in areas such as the S2 and the SMG. However, the PCS is of great interest in the context of this thesis. In chapter 5, fMRI results showed activity overlap with posterior regions of the S1 hand area. This region overlaps with PCS, and from visual inspection of the left panel in Figures 8.4 and 8.5, there seems to be a slight overlap with areas which could be considered the posterior areas of the S1 hand area. It is possible that a significant difference over such a large area is also a consequence of the involvement of the posterior areas of the S1 in response to the observation of the distorted finger postures compared to standard configurations, as seen in the fMRI results of Chapter 5.

8.5.5 Conclusion

In conclusion, in this chapter I attempted to provide a time-line of the brain structures involved in the processing of distorted fingers postures. In earlier latencies (<200 ms), results showed the expected involvement of the visual processing areas such as the lateral occipital cortex, fusiform gyrus, and inferior and middle temporal gyri. From 200 ms of stimulus onset, results showed a larger involvement of somatosensory integration areas such the as intra-parietal sulcus, par opercularis, the secondary somatosensory cortex and the supramarginal gyrus. The later latecies of these responses are in line with previous literature, and expand previous fMRI studies of multisensory integration by demonstrating

the spatio-temporal profile of such a response. Statistical analyses of the control stimuli did not show this late network, thereby confirming these results and the choice of chairs as control stimuli. Therefore, in this chapter I was able to demonstrate the underlying trigger (visual) of the embodied simulation; and the integration of proprioceptive and visual information as expressed by sustained activity of areas involved in multisensory representation.

Chapter 9

General Discussion

9.1 Overview

This thesis explored the involvement of the somatosensory regions and visual areas sensitive to body part images in the creation of an embodied simulation response. In the introductory chapter (section 1.1), I explain embodied simulation as a mechanism that uses areas related to the processing of first-person or direct somatosensory experience in order to simulate somatosensory experience from images that imply such experience. This mechanism depends on preexisting body information (i.e., body schema) and interacts with the visual areas related to body observation, allowing the observer to achieve a 'visceral' understanding of what is happening to the observed body. In the following sections, I discuss how the results of the experiments in this thesis support this assertion.

9.2 Main findings

If the definition of embodied simulation is accurate, then when biologically salient stimuli related to a specific body part are visually presented, there should be an overlap of activity with tactile stimulation of the same body part. The

results of Chapter 5 confirm this hypothesis. Using a tactile localiser of the finger areas in the primary somatosensory cortex, in combination with the parcellation of the different Brodmann Areas (BA) in this region, I found significant activation in contrast for the observation of *Distorted Hands>Standard Hands* in BA 2, which was mostly right lateralised. This finding somewhat tentatively addressed the first step in this investigation, which lead to the next question of 'Can this difference between distorted and standard hands be traced to the visual areas involved in the representation of bodies?' To answer this question I conducted two EEG experiments: first to identify whether the lateral occipital N1 ERP component demonstrates a sensitive response to hands in comparison to whole-bodies; then use this component to ask targeted questions about distorted hands representation in the visual areas. The result of the first experiment showed a larger N1 response to images of hands compared to whole-bodies which motivated the use of this component for the next experiment. In the second experiment, it was found that distorted hands elicited a larger right-lateralised N1 peak (compared to standard hands), compared to the same contrast for chairs in distorted and standard configurations. With this, I finalised the second step in this thesis; I showed that differences between the salience of distorted hands and chairs can be traced to early latencies in the visual processing stream. Furthermore, these differences cannot be explained just via increased object-based attention, as the comparison between control conditions did not elicit the same response. In the final experiment and third step of this exploration, I outlined the spatio-temporal relationship between the visual areas and somatosensory areas using MEG. Since the results of the EEG experiment which compared hands and chairs conditions elicited interesting results, I used a very similar paradigm to

address this step. The source analysis of these response estimates for different conditions revealed a complex temporal processing of these salient and abnormal finger postures. First, unlike the EEG experiment, significant differences for the contrasts *Distorted Hands* > *Standard Hands* showed sustained involvement of the fusiform and inferior temporal areas around 150 ms from stimulus onset. Subsequently from 250 ms, somatosensory areas and multi-sensory integration areas became active in parallel with sustained activity of the body-part observation processing areas. This last step converged both the ERP and fMRI findings, and demonstrated that visual representation of biologically salient distortions leads to a hierarchical processing stream of visual and somatosensory information.

9.3 Visual attention or embodied simulation

One common interpretation offered by both the fMRI and MEG experiments is that the parietal areas (including S1) are the centres supporting embodied simulation. One potential confound of this explanation is that activity patterns observed are also associated with the control of visual attention, rather than a body-specific mechanism. In the review by Corbetta and Shulman (2002), it was put forward that the bilateral IPS, the extrastriate visual areas, the right hemispheric SMG, insula, and ventral frontal cortex compose the dorsal attention network. This network is activated by directional prompts to manipulate the focus of attention to a location in the visual field, or to specific features of an object. Damage or physiological manipulation of the areas in this network can to lead to visuo-spatial neglect, decline in attention related tasks, impairment in social perception tasks, and also decreases proprioceptive experience such as direct touch perception and bodily-self consciousness (Farrell & Robertson, 2000; Maravita et al., 2003; Blanke et al., 2005; Ebisch et al., 2008; Alho, Salminen, Sams, Hietanen

& Nummenmaa, 2015). Furthermore, it is suggested that activity in areas such as the temporal-parietal junction and SMG reflect an interruption of ongoing activity to redirect functioning to areas that are involved in the processing of the salient modality (Corbetta & Shulman, 2002; Ionta et al., 2011). The attention network explanation fits with the results of the fMRI experiment and MEG results (see Figure 9.1), and is based on a wide range of literature of multisensory integration. Therefore, it could be said that just attention is responsible for the brain activity elicited by the observation to the distorted hands, and that the biological salience of these stimuli is not the key factor behind the result observed. However, crucial details in the thesis point towards an alternative explanation.

First, the results of the behavioural experiment in Chapter 4, where repetition priming was used, demonstrate how perspective influenced accuracy in the detection of finger distortions. In this experiment, a finger distortion image was either primed by a larger distortion of the same finger, or by a natural hand in congruent or incongruent perspective (ego- vs. allocentric). The results showed that subjects engage with the orientation of the hand in the priming event to determine whether or not it is distorted. If both the prime and the target events are distorted fingers in congruent and egocentric perspective, results showed a better distortion discrimination compared to the unprimed condition. This result alone supports the idea that the attention network is at play; subjects create a frame of reference in whatever perspective has been primed by a finger distortion, and then they become primed to attend to an object in that orientation, leading to an improvement in detection. However, if the prime is a finger distortion in an incongruent perspective, the accuracy is significantly decreased, even compared to the unprimed condition. This finding is particularly pertinent to the discus-

sion of the involvement of the attention network in the response to distorted hands. This suggests that subjects mentally rotate the observed hand to match the position of the frame of reference created during the priming stage (previously seen). Then, they compare it with the known body schema of the hand aspect to decide whether there is an abnormality. This finding therefore, points towards a mechanism that relies on the attention network, but that also relies on sensorimotor integration of different modalities in order to make inferences regarding the aspect of the finger.

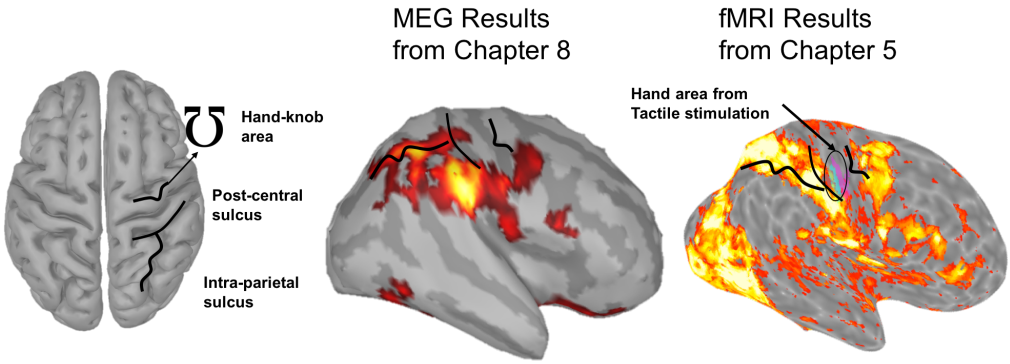

Figure 9.1: Comparison of the results between fMRI and MEG (time window of 270-400 ms) for distorted vs. standard finger postures contrast. Also note the black line highlighting interesting anatomical landmarks such as the omega-shapped hand-knob area (Yousry et al., 1997). Note similar pattern between results MEG and fMRI results.

Second, if attention was the only process at play in the processing of distorted fingers, then primary somatosensory cortex involvement would not be expected. This was the key hypothesis behind Chan and Baker's (2015) results. In this fMRI study, they reported no overlap in activation between observed touch and experienced touch to the hand over the somatosensory hand area. They explained that similar studies (e.g., Kuehn et al., 2013) used liberal methods of ROI drawing, overestimating the area of BA 2, including regions of the IPS, which is a key area in directing attention to salient features of a stimulus (Meeren et al., 2016). But the result of their analysis can also be explained by the use of conservative

restrictions on what the primary somatosensory cortex is, as they excluded BA 2 from the analysis. Several cytoarchitectonic and functional studies that explore the composition of the S1 have converged on the conclusion the BA 2 is part of the S1 (Grefkes et al., 2001; Grezes et al., 2007). In particular, Martuzzi et al. (2015) demonstrated superior involvement of BA 2 in the representation of visual-touch illusions (task highly dependent on visual and somatosensory integration), and numerous others for direct tactile stimulation (for example see Sanchez-Panchuelo et al., 2012; Martuzzi et al., 2014). The fMRI results in Chapter 5, further argues against the claim by Chan & Baker, 2015 by showing activity patterns elicited by the observation of distorted fingers overlaps with BA 2 regions. Furthermore, the fMRI resolution was larger than other similar studies, and the ROIs were defined based on a probabilistic parcellation of the whole brain, in combination with a tactile localiser that creates conservative ROIs (explained below) with respects to finger response preference. These facts add further weight to the argument that an embodied simulation network, which is driven by more than just visual attention to the hand, is responsible for the results observed.

Third, in both EEG and MEG studies, distorted chairs do not show similar response patterns compared to distorted hands. In the EEG experiment, the distortion effect of chairs was smaller particularly over the right hemisphere occipito-parietal electrodes. And, whilst they are both visually abnormal, only the distorted hands induced a larger and sustained N1 response. Furthermore, this result is expanded by the analysis of the source localisation of the same condition in the MEG experiment. While the distorted hands showed involvement of similar areas compared to those in the attention network, the distorted chairs condition did not show parietal involvement in any latency of interest. In comparison

with Meeren et al. (2016), IPS activity was not found in within similar latencies, and IPS activity found within 130 ms of onset when comparing fearful and neutral body postures. The spatio-temporal evolution of this difference is similar to what was found in the MEG experiment and could reflect the involvement of a similar mechanism of attention to salient body information. Consequently, the differences at later latencies in the MEG experiment perhaps reflect a fine grain analysis of the observed stimuli. This would also explain the involvement of the attention network, which in turn, leads to the involvement of the somatosensory areas.

9.4 Limitations and future work

In this section, I expand on some of the limitations of this thesis and how they can be addressed in the future. For instance in the fMRI experiment, there are two limitations: First, the method for analysing the data of the finger localiser paradigm is not very good at detecting overlapping responses. Analysis of the travelling wave protocol depends on a differential statistical method that attributes a single stimulation (e.g., stimulation of the index finger) to a specific voxel in an all-or-nothing approach. Therefore, overlapping responses to finger stimulation are either unidentified due to lack of coherence with the predictive model, or are classified as belonging to the finger with the largest response (Besle et al., 2014). It means that this method for defining touch-sensitive areas in the S1 may be overly conservative. BA 2 receptive-fields are large and respond to more than one finger stimulation, leading to some voxels in the posterior S1 to be ignored by this method. This was demonstrated in (Besle et al., 2014), where finger-specific activity using a similar travelling wave paradigm, and a coherence based analysis was compared to tactile responses using an event-related

paradigm, and a general linear model based analysis. They found that finger specificity in the S1 was better in the travelling wave protocol, however, in the event-related analysis results showed larger involvement of the posterior areas of the S1 but less specificity. Another consideration is the type of stimuli used. The BA 2 is not as responsive to touch driven by mechanical instruments such as piezo-electric devices (as used in chapter 5) in comparison to other more natural tactile stimuli. A recent study demonstrated this by comparing S1 activity in response to natural touch as opposed to mechanical touch (van der Zwaag, Gruetter & Martuzzi, 2015). They found that with natural touch, involvement of the BA 1 and 2 increased significantly, with BA 2 showing the larger effect (van der Zwaag et al., 2015). More importantly, the average ratio of significant voxels responsive to natural stroking vs. mechanical stimulation within BA 2 was 38% in comparison with 3%. These findings further demonstrate the conservative nature of the travelling wave method, but despite these factors, the analysis of Distorted>Standard finger postures still showed significant overlap with BA 2 ROI. This prompts future research using localisers such as in van der Zwaag et al.'s (2015) study.

Another limitation of this thesis was that I was not able to demonstrate within finger-specific response to the observation of hand images with abnormalities in that same finger. This means that the response may not be exactly localised to ROI of the finger, which goes against the embodied simulation definition I proposed. However, as explained above, the deliberately conservative localiser method may have missed parts of the BA 2, raising interesting research questions: for instance, if embodied simulation is truly occurring in responses to the observation of abnormal fingers, then another type of body stimuli should

elicit similar response. The stimuli development procedure used here to generate images of hands and abnormalities can be easily conducted using the face, and distortions to specific areas of the face could be applied. A recent study has shown topographical organisation of the face , or 'faciotopy', in the extrastriate area responsive to visual stimuli of faces (Henriksson, Mur & Kriegeskorte, 2015). Therefore, two potential studies could be conducted to investigate the link between response patterns within these 'faciotopic' areas on the visual cortex, and corresponding S1 activity profile. The first study would be a 7T study similar to the one reported here, but using observed face abnormalities and tactile localisers (similar to Moulton et al., 2009; Huang, Chen & Sereno, 2017) for those same facial areas. The second study would be conducted using MEG, and it would aim to confirm the spatio-temporal dynamics observed in the MEG experiment reported here. This could be paired with the ROIs developed in the fMRI study and more precise time-lines of the embodied simulation network can be achieved.

Another limitation of this thesis, and in particular in the MEG study, is that there is no test whether activity in visual areas at early latencies is actually predicting the later involvement the parietal areas. Although such an investigation would be feasible due to the high temporal resolution of MEG, responses to hand in the occiptal cortex were not possible due to lack of independent functional localisers. Therefore, an investigation regarding this relationship is necessary to formalise the relationship between imaging modalities that I outline here.

9.5 Final conclusion

This thesis provides experimental support for a so far untested model of vicarious perception (Keysers et al., 2010): Images of distorted finger postures elicit the activity in the S1 with larger involvement of the posterior S1. Furthermore,

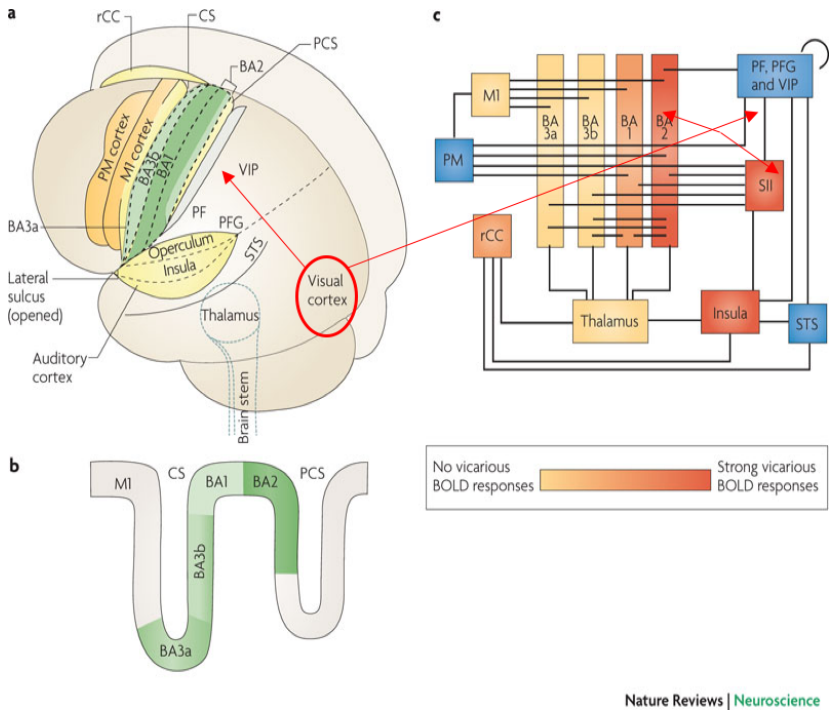

Figure 9.2: Depiction of the vicarious somatosensation model extracted from Keysers et al., 2010 and modified. Note red line, and oval added to the image to indicate that their model does not address the involvement of the visual areas.

as illustrated in Figure 9.2, this model does not include the contributions from the visual areas.

Even though the exclusion of the visual areas was likely due to it being outside of the scope the authors' argument, my thesis demonstrates how they are involved in the representation of abnormal postures. In Figure 9.3, I propose an expanded model of vicarious experience, which explains how embodied simulation arises from the interplay between visual, somatosensory, and multisensory areas.

This model tentatively claims (as involvement was not demonstrated sufficiently in this thesis) that the insula is the area that dictates when, and to what, embodied simulation will happen. The insula acts as a relay station of proprioception that prompts the reappraisal of the stimuli, which in turn triggers the involvement of areas in the parietal and somatosensory cortices.

Finally, following on from my studies, all addressing embodied simulation

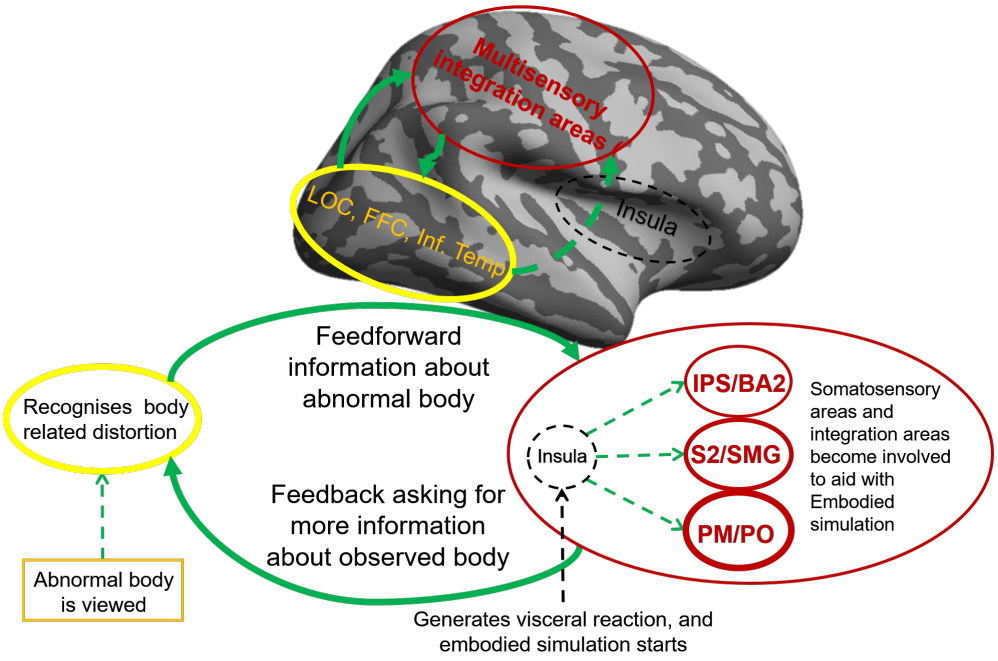

Figure 9.3: The model that includes how visual areas integrate with information about abnormal bodies into the larger multisensory network. In the top panel, a schematic of this process with the green lines depicting the communication between areas. In the bottom panel, an elaborate representation of the same schematic. Note that the involvement of the insula should be part of the multisensory areas, however, there was not sufficient evidence to include this with certainty. IPS- intra-parietal sulcus, BA 2- Brodmann Area 2, S2- secondary somatosensory cortex, SMG- supramarginal gyrus, PM- pre-motor cortex, PO- pars opercularis.

from a general population, one question remains- what does a faulty embodied simulation network mean for healthy functioning? I can only speculate that a poor integration of visual and somatosensory processes can lead to either of the two extremes: 1) inability to experience what others are experiencing may lead to a wide range of callous tendencies; or 2) people that are unable to separate their own somatosensory experience from another person's experience may have serious difficulties in social interactions. In between this wide spectrum, are most of us.

Appendix A

Empathy for Pain Scale questionnaire

Giummarra et al., 2015. See **Images of Distorted Fingers Activate Posterior Somatosensory Cortex: An Ultra High-Field fMRI Investigation**

Caulfield HOSPITAL

MONASH University Medicine, Nursing and Health Sciences

TheAlfred

MAPrc We mend minds Monash Alfred Psychiatry Research Centre

1. When you see a person undergoing a **surgical procedure** (*e.g., on a television hospital drama)* do you feel:					
	Please check ONE box for EACH statement				
	Strongly disagree				strongly agree
1) Distressed and/or upset	☐1	☐2	☐3	☐4	☐5
2) General discomfort	☐1	☐2	☐3	☐4	☐5
3) Disgust	☐1	☐2	☐3	☐4	☐5
4) A sense of what it feels like to be the person in that situation	☐1	☐2	☐3	☐4	☐5
5) "gut" feelings (e.g., nauseated)	☐1	☐2	☐3	☐4	☐5
6) Restless or a general desire to move	☐1	☐2	☐3	☐4	☐5
7) Afraid of fearful	☐1	☐2	☐3	☐4	☐5
8) A need to look away	☐1	☐2	☐3	☐4	☐5
9) A feeling of compassion for the person in that situation	☐1	☐2	☐3	☐4	☐5
10) A need to supervise or get help	☐1	☐2	☐3	☐4	☐5
11) Bodily sensations (e.g., tingling)	☐1	☐2	☐3	☐4	☐5
12) Bodily pain (e.g., stabbing, throbbing, etc.)	☐1	☐2	☐3	☐4	☐5
13) Please **describe your experiences** when seeing a surgical procedure:	.....				
	.....				

2. When you see a person who has recently had a **surgical procedure** in real life (*e.g., they have stitches or bandaged amputation stump*) do you feel:					
	Please check ONE box for EACH statement				
	Strongly disagree				strongly agree
1) Distressed and/or upset	☐1	☐2	☐3	☐4	☐5
2) General discomfort	☐1	☐2	☐3	☐4	☐5
3) Disgust	☐1	☐2	☐3	☐4	☐5
4) A sense of what it feels like to be the person in that situation	☐1	☐2	☐3	☐4	☐5
5) "gut" feelings (e.g., nauseated)	☐1	☐2	☐3	☐4	☐5
6) Restless or a general desire to move	☐1	☐2	☐3	☐4	☐5
7) Afraid of fearful	☐1	☐2	☐3	☐4	☐5
8) A need to look away	☐1	☐2	☐3	☐4	☐5
9) A feeling of compassion for the person in that situation	☐1	☐2	☐3	☐4	☐5
10) A need to supervise or get help	☐1	☐2	☐3	☐4	☐5
11) Bodily sensations (e.g., tingling)	☐1	☐2	☐3	☐4	☐5
12) Bodily pain (e.g., stabbing, throbbing, etc.)	☐1	☐2	☐3	☐4	☐5
13) Please **describe your experiences** when you see a person who has recently had a surgical procedure:	.....				
	.....				
14) Please **describe the situations involving surgery** that trigger these emotional or sensory experiences (i.e., experiences from items 1-14, above):	.....				
	.....				

3. When you see a person being **physically assaulted**, do you feel:					
	Please check ONE box for EACH statement				
	Strongly disagree				strongly agree
1) Distressed and/or upset	☐1	☐2	☐3	☐4	☐5
2) General discomfort	☐1	☐2	☐3	☐4	☐5
3) Disgust	☐1	☐2	☐3	☐4	☐5
4) A sense of what it feels like to be the person in that situation	☐1	☐2	☐3	☐4	☐5
5) "gut" feelings (e.g., nauseated)	☐1	☐2	☐3	☐4	☐5
6) Restless or a general desire to move	☐1	☐2	☐3	☐4	☐5
7) Afraid or fearful	☐1	☐2	☐3	☐4	☐5
8) A need to look away	☐1	☐2	☐3	☐4	☐5
9) A feeling of compassion for the person in that situation	☐1	☐2	☐3	☐4	☐5
10) A need to supervise or get help	☐1	☐2	☐3	☐4	☐5
11) Bodily sensations (e.g., tingling)	☐1	☐2	☐3	☐4	☐5
12) Bodily pain (e.g., stabbing, throbbing, etc.)	☐1	☐2	☐3	☐4	☐5
13) Please **describe your experiences** when you see a person being physically assaulted:	.....				
	.....				
14) Please **describe situations involving physical assault** that trigger these emotional or sensory experiences (i.e., experiences from items 1-14, above):	.....				
	.....				

4. When you see a **person being accidentally injured** *(e.g., major injuries in a car accident, or minor injuries from falling over)* do you feel:

	Please check ONE box for EACH statement Strongly disagree .....strongly agree
1) Distressed and/or upset	☐1 ☐2 ☐3 ☐4 ☐5
2) General discomfort	☐1 ☐2 ☐3 ☐4 ☐5
3) Disgust	☐1 ☐2 ☐3 ☐4 ☐5
4) A sense of what it feels like to be the person in that situation	☐1 ☐2 ☐3 ☐4 ☐5
5) "gut" feelings (e.g., nauseated)	☐1 ☐2 ☐3 ☐4 ☐5
6) Restless or a general desire to move	☐1 ☐2 ☐3 ☐4 ☐5
7) Afraid of fearful	☐1 ☐2 ☐3 ☐4 ☐5
8) A need to look away	☐1 ☐2 ☐3 ☐4 ☐5
9) A feeling of compassion for the person in that situation	☐1 ☐2 ☐3 ☐4 ☐5
10) A need to supervise or get help	☐1 ☐2 ☐3 ☐4 ☐5
11) Bodily sensations (e.g., tingling)	☐1 ☐2 ☐3 ☐4 ☐5
12) Bodily pain (e.g., stabbing, throbbing, etc.)	☐1 ☐2 ☐3 ☐4 ☐5
13) Please **describe your experiences** when you see a person being accidentally injured:	....
14) Please **describe situations involving accidental injury** that trigger these emotional or sensory experiences (i.e., experiences from items 1-14, above):	....

If you experience no sensations like tingling or pain for the situation described in section 2, please check this box ☐ and do not answer the following questions.

1. Do you experience pain triggered when you:

Please check ONE box for EACH statement

Strongly disagree .....strongly agree

	1	2	3	4	5
a) see another person in pain in real life	☐	☐	☐	☐	☐
b) hear someone describe an injury or pain	☐	☐	☐	☐	☐
c) see another person injured or in pain on TV	☐	☐	☐	☐	☐
d) imagine another person in pain	☐	☐	☐	☐	☐

2. Have you always experienced pain when seeing others in pain?

☐ YES ☐ NO ☐ Don't know

If you answered "no", how old were you when these experiences started, or was there a triggering incident?

Please describe: .....

.....

3. Where on YOUR body do you experience pain when seeing another person injured or in pain?

Please check ONE box for EACH statement

Strongly disagree .....strongly agree

	1	2	3	4	5
a) **In the same body part** (i.e., if you see someone hurt *their* left leg *your* left leg hurts)	☐	☐	☐	☐	☐
b) **In no specific part of your body**	☐	☐	☐	☐	☐
c) **In other body parts.**	☐	☐	☐	☐	☐
Please specify which body parts from the list below:					
i. Pelvis/genitals	☐	☐	☐	☐	☐
ii. Leg or legs	☐	☐	☐	☐	☐
iii. Arms	☐	☐	☐	☐	☐
iv. Chest, or spine	☐	☐	☐	☐	☐
v. stomach	☐	☐	☐	☐	☐
d) Have you experienced either of the following in the body part(s) where you experience this pain?					
i. previous traumatic/surgical injury	☐	☐	☐	☐	☐
ii. past or ongoing pain	☐	☐	☐	☐	☐

Please describe any surgery, injury or pain in the body parts where you experience your pain to be triggered when seeing others injured or in pain:

.....

.....

4. What does YOUR pain feel like when you see another person injured or in pain?

Please check ONE box for EACH statement

Strongly disagree .....strongly agree

It feels like:

	1	2	3	4	5
(a) the other person's pain	☐	☐	☐	☐	☐
(b) a "general" pain	☐	☐	☐	☐	☐
(c) my own previous or ongoing pain	☐	☐	☐	☐	☐

5. Please describe what YOUR pain feels like when you see others injured or in pain

.....

.....

.....

6. Does a more intense/dangerous situation trigger more intense pain for you? *E.g., seeing a person fall over and break their leg compared to seeing them fall and sprain their ankle.*	**Please check ONE box** *Strongly disagree.....strongly agree* ☐1 ☐2 ☐3 ☐4 ☐5
7. What is the usual intensity of the <u>pain</u> that YOU feel when you see another person injured or in pain?	0 1 2 3 4 5 6 7 8 9 10 No pain most intense pain

8. Do you avoid triggers, no longer watch particular television programs, look away because you worry that it might trigger an experience of pain?

.....

.....

If you have any further comments about your pain please write them here:

.....

.....

.....

.....

Appendix B

Supplementary Results

B.1 Brodmann Areas betas

B.2 Average betas for distorted finger observation in Finger ROIs created in the travelling wave paradigm

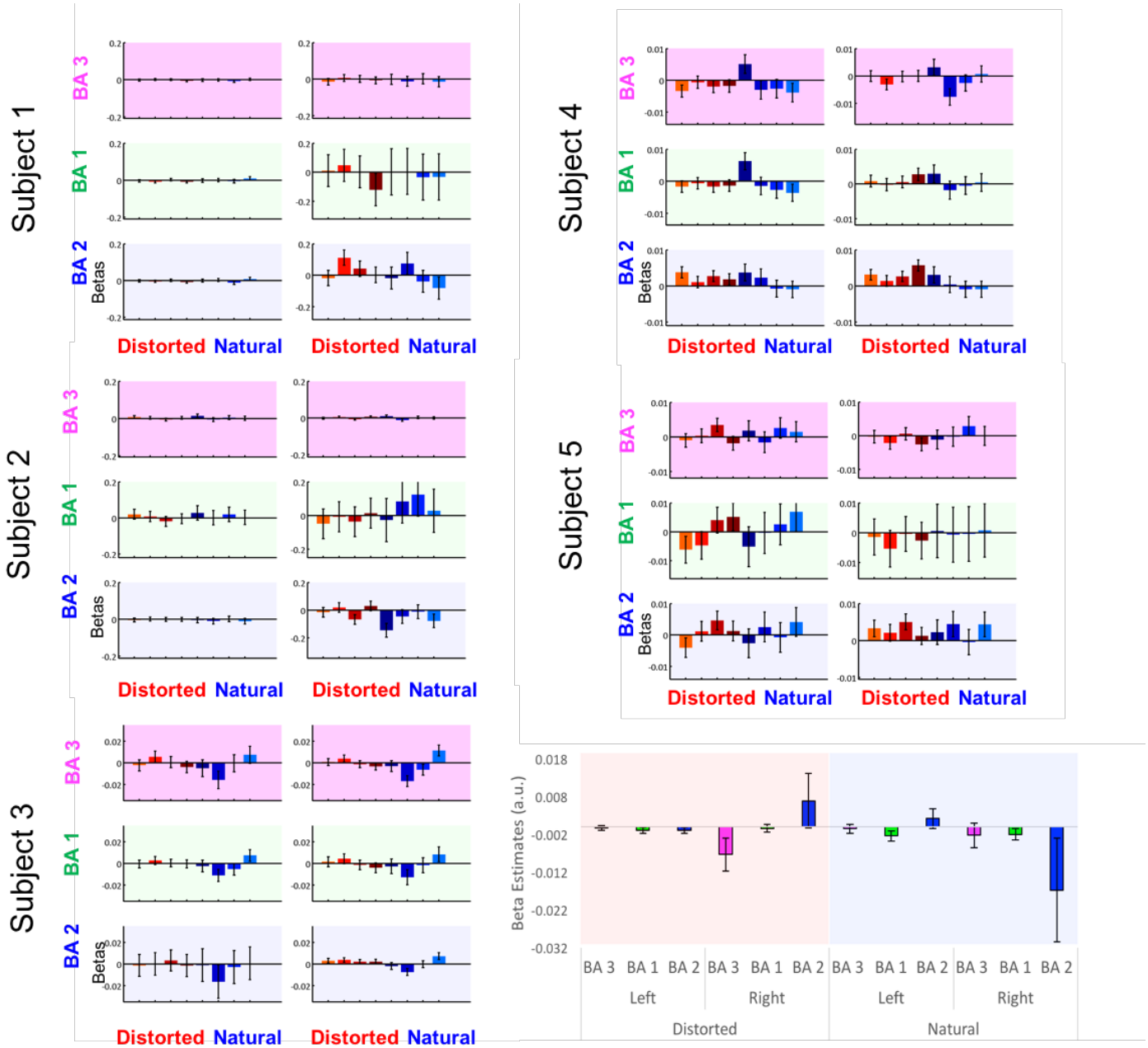

Figure B.1: Bar graphs depicting the average of the beta estimates for all the distorted conditions (in warm colours) and natural conditions (in cold colours) for all 5 subjects. At the bottom left, a bar graph the group average is presented. Standard error of the mean in all the graphs in seen in the error bars.

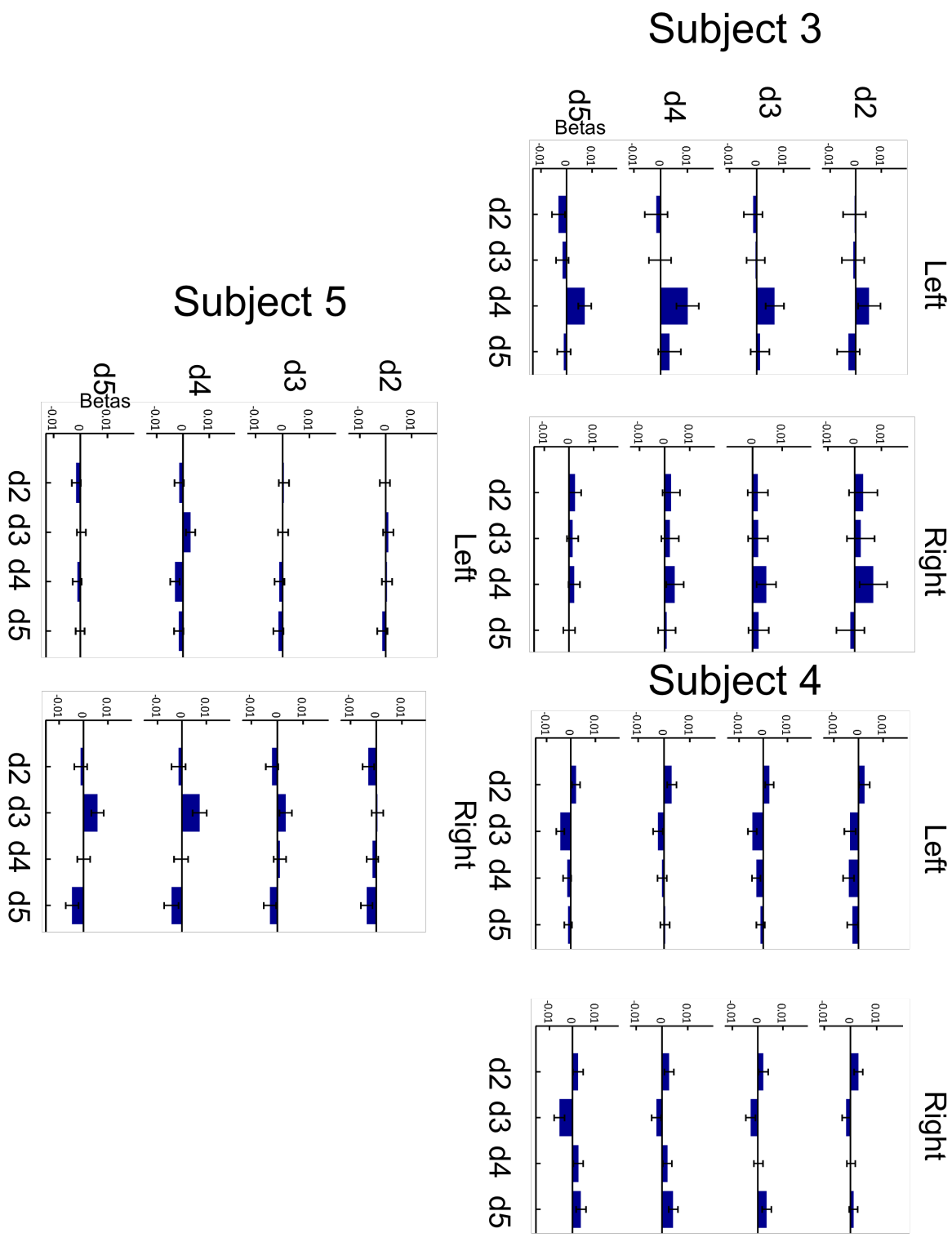

Figure B.2: Bar graphs of each subject with over 10% overlap of significant activity at any BA ROI showing the average beta estimate for each distorted finger conditions at each corresponding tactile finger ROI (left and right hemispheres) created in the travelling wave paradigm. These estimates were calculated from a GLM using using regressors for each observation of a specific finger distortion - i.e. the HRF was modelled as the convolution of 4 (distortions) 5 second regressors that started at the onset of each distorted finger observation. This GLM was applied the volume of the S1 where the main analysis was conducted and for each tactile finger ROI, and the betas for each finger distortion observation within the ROIs was calculated creating a matrix of 4 (distorted finger observation) $\times$ 4 (tactile finger ROIs).

Appendix C

Suplementary Material for Hands vs. Chair article

See **Lateral Occipital N1 Responses to Hands and Distorted Fingers**

Lateralized occipito-temporal N1 responses to images of salient distorted finger postures

Miguel G. Espirito Santo, Hsin-Yuan Chen, Martin Schürmann

Supplementary Methods (page 1), Supplementary Tables 1-3 (p 2-5), Supplementary Results (p 5-6)

Supplementary Methods

Hand stimuli were created using realistic 3D models of actual people's hands who participated in previous experiments conducted by the authors. In order to create these models, right hand dorsal and palmar sides were photographed (approximately 30-40 pictures each) from multiple angles, and then the pictures were uploaded separately onto Autodesk® 123D Catch. This free software allows photos to be uploaded, then through intensity mapping algorithms, creates a 3D mesh of the uploaded photos for each side of the hand. The models created through this software were then processed using Blender 3D®, a free 3D modelling software (https://www.blender.org). for 3D mesh post-processing and texture fixes.

Blender provides an API which allows easy access to edit any interfaced data and allowed applying distortions to the hands and chair stimuli consistently. For each of the hand models, the dorsal side with the wrist structure was parallel to the camera. Then the structure controlling the wrist was rotated by 1.5°, 1°, 8.3° (x,y,z) in order to mimic a similar perspective to that of viewing your own hand. A 40° rotation was applied anticlockwise along the x- and z-axis for each finger (except the thumb) to the proximal interphalangeal joint (between the proximal and intermediate phalanges) in order to mimic an abnormality as they might occur after an accident (see Figure 1A). Saturation was set to 0, contrast to 2.5, and brightness to 0.8, Then hands were rendered with Blender camera presets (12:11 aspect ratio) with a focal length 35 mm, and 800 x 800 pixels resolution. Using this procedure, 6 individuals' hands were modelled. Due to inter-individual differences in hand size and shape, manual adjustments were made in order to keep the ratio of hand to camera as similar between models as possible. Per hand, 8 images (2 per finger) of distorted finger postures were created. Out of these, 4 images (1 per finger) were randomly selected as stimuli for the experiment. For natural finger postures, 4 images of each hand were created. The whole procedure resulted in 48 images of hands.

Chair stimuli were created using a similar method through modification of 6 freely available templates (http://www.blendswap.com/blends/view/40140, user sizzler, license: CC-BY). Using Blender 3D, distortions were applied to the legs of the chair, in order to create a geometrically matched control for distorted hands As the legs of the chairs do not have any specific landmarks, the distortions were applied at 1/3 third of the leg proximally to the seating base (see Figure 1A) in order to mimic the placement of the distortions on the fingers. The chairs were placed in similar position as the hands, with legs - as control proxies for the fingers – pointing upwards in diagonal fashion, and the chair was rotated 45° in the z-axis to maximize viewing of all the legs. Using this procedure, 6 different chairs were modelled. The same script (including camera parameters) was used to create the distortions for each of the chairs, creating 8 distorted images (2 distortions for each of 4 legs). Out of these, 4 images (1 per leg) were randomly selected as stimuli for the experiment. For standard chairs, 4 images of each chair were created. The whole procedure resulted in 48 images of hands.

In order to hide the end of the hand model, as this may distract from the finger distortion, a Gaussian filter was applied to centre of the image such that the edges of the images, and consequently the end of model, were blurred while the centre of the image remained visible (see Figure 1A).

Supplementary Table 1a: P1 amplitudes, separate by stimulus type, configuration, and hemisphere (electrodes PO3 and PO4). The reasons to choose PO3 and PO4 for exploratory analysis of P1 responses were (a) clearly defined P1 responses in grand averages and (b) lowest variability across subjects (measured as SD, compared with P7/P8, P9/10, and PO7/PO8, the 6 electrodes of interest for N1 in main analysis). PO3/PO4 were also among the electrodes studied in Thierry et al. 2007.

Stimulus type	Configuration	Hemisphere	Mean	SEM
Hands	Distorted	Left (PO3)	4.042	0.415
		Right (PO4)	3.366	0.433
	Standard/Natural	Left (PO3)	3.706	0.304
		Right (PO4)	3.308	0.416
Chairs	Distorted	Left (PO3)	2.166	0.328
		Right (PO4)	2.530	0.467
	Standard/Natural	Left (PO3)	2.056	0.373
		Right (PO4)	2.845	0.467

Supplementary Table 1b: ANOVA, all conditions, on P1 amplitudes in per-condition waveforms (Supplementary Table 1a, above), all factors within-subject. Exploratory analysis.

	df	F	p	η_p^2
stimulus type (hand, chair)	**1,13**	**28.500**	**<0.001**	**0.687**
configuration (distorted, natural/standard)	1,13	0.135	0.719	0.010
hemisphere (left, right)	1,13	0.002	0.967	<0.001
stimulus type X configuration	1,13	1.208	0.292	0.085
stimulus type X hemisphere (footnote 1)	**1,13**	**6.559**	**0.024**	**0.335**
configuration X hemisphere	1,13	3.435	0.087	0.209
stimulus type X configuration X hemisphere	1,13	0.162	0.694	0.012

Footnote 1: To facilitate interpretation of the stimulus type X hemisphere interaction, paired t tests were run on P1 amplitudes (all averaged across distorted and standard/natural conditions), with the following results: Hands PO3 (left hemisphere) vs PO4 (right hemisphere), $t(13) = 1.205$, $p = 0.250$, Cohen's $d = 0.32$; Chairs PO3 vs PO4, $t(13) = -1.203$, $d = -0.27$; PO3 hands vs chairs, $t(13)=5.450$, $p < 0.001$, $d = 1.45$; PO4 hands vs chairs, $t(13) = 2.142$, $p = 0.052$, $d = 0.57$. The latter two results, $p < 0.001$ and $p = 0.052$, reflect stronger P1 responses to hands than to chairs, with a particularly strong difference in PO3 (left hemisphere - note that all hand images shown were of right hands). To facilitate interpretation of the configuration X hemisphere interaction (observed as a trend), paired t tests were run on P1 amplitudes (averaged across stimulus types, hands and chairs), with the following results: Distorted PO3 vs Distorted PO4, $t(13) = 0.313$, $p = 0.759$, $d = 0.203$; Standard PO3 vs Standard PO4, $t(13) = -0.449$, $p = 0.661$, $d = -0.120$; Distorted PO3 vs Standard PO3, $t(13) = 1.151$, $p = 0.270$, $d = 0.308$; Distorted PO4 vs Standard PO4, $t(13) = -1.115$, $p = 0.285$, $d = -0.298$.

Supplementary Table 2a: ANOVA, all conditions, N1 amplitudes in per-condition waveforms (complementary with **Figure 2A, left panel**), all factors within-subjects.

	df	F	p	η_p^2
stimulus type (hand, chair)	1,13	1.582	0.231	0.109
configuration (distorted, natural/standard)	1,13	0.001	0.970	0.000
hemisphere (left, right)	1,13	0.020	0.889	0.002
stimulus type X configuration	**1,13**	**7.009**	**0.020**	**0.350**
stimulus type X hemisphere	1,13	1.760	0.207	0.119
configuration X hemisphere	**1,13**	**13.879**	**0.003**	**0.516**
stimulus type X configuration X hemisphere	1,13	0.583	0.459	0.043

Supplementary Table 2b: Follow-up ANOVA, hands only, all factors within-subjects.

	df	F	p	η_p^2
configuration (distorted, natural/standard)	**1,13**	**3.624**	**0.079**	**0.218**
hemisphere (left, right)	1,13	0.493	0.495	0.037
configuration X hemisphere	1,13	0.953	0.347	0.068

Supplementary Table 2c: Follow-up ANOVA, chairs only, all factors within-subjects.

	df	F	p	η_p^2
configuration (distorted, natural/standard)	1,13	2.586	0.132	0.166
hemisphere (left, right)	1,13	0.840	0.376	0.061
configuration X hemisphere	**1,13**	**5.859**	**0.031**	**0.311**

Supplementary Table 3a: ANOVA, all conditions, N1 latencies in per-condition waveforms (complementary with **Figure 2A, right panel**), all factors within-subjects.

	df	F	p	η_p^2
stimulus type (hand, chair)	**1,13**	**11.699**	**0.005**	**0.474**
configuration (distorted, natural/standard)	1,13	0.526	0.481	0.039
hemisphere (left, right)	1,13	0.094	0.764	0.007
stimulus type X configuration	1,13	1.065	0.321	0.076
stimulus type X hemisphere	**1,13**	**11.654**	**0.005**	**0.473**
configuration X hemiphere	1,13	0.711	0.414	0.052
stimulus type X configuration X hemisphere	1,13	0.170	0.687	0.013

Supplementary Table 3b: Follow-up ANOVA, N1 latencies, hands only, all factors within-subjects.

	df	F	p	η_p^2
configuration (distorted, natural/standard)	**1,13**	**16.532**	**0.001**	**0.560**
hemisphere (left, right)	1,13	2.638	0.128	0.169
configuration X hemisphere	1,13	0.656	0.432	0.048

Supplementary Table 3c: Follow-up ANOVA, N1 latencies, chairs only, all factors within-subjects.

	df	F	p	η_p^2
configuration (distorted, natural/standard)	1,13	0.017	0.897	0.001
hemisphere (left, right)	**1,13**	**3.197**	**0.097**	**0.197**
configuration X hemisphere	1,13	0.441	0.518	0.033

Supplementary Results

Complementary to the hypothesis-driven analysis of N1 responses (with electrodes of interest and time window chosen on the basis of research literature), exploratory analysis was performed on responses to hands later than N1. The purpose of this analysis was to compare EEG responses in the current study with the bilateral MEG responses to distorted hands in an earlier MEG study (Avikainen et al. 2003). In the MEG study, differences between distorted and natural hands started at 260 ms after stimulus onset and were most consistent across subjects in a 400 to 600 ms time window. Consequently, the time window for EEG analysis was chosen to start at 250 ms and to end at 500 ms (end of segmented EEG trials).

In ANOVA of EEG amplitudes (averaged between 250 and 500 ms), neither of the main effects (configuration: distorted, natural; hemisphere: left, right) nor the configuration X hemisphere interaction was significant (Supplementary Table 4a).

The MEG parameter was source strength (always positive) whereas the EEG parameter was amplitude relative to baseline (positive or negative). Therefore, in an additional analysis step, EEG responses were assessed in terms of root-mean-square (rms) amplitudes (always positive). Again, in ANOVA of rms EEG amplitudes (250 to 500 ms), neither of the main effects (configuration; hemisphere) nor the configuration X hemisphere interaction was significant (Supplementary Table 4b).

Although the MEG study and the current EEG study have divergent results regarding post-N1 responses, this divergence cannot be interpreted as a difference of MEG vs EEG measurements, because there are more obvious explanations. The current EEG study was not designed to match the experimental conditions of the MEG study (stimulus duration 2 s, 15° x 17° of visual angle). Instead, we used parameters as in earlier EEG studies of N1 responses to whole bodies and body parts (here 200 ms duration and 4° x 4° of visual angle, compare with Thierry et al. 2006 - same duration, same size - and with Taylor et al. 2010 - duration 300 ms, same size). This approach allowed hypothesis-driven analysis, in line with our aim to enhance sensitivity for distortion-related responses at N1 latency (earlier than what was found in MEG), rather than replicating the MEG study. Note that in the MEG setup the time window of distorted vs natural differences is within stimulus duration whereas in the EEG setup, the 250 to 500 ms window is after stimulus offset.

Critically, the MEG study and our current study were also different in terms of the task for the subject: in the two conditions of the MEG study, subjects either detected stimulus repeats in a 1-back task or imitated the previously seen hand posture when an imperative (non-hand) stimulus was shown. In the current EEG study, subjects had to mentally count occurrences of a shadow superimposed on some of the stimuli. The MEG study therefore required processing of hand postures for demands of the 1-back and imitation tasks whereas in our study postures were entirely irrelevant to the task. It is all the more remarkable that our hand postures, although irrelevant to the task, still elicited distorted vs natural response differences at N1 latency (see Discussion, section "Task demands").

Supplementary Table 4a: ANOVA, hands only, mean amplitudes 250 to 500 ms, all factors within-subjects.

	df	F	p	η_p^2
configuration (distorted, natural/standard)	1,13	0.034	0.856	0.003
hemisphere (left, right)	1,13	1.642	0.222	0.112
configuration X hemisphere	1,13	1.019	0.331	0.073

Supplementary Table 4b: ANOVA, hands only, mean rms 250 to 500 ms, all factors within-subjects.

	df	F	p	η_p^2
configuration (distorted, natural/standard)	1,13	1.406	0.257	0.098
hemisphere (left, right)	1,13	0.966	0.344	0.069
configuration X hemisphere	1,13	0.014	0.909	0.001

References for Supplementary Material

Avikainen, S., Liuhanen, S., Schürmann, M. & Hari, R. Enhanced extrastriate activation during observation of distorted finger postures. J. Cogn. Neurosci, 15, 658-663 (2003).

Thierry, G. et al. An event-related potential component sensitive to images of the human body. NeuroImage 32, 871-879 (2006).

Thierry, G., Martin, C.D., Downing, P. & Pegna, A.J. Controlling for interstimulus perceptual variance abolishes N170 face selectivity. Nat. Neurosci. 10, 505-511 (2007).

Taylor, J.C., Roberts, M.V., Downing, P.E. & Thierry, G. Functional characterisation of the extrastriate body area based on the N1 ERP component. Brain Cogn. 73, 153-159 (2010).

References

Adolphs, R., Damasio, H., Tranel, D., Cooper, G. & Damasio, A. R. (2000). A role for somatosensory cortices in the visual recognition of emotion as revealed by three-dimensional lesion mapping. *Journal of neuroscience*, *20*(7), 2683–2690.

Alho, J., Salminen, N., Sams, M., Hietanen, J. K. & Nummenmaa, L. (2015). Facilitated early cortical processing of nude human bodies. *Biological psychology*, *109*, 103–110.

Allison, T., McCarthy, G. & Wood, C. C. (1992). The relationship between human long-latency somatosensory evoked potentials recorded from the cortical surface and from the scalp. *Electroencephalography and Clinical Neurophysiology/Evoked Potentials Section*, *84*(4), 301–314.

Andersson, J. L., Jenkinson, M., Smith, S. et al. (2007). Non-linear registration, aka spatial normalisation fmrib technical report tr07ja2. *FMRIB Analysis Group of the University of Oxford*, *2*.

Avikainen, S., Liuhanen, S., Schürmann, M. & Hari, R. (2003). Enhanced extrastriate activation during observation of distorted finger postures. *Journal of Cognitive Neuroscience*, *15*(5), 658–663.

Baillet, S. (2017). Magnetoencephalography for brain electrophysiology and imaging. *Nature Neuroscience*, *20*(3), 327–339.

Bandettini, P. A., Wong, E. C., Hinks, R. S., Tikofsky, R. S. & Hyde, J. S. (1992). Time course epi of human brain function during task activation. *Magnetic Resonance in Medicine*, *25*(2), 390–397.

Banissy, M. J., Kadosh, R. C., Maus, G. W., Walsh, V. & Ward, J. (2009). Prevalence, characteristics and a neurocognitive model of mirror-touch syn-

aesthesia. *Experimental brain research*, *198*(2-3), 261–272.

Baumgaertner, A., Buccino, G., Lange, R., McNamara, A. & Binkofski, F. (2007). Polymodal conceptual processing of human biological actions in the left inferior frontal lobe. *European Journal of Neuroscience*, *25*(3), 881–889.

Baumgartner, C., Doppelbauer, A., Deecke, L., Barth, D., Zeitlhofer, J., Lindinger, G. & Sutherling, W. (1991). Neuromagnetic investigation of somatotopy of human hand somatosensory cortex. *Experimental Brain Research*, *87*(3), 641–648.

Benjamini, Y. & Hochberg, Y. (1995). Controlling the false discovery rate: a practical and powerful approach to multiple testing. *Journal of the Royal Statistical Society. Series B (Methodological)*, 289–300.

Benjamini, Y., Krieger, A. M. & Yekutieli, D. (2006). Adaptive linear step-up procedures that control the false discovery rate. *Biometrika*, *93*(3), 491–507.

Bentin, S., Allison, T., Puce, A., Perez, E. & McCarthy, G. (1996). Electrophysiological studies of face perception in humans. *Journal of Cognitive Neuroscience*, *8*(6), 551–565.

Berger, H. (1929). Über das elektrenkephalogramm des menschen. *European Archives of Psychiatry and Clinical Neuroscience*, *87*(1), 527–570.

Besle, J., Sánchez-Panchuelo, R.-M., Bowtell, R., Francis, S. & Schluppeck, D. (2013). Single-subject fmri mapping at 7 t of the representation of fingertips in s1: a comparison of event-related and phase-encoding designs. *Journal of Neurophysiology*, *109*(9), 2293–2305.

Besle, J., Sánchez-Panchuelo, R.-M., Bowtell, R., Francis, S. & Schluppeck, D. (2014). Event-related fmri at 7t reveals overlapping cortical representations

for adjacent fingertips in s1 of individual subjects. *Human Brain Mapping*, *35*(5), 2027–2043.

Bigdely-Shamlo, N., Mullen, T., Kothe, C., Su, K.-M. & Robbins, K. A. (2015). The prep pipeline: standardized preprocessing for large-scale eeg analysis. *Frontiers in neuroinformatics*, *9*, 16.

Björnsdotter, M. & Olausson, H. (2011). Vicarious responses to social touch in posterior insular cortex are tuned to pleasant caressing speeds. *Journal of Neuroscience*, *31*(26), 9554–9562.

Blaimer, M., Breuer, F., Mueller, M., Heidemann, R. M., Griswold, M. A. & Jakob, P. M. (2004). Smash, sense, pils, grappa: how to choose the optimal method. *Topics in Magnetic Resonance Imaging*, *15*(4), 223–236.

Blakemore, S.-J., Bristow, D., Bird, G., Frith, C. & Ward, J. (2005). Somatosensory activations during the observation of touch and a case of vision–touch synaesthesia. *Brain*, *128*(7), 1571–1583.

Blanke, O., Mohr, C., Michel, C. M., Pascual-Leone, A., Brugger, P., Seeck, M., ... Thut, G. (2005). Linking out-of-body experience and self processing to mental own-body imagery at the temporoparietal junction. *Journal of Neuroscience*, *25*(3), 550–557.

Bloch, F., Hansen, W. W. & Packard, M. (1946). The nuclear induction experiment. *Physical Review*, *70*, 474.

Bolognini, N., Rossetti, A., Fusaro, M., Vallar, G. & Miniussi, C. (2014). Sharing social touch in the primary somatosensory cortex. *Current Biology*, *24*(13), 1513–1517.

Borhani, K., Borgomaneri, S., Làdavas, E. & Bertini, C. (2016). The effect of alexithymia on early visual processing of emotional body postures. *Biolo-*

gical Psychology, *115*, 1–8.

Borhani, K., Làdavas, E., Maier, M. E., Avenanti, A. & Bertini, C. (2015). Emotional and movement-related body postures modulate visual processing. *Social Cognitive and Affective Neuroscience*, *10*(8), 1092–1101.

Borod, J. C., Cicero, B. A., Obler, L. K., Welkowitz, J., Erhan, H. M., Santschi, C., ... Whalen, J. R. (1998). Right hemisphere emotional perception: Evidence across multiple channels. *NEUROPSYCHOLOGY-NEW YORK-*, *12*, 446–458.

Botvinick, M. & Cohen, J. (1998). Rubber hands' feel'touch that eyes see. *Nature*, *391*(6669), 756.

Bowers, D. & Heilman, K. M. (1980). Pseudoneglect: effects of hemispace on a tactile line bisection task. *Neuropsychologia*, *18*(4), 491–498.

Boynton, G. M., Engel, S. A., Glover, G. H. & Heeger, D. J. (1996). Linear systems analysis of functional magnetic resonance imaging in human v1. *Journal of Neuroscience*, *16*(13), 4207–4221.

Bracci, S., Cavina-Pratesi, C., Ietswaart, M., Caramazza, A. & Peelen, M. V. (2012). Closely overlapping responses to tools and hands in left lateral occipitotemporal cortex. *Journal of Neurophysiology*, *107*(5), 1443–1456.

Bracci, S., Ietswaart, M., Peelen, M. V. & Cavina-Pratesi, C. (2010). Dissociable neural responses to hands and non-hand body parts in human left extrastriate visual cortex. *Journal of Neurophysiology*, *103*(6), 3389–3397.

Brady, N., Maguinness, C. & Choisdealbha, Á. N. (2011). My hand or yours? markedly different sensitivity to egocentric and allocentric views in the hand laterality task. *PloS one*, *6*(8), e23316.

Brookes, M. & Singh, K. (2013). Methods in mind. *Physics World*, *26*(5), 39–44.

Brown, L. E., Morrissey, B. F. & Goodale, M. A. (2009). Vision in the palm of your hand. *Neuropsychologia*, *47*(6), 1621–1626.

Buccino, G., Lui, F., Canessa, N., Patteri, I., Lagravinese, G., Benuzzi, F., ... Rizzolatti, G. (2004). Neural circuits involved in the recognition of actions performed by nonconspecifics: An fmri study. *Journal of Cognitive Neuroscience*, *16*(1), 114–126.

Bufalari, I., Aprile, T., Avenanti, A., Di Russo, F. & Aglioti, S. M. (2007). Empathy for pain and touch in the human somatosensory cortex. *Cerebral Cortex*, *17*(11), 2553–2561.

Buxbaum, L. J., Johnson-Frey, S. H. & Bartlett-Williams, M. (2005). Deficient internal models for planning hand–object interactions in apraxia. *Neuropsychologia*, *43*(6), 917–929.

Calvo-Merino, B., Urgesi, C., Orgs, G., Aglioti, S. M. & Haggard, P. (2010). Extrastriate body area underlies aesthetic evaluation of body stimuli. *Experimental brain research*, *204*(3), 447–456.

Carandini, M. & Ferster, D. (1997). A tonic hyperpolarization underlying contrast adaptation in cat visual cortex. *Science*, *276*(5314), 949–952.

Cardini, F., Longo, M. R. & Haggard, P. (2011). Vision of the body modulates somatosensory intracortical inhibition. *Cerebral Cortex*, *21*(9), 2014–2022.

Chan & Baker, C. I. (2015). Seeing is not feeling: posterior parietal but not somatosensory cortex engagement during touch observation. *Journal of Neuroscience*, *35*(4), 1468–1480.

Chan, Kravitz, D. J., Truong, S., Arizpe, J. & Baker, C. I. (2010). Cortical representations of bodies and faces are strongest in commonly experienced configurations. *Nature Neuroscience*, *13*(4), 417–418.

Chen, Babiloni, C., Ferretti, A., Perrucci, M. G., Romani, G. L., Rossini, P. M., ... Del Gratta, C. (2008). Human secondary somatosensory cortex is involved in the processing of somatosensory rare stimuli: an fmri study. *Neuroimage*, *40*(4), 1765–1771.

Chen, Dammers, J., Boers, F., Leiberg, S., Edgar, J. C., Roberts, T. P. & Mathiak, K. (2009). The temporal dynamics of insula activity to disgust and happy facial expressions: a magnetoencephalography study. *Neuroimage*, *47*(4), 1921–1928.

Cheng, Yang, C., Lin, C., Lee, P. & Decety, J. (2008). The perception of pain in others suppresses somatosensory oscillations: a magnetoencephalography study. *Neuroimage*, *40*(4), 1833–1840.

Cheng, J., Zhang, T., Ruangwattanapaisarn, N., Alley, M. T., Uecker, M., Pauly, J. M., ... Vasanawala, S. S. (2015). Free-breathing pediatric mri with nonrigid motion correction and acceleration. *Journal of Magnetic Resonance Imaging*, *42*(2), 407–420.

Collins, D. L., Neelin, P., Peters, T. M. & Evans, A. C. (1994). Automatic 3d intersubject registration of mr volumetric data in standardized talairach space. *Journal of Computer Assisted Tomography*, *18*(2), 192–205.

Corbetta, M. & Shulman, G. L. (2002). Control of goal-directed and stimulus-driven attention in the brain. *Nature reviews neuroscience*, *3*(3), 201–215.

Corradi-Dell'Acqua, C. & Tessari, A. (2010). Is the body in the eye of the beholder?: visual processing of bodies in individuals with anomalous anatomical sensory and motor features. *Neuropsychologia*, *48*(3), 689–702.

Cosman, J. D. & Vecera, S. P. (2010). Attention affects visual perceptual processing near the hand. *Psychological Science*, *21*(9), 1254–1258.

Costantini, M., Galati, G., Ferretti, A., Caulo, M., Tartaro, A., Romani, G. L. & Aglioti, S. M. (2005). Neural systems underlying observation of humanly impossible movements: an fmri study. *Cerebral Cortex*, *15*(11), 1761–1767.

Costantini, M., Galati, G., Romani, G. L. & Aglioti, S. M. (2008). Empathic neural reactivity to noxious stimuli delivered to body parts and non-corporeal objects. *European Journal of Neuroscience*, *28*(6), 1222–1230.

Costanzo, R. M. & Gardner, E. P. (1980). A quantitative analysis of responses of direction-sensitive neurons in somatosensory cortex of awake monkeys. *Journal of Neurophysiology*, *43*(5), 1319–1341.

Craig, A. D. (2002a). How do you feel? interoception: the sense of the physiological condition of the body. *Nature reviews neuroscience*, *3*(8), 655–666.

Craig, A. D. (2002b). Opinion: How do you feel? interoception: the sense of the physiological condition of the body. *Nature reviews. Neuroscience*, *3*(8), 655.

Cross, E. S., Mackie, E. C., Wolford, G. & Hamilton, A. F. d. C. (2010). Contorted and ordinary body postures in the human brain. *Experimental Brain Research*, *204*(3), 397–407.

Dale, A. M., Liu, A. K., Fischl, B. R., Buckner, R. L., Belliveau, J. W., Lewine, J. D. & Halgren, E. (2000). Dynamic statistical parametric mapping: combining fmri and meg for high-resolution imaging of cortical activity. *Neuron*, *26*(1), 55–67.

Dale, A. M. & Sereno, M. I. (1993). Improved localizadon of cortical activity by combining eeg and meg with mri cortical surface reconstruction: a linear approach. *Journal of cognitive neuroscience*, *5*(2), 162–176.

Damasio, A. R., Everitt, B. J. & Bishop, D. (1996). The somatic marker hypothesis and the possible functions of the prefrontal cortex. *Philosophical transactions: Biological sciences*, 1413–1420.

Davoli, C. C. & Brockmole, J. R. (2012). The hands shield attention from visual interference. *Attention, Perception, & Psychophysics*, *74*(7), 1386–1390.

De Cesarei, A., Mastria, S. & Codispoti, M. (2013). Early spatial frequency processing of natural images: an erp study. *PloS one*, *8*(5), e65103.

de Gelder, B., Van den Stock, J., Meeren, H. K., Sinke, C. B., Kret, M. E. & Tamietto, M. (2010). Standing up for the body. recent progress in uncovering the networks involved in the perception of bodies and bodily expressions. *Neuroscience & Biobehavioral Reviews*, *34*(4), 513–527.

Delorme, A., Mullen, T., Kothe, C., Acar, Z. A., Bigdely-Shamlo, N., Vankov, A. & Makeig, S. (2011). Eeglab, sift, nft, bcilab, and erica: new tools for advanced eeg processing. *Computational intelligence and neuroscience*, *2011*, 10.

D'Entremont, B., Hains, S. & Muir, D. (1997). A demonstration of gaze following in 3-to 6-month-olds. *Infant Behavior and Development*, *20*(4), 569–572.

De Schotten, M. T., Dell'Acqua, F., Forkel, S. J., Simmons, A., Vergani, F., Murphy, D. G. & Catani, M. (2011). A lateralized brain network for visuospatial attention. *Nature neuroscience*, *14*(10), 1245–1246.

Desikan, R. S., Ségonne, F., Fischl, B., Quinn, B. T., Dickerson, B. C., Blacker, D., ... others (2006). An automated labeling system for subdividing the human cerebral cortex on mri scans into gyral based regions of interest. *Neuroimage*, *31*(3), 968–980.

Dinstein, I., Hasson, U., Rubin, N. & Heeger, D. J. (2007). Brain areas selective

for both observed and executed movements. *Journal of Neurophysiology*, *98*(3), 1415–1427.

Donner, T. H. & Siegel, M. (2011). A framework for local cortical oscillation patterns. *Trends in cognitive sciences*, *15*(5), 191–199.

Downing, P. E., Jiang, Y., Shuman, M. & Kanwisher, N. (2001). A cortical area selective for visual processing of the human body. *Science*, *293*(5539), 2470–2473.

Downing, P. E. & Peelen, M. V. (2011). The role of occipitotemporal body-selective regions in person perception. *Cognitive Neuroscience*, *2*(3-4), 186–203.

Downing, P. E. & Peelen, M. V. (2016). Body selectivity in occipitotemporal cortex: Causal evidence. *Neuropsychologia*, *83*, 138–148.

Ebisch, S. J., Perrucci, M. G., Ferretti, A., Del Gratta, C., Romani, G. L. & Gallese, V. (2008). The sense of touch: embodied simulation in a visuotactile mirroring mechanism for observed animate or inanimate touch. *Journal of Cognitive Neuroscience*, *20*(9), 1611–1623.

Eickhoff, S. B., Grefkes, C., Fink, G. R. & Zilles, K. (2008). Functional lateralization of face, hand, and trunk representation in anatomically defined human somatosensory areas. *Cerebral Cortex*, *18*(12), 2820–2830.

Eickhoff, S. B., Schleicher, A., Zilles, K. & Amunts, K. (2005). The human parietal operculum. i. cytoarchitectonic mapping of subdivisions. *Cerebral cortex*, *16*(2), 254–267.

Eimer, M. & Holmes, A. (2007). Event-related brain potential correlates of emotional face processing. *Neuropsychologia*, *45*(1), 15–31.

Engel, S. A., Glover, G. H. & Wandell, B. A. (1997). Retinotopic organization

in human visual cortex and the spatial precision of functional mri. *Cerebral Cortex (New York, NY: 1991)*, *7*(2), 181–192.

Farahani, K., Sinha, U., Sinha, S., Chiu, L. C. & Lufkin, R. B. (1990). Effect of field strength on susceptibility artifacts in magnetic resonance imaging. *Computerized Medical Imaging and Graphics*, *14*(6), 409–413.

Farrell, M. J. & Robertson, I. H. (2000). The automatic updating of egocentric spatial relationships and its impairment due to right posterior cortical lesions. *Neuropsychologia*, *38*(5), 585–595.

Ferri, Frassinetti, F., Ardizzi, M., Costantini, M. & Gallese, V. (2012). A sensorimotor network for the bodily self. *Journal of Cognitive Neuroscience*, *24*(7), 1584–1595.

Ferri, S., Kolster, H., Jastorff, J. & Orban, G. A. (2013). The overlap of the eba and the mt/v5 cluster. *Neuroimage*, *66*, 412–425.

Fischl, B. (2012). Freesurfer. *NeuroImage*, *62*(2), 774–781.

Fischl, B., Rajendran, N., Busa, E., Augustinack, J., Hinds, O., Yeo, B. T., ... Zilles, K. (2007). Cortical folding patterns and predicting cytoarchitecture. *Cerebral Cortex*, *18*(8), 1973–1980.

Fischl, B., Sereno, M. I., Tootell, R. B., Dale, A. M. et al. (1999). High-resolution intersubject averaging and a coordinate system for the cortical surface. *Human brain mapping*, *8*(4), 272–284.

Flaisch, T. & Schupp, H. T. (2012). Tracing the time course of emotion perception: the impact of stimulus physics and semantics on gesture processing. *Social cognitive and affective neuroscience*, *8*(7), 820–827.

Francis, S., Kelly, E., Bowtell, R., Dunseath, W., Folger, S. & McGlone, F. (2000). fmri of the responses to vibratory stimulation of digit tips. *Neuroimage*,

11(3), 188–202.

Fuchs, X., Riemer, M., Diers, M., Flor, H. & Trojan, J. (2016). Perceptual drifts of real and artificial limbs in the rubber hand illusion. *Scientific reports*, *6*.

Gallese, V. (2005). Embodied simulation: From neurons to phenomenal experience. *Phenomenology and the Cognitive Sciences*, *4*(1), 23–48.

Gallese, V. (2007). Before and below 'theory of mind': embodied simulation and the neural correlates of social cognition. *Philosophical Transactions of the Royal Society of London B: Biological Sciences*, *362*(1480), 659–669.

Gallese, V., Fadiga, L., Fogassi, L. & Rizzolatti, G. (2002). Action representation and the inferior parietal lobule. In W. Prinz & B. Hommel (Eds.), *Common mechanisms in perception and action: Attention & performance vol xix.* Oxford: Oxford University Press.

Gallese, V. & Lakoff, G. (2005). The brain's concepts: The role of the sensory-motor system in conceptual knowledge. *Cognitive neuropsychology*, *22*(3-4), 455–479.

Gao, X., Deng, X., Chen, N., Luo, W., Hu, L., Jackson, T. & Chen, H. (2011). Attentional biases among body-dissatisfied young women: An erp study with rapid serial visual presentation. *International Journal of Psychophysiology*, *82*(2), 133–142.

Gazzola, V., Aziz-Zadeh, L. & Keysers, C. (2006). Empathy and the somatotopic auditory mirror system in humans. *Current biology*, *16*(18), 1824–1829.

Genovese, C. R., Lazar, N. A. & Nichols, T. (2002). Thresholding of statistical maps in functional neuroimaging using the false discovery rate. *NeuroImage*, *15*(4), 870–878.

Geyer, S., Schleicher, A. & Zilles, K. (1997). The somatosensory cortex of human: cytoarchitecture and regional distributions of receptor-binding sites. *Neuroimage*, *6*(1), 27–45.

Geyer, S., Schleicher, A. & Zilles, K. (1999). Areas 3a, 3b, and 1 of human primary somatosensory cortex: 1. microstructural organization and interindividual variability. *Neuroimage*, *10*(1), 63–83.

Geyer, S., Schormann, T., Mohlberg, H. & Zilles, K. (2000). Areas 3a, 3b, and 1 of human primary somatosensory cortex: 2. spatial normalization to standard anatomical space. *Neuroimage*, *11*(6), 684–696.

Giummarra, M., Fitzgibbon, B., Georgiou-Karistianis, N., Beukelman, M., Verdejo-Garcia, A., Blumberg, Z., ... Gibson, S. (2015). Affective, sensory and empathic sharing of another's pain: The empathy for pain scale. *European Journal of Pain*, *19*(6), 807–816.

Gordon, G. R., Choi, H. B., Ellis-Davies, G. C. & MacVicar, B. A. (2008). Brain metabolic state dictates the polarity of astrocyte control over the cerebrovasculature. *Nature*, *456*(7223), 745.

Grefkes, C., Geyer, S., Schormann, T., Roland, P. & Zilles, K. (2001). Human somatosensory area 2: observer-independent cytoarchitectonic mapping, interindividual variability, and population map. *Neuroimage*, *14*(3), 617–631.

Grezes, J., Pichon, S. & De Gelder, B. (2007). Perceiving fear in dynamic body expressions. *Neuroimage*, *35*(2), 959–967.

Grill-Spector, K., Henson, R. & Martin, A. (2006). Repetition and the brain: neural models of stimulus-specific effects. *Trends in cognitive sciences*, *10*(1), 14–23.

Grill-Spector, K., Kushnir, T., Edelman, S., Avidan, G., Itzchak, Y. & Malach, R. (1999). Differential processing of objects under various viewing conditions in the human lateral occipital complex. *Neuron*, *24*(1), 187–203.

Grill-Spector, K., Sayres, R. & Ress, D. (2006). High-resolution imaging reveals highly selective nonface clusters in the fusiform face area. *Nature neuroscience*, *9*(9), 1177.

Grivaz, P., Blanke, O. & Serino, A. (2017). Common and distinct brain regions processing multisensory bodily signals for peripersonal space and body ownership. *NeuroImage*, *147*, 602–618.

Groppe, D. M., Urbach, T. P. & Kutas, M. (2011). Mass univariate analysis of event-related brain potentials/fields i: A critical tutorial review. *Psychophysiology*, *48*(12), 1711–1725.

Groves, K., Kennett, S. & Gillmeister, H. (2017). Evidence for erp biomarkers of eating disorder symptoms in women. *Biological Psychology*, *123*, 205–219.

Halgren, E., Raij, T., Marinkovic, K., Jousmäki, V. & Hari, R. (2000). Cognitive response profile of the human fusiform face area as determined by meg. *Cerebral cortex*, *10*(1), 69–81.

Hämäläinen, M., Hari, R., Ilmoniemi, R. J., Knuutila, J. & Lounasmaa, O. V. (1993). Magnetoencephalography—theory, instrumentation, and applications to noninvasive studies of the working human brain. *Reviews of modern Physics*, *65*(2), 413.

Hari, R. & Puce, A. (2017). *Meg-eeg primer*. Oxford University Press.

Henriksson, L., Mur, M. & Kriegeskorte, N. (2015). Faciotopy—a face-feature map with face-like topology in the human occipital face area. *Cortex*, *72*, 156–167.

Henson, R. & Rugg, M. (2003). Neural response suppression, haemodynamic repetition effects, and behavioural priming. *Neuropsychologia*, *41*(3), 263–270.

Herbert, B. M., Herbert, C. & Pollatos, O. (2011). On the relationship between interoceptive awareness and alexithymia: is interoceptive awareness related to emotional awareness? *Journal of Personality*, *79*(5), 1149–1175.

Hesslow, G. (2002). Conscious thought as simulation of behaviour and perception. *Trends in cognitive sciences*, *6*(6), 242–247.

Hinkley, L. B., Krubitzer, L. A., Nagarajan, S. S. & Disbrow, E. A. (2007). Sensorimotor integration in s2, pv, and parietal rostroventral areas of the human sylvian fissure. *Journal of neurophysiology*, *97*(2), 1288–1297.

Huang, Chen, C.-f. & Sereno, M. I. (2017). Mapping the complex topological organization of the human parietal face area. *NeuroImage*.

Huang, Mosher, J. C. & Leahy, R. (1999). A sensor-weighted overlapping-sphere head model and exhaustive head model comparison for meg. *Physics in Medicine & Biology*, *44*(2), 423.

Hyvärinen, J. & Poranen, A. (1978). Movement-sensitive and direction and orientation-selective cutaneous receptive fields in the hand area of the post-central gyrus in monkeys. *The Journal of Physiology*, *283*(1), 523–537.

Ionta, S. & Blanke, O. (2009). Differential influence of hands posture on mental rotation of hands and feet in left and right handers. *Experimental Brain Research*, *195*(2), 207–217.

Ionta, S., Heydrich, L., Lenggenhager, B., Mouthon, M., Fornari, E., Chapuis, D., ... Blanke, O. (2011). Multisensory mechanisms in temporo-parietal cortex support self-location and first-person perspective. *Neuron*, *70*(2),

363–374.

Ionta, S., Sforza, A., Funato, M. & Blanke, O. (2013). Anatomically plausible illusory posture affects mental rotation of body parts. *Cognitive, Affective, & Behavioral Neuroscience*, *13*(1), 197–209.

Iriki, A., Tanaka, M. & Iwamura, Y. (1996). Coding of modified body schema during tool use by macaque postcentral neurones. *Neuroreport*, *7*(14), 2325–2330.

Ishida, H., Nakajima, K., Inase, M. & Murata, A. (2010). Shared mapping of own and others' bodies in visuotactile bimodal area of monkey parietal cortex. *Journal of Cognitive Neuroscience*, *22*(1), 83–96.

Iwamura, Y. (1998). Hierarchical somatosensory processing. *Current Opinion in Neurobiology*, *8*(4), 522–528.

Iwamura, Y., Iriki, A. & Tanaka, M. (1994). Bilateral hand representation in the postcentral somatosensory cortex. *Nature*, *369*(6481), 554–556.

Iwamura, Y. & Tanaka, M. (1991). Organization of the first somatosensory cortex for manipulation of objects: an analysis of behavioral changes induced by muscimol injection into identified cortical loci of awake monkeys. In *Information processing in the somatosensory system* (pp. 371–380). Springer.

Iwamura, Y., Tanaka, M., Iriki, A., Taoka, M. & Toda, T. (2002). Processing of tactile and kinesthetic signals from bilateral sides of the body in the postcentral gyrus of awake monkeys. *Behavioural Brain Research*, *135*(1), 185–190.

Jackson, P. L., Brunet, E., Meltzoff, A. N. & Decety, J. (2006). Empathy examined through the neural mechanisms involved in imagining how i feel versus how you feel pain. *Neuropsychologia*, *44*(5), 752–761.

Jung, T.-P., Makeig, S., Humphries, C., Lee, T.-W., Mckeown, M. J., Iragui, V. & Sejnowski, T. J. (2000). Removing electroencephalographic artifacts by blind source separation. *Psychophysiology*, *37*(2), 163–178.

Jung, T.-P., Makeig, S., Westerfield, M., Townsend, J., Courchesne, E. & Sejnowski, T. J. (2000). Removal of eye activity artifacts from visual event-related potentials in normal and clinical subjects. *Clinical Neurophysiology*, *111*(10), 1745–1758.

Kaas, J. H. (1983). What, if anything, is si? organization of first somatosensory area of cortex. *Physiological Reviews*, *63*(1), 206–231.

Kaas, J. H. (1993). The functional organization of somatosensory cortex in primates. *Annals of Anatomy-Anatomischer Anzeiger*, *175*(6), 509–518.

Kaas, J. H. (2004). Evolution of somatosensory and motor cortex in primates. *The Anatomical Record*, *281*(1), 1148–1156.

Kalaska, J. F., Scott, S. H., Cisek, P. & Sergio, L. E. (1997). Cortical control of reaching movements. *Current opinion in neurobiology*, *7*(6), 849–859.

Keysers, C. & Gazzola, V. (2009). Expanding the mirror: vicarious activity for actions, emotions, and sensations. *Current Opinion in Neurobiology*, *19*(6), 666–671.

Keysers, C., Kaas, J. H. & Gazzola, V. (2010). Somatosensation in social perception. *Nature reviews. Neuroscience*, *11*(6), 417.

Keysers, C., Wicker, B., Gazzola, V., Anton, J.-L., Fogassi, L. & Gallese, V. (2004). A touching sight: Sii/pv activation during the observation and experience of touch. *Neuron*, *42*(2), 335–346.

Killackey, H., Gould, H., Cusick, C., Pons, T. & Kaas, J. (1983). The relation of corpus callosum connections to architectonic fields and body surface maps in

sensorimotor cortex of new and old world monkeys. *Journal of Comparative Neurology*, *219*(4), 384–419.

Krüger, G., Kastrup, A. & Glover, G. H. (2001). Neuroimaging at 1.5 t and 3.0 t: comparison of oxygenation-sensitive magnetic resonance imaging. *Magnetic Resonance in Medicine*, *45*(4), 595–604.

Kuehn, E., Mueller, K., Turner, R. & Schütz-Bosbach, S. (2014). The functional architecture of s1 during touch observation described with 7 t fmri. *Brain Structure and Function*, *219*(1), 119–140.

Kuehn, E., Trampel, R., Mueller, K., Turner, R. & Schütz-Bosbach, S. (2013). Judging roughness by sight—a 7-tesla fmri study on responsivity of the primary somatosensory cortex during observed touch of self and others. *Human Brain Mapping*, *34*(8), 1882–1895.

Kwong, K. K., Belliveau, J. W., Chesler, D. A., Goldberg, I. E., Weisskoff, R. M., Poncelet, B. P., ... Turner, R. (1992). Dynamic magnetic resonance imaging of human brain activity during primary sensory stimulation. *Proceedings of the National Academy of Sciences*, *89*(12), 5675–5679.

Lakens, D. (2013). Calculating and reporting effect sizes to facilitate cumulative science: a practical primer for t-tests and anovas. *Frontiers in psychology*, *4*.

Lamm, C., Nusbaum, H. C., Meltzoff, A. N. & Decety, J. (2007). What are you feeling? using functional magnetic resonance imaging to assess the modulation of sensory and affective responses during empathy for pain. *PloS one*, *2*(12), e1292.

Lancaster, J. L., Tordesillas-Gutiérrez, D., Martinez, M., Salinas, F., Evans, A., Zilles, K., ... Fox, P. T. (2007). Bias between mni and talairach

coordinates analyzed using the icbm-152 brain template. *Human brain mapping*, *28*(11), 1194–1205.

Langton, S. R., Watt, R. J. & Bruce, V. (2000). Do the eyes have it? cues to the direction of social attention. *Trends in cognitive sciences*, *4*(2), 50–59.

Lauritzen, M. (2005). Reading vascular changes in brain imaging: is dendritic calcium the key? *Nature reviews. Neuroscience*, *6*(1), 77.

Lederman, S. J. & Klatzky, R. L. (2009). Haptic perception: A tutorial. *Attention, Perception, & Psychophysics*, *71*(7), 1439–1459.

Limanowski, J. & Blankenburg, F. (2016). Integration of visual and proprioceptive limb position information in human posterior parietal, premotor, and extrastriate cortex. *Journal of Neuroscience*, *36*(9), 2582–2589.

Ljunggren, S. (1983). A simple graphical representation of fourier-based imaging methods. *Journal of Magnetic Resonance (1969)*, *54*(2), 338–343.

Logothetis, N. K., Pauls, J., Augath, M., Trinath, T. & Oeltermann, A. (2001). Neurophysiological investigation of the basis of the fmri signal. *Nature*, *412*(6843), 150.

Luck, S. J., Woodman, G. F. & Vogel, E. K. (2000). Event-related potential studies of attention. *Trends in cognitive sciences*, *4*(11), 432–440.

Luhmann, T., Robson, S., Kyle, S. & Boehm, J. (2014). *Close-range photogrammetry and 3d imaging*. Walter de Gruyter.

Makeig, S., Jung, T.-P., Bell, A. J., Ghahremani, D. & Sejnowski, T. J. (1997). Blind separation of auditory event-related brain responses into independent components. *Proceedings of the National Academy of Sciences*, *94*(20), 10979–10984.

Maldjian, J. A., Gottschalk, A., Patel, R. S., Pincus, D., Detre, J. A. & Alsop,

D. C. (1999). Mapping of secondary somatosensory cortex activation induced by vibrational stimulation: an fmri study. *Brain Research*, *824*(2), 291–295.

Maravita, A., McNeil, J., Malhotra, P., Greenwood, R., Husain, M. & Driver, J. (2003). Prism adaptation can improve contralesional tactile perception in neglect. *Neurology*, *60*(11), 1829–1831.

Martuzzi, R., Van Der Zwaag, W., Dieguez, S., Serino, A., Gruetter, R. & Blanke, O. (2015). Distinct contributions of brodmann areas 1 and 2 to body ownership. *Social Cognitive and Affective Neuroscience*, *10*(11), 1449–1459.

Martuzzi, R., van der Zwaag, W., Farthouat, J., Gruetter, R. & Blanke, O. (2014). Human finger somatotopy in areas 3b, 1, and 2: a 7t fmri study using a natural stimulus. *Human Brain Mapping*, *35*(1), 213–226.

Matarić, M. J. & Pomplun, M. (1998). Fixation behavior in observation and imitation of human movement. *Cognitive Brain Research*, *7*(2), 191–202.

McKone, E., Kanwisher, N. & Duchaine, B. C. (2007). Can generic expertise explain special processing for faces? *Trends in cognitive sciences*, *11*(1), 8–15.

Meeren, H. K., Hadjikhani, N., Ahlfors, S. P., Hämäläinen, M. S. & de Gelder, B. (2008). Early category-specific cortical activation revealed by visual stimulus inversion. *PLoS One*, *3*(10), e3503.

Meeren, H. K., Hadjikhani, N., Ahlfors, S. P., Hämäläinen, M. S. & De Gelder, B. (2016). Early preferential responses to fear stimuli in human right dorsal visual stream-a meg study. *Scientific Reports*, *6*, 24831.

Meeren, H. K., van Heijnsbergen, C. C. & de Gelder, B. (2005). Rapid perceptual integration of facial expression and emotional body language. *Proceedings of*

the National Academy of Sciences of the United States of America, *102*(45), 16518–16523.

Méndez-Bértolo, C., Moratti, S., Toledano, R., Lopez-Sosa, F., Martínez-Alvarez, R., Mah, Y. H., ... Strange, B. A. (2016). A fast pathway for fear in human amygdala. *Nature neuroscience*, *19*(8), 1041–1049.

Miller, K. L., Bartsch, A. J. & Smith, S. M. (2015). Simultaneous multi-slice imaging for resting-state fmri. *MAGNETOM Flash*, *63*, 70–77.

Moeller, S., Yacoub, E., Olman, C. A., Auerbach, E., Strupp, J., Harel, N. & Uğurbil, K. (2010). Multiband multislice ge-epi at 7 tesla, with 16-fold acceleration using partial parallel imaging with application to high spatial and temporal whole-brain fmri. *Magnetic Resonance in Medicine*, *63*(5), 1144–1153.

Möhring, N., Shen, C. & Neuhaus, A. H. (2014). Spatiotemporal dynamics of early cortical gesture processing. *NeuroImage*, *99*, 42–49.

Morrisey, M. N. & Rutherford, M. (2013). Do hands attract attention? *Visual Cognition*, *21*(5), 647–672.

Morrison, I. & Downing, P. E. (2007). Organization of felt and seen pain responses in anterior cingulate cortex. *Neuroimage*, *37*(2), 642–651.

Morrison, I., Löken, L. S., Minde, J., Wessberg, J., Perini, I., Nennesmo, I. & Olausson, H. (2011). Reduced c-afferent fibre density affects perceived pleasantness and empathy for touch. *Brain*, *134*(4), 1116–1126.

Morrison, I., Peelen, M. V. & Downing, P. E. (2006). The sight of others' pain modulates motor processing in human cingulate cortex. *Cerebral cortex*, *17*(9), 2214–2222.

Mougin, O., Abdel-Fahim, R., Dineen, R., Pitiot, A., Evangelou, N. & Gowland,

P. (2016). Imaging gray matter with concomitant null point imaging from the phase sensitive inversion recovery sequence. *Magnetic resonance in medicine*, *76*(5), 1512–1516.

Moulton, E. A., Pendse, G., Morris, S., Aiello-Lammens, M., Becerra, L. & Borsook, D. (2009). Segmentally arranged somatotopy within the face representation of human primary somatosensory cortex. *Human brain mapping*, *30*(3), 757–765.

Murata, A., Fadiga, L., Fogassi, L., Gallese, V., Raos, V. & Rizzolatti, G. (1997). Object representation in the ventral premotor cortex (area f5) of the monkey. *Journal of neurophysiology*, *78*(4), 2226–2230.

Najt, P., Bayer, U. & Hausmann, M. (2013). Models of hemispheric specialization in facial emotion perception—a reevaluation. *Emotion*, *13*(1), 159.

Nakashima, T., Kaneko, K., Goto, Y., Abe, T., Mitsudo, T., Ogata, K., ... Tobimatsu, S. (2008). Early erp components differentially extract facial features: evidence for spatial frequency-and-contrast detectors. *Neuroscience Research*, *62*(4), 225–235.

Nestares, O. & Heeger, D. J. (2000). Robust multiresolution alignment of mri brain volumes. *Magnetic Resonance in Medicine*, *43*(5), 705–715.

Nunes, R., Hajnal, J., Golay, X. & Larkman, D. (2006). Simultaneous slice excitation and reconstruction for single shot epi. In *Proceedings of the 14th annual meeting of ismrm, seattle, washington, usa* (p. 293).

Oberman, L. M., Winkielman, P. & Ramachandran, V. S. (2007). Face to face: Blocking facial mimicry can selectively impair recognition of emotional expressions. *Social Neuroscience*, *2*(3-4), 167–178.

Ogawa, S., Lee, T.-M., Kay, A. R. & Tank, D. W. (1990). Brain magnetic reson-

ance imaging with contrast dependent on blood oxygenation. *Proceedings of the National Academy of Sciences*, *87*(24), 9868–9872.

Ogawa, S., Menon, R., Tank, D., Kim, S., Merkle, H., Ellermann, J. & Ugurbil, K. (1993). Functional brain mapping by blood oxygenation level-dependent contrast magnetic resonance imaging. a comparison of signal characteristics with a biophysical model. *Biophysical journal*, *64*(3), 803–812.

Ohgami, Y., Matsuo, K., Uchida, N. & Nakai, T. (2004). An fmri study of tool-use gestures: body part as object and pantomime. *Neuroreport*, *15*(12), 1903–1906.

Olausson, H. W., Cole, J., Vallbo, Å., McGlone, F., Elam, M., Krämer, H. H., ... Bushnell, M. C. (2008). Unmyelinated tactile afferents have opposite effects on insular and somatosensory cortical processing. *Neuroscience letters*, *436*(2), 128–132.

Olausson, H. W., Lamarre, Y., Backlund, H., Morin, C., Wallin, B., Starck, G., ... others (2002). Unmyelinated tactile afferents signal touch and project to insular cortex. *Nature neuroscience*, *5*(9), 900.

Oostenveld, R., Fries, P., Maris, E. & Schoffelen, J.-M. (2011). Fieldtrip: open source software for advanced analysis of meg, eeg, and invasive electrophysiological data. *Computational intelligence and neuroscience*, *2011*, 1.

Op de Beeck, H. P., Brants, M., Baeck, A. & Wagemans, J. (2010). Distributed subordinate specificity for bodies, faces, and buildings in human ventral visual cortex. *Neuroimage*, *49*(4), 3414–3425.

Orlov, T., Makin, T. R. & Zohary, E. (2010). Topographic representation of the human body in the occipitotemporal cortex. *Neuron*, *68*(3), 586–600.

Orlov, T., Porat, Y., Makin, T. R. & Zohary, E. (2014). Hands in motion: an

upper-limb-selective area in the occipitotemporal cortex shows sensitivity to viewed hand kinematics. *Journal of Neuroscience*, *34*(14), 4882–4895.

Overduin, S. A. & Servos, P. (2004). Distributed digit somatotopy in primary somatosensory cortex. *NeuroImage*, *23*(2), 462–472.

Overduin, S. A. & Servos, P. (2008). Symmetric sensorimotor somatotopy. *PLoS One*, *3*(1), e1505.

Overney, L. S., Michel, C. M., Harris, I. M. & Pegna, A. J. (2005). Cerebral processes in mental transformations of body parts: recognition prior to rotation. *Cognitive brain research*, *25*(3), 722–734.

Parks, N. A., Gannon, M. A., Long, S. M. & Young, M. E. (2016). Bootstrap signal-to-noise confidence intervals: an objective method for subject exclusion and quality control in erp studies. *Frontiers in human neuroscience*, *10*, 50.

Parsons, L. M. (1994). Temporal and kinematic properties of motor behavior reflected in mentally simulated action. *Journal of Experimental Psychology: Human Perception and Performance*, *20*(4), 709.

Pauling, L. & Coryell, C. D. (1936). The magnetic properties and structure of hemoglobin, oxyhemoglobin and carbonmonoxyhemoglobin. *Proceedings of the National Academy of Sciences*, *22*(4), 210–216.

Pavlova, M., Lutzenberger, W., Sokolov, A. & Birbaumer, N. (2004). Dissociable cortical processing of recognizable and non-recognizable biological movement: analysing gamma meg activity. *Cerebral Cortex*, *14*(2), 181–188.

Peelen, M. V. & Downing, P. E. (2005). Selectivity for the human body in the fusiform gyrus. *Journal of neurophysiology*, *93*(1), 603–608.

Peelen, M. V., Wiggett, A. J. & Downing, P. E. (2006). Patterns of fmri activ-

ity dissociate overlapping functional brain areas that respond to biological motion. *Neuron*, *49*(6), 815–822.

Penfield, W. & Boldrey, E. (1937). Somatic motor and sensory representation in the cerebral cortex of man as studied by electrical stimulation. *Brain: A Journal of Neurology*.

Pfurtscheller, G. & Lopes da Silva, F. (1999). Event-related eeg/meg synchronization and desynchronization: basic principles. *Clinical neurophysiology*, *110*(11), 1842–1857.

Pihko, E., Nangini, C., Jousmäki, V. & Hari, R. (2010). Observing touch activates human primary somatosensory cortex. *European Journal of Neuroscience*, *31*(10), 1836–1843.

Pons, T. & Kaas, J. (1986). Corticocortical connections of area 2 of somatosensory cortex in macaque monkeys: a correlative anatomical and electrophysiological study. *Journal of Comparative Neurology*, *248*(3), 313–335.

Poole, M. & Bowtell, R. (2008). Volume parcellation for improved dynamic shimming. *Magnetic Resonance Materials in Physics, Biology and Medicine*, *21*(1), 31–40.

Pouga, L., Berthoz, S., de Gelder, B. & Grezes, J. (2010). Individual differences in socioaffective skills influence the neural bases of fear processing: the case of alexithymia. *Human Brain Mapping*, *31*(10), 1469–1481.

Purcell, E. M., Torrey, H. C. & Pound, R. V. (1946). Resonance absorption by nuclear magnetic moments in a solid. *Physical Review*, *69*(1-2), 37.

Qian, C., Al-Aidroos, N., West, G., Abrams, R. A. & Pratt, J. (2012). The visual p2 is attenuated for attended objects near the hands. *Cognitive neuroscience*, *3*(2), 98–104.

Randolph, M. & Semmes, J. (1974). Behavioral consequences of selective subtotal ablations in the postcentral gyrus ofmacaca mulatta. *Brain Research*, *70*(1), 55–70.

Reed, C. L. (2002). What is the body schema? In W. Prinz & A. Weltoff (Eds.), *The imitative mind: Development, evolution, and brain bases (pp. 233-243).* Cambrige, UK: Cambrige University Press.

Reed, C. L., Grubb, J. D. & Steele, C. (2006). Hands up: attentional prioritization of space near the hand. *Journal of Experimental Psychology: Human Perception and Performance*, *32*(1), 166.

Rizzolatti, G., Fadiga, L., Gallese, V. & Fogassi, L. (1996). Premotor cortex and the recognition of motor actions. *Cognitive Brain Research*, *3*(2), 131–141.

Rizzolatti, G., Fogassi, L. & Gallese, V. (2002). Motor and cognitive functions of the ventral premotor cortex. *Current opinion in neurobiology*, *12*(2), 149–154.

Rosen, B. R., Buckner, R. L. & Dale, A. M. (1998). Event-related functional mri: past, present, and future. *Proceedings of the National Academy of Sciences*, *95*(3), 773–780.

Rossion, B. & Jacques, C. (2008). Does physical interstimulus variance account for early electrophysiological face sensitive responses in the human brain? ten lessons on the n170. *Neuroimage*, *39*(4), 1959–1979.

Rotshtein, P., Richardson, M. P., Winston, J. S., Kiebel, S. J., Vuilleumier, P., Eimer, M., ... Dolan, R. J. (2010). Amygdala damage affects event-related potentials for fearful faces at specific time windows. *Human brain mapping*, *31*(7), 1089–1105.

Rushworth, M. F., Krams, M. & Passingham, R. E. (2001). The attentional

role of the left parietal cortex: the distinct lateralization and localization of motor attention in the human brain. *Journal of cognitive neuroscience*, *13*(5), 698–710.

Sanchez-Panchuelo, R. M., Besle, J., Beckett, A., Bowtell, R., Schluppeck, D. & Francis, S. (2012). Within-digit functional parcellation of brodmann areas of the human primary somatosensory cortex using functional magnetic resonance imaging at 7 tesla. *Journal of Neuroscience*, *32*(45), 15815–15822.

Sanchez-Panchuelo, R. M., Francis, S., Bowtell, R. & Schluppeck, D. (2010). Mapping human somatosensory cortex in individual subjects with 7t functional mri. *Journal of Neurophysiology*, *103*(5), 2544–2556.

Santo, M. G. E., Chen, H.-Y. & Schürmann, M. (2017). Lateralized occipito-temporal n1 responses to images of salient distorted finger postures. *Scientific Reports*, *7*(1), 14129.

Santo, M. G. E., Maxim, O. S. & Schürmann, M. (2017). N1 responses to images of hands in occipito-temporal event-related potentials. *Neuropsychologia*, *106*, 83–89.

Schaefer, M., Heinze, H.-J. & Rotte, M. (2012). Embodied empathy for tactile events: interindividual differences and vicarious somatosensory responses during touch observation. *Neuroimage*, *60*(2), 952–957.

Schürmann, M., Hlushchuk, Y. & Hari, R. (2011). Embodied visual perception of distorted finger postures. *Human Brain Mapping*, *32*(4), 612–623.

Scouten, A., Papademetris, X. & Constable, R. (2006). Spatial resolution, signal-to-noise ratio, and smoothing in multi-subject functional mri studies. *NeuroImage*, *30*(3), 787–793.

Sel, A., Forster, B. & Calvo-Merino, B. (2014). The emotional homunculus: Erp evidence for independent somatosensory responses during facial emotional processing. *Journal of Neuroscience*, *34*(9), 3263–3267.

Sereno, M., Belliveau, J., Dale, A. M., Repas, J. B., Kwong, K. K., Brady, T., ... Tootell, R. (1995). Borders of multiple visual areas in humans revealed by functional magnetic resonance imaging. *Science*, *268*, 889–893.

Shobe, E. R. (2014). Independent and collaborative contributions of the cerebral hemispheres to emotional processing. *Frontiers in human neuroscience*, *8*.

Sifneos, P. E. (1971). Change in patients' motivation for psychotherapy. *American Journal of Psychiatry*, *128*(6), 718–721.

Silani, G., Lamm, C., Ruff, C. C. & Singer, T. (2013). Right supramarginal gyrus is crucial to overcome emotional egocentricity bias in social judgments. *Journal of Neuroscience*, *33*(39), 15466–15476.

Singer, T., Seymour, B., O'doherty, J., Kaube, H., Dolan, R. J. & Frith, C. D. (2004). Empathy for pain involves the affective but not sensory components of pain. *Science*, *303*(5661), 1157–1162.

Slaughter, V., Nielsen, M. & Enchelmaier, P. (2008). Interacting socially with human hands at 24 months of age. *Infancy*, *13*(2), 185–195.

Smith, S. M., Jenkinson, M., Woolrich, M. W., Beckmann, C. F., Behrens, T. E., Johansen-Berg, H., ... others (2004). Advances in functional and structural mr image analysis and implementation as fsl. *Neuroimage*, *23*, S208–S219.

Stekelenburg, J. J. & de Gelder, B. (2004). The neural correlates of perceiving human bodies: an erp study on the body-inversion effect. *Neuroreport*, *15*(5), 777–780.

Stippich, C., Hofmann, R., Kapfer, D., Hempel, E., Heiland, S., Jansen, O. &

Sartor, K. (1999). Somatotopic mapping of the human primary somatosensory cortex by fully automated tactile stimulation using functional magnetic resonance imaging. *Neuroscience letters*, *277*(1), 25–28.

Striem-Amit, E. & Amedi, A. (2014). Visual cortex extrastriate body-selective area activation in congenitally blind people "seeing" by using sounds. *Current Biology*, *24*(6), 687–692.

Sun, H.-C., Welchman, A. E., Chang, D. H. & Di Luca, M. (2016). Look but don't touch: Visual cues to surface structure drive somatosensory cortex. *NeuroImage*, *128*, 353–361.

Tadel, F., Baillet, S., Mosher, J. C., Pantazis, D. & Leahy, R. M. (2011). Brainstorm: a user-friendly application for meg/eeg analysis. *Computational intelligence and neuroscience*, *2011*, 8.

Talairach, J. & Tournoux, P. (1988). Co-planar stereotaxic atlas of the human brain. 3-dimensional proportional system: an approach to cerebral imaging.

Taylor, Kim, J. H. & Ress, D. (2018). Characterization of the hemodynamic response function across the majority of human cerebral cortex. *NeuroImage*, *173*, 322–331.

Taylor & Parker, J. D. (1991). The alexithymia construct: a potential paradigm for psychosomatic medicine. *Psychosomatics*, *32*(2), 153–164.

Taylor, Roberts, M. V., Downing, P. E. & Thierry, G. (2010). Functional characterisation of the extrastriate body area based on the n1 erp component. *Brain and cognition*, *73*(3), 153–159.

Taylor, Wiggett, A. J. & Downing, P. E. (2007). Functional mri analysis of body and body part representations in the extrastriate and fusiform body areas. *Journal of neurophysiology*, *98*(3), 1626–1633.

Thierry, G., Pegna, A. J., Dodds, C., Roberts, M., Basan, S. & Downing, P. (2006). An event-related potential component sensitive to images of the human body. *Neuroimage*, *32*(2), 871–879.

Thulborn, K. R., Waterton, J. C., Matthews, P. M. & Radda, G. K. (1982). Oxygenation dependence of the transverse relaxation time of water protons in whole blood at high field. *Biochimica et Biophysica Acta (BBA)-General Subjects*, *714*(2), 265–270.

Triantafyllou, C., Hoge, R., Krueger, G., Wiggins, C., Potthast, A., Wiggins, G. & Wald, L. (2005). Comparison of physiological noise at 1.5 t, 3 t and 7 t and optimization of fmri acquisition parameters. *NeuroImage*, *26*(1), 243–250.

Tsakiris, M. & Haggard, P. (2005). The rubber hand illusion revisited: visuotactile integration and self-attribution. *Journal of Experimental Psychology: Human Perception and Performance*, *31*(1), 80.

Turner, R. (2002). How much cortex can a vein drain? downstream dilution of activation-related cerebral blood oxygenation changes. *Neuroimage*, *16*(4), 1062–1067.

Turner, R., Bihan, D. L., Moonen, C. T., Despres, D. & Frank, J. (1991). Echo-planar time course mri of cat brain oxygenation changes. *Magnetic Resonance in Medicine*, *22*(1), 159–166.

Umilta, M. A., Kohler, E., Gallese, V., Fogassi, L., Fadiga, L., Keysers, C. & Rizzolatti, G. (2001). I know what you are doing: A neurophysiological study. *Neuron*, *31*(1), 155–165.

Urgesi, C., Calvo-Merino, B., Haggard, P. & Aglioti, S. M. (2007). Transcranial magnetic stimulation reveals two cortical pathways for visual body

processing. *Journal of Neuroscience*, *27*(30), 8023–8030.

Van de Moortele, P.-F., Auerbach, E. J., Olman, C., Yacoub, E., Uğurbil, K. & Moeller, S. (2009). T 1 weighted brain images at 7 tesla unbiased for proton density, t 2∗ contrast and rf coil receive b 1 sensitivity with simultaneous vessel visualization. *Neuroimage*, *46*(2), 432–446.

van der Zwaag, W., Gruetter, R. & Martuzzi, R. (2015). Stroking or buzzing? a comparison of somatosensory touch stimuli using 7 tesla fmri. *PloS one*, *10*(8), e0134610.

Van Heijnsbergen, C., Meeren, H., Grezes, J. & de Gelder, B. (2007). Rapid detection of fear in body expressions, an erp study. *Brain research*, *1186*, 233–241.

van Stralen, H. E., van Zandvoort, M. J., Hoppenbrouwers, S. S., Vissers, L. M., Kappelle, L. J. & Dijkerman, H. C. (2014). Affective touch modulates the rubber hand illusion. *Cognition*, *131*(1), 147–158.

Vuilleumier, P., Henson, R., Driver, J. & Dolan, R. (2002). Multiple levels of visual object constancy revealed by event-related fmri of repetition priming. *Nature neuroscience*, *5*(5), 491.

Wang, X., Merzenich, M. M., Sameshima, K. & Jenkins, W. M. (1995). Remodelling of hand representation in adult cortex determined by timing of tactile stimulation. *Nature*, *378*(6552), 71.

Wasaka, T. & Kakigi, R. (2012). The effect of unpredicted visual feedback on activation in the secondary somatosensory cortex during movement execution. *BMC neuroscience*, *13*(1), 138.

Weibull, A., Gustavsson, H., Mattsson, S. & Svensson, J. (2008). Investigation of spatial resolution, partial volume effects and smoothing in functional mri

using artificial 3d time series. *NeuroImage*, *41*(2), 346–353.

Weiner, K. S. & Grill-Spector, K. (2011). Not one extrastriate body area: using anatomical landmarks, hmt+, and visual field maps to parcellate limb-selective activations in human lateral occipitotemporal cortex. *Neuroimage*, *56*(4), 2183–2199.

Wig, G. S., Grafton, S. T., Demos, K. E. & Kelley, W. M. (2005). Reductions in neural activity underlie behavioral components of repetition priming. *Nature neuroscience*, *8*(9), 1228–1233.

Wilson, P., Maruff, P., Butson, M., Williams, J., Lum, J. & Thomas, P. (2004). Internal representation of movement in children with developmental co-ordination disorder: a mental rotation task. *Developmental medicine and child neurology*, *46*(11), 754–759.

Winkler, I., Haufe, S. & Tangermann, M. (2011). Automatic classification of artifactual ica-components for artifact removal in eeg signals. *Behavioral and Brain Functions*, *7*(1), 30.

Xiang, J.-Z. & Brown, M. (1998). Differential neuronal encoding of novelty, familiarity and recency in regions of the anterior temporal lobe. *Neuropharmacology*, *37*(4), 657–676.

Yacoub, E., Shmuel, A., Pfeuffer, J., De Moortele, V., Adriany, G., Andersen, P., ... others (2001). Imaging brain function in humans at 7 tesla. *Magnetic Resonance in Medicine*, *45*(4), 588–594.

Yacoub, E., Shmuel, A., Pfeuffer, J., De Moortele, V., Adriany, G., Ugurbil, K., ... others (2001). Investigation of the initial dip in fmri at 7 tesla. *NMR in Biomedicine*, *14*(7-8), 408–412.

Yang, Y., Wen, H., Mattay, V. S., Balaban, R. S., Frank, J. A. & Duyn, J. H.

(1999). Comparison of 3d bold functional mri with spiral acquisition at 1.5 and 4.0 t. *NeuroImage*, *9*(4), 446–451.

Yau, J. M., Connor, C. E. & Hsiao, S. S. (2013). Representation of tactile curvature in macaque somatosensory area 2. *Journal of Neurophysiology*, *109*(12), 2999–3012.

Yousry, T., Schmid, U., Alkadhi, H., Schmidt, D., Peraud, A., Buettner, A. & Winkler, P. (1997). Localization of the motor hand area to a knob on the precentral gyrus. a new landmark. *Brain: a journal of neurology*, *120*(1), 141–157.

Yu, C. & Smith, L. B. (2013). Joint attention without gaze following: Human infants and their parents coordinate visual attention to objects through eye-hand coordination. *PloS one*, *8*(11), e79659.

Zopf, R. & Williams, M. A. (2013). Preference for orientations commonly viewed for one's own hand in the anterior intraparietal cortex. *PloS one*, *8*(1), e53812.